A lipid nanocapsule formulation for drug delivery to the retina

Dileep Urimi

Thesis for the degree of Philosophiae Doctor

August 2023

School of Health Sciences

FACULTY OF PHARMACEUTICAL SCIENCES

UNIVERSITY OF ICELAND

A lipid nanocapsule formulation for drug delivery to the retina

Dileep Urimi

Thesis for the degree of Philosophiae Doctor

Supervisor(s)

Nicolaas Schipper PhD
Ronja Widenbring PhD
Prof. Þorsteinn Loftsson PhD

Doctoral committee

Prof. Þorsteinn Loftsson PhD
Nicolaas Schipper PhD
Anna Fureby PhD
Prof. Hákon Hrafn Sigurðsson PhD

August 2023

School of Health Sciences

FACULTY OF PHARMACEUTICAL SCIENCES

UNIVERSITY OF ICELAND

Þróun fitusækinna nanóhylkja fyrir lyfjagjöf til sjónhimnu

Dileep Urimi

Ritgerð til doktorsgráðu

Leiðbeinandi/leiðbeinendur

Nicolaas Schipper PhD
Ronja Widenbring PhD
Prof. Þorsteinn Loftsson PhD

Doktorsnefnd

Prof. Þorsteinn Loftsson PhD
Nicolaas Schipper PhD
Anna Fureby PhD
Prof. Hákon Hrafn Sigurðsson PhD

Ágúst 2023

Heilbrigðisvísindasvið
LYFJAFRÆÐIDEILD
HÁSKÓLI ÍSLANDS

ISBN 978-9935-9689-2-0

ORCID: 0000-0002-1463-4990

Reykjavik, Iceland 2023

Ágrip

Arftengd sjónhimnuhrörnun (retinal degeneration, RD) er samheiti á sjaldgæfum og ólæknandi taugahrörnunarsjúkdómum í sjónhimnu sem einkennast af stig vaxandi tapi á sjónviðtakafrumum. Í byrjun verður sjúklingurinn var við næturblindu en síðan tapi á útlægri og miðlægri sjón sem að lokum leiðir til blindu. Erfiðleika við meðhöndlunar sjúkdómsins má rekja til mikils erfðafræðilegs fjölbreytileika hans og takmarkaðrar þekkingu á orsökum sjúkdómsins sem gerir lyfjaþróun erfiða, sem og erfiðleika við að koma lyfjum til sjónhimnunnar. Það er talið að í sumum tilfellum megi rekja sjúkdóminn til hækkunar á styrk hringlaga gúanósíns-3′,5′-mónófosfats (cyclic guanosine-3′,5′-monophosphate, cGMP) í ljósviðtakafrumum. Því voru cGMP hemlar (cGMP inhibitors) samtengdir sem eiga að hindra cGMP viðtaka. Einn slíkur er DF003 og hefur virkni hans verið sannreynd í RD rannsóknum. Fitusækin nanó-hylki (lipid nanocapsules, LNCs) voru valin sem flutningskerfi fyrir DF003. Slík hylki hafa áður verið notuð við lyfjagjafir, meðal annars fyrir peptíð-lyf. Rannsóknirnar fólust í eðlisefnarfæðilegum rannsóknum á nanó-hylkjunum og hvernig slík flutningskerfi virka fyrir DF003. Til að ná sem bestum árangri var samsetning nanó-hylkjanna aðlöguð að lyfinu DF003. Við rannsóknirnar var m.a. notast við svínsaugu og einangraðar sjónhimnur úr músum.

Fyrsta greinin (grein I) lýsir hvernig samsetning nanó-hylkjanna var aðlöguð að lyfinu DF003. Nanó-hylkin voru rannsökuð með tilliti til kornastærðar, stærðardreifingar (polydispersity index, PDI), lyfjahleðslu og upptöku lyfs (entrapment efficiency). Lyfið losnaði með jöfnum hraða úr hylkjunum í a.m.k. 6 daga, bæði í vatni og gerviglerhlaupi (þ.e. hýalúrónsýru lausn). Einnig var framleiðsla á nanó-hylkjunum aukin frá örfáum millilítrum upp í einn lítra. Nanó-hylkin voru einnig frostþurrkuð til að auka geymsluþol þeirra. Bæði óhlaðnar og lyfjahlaðnar samsetningar voru frostþurrkaðar með mismunandi styrk af frostvarnarefnum, þ.e. súkrósa, trehalósa og raffínósa. Í grein II er ítarleg rannsókn á uppbyggingu nanó-hylkja lýst þar sem beitt var tækni sem byggist á endurvörpun geisla (small-angle scattering). Rannsóknirnar sýndu að bæði óhlaðin og lyfjahlaðin nanó-hylki hafa kjarna-skel uppbyggingu. Til að skilja hegðun nanó-hylkjanna við augnlyfjagjöf voru framkvæmdar nokkrar in vitro og ex vivo rannsóknir þar sem m.a. lyfjaflutningur í gegnum himnur úr svínsaugum sem komið hafði verið fyrir Franz-sellum var mældur. Einnig var dreifing lyfs í svínsaugum eftir innsprautun í glerhlaup (intravitreal injection) mæld auk þess sem mat var lagt á eituráhrif og virkni á óhlöðnum og lyfjahlöðnum nanó-hylkjum í vefjasýnum úr músum. Þessar niðurstöður voru birtar í grein III.

Í stuttu máli sýndu rannsóknirnar að hægt er að nota fitusækin nanó-hylki sem augnlyfjaferjur og að þau geta ferjað cGMP hemlann DF003 til sjónhimnunnar.

Lykilorð: Nanó-hylki, sjónhimnuhrörnun, DF003, kjarna-skel uppbyggingu, augnlyfjagjöf

Abstract

Inherited retinal degeneration (RD), a rare neurodegenerative group of retinal blinding disorders and is characterized by a progressive loss of retinal photoreceptor cells that are responsible for vision. The symptoms of RD include onset of night blindness, followed by a loss of peripheral and central vision leading to a complete loss of vision. To date RD type diseases are untreatable, leaving a huge impact on patient population. The lack of valid treatments can be attributed primarily to a vast genetic diversity of the disease, obstructing identification of a common therapeutic target compound. Further, the development of a valid treatment is hindered by a lack of effective delivery mechanisms for potential drug candidates to be available at retinal photoreceptor cells, primarily due to access limiting ocular barriers. The mechanism(s) involved in the degeneration of retinal photoreceptors is still not fully understood, despite the huge progress made over the years. One of the several mechanisms that explains the degeneration points to a higher level of cyclic guanosine- 3′,5′-monophosphate (cGMP) in photoreceptor cells and this mechanism has been commonly found in various forms of RD. Thus, cGMP analogues were prepared to inhibit cGMP-activated targets within the photoreceptor cells. DF003 (or CN03) is one such analogue that was extensively evaluated and showed promising potential to be used in the treatment of RD.

In order to deliver the lead compound (DF003) to the retinal photoreceptors, lipid nanocapsule formulation (LNCs) was chosen as a carrier system. LNCs have been widely evaluated for various drug delivery applications owing to their versatile nature and their ability to carry a wide range of drug molecules including peptides. These nanoparticles have been shown to be promising in preclinical testing for various drug candidates. Hence, this study aimed at understanding the suitability of LNCs as a drug delivery carrier for DF003 to be used in ocular administration. The work includes formulation preparation with DF003, optimization and characterization, nanoscale evaluation of internal structure of LNCs, performance evaluation using porcine eyeballs and retinal explants derived from retinas of diseases mouse models. This work also includes the possibility of freeze-drying the formulation both with and without drug to enhance the long-term storage stability.

LNCs were prepared with a phase inversion process. In **Paper I**, the screening of formulation was performed by varying the composition of Labrafac™ and Kolliphor® that forms the core and shell of the nanoparticles, respectively with an aim to study their influence on physico-chemical attributes of the resulting LNCs. Formulations were characterized for particle size, polydispersity index/particle size distribution (PDI), drug loading, and entrapment efficiency. Formulation with selected composition was

characterized for additional parameters i.e., morphology using cryo-transmission electron microscopy (cryo-TEM), stability, and *in vitro* drug release. It was observed that particle size and entrapment efficiency (EE) were significantly dependent on the proportion of Kolliphor® in the composition. With an increase in Kolliphor®, a proportionate increase in EE and a decrease in particle size was noticed. Whereas an increase in Labrafac™ did not change the EE significantly, however, a higher particle size was evident owing to a lower surfactant to oil ratio. Additionally, the drug release from the formulation was sustained for a period of up to 6 days both in phosphate buffer and in vitreous component i.e., hyaluronic acid (HA) solution. Further, the stability testing data indicated the absence of an unfavorable interaction between LNCs and HA. In addition to lab-scale testing, LNCs were successfully upscaled to volumes of 1 L and 10 L using different processes and the resulted LNCs were having similar characteristics to those prepared at lab-scale.

The selected composition was further used for developing freeze-dried LNCs and for the work described in **Paper II**, and **Paper III**. With the objective of facilitating the long-term storage of LNCs, the formulation was subjected to freeze-drying. The resulting freeze-dried material was characterized after reconstitution to the initial volume to assess the impact of freeze-drying on the physico-chemical characteristics of the LNCs. Both unloaded and drug-loaded formulations were freeze dried with different concentrations of cryoprotectants, namely sucrose, trehalose and raffinose. Out of these, sucrose showed a better preservation of LNCs characteristics especially particle size and PDI, even though a slight increase in size was evident after reconstitution. Nevertheless, interesting findings were seen with freeze-drying of LNCs under varied conditions.

The structure of LNCs with and without the drug presence was investigated using small-angle scattering techniques namely, small-angle X-ray scattering (SAXS) and small-angle neutron scattering (SANS). The findings from these techniques were combined with DLS and cryo-TEM data to understand the internal structural information of LNCs. Combined analysis of the data from these techniques revealed the presence of a core-shell spherical structure that was unable to be seen with cryo-TEM. Upon drug loading, the overall core-shell structure was retained, however, interestingly the thickness of the shell increased in the order of 1 nm due to the predominant drug localization in the shell region. These findings were published in **Paper II**.

To understand the behavior of these nanoparticles in relation to their ocular administration, several *in vitro* and *ex vivo* tests were performed. These include permeability testing across excised tissues from isolated porcine eye balls using Franz-diffusion cell system, ocular distribution of fluorescently labelled LNCs in intact porcine eye balls following intravitreal (IVT) injection, toxicity and efficacy evaluation of unloaded and drug-loaded LNCs, respectively using retinal explant cultures obtained from mouse models. Data from the permeability testing showed that this formulation is

not well suited for topical administration as eye drops. This led us to further evaluate the alternative administration routes. IVT administration of DiO-loaded LNCs demonstrated the distribution of LNCs across the vitreous, with the DiO signal evident from most of the ocular tissues. These nanoparticles showed well tolerability with only a slight increase in the number of dying photoreceptors after *ex vivo* exposure to concentrations of 10 mg/mL in the retinal cultures. Furthermore, the drug-loaded LNCs showed similar pharmacological effect to that of free drug solution upon testing with retinal explants derived from retinal degeneration *rd1* mouse model, despite the fact that most of the drug is associated with the nanoparticles. These findings were published in **Paper III**. Taking together the information from these papers, LNCs showed considerable potential for ocular application and are therefore suitable for further evaluation.

In summary, this thesis gives a comprehensive information about the understanding of LNCs as a drug carrier system and its suitability for ocular application, in particular for the retinal delivery of DF003.

Keywords:

Lipid nanocapsules, retinal degeneration, DF003, core-shell structure, ocular administration

Acknowledgements

This study was carried out during the period of 2018-2023 at Department of Chemical Process and Pharmaceutical Development, RISE Research Institutes of Sweden, Södertälje and Stockholm. The project received funding from *trans*Med, a European Union Horizon 2020 research and innovation programme under the Marie Sklodowska-Curie grant agreement No 765441.

I would like to express my sincere appreciation to everyone who directly or indirectly assisted me during my journey towards this milestone.

I greatly and endlessly thank Dr. Nicolaas Schipper (Co), my supervisor at RISE for offering me with this wonderful opportunity to work as a PhD student in *trans*Med project. My deepest gratitude to Co for knowledge sharing, scientific expertise and all the discussions. A big THANK YOU for providing me ample opportunities and freedom at work, and for being a constant support both professionally and personally.

I would like to thank Ronja, my co-supervisor at RISE for knowledge sharing, continued support and for being extremely reachable.

Being away from supervisor and the degree awarding university is never an easy thing. However, I am extremely obliged for Prof. Thorsteinn Loftsson, my supervisor at University of Iceland for his guidance, constant support, and for making administrative things much easier.

I would like to thank Maja Hellsing for encouraging me to learn scattering techniques. Thanks for your patience, support and all the discussions during the scattering data analysis.

I would like to thank the members of doctoral committee: Prof. Thorsteinn Loftsson, Dr. Anna Fureby, and Prof. Hákon Hrafn Sigurðsson for their evaluation and feedback on the thesis.

I would like to thank Per Wessman, my reporting manager at RISE who provided a lot of scientific input in the project and for knowledge sharing. Thank you for being a great support.

I would like to thank Ylva Rosell for being so selfless, genuine and for offering care both at work and in my personal life.

I would like to thank my co-PhD students and friends, Oswalso, Kristina, and Monica at RISE, who always there to reach out to, both at work and off the work. A lot of

appreciation for both Oswaldo and Kristina for making me feel comfortable in very early days of my relocation to Sweden. Thanks for all the discussions and hangouts during these years.

I would like to thank all my colleagues at RISE in both Södertälje and Stockholm for their kindness, support and for their inclusiveness.

My special thanks to all the co-authors involved in the studies described in the thesis for their great collaboration, discussions and for their scientific support.

I would like to express sincere appreciation to Matej, Erico and Anna for hosting my secondment and for all the help and discussions.

I would like to thank Sara for proof-reading and feedback on the thesis.

I am extremely happy for being a part of *trans*Med consortium. I would like to thank everyone involved in *trans*Med network for arranging the consortium meetings, providing resources and opportunities to learn many different research topics. I would like to thank all the research investigators in *trans*Med consortium for their feedback, guidance, and scientific discussions. I would also like to thank all my co-PhD students in *trans*Med consortium for all the time spent during the consortium meetings, workshops and after-work hangouts.

Finally, I must say, I am forever grateful to my parents, Poorna Chandra Rao and Nirmala for their countless sacrifices and compromises in providing resources for my education, which made me to who I am today. I am sure you will feel proud of this achievement. I am always indebted to my brother, Uday who kept believing in me and for being a backbone throughout these years. Mounica, my wife and my better-half who always believes me more than I do myself, thank you for showing unconditional love and support. This PhD journey wouldn't have been completed without your constant support and motivation. To our little daughters, Kethana and Riyasri who made us to enter a new life which is more colourful than ever. I also would like to thank my extended family and friends for their constant support and motivation.

Contents

List of Abbreviations

2D	2- dimensional
Å	Angstrom
AMD	Age related macular degeneration
ANOVA	Analysis of variance
API	Active pharmaceutical ingredient
AUC	area under the curve
BRB	Blood retinal barrier
CDS	Chromatography Data System
CFU	Colony forming unit
cGMP	cyclic guanosine- 3′,5′-monophosphate
cLNC	Cationic lipid nanocapsule
CN03/DF003	Drug compound
CNGC	Cyclic nucleotide-gated ion channel
cryo-TEM	cryogenic transmission electron microscopy
CsA	Cyclosporine
CSNB	Congenital stationary night blindness
D_2O,	Deuterium oxide
DAPI	4′,6-diamidino-2-phenylindole
dC10	decanoic-d19 acid (deuterated)
dC8	octanoic-d15 (deuterated)
DCR	Derived count rate
DiO	Dioctadecyl-3,3,3,3 Tetramethylindodicarbocyanine
d-LNC	Deuterated lipid nanocapsule
DLS	Dynamic light scattering
D_{max}	The maximum dimension
DSPE-PEG2000	1,2-distearoyl-sn-glycero-3-phosphoethanolamine-N-[methoxy(polyethylene glycol)-2000]
EE	Entrapment efficiency
FALNC	Folate-modified lipid nanocapsules
GRAS	Generally regarded as safe
HA	hyaluronic acid
HCl	Hydrochloric acid
HEPES	4-(2-Hydroxyethyl)piperazine-1-ethanesulfonic acid
HIV	Human immunodeficiency virus
HLB	Hydrophilic-lipophilic balance

h-LNC	Hydrogenated lipid nanocapsule
HPLC	high-performance liquid chromatography
INL	Inner nuclear layer
IOP	Intraocular pressure
IV	Intravenous
IVT	Intravitreal
LCA	Leber congenital amaurosis
LNC	lipid nanocapsule
LNP	Lipid nanoparticle
MMR	mass mixing ratio
mRNA	Messenger ribonucleic acid
MWCO	Molecular weight cut-off
NLC	nanostructured lipid carriers
ONL	Outer nuclear layer
PBS	phosphate buffered saline
PDE6	phosphodiesterase-6
PdI	Polydispersity index
PEG	Polyethylene glycol
PFA	paraformaldehyde
PIT	Phase inversion temperature
PKG	Protein Kinase G
PLGA	Poly Lactic-co-Glycolic Acid
POPC	1-palmitoyl-2-oleoyl-sn-glycero-3-phosphocholine
Rg	Radius of gyration
RoA	Route of administration
RP	Retinitis Pigmentosa
RPE	Retinal pigment epithelium
SANS	Small-angle neutron scattering
SAXS	Small-angle X-ray scattering
SD	Standard deviation
SLD	scattering length density
SLN	solid lipid nanoparticles
TAMC	Total Aerobic Microbial Count
TSA	tryptic soy agar
TUNEL	Terminal deoxynucleotidyl transferase dUTP nick end labeling
UPLC	Ultra-performance liquid chromatography
UV	Ultraviolet
VEGF	Vascular endothelial growth factor
WT	Wild-type

List of Figures

List of Tables

List of Original Papers

This thesis is based on the following original publications, which are referred to in the text by their Roman numerals (I, II, III):

I. Urimi, D., Widenbring, R., García, R. O. P., Gedda, L., Edwards, K., Loftsson, T., & Schipper, N. (2021). Formulation development and upscaling of lipid nanocapsules as a drug delivery system for a novel cyclic GMP analogue intended for retinal drug delivery. International Journal of Pharmaceutics, 602, 120640.

II. Urimi, D., Hellsing, M., Mahmoudi, N., Soderberg, C., Widenbring, R., Gedda, L., ... & Schipper, N. (2022). Structural Characterization Study of a Lipid Nanocapsule Formulation Intended for Drug Delivery Applications Using Small-Angle Scattering Techniques. Molecular Pharmaceutics, 19(4), 1068-1077.

III. Christensen, G., Urimi, D., Lorenzo-Soler, L., Schipper, N., & Paquet-Durand, F. (2023). Ocular permeability, intraocular biodistribution of lipid nanocapsule formulation intended for retinal drug delivery. European Journal of Pharmaceutics and Biopharmaceutics, 187, 175-183.

Some unpublished data are also presented in the thesis.

In addition, other scientific publications that are not part of this thesis:

I. Christensen, G., Barut, L., Urimi, D., Schipper, N., & Paquet-Durand, F. (2021). Investigating Ex Vivo Animal Models to Test the Performance of Intravitreal Liposomal Drug Delivery Systems. Pharmaceutics, 13(7), 1013.

II. Christensen, G., Chen, Y., Urimi, D., Schipper, N., & Paquet-Durand, F. (2022). Pyruvate-conjugation of PEGylated liposomes effectively enhances their uptake in retinal photoreceptors. bioRxiv, 2022-11.

Declaration of Contribution

The doctoral student, Dileep Urimi planned the research work for the studies included in the thesis, drafted the manuscripts, and wrote the thesis with the guidance of his supervisors and co-supervisors, the doctoral committee and in close co-operation with the co-authors of each study.

1 Introduction

1.1 Inherited retinal degeneration (RD) and the role of cGMP

Inherited retinal degeneration (RD) relates to a group of rare neurodegenerative blinding disorders that result in the progressive loss of retinal photoreceptors, eventually leading to blindness (Paquet-Durand et al., 2009; Sahaboglu et al., 2013; Sancho-Pelluz et al., 2008). Retinitis Pigmentosa (RP) constitutes the most common form of RD, although many different forms are existent. These include Leber congenital amaurosis (LCA), Usher syndrome, Congenital stationary night blindness (CSNB) etc., (Chen et al., 2021; Farrar et al., 2017). RD initiates with the loss of rod cells that triggers the subsequent loss of cone cells. This leads to an initial loss of night vision followed by reduced visual acuity and a gradual narrowing of the visual field, ultimately leading to a complete blindness thereby significantly affecting the quality of life (Cross et al., 2022; O'Neal & Luther, 2021; Tolone et al., 2019; Vighi et al., 2018). It was reported that RD affects 1 in 2000 individuals with more than 2 million reported cases worldwide (Chen et al., 2021). RD type disorders are characterized by a high genetic heterogenicity (Chizzolini et al., 2011; Farrar et al., 2017) with as many as 280 identified genes associated with various forms of RD (https://sph.uth.edu/retnet/; information retrieved in September 2022). Limited knowledge underlying the disease mechanism, vast genetic diversity coupled with various ocular barriers that limits the drug availability to the retinal photoreceptors represent some of the major causes for lack of effective therapies till date (Liu & Liu, 2019). Figure 1 represents the schematic of a healthy retina, and of the retina in RD (Tolone et al., 2019).

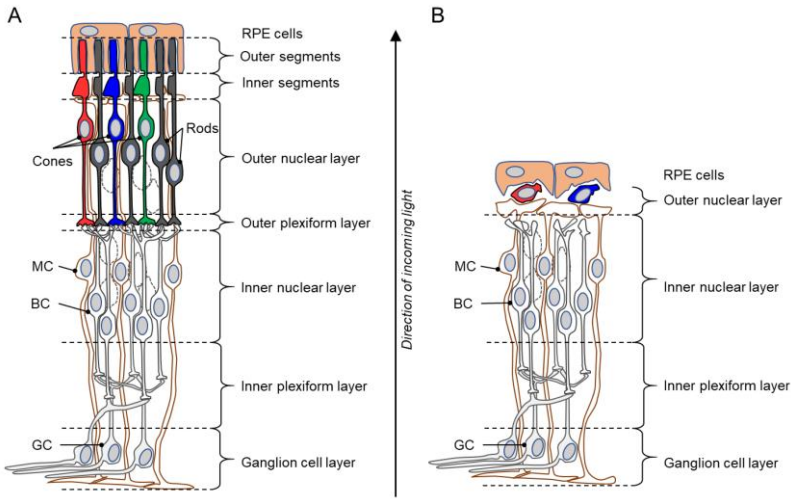

Figure 1. Schematic representation of a (A) healthy retina and, (B) retina in inherited retinal degeneration (RD). In healthy retina (A), various layers of different cell types are shown from the retinal pigment epithelium (RPE) to the ganglion cell layer. Rod photoreceptors are labelled black while cones are labelled with different colors. Retina in RD (B), outer plexiform layer has disappeared and the photoreceptors in the outer nuclear layer are lost almost completely, however, a few numbers of cone photoreceptors may still be present. BC = bipolar cell; GC = ganglion cell; MC = Müller glial cell. Note that the retinal structure has been simplified for clarity and that not all retinal cell types are shown. Adapted from *A. Tolone* et al. (Tolone et al., 2019)

Elevated levels of cGMP (cyclic guanosine- 3′,5′-monophosphate) in retinal photoreceptors are a common feature in several genetically different forms of RD. Thus, the role of cGMP in photoreceptor cell death has been evaluated in the literature. cGMP is a key molecule for photoreceptor signal transduction cascade where phosphodiesterase-6 (PDE6) is involved in the degradation of photoreceptor cGMP. Mutations affecting rod-specific *Pde6b* gene results in accumulation of cGMP in rods. These elevated levels results in overactivation of cGMP effectors i.e., Protein Kinase G (PKG) and Cyclic nucleotide–gated ion channel (CNGC) channels in photoreceptors that drives a rapid death of rod cells and subsequently results in cone cell loss (Vighi et al., 2018). Thereby, targeting the cGMP-dependent overactivation of PKG and CNGC in photoreceptors is a potential option in therapy development for RD treatment (Farber & Lolley, 1974; Marigo et al., 2018; Tolone et al., 2019; Vighi et al., 2018).

Based on this mechanistic insight, a novel class of cGMP analogues were developed in recent years to inhibit cGMP-activated targets within photoreceptors (Ekström et al., 2019; Vighi et al., 2018). These analogues have shown to be potentially effective in the treatment of RD. One such analogue, DF003 (or sometimes referred to as CN03; Figure 2), was found to inhibit both PKG and CNGC and thus proved to be effective against photoreceptor cell death. Preclinical evaluation of DF003 demonstrated the morphological and functional preservation of rod and cone photoreceptors, in RD

mouse models (*rd1*, *rd2*, and *rd10* animal models) confirming the cGMP-PKG signaling as a target for the treatment of RD (Tolone et al., 2021; Vighi et al., 2018). Further, DF003 compound showed no strong toxicological outcomes upon administration to mice and rats. This has led to further development of cGMP analogues. CN238, a novel 2nd generation analogue which structurally resembles DF003 demonstrated improved potency in preserving photoreceptor viability and function when tested in *in vitro* RD mouse models (*rd1* and *rd10* animal models) (Genieser et al., 2018; Tolone et al., 2021). In the present work, DF003 was chosen as a drug molecule owing to its strong protective effect on retinal photoreceptor cells.

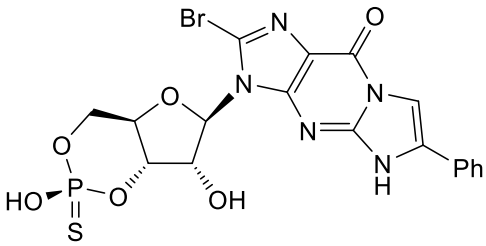

Figure 2. Molecular structure of DF003/CN03

1.2 Approaches for retinal drug delivery

Targeted drug delivery to the retina is challenging and is currently under thorough investigation (Xiaonan Huang & Ying Chau, 2019; Mandal et al., 2017). Drugs can be delivered to the retina in many ways for e.g., topical eye drops, intravenous injection, and intraocular injections namely subconjunctival, transscleral, subretinal, suprachoroidal, and intravitreal injections (Figure 3). Each of these routes are associated with both advantages and disadvantages, some of which are listed in Table 1. Topical drug administration is non-invasive and is by far the most patient compliant. However, drugs administered by this route will have to cross numerous barriers including the cornea. In spite of the barrier properties, the topical route is the first choice of administration, especially for treating diseases associated with the anterior chamber of the eye, for e.g., uveitis, dry-eye diseases for which commercial formulations are available as eye drops. Unfortunately, these barrier properties intensify when the diseases target is located in the posterior chamber, for instance the retina, for which sub-therapeutic drug concentrations are often reported following the topical administration. For this reason, despite the poor patient acceptability, intravitreal injection is the preferred administration route for retinal applications and are clinically used in the delivery of anti-VEGF proteins for e.g., bevacizumab, ranibizumab, aflibercept, in the treatment of wet age related macular degeneration (AMD) (Del Amo et al., 2017). Small molecule drugs given by intravitreal injections suffer from rapid clearance and thus poor pharmacokinetics that necessitate increased dosing frequency (Del Amo et al., 2017; Li et al., 2020). This can result in various complications such as

retinal detachment, vitreous haemorrhage, etc as mentioned in Table 1. Thus, the ideal route for drug administration for treating various diseases of the eye is not yet fully accomplished. Undeniably this needs to be specifically studied for individual retinal diseases.

Various formulation approaches to increase exposure and reduce injection frequency are currently under investigation both preclinically and clinically for the treatment of retinal diseases. Some of these include intravitreal administration of nanoparticles, microparticles, intravitreal implants, hydrogels, and combination approaches and each of these associated with both advantages and limitations (Kim & Woo, 2021). The choice of a specific delivery system is dependent on various factors including the properties of the drug molecule, dosing frequency, required bioavailability, and toxicological effects of the carrier system. Nevertheless, achieving a higher therapeutic concentration for a chronic treatment while minimizing the adverse effects is challenging. Owing to this, very few clinical treatments are available despite the extensive preclinical progress.

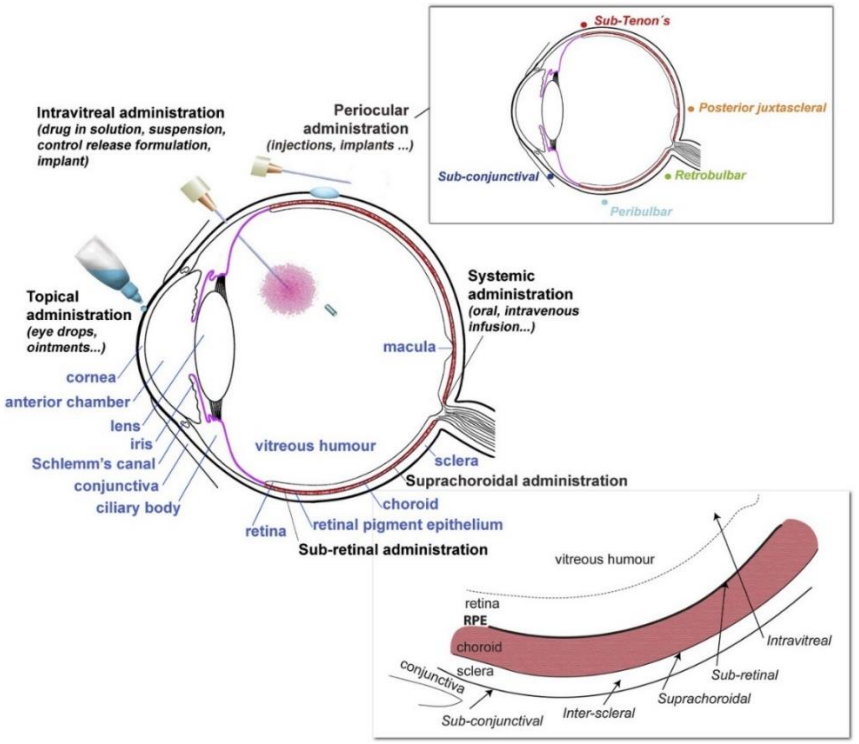

Figure 3. Routes of drug administration for drug delivery to the retina, adapted from *del Amo* et al. (Del Amo et al., 2017)

Table 1. Barriers, advantages, and drawbacks of various routes of retinal drug delivery (Agrahari et al., 2017; Duvvuri et al., 2003; Kaur & Kakkar, 2014; Meyer et al., 2016; Yamada & Olsen, 2016)

Route of administration (RoA)	**Barriers for drug availability to retina**	**Advantages**	**Drawbacks**
Systemic/ intravenous	Blood retinal barrier (BRB)	Relatively non-invasive	Systemic drug toxicity. Higher drug doses are frequently needed. Efflux transporters expressed on RPE may impede drug permeation from choroid to the retina.
Topical	Permeability and diffusional barrier properties of cornea, aqueous humor and lens	Patient friendly administration Flexibility with the dosage frequency	Faster drug clearance. Conjunctival absorption. Difficult to maintain therapeutic drug concentration at the retina.
Transscleral	Scleral permeability for large molecules	Relatively safe Better diffusion kinetics for small and hydrophilic molecules	Poor pharmacokinetics for macromolecules and less hydrophilic compounds. Small drug molecules may get eliminated via conjunctival, episcleral blood, and lymphatic flow.
Suprachoroidal	-	Better drug availability to retina in comparison to transscleral route of administration	Damage to the retinal pigment epithelium may be a concern. Postoperative inflammation and choroid haemorrhage.
Intravitreal	-	Absence of systemic side effects High therapeutic drug concentration	Invasive and patient non-compliance. Injection associated infections. Retinal detachment Increase in intraocular pressure (IOP).
Subretinal	-	Immediate access of drug to the retina	Retinal detachment.

1.3 Application of nanoparticulate formulations for ocular drug delivery

Among the various formulation strategies, nanoparticles of different types have been extensively studied for drug delivery to the retina. Application of nanoparticles in drug delivery offers numerous advantages, notably their enhanced tissue permeability, drug targeting ability and improving the pharmacokinetic properties of various drug molecules (Germain et al., 2020; Lombardo et al., 2019; Ventola, 2017). In the case of ocular drug delivery, nanoparticles demonstrate improved permeation characteristics across ocular tissues enabling the investigation of topical route for retinal drug delivery applications although clinical translation of preclinical research is still limited. Further, intravitreally administered nanoparticulate formulations enabled sustained release of drugs and thereby improved the intravitreal half-life of loaded drugs (Abrishami et al., 2009; Kang-Mieler et al., 2017; Kang-Mieler et al., 2014; Kim & Woo, 2021; Zeng et al., 1993). In addition, many researchers have evaluated functionalized nanoparticles (surface modified with various agents) for targeted drug delivery to the retina (Gross et al., 2013; Li et al., 2020; Salehi-Had et al., 2011; Singh et al., 2009).

Various types of nanoparticles such as micelles, polymeric nanoparticles, lipid-based nanoparticles and nanoparticles combined with hydrogel systems have been investigated for various routes of ocular administration preclinically and clinically (Kang-Mieler et al., 2020; Kaur & Kakkar, 2014; Kim & Woo, 2021; Li et al., 2020). Among these, lipid-based nanoparticles such as liposomes, solid lipid nanoparticles and other lipid vehicles are essentially superior to the other nanoformulations due to their low toxicity, limited immunogenicity, better biocompatibility, biodegradability and their ability to increase the bioavailability of a wide range of molecules (Balguri et al., 2016; Battaglia et al., 2016; Ghasemiyeh & Mohammadi-Samani, 2018; Li et al., 2020; Sánchez-López et al., 2017; Zhang et al., 2013). Some examples of lipid-based systems used in the treatment of retinal diseases are described here. Sai et al. evaluated the use of solid lipid nanoparticles (SLNs) and nanostructured lipid carriers (NLCs) as topical eye drops for delivery of indomethacin to posterior ocular tissues. They observed a higher drug availability in posterior ocular tissues upon loading into nanoparticles compared to the solution formulations (Balguri et al., 2016). Patrizia *et al*. found higher vitreous and retinal concentrations of Tobramycin following topical ophthalmic administration in the form of SLNs and this was reported to be due to the permeability enhancing nature of SLNs (Chetoni et al., 2016). Similarly, several reports suggested the efficacy of liposomes (Dos Santos et al., 2020; Lai et al., 2019; Natarajan et al., 2012; Natarajan et al., 2014; Liesbeth Peeters et al., 2005; Shen & Tu, 2007; Zhang et al., 2010) and lipid nanocapsules (LNCs) (Eldesouky et al., 2021; Formica et al., 2020; Formica et al., 2021; Sun et al., 2020) in enhancing the ocular permeation and bioavailability followed by both topical and intraocular administration. This remarkable potential of liposomes led to a huge clinical success and liposomes loaded with Doxorubicin or Amphotericin B are now commercially available to treat cancer and

fungal infections respectively (Lim et al., 2012). Further, various liposomal and other lipid-based formulations are currently under clinical trials for the treatment of various diseases (Table 2). The work described in the thesis focused on evaluation of LNCs as a carrier system for delivering the cGMP analogue, DF003 to the retinal photoreceptors. The use and preparation of LNCs as drug carriers is described in more detail below.

Table 2. Examples of lipid based nanoformulations currently in clinical trials

Formulation	Drug	Indication	Clinical trial information* Identifier/phase/status
SLNs loaded gel for topical applications	Oxiconazole nitrate	Tinea Pedis	NCT03823040 Phase I Completed
Lipid nanoparticles	mRNA	Respiratory syncytial virus infection	NCT05639894 Phase I/II (Recruiting)
Liposome Injection	Mitoxantrone Hydrochloride	Neuromyelitis Optica Spectrum Disorder	NCT05551598 Phase II (Not yet recruiting)
Liposomes	Daunorubicin-Cytarabine	Acute myeloid leukemia	NCT03629171 Phase II (Recruiting)
Liposomes	Daunorubicin	Acute myeloid leukemia	NCT02724163 Phase III (Recruiting)
Pegylated liposomes	Doxorubicin	Kaposi Sarcoma in people living with HIV	NCT05411237 Phase III (Not yet recruiting)
Liposomes	Bupivacaine	Fibroid Uterus	NCT04272086 Phase IV (Recruiting)

*Information was retrieved from https://clinicaltrials.gov/ on 10 February 2023.

1.4 Lipid nanocapsules (LNCs): an overview

1.4.1 LNCs as drug delivery carriers

Lipid nanocapsules (LNCs) are nanoparticles prepared by a solvent-free, low-energy phase inversion method which has been well documented in previous reports (Heurtault et al., 2002; Hirsjärvi et al., 2013; Huynh et al., 2009; Thomas & Lagarce, 2013; Valcourt et al., 2016). These nanoparticles are mainly composed of an oily core formed by medium chain triglycerides (commercially available as Labrafac™ lipophile WL 1349) which is surrounded and stabilized by a combination of Polyethylene glycol

(15)-hydroxystearate (Kolliphor® HS 15) and phospholipids (Heurtault et al., 2002; Mouzouvi et al., 2017; Valcourt et al., 2016; Vonarbourg et al., 2005). In general, LNCs are biocompatible as the components of LNCs are pharmaceutically acceptable and are GRAS listed (generally recognized as safe) (Minkov et al., 2005a, 2005b; Vonarbourg et al., 2005). Apart from being non-toxic, these nanoparticles offer various advantages including the possibility to load both hydrophilic and lipophilic molecules, and the possibility to prepare particles of different sizes with a narrow size distribution to meet a specific application of interest (Minkov et al., 2005a; Thomas & Lagarce, 2013; Vonarbourg et al., 2005). Owing to their numerous advantages, LNCs were evaluated for many drug delivery applications including antibiotic resistance, cancer, and to treat ocular conditions like age related macular degeneration. Moreover, they have been tested for various routes of administrations where LNCs showed promising outcomes (Table 3) (Abdel-Mottaleb et al., 2011; Formica et al., 2020; Formica et al., 2021; Groo et al., 2018; Hureaux et al., 2009; Huynh et al., 2009; Alf Lamprecht et al., 2002; Malzert-Fréon et al., 2006; Sun et al., 2020; Umerska et al., 2016; Zhai et al., 2018).

Table 3. Applications of LNCs as drug delivery systems described in literature.

Formulation	Drug	Disease area	RoA	*In vitro/ in vivo* testing	Major study outcome	Reference
LNCs	Efavirenz (EFV)	Gut permeation study	Oral	*Ex vivo* permeation using rat intestine	Increased *ex vivo* intestinal permeation of EFV-LNCs (47.29 ± 0.27 µg/cm^2) compared to free EFV (26.28 ± 0.27 µg/cm^2)	(Varshosaz et al., 2018)
LNCs	Efavirenz (EFV)	Viral infections	-	-	Sustained drug release was observed with EFV-LNCs	(Mukubwa et al., 2022)
LNCs	Tanshinone IIA (TSIIA)	Cancer	Oral	*In vivo* testing in male Wistar rats	Significant bioavailability enhancement with TSIIA-LNCs compared to TSIIA suspension	(Ashour et al., 2020)
LNCs	Resveratrol (RSV)	Acute Lung injury (ALI)	Oral	*In vivo* testing in male albino rats	RSV-LNCs showed beneficial role in prevention of ALI detrimental effects, compared to RSV alone	(Albanawany et al., 2022)
LNCs	Praziquantel (PZQ)	Schistosomiasis	Oral	*In vivo* testing in mice	Enhanced drug efficacy with PZQ-LNCs compared to PZG.	(Amara et al., 2018)
Phospholipid complex loaded LNCs	Tetrandrine-phospholipid complex (TPC)	Cancer, multidrug resistance	Oral	*In vivo* testing in Male Sprague-Dawley rats	Significant improvement in relative bioavailability with TPC-LNCs (2.1-fold compared to tetrandrine tablets	(Zhao et al., 2013)

Formulation	**Drug**	**Disease area**	**RoA**	***In vitro/ in vivo* testing**	**Major study outcome**	**Reference**
Cationic lipid nanocapsules (cLNCs)	Fondaparinux (Fp)	Anticoagulant therapy	Oral	*In vivo* studies in Male Wistar rats	Increased oral absolute bioavailability (up to ~21%) with LNCs compared to free Fp	(Ramadan et al., 2011)
Reverse Micelle Loaded LNCs (RMLNC)	Gallic acid (GA)	Hepatic Fibrosis	Oral	*In vivo* studies male Sprague-Dawley rats, *in vitro* cell assays	GA-RMLNC displayed higher anti-proliferative activities,	(Radwan et al., 2020)
LNCs surface modified with hyaluronic acid (HA) and Phosphatidyl serine	Tanshinone IIA	Hepatic fibrosis	Intraperitoneal	*In vivo* studies in adult male Wistar rats, in vitro cell assays.	2.4-fold increase in $AUC_{0-\infty}$ with LNCs compared to TSIIA suspension; Surface modification led to ~1.5-fold increase in hepatic accumulation compared to unmodified LNCs	(Ashour et al., 2021)
LNCs	Nimodipine (NM)	Subarachnoid haemorrhage induced vasospasm	Intranasal	*In vivo* study in Wistar rats	Intranasal delivery of NM-LNC was capable to deliver the same amount of NM at brain tissue compared with IV administration of the NM solution	(Mohsen et al., 2020)
LNCs	Paclitaxel	Lung fibrosis	Endotracheal spray	*In vivo* testing in Sprague-Dawley rats	Both blank and PTX-LNCs induces a short-term alveolar inflammation with no residual lesions in rats at	(Hureaux et al., 2017)

Formulation	Drug	Disease area	RoA	*In vitro/ in vivo* testing	Major study outcome	Reference
					day 60	
LNCs	Paclitaxel	Cancer	Pulmonary delivery by nebulisation	*In vitro* cytotoxicity study	Similar IC50 was observed with nebulized PTX-LNCs and fresh PTX-LNCs	(Hureaux et al., 2009)
LNCs	Paclitaxel (PTX)	Cancer	Intravenous	*In vivo* testing in Wistar rats	Increased mean survival times with PTX-LNCs compared to free PTX	(Lacoeuille et al., 2007)
LNCs	Curcumin	Cancer	Intravenous	*In vivo* testing in Fischer F344 female rats, in vitro cell assays	Improved pharmacokinetics upon loading into LNCs, improved anti-cancer activity in cell assays	(Lollo et al., 2018)
LNCs	Ferrocenyl diphenol tamoxifen derivative	Cancer	Intratumoural subcutaneous	*In vivo* testing in Syngeneic Fischer F344 female rats, in vitro cell assays	Better internalization, selective cytotoxicity, reduced the tumour mass and volume	(Allard et al., 2008)
Folate-modified lipid nanocapsules (FALNC)	Quercetin	Cancer	-	*In vivo* testing in rats, in vitro cell assays	Improved biological activity for QT upon loading into LNCs	(Ding et al., 2014)
LNCs	Etoposide	Cancer	-	*In vitro* cell assays	Higher growth inhibition for ETO-LNCs compared to free ETO	(Lamprecht & Benoit, 2006)

Formulation	Drug	Disease area	RoA	*In vitro/ in vivo* testing	Major study outcome	Reference
LNCs	Imatinib	Cancer	-	*In vitro* cell assays	Pharmacological effect of Imatinib was maintained with loading into LNCs	(Molaahmadi et al., 2019)
LNCs	Apigenin (AP)	Cancer	-	*In vitro* cell assays	Significant inhibition rate to HepG2 cells and MCF-7 cells with AP-LNCs	(Ding et al., 2013)
LNCs	Tripentone	Cancer	-	*In vitro* cell assays	Complete recovery from cytotoxic activity of tripentone after its encapsulation in LNCs	(Malzert-Fréon et al., 2006)
LNCs	EAPB0503	Cancer	-	*In vitro* cell assays	Significant improvement is drug solubility with LNCs, preservation of cyto-toxic effect after loading into LNCs	(Chouchou et al., 2017)
LNCs	Erlotinib hydrochloride (ERLO)	Pancreatic cancers	-	*In vitro* cell assays	Comparable efficacy of ERLO-LNCs on pancreatic adenocarcinoma cells, to that of free ERLO	(Vrignaud et al., 2012)
LNCs	Cisplatin (CDDP)	Hepatocellular Carcinoma	-	*In vitro* cell assays	CDDP-LNCs exhibited much stronger cell killing potency than free CDDP, with the IC50 values decreased from 17.93 to 3.53 and 5.16 μM after 72-h incubation.	(Zhai et al., 2018)

Formulation	Drug	Disease area	RoA	*In vitro/ in vivo* testing	Major study outcome	Reference
LNCs	Sorafenib (SFN)	Glioblastoma	Intratumoral injection	*In vitro* cell assays, *in vivo* studies using female Swiss nude mice	SFN-LNCs were more effective than free SFN in inducing early tumor vascular normalization	(Clavreul et al., 2018)
LNCs loaded in Chitosan/Poloxamer *in situ* Gel	Cyclosporine (CsA)	Dry eye disease	Topical	*In vivo* studies using Male rabbits, Ex vivo studies using bovine cornea	Increased corneal mucoadhesion for LNC-in situ gel combination, CsA-LNCs showed comparable efficacy to that of marketed CsA nanoemulsion.	(Eldesouky et al., 2021)
LNCs	Triamcinolone acetonide	Endotoxin-induced uveitis	Subconjunctival injection	*In vivo* studies using albino male white rabbits, *in vitro* cell assays	TA-LNCs showed a high anti-inflammatory activity, improved therapeutic efficacy in the endotoxin-induced uveitis/rabbit model, compared to commercial TA suspension	(Formica et al., 2020)
LNCs	Bevacizumab (BVZ) + Triamcinolone acetonide (TA)	Neovascular ocular pathologies	-	*In vitro* cell assays	BVZ-TA-LNC significantly prevented the capillary formation induced by the vascular endothelium growth factor.	(Formica et al., 2021)
LNCs	Astragaloside-IV (ASIV)	Age-related macular degeneration	Topical eye drops	*In vivo* studies in Sprague-Dawley rats, Japanese	With ASIV-LNCs, a significant reduction in apoptosis rate was seen. Also, ASIV-LNCs showed	(Sun et al., 2020)

Formulation	Drug	Disease area	RoA	*In vitro/ in vivo* testing	Major study outcome	Reference
		(AMD)		white rabbits, wild-type mice	good protective effect on morphology and functions of the retina.	
LNCs	microRNA (miR-155)	Intervertebral disc degeneration disease	Percutaneous	*In vivo* studies in healthy female sheep, in vitro cell assays	LNCs demonstrated stability and efficacy of loaded miR.	(Le Moal et al., 2022)
Reverse micelle loaded LNCs	Antimicrobial peptides (AMPs), AP138	Anti-bacterial resistance	-	*In vitro* cell assays	Resistant to enzymatic degradation, preservation of antimicrobial activity	(Groo et al., 2018)
LNCs	Flavanoids quercetin (QC), (–)-epigallocatechin-3-gallate [(–)-EGCG]	Cancer, anti-inflammatory	-	-	100 fold increase in apparent solubility of QC, improved stability of (–)-EGCG with loading into LNCs	(Barras et al., 2009)

1.4.2 Structure of LNCs

LNCs prepared by the phase inversion process have a hybrid structure between polymeric nanoparticles and liposomes because of their oily core which is surrounded by a tensioactive rigid membrane. The oily core is formed by medium chain triglycerides (commercially available as Labrafac™ lipophile WL 1349). This oily core is surrounded and stabilized by a combination of Polyethylene glycol (15)-hydroxystearate (Kolliphor® HS 15) and phospholipids (Heurtault et al., 2002; Mouzouvi et al., 2017; Valcourt et al., 2016; Vonarbourg et al., 2005) that together form the shell. The presence of a core-shell structure was initially demonstrated by B. Heurtault et al., (Heurtault et al., 2003; Heurtault et al., 2002) wherein the thermal and interfacial behaviour of individual components, physical mixture of components and the LNCs were measured and related to the structure of LNCs. According to their observations, phospholipid molecules (commercially available as Lipoid category) are in contact with Labrafac™ inside the nanocapsules, whereas Kolliphor® molecules are positioned on the surface of the nanocapsules and orients towards the aqueous phase (Figure 4). A direct measurement of this core-shell structure would be desired to confirm the structure of the LNCs in more detail. This is a part of the investigations in this thesis and accordingly, in **Paper II**, SAXS and SANS techniques were used to determine and confirm the structure of the LNC at molecular level.

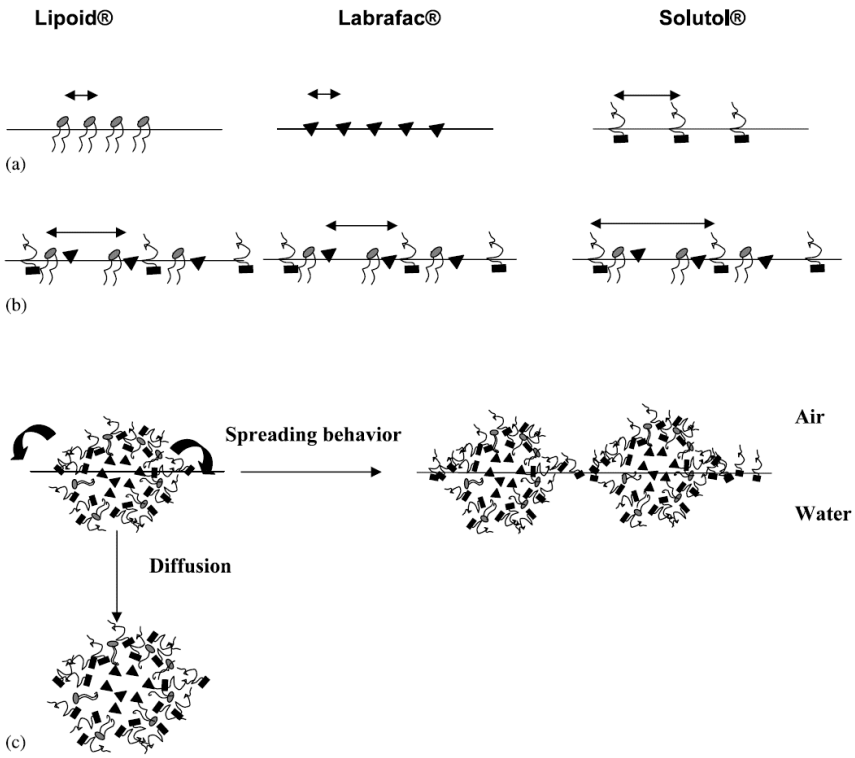

Figure 4. Interfacial behaviour (a) of the pure component, (b) of the mixture of the three components, and (c) nanocapsule structural behaviour at the air/water interface with partial Kolliphor® release from nanocapsules during the spreading and diffusion of nanocapsules. (Adapted from B. Heurtault et al. (Heurtault et al., 2003))

1.4.3 Formation of LNCs

LNCs are prepared by a phase inversion process wherein the components are heated from room temperature to a temperature above the phase inversion temperature (PIT) resulting in the formation of a W/O emulsion. This is followed by cooling the mixture to a temperature below the PIT during which the W/O emulsion transforms into a O/W emulsion. Several of these heating-cooling cycles are applied (usually 3) followed by an irreversible shock to the system by diluting with cold water at the beginning of the phase inversion process when the mixture turns translucent. This results in the formation of stable nanocapsules with a narrow particle size distribution. A schematic representation of the structure of LNCs is showed in Figure 5.

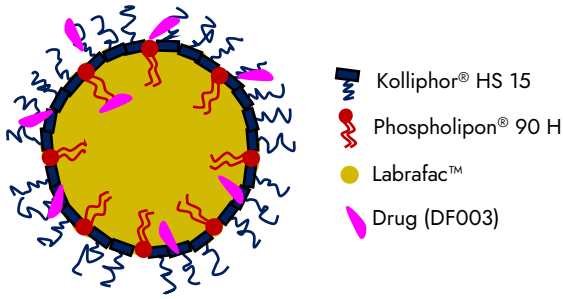

Figure 5. Schematic representation of LNC structure

1.4.3.1 Phase inversion process

A phase inversion emulsification is a low-energy process capable of producing fine and stable nanoparticles. This process is governed by a change in temperature rather than a change in system composition. This process was first introduced by Shinoda and Saito (Shinoda & Saito, 1969). Non-ionic surfactants, for instance Kolliphor®, which is a Polyoxyethylated 12-hydroxystearic acid is an O/W emulsifier with a HLB of 16 that favours the formation of O/W emulsions (Shaukat & Kolter, 2019). It was reported that, non-ionic surfactants become more hydrophobic and oil soluble upon increase in temperature due to dehydration of polar head groups thereby resulting a change in HLB (Shinoda & Kunieda, 1983). At low temperatures, the surfactant monolayer has a large positive spontaneous curvature that favours the formation of O/W emulsion, and this curvature becomes negative upon increasing the temperatures that favours the formation of a W/O emulsion. The temperature or a temperature zone where this transition happens is referred to as phase inversion temperature (PIT), at which hydrophilic and lipophilic properties of non-ionic surfactants are balanced. At PIT, the spontaneous curvature become close to zero suggesting the formation of a bicontinuous microemulsion which is a surfactant rich phase that coexists with excess water and oil phases in equilibrium (Förster et al., 1990; Huynh et al., 2009; Perazzo et al., 2015; Solans et al., 2005). These changes in the emulsion configuration can be described by changes in conductivity values. At low temperatures, with a resulting O/W emulsion, the emulsion exhibits higher conductivity which decreases rapidly to almost 0 mS/cm when the emulsion transitions into W/O type with an increase in temperature (Huynh et al., 2009). With an addition of salts to this kind of systems, it is possible to alter the phase inversion temperature. Nicolas Anton et al., reported that the phase inversion zone shifts to a lower temperatures with an increase in salt concentration (Anton et al., 2007) that enables the loading of thermosensitive drugs in to the emulsions.

2 Aims

The work described in the thesis largely aims at development of LNCs as a delivery system for DF003 for retinal applications. This work included formulation development with DF003, physico-chemical characterization, investigation of internal structure, performance evaluation using *in vitro* and *ex vivo* methods, and investigating the system for further developability i.e., upscaling and lyophilization process development.

The specific aims of this work were:

i. Preparation and evaluation of LNCs formulation loaded with DF003.
ii. Investigating the suitability of phase inversion process for manufacturing LNCs at higher volume scales.
iii. Development and evaluation of freeze dried LNCs for enhancing the long-term storage stability.
iv. Investigation of structural aspects of the LNCs using synchrotron- and neutron-based scattering techniques.
v. Investigation of *in vitro* and *ex vivo* performance of LNCs to check for their suitability for ocular administration.

3 Materials

The drug compound, DF003 (β-phenyl-1,N2-etheno-8-bromoguanosine-3′,5′-cyclic monophosphorothiotic acid, sometimes referred to as CN03), was synthesized within RISE Research Institutes of Sweden (Södertälje, Sweden) as part of the *trans*Med project (H2020-MSCA-765441) (Pérez et al., 2021). Labrafac™ lipophile WL 1349 (Medium chain triglycerides, Ph. Eur. Grade), Kolliphor® HS 15 (polyethylene glycol (15)-hydroxystearate, Ph. Eur. Grade), were obtained from Gattefossé (France), and BASF, Germany respectively. Phospholipids namely Phospholipon® 90 H (hydrogenated phosphatidylcholine ≥ 90 %), Phospholipon® 80 H (hydrogenated phosphatidylcholine ≥ 70 %), Lipoid S 75 (phosphatidylcholine approx. 70 % with predominantly unsaturated fatty acids) and Lipoid S PC-3 (hydrogenated phosphatidylcholine ≥ 98 %) were obtained from Lipoid GmbH, Germany. 100 kD Float-A-Lyzer® G2 Dialysis Devices, 50 kD Amicon Ultra-0.5 Centrifugal Filter Units, 1-palmitoyl-2-oleoyl-sn-glycero-3-phosphocholine (POPC), cholesterol (≥ 99.0 %), 1,2-distearoyl-sn-glycero-3-phosphoethanolamine-N-[methoxy(polyethylene glycol)-2000] (ammonium salt) (DSPE-PEG2000), 3,3′-Dioctadecyl-oxacarbocyanin-perchlorate, dioctadecyl-3,3,3,3 Tetramethylindodicarbocyanine (DiO), Sodium phosphate dibasic dihydrate ($Na_2HPO_4 \cdot 2H_2O$), sodium dihydrogen phosphate (NaH_2PO_4), phosphate buffered saline (PBS), octanoic-d_{15} acid (≥ 98 atom % D), decanoic-d_{19} acid (98 atom % D), chloroform, 4 % paraformaldehyde in PBS (PFA), sucrose (BioXtra, ≥ 99.5 %), trehalose (Emprove® Expert), D-(+)-Raffinose pentahydrate (≥ 99.0 %), N-(2-Hydroxyethyl)piperazine-N′-(2-ethanesulfonic acid), 4-(2-Hydroxyethyl)piperazine-1-ethanesulfonic acid (HEPES; BioUltra, ≥ 99.5 %), sodium chloride (BioUltra, ≥ 99.5 %), In Situ Cell Death Detection Kit for TUNEL assay (TMR red) were purchased from Sigma-Aldrich, Germany. Deuterium oxide (99.9 atom % D, Cambridge Isotope Laboratories) was purchased from Fisher Scientific, Sweden. Ultrapure milli-Q water (ELGA, Purelab Prima) made in-house was utilized for all experiments. All organic solvents used were of high-performance liquid chromatography (HPLC) grade. All other excipients and reagents were of analytical grade, unless specified otherwise.

4 Methods

4.1 UPLC-UV method for quantification of DF003

Quantification of DF003 was performed using UPLC equipped with a UV detector (ACQUITY UPLC, Waters Corporation). The UPLC system consisted of Acquity BEH shield RP18 column (2.1 mm internal diameter, particle size 1.7 µm), pump for mobile phases, column oven, and a UV detector. Samples were diluted in suitable solvents and eluted using the parameters described in Table 4. Data was processed and analysed using Thermo Scientific™ Chromeleon™ 6.8 Chromatography Data System (CDS) software. For drug quantification purposes, a standard curve was generated with known sample concentrations of 1-100 µg/mL prepared in 30 % Acetonitrile.

Table 4. UPLC-UV method for quantification of DF003

Parameter	Description
Mobile phase A	5 mM ammonium acetate
Mobile phase B	Acetonitrile
Type of elusion	Gradient (100 % A to 100 % B over 10 min)
Mobile phase flow rate	0.5 mL/min
Sample injection volume	2 µL
Column temperature	40 °C
Detection wavelength	256 nm

4.2 Solubility studies of DF003

Solubility evaluation of DF003 was performed in both buffers (purified water, 0.1 N HCl with pH 1.5, Phosphate buffer with pH 7.2–7.4), and LNC formulation components (Labrafac™ and Kolliphor®). For solubility testing in aqueous buffers, an excess of drug compound was weighed in individual glass vials each containing 1mL of test buffer and kept under constant mixing for 48 hrs at 25 °C. For solubility testing in formulation components, excess drug compound was added to individual glass vials each containing 0.5g of either of the test component and the vials were maintained under constant mixing at 37 °C for 3 h and 6 h respectively for Labrafac™ or Kolliphor®. Vials were observed at different time points and ensured for the presence of excess drug throughout the mixing duration. At the end of specified mixing time, excess drug compound was removed by centrifugation for 30 min at 14000*g* followed by filtration. Clear aqueous samples were diluted in 30 % acetonitrile while ethanol was used for diluting the formulation components. Drug quantification was performed using UPLC-UV as described previously.

4.3 Preparation of LNCs

4.3.1 Lab-scale preparation and optimization of LNCs

Phase inversion technique was used for preparation of LNCs based on the procedure earlier described by Valcourt et al. (Valcourt et al., 2016). The preparation process includes mixing and heating of Labrafac™, Kolliphor®, phospholipid, sodium chloride and water (17 % w/v) to 50 °C until all the components dissolve. For drug-loaded LNCs, DF003 was included in this mixture. The resulting dispersion was then heated to 90 °C and then cooled back to 60 °C, typically above and below the phase inversion temperature of the composition. Three such heat-cool cycles were applied to the dispersion. During the last cooling cycle, when the temperature approaches to phase-inversion which can be characterized by a visual transition from opaque to translucent state, excess cold water (2-8 °C) was added. This resulted in the spontaneous formation of LNCs.

As part of the optimization process, compositional effects on the physico-chemical properties of the formulation were evaluated. For this, different proportions of Labrafac™ (6.2 and 9.3 % w/v), Kolliphor® (4.8, 7.2, and 9.6 % w/v), phospholipid (0 and 0.4 % w/v), and various phospholipids namely Phospholipon® 90 H, Phospholipon® 80 H, Lipoid S 75, and Lipoid S PC-3 were screened. Also, drug to lipid ratios of 1:32 and 1:64 was tested. The resulting LNCs were characterized for particle size, size distribution, zeta potential, % entrapment efficiency (EE) and drug loading.

DiO (a lipophilic and green fluorescent dye) loaded LNCs were prepared in the same manner described above by including the DiO in the mixture before starting heat-cool cycles. For SANS experiments, deuterated LNCs (referred to as d-LNCs hereafter, were also prepared in the same way as mentioned above. The only change was that 5 % of Labrafac™ was replaced with a mixture of octanoic-d15 (dC8) and decanoic-d19 acid (dC10). The ratio of dC8/dC10 used corresponded to 54.0 %:45.2 % and this was based on the proportion of C8/C10 fatty acids as per the certificate of analysis of Labrafac™ (batch number 165157). This resulted in LNCs with higher neutron contrast in the core which are suitable for SANS experiments. Furthermore, h-LNCs and d-LNCs were prepared in both D_2O and H_2O.

LNCs used in all the experiments were filtered using a 0.22 µm membrane filter prior to characterization and further use. Schematic representation of LNCs preparation is presented in Figure 6. Optimized composition of h-LNCs and d-LNCs used for various studies is given in Table 5.

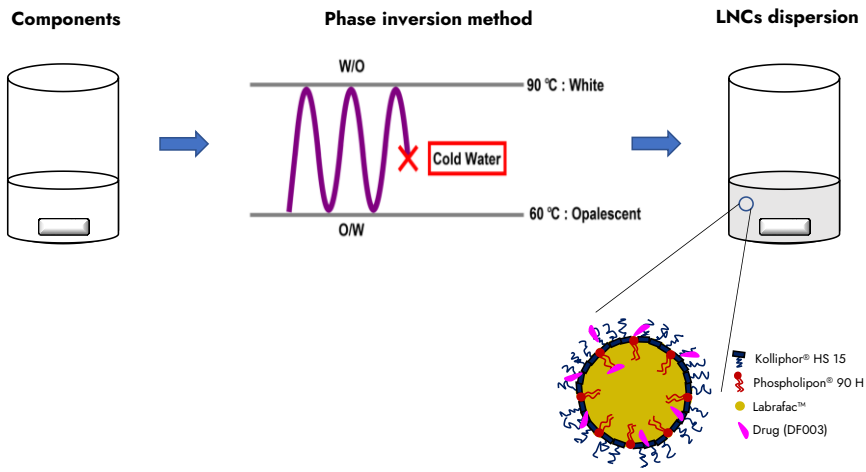

Figure 6. Preparation of LNCs by a phase inversion method

Table 5. Composition of h-LNCs and d-LNCs

Excipient	Composition of h-LNCs (% w/v)	Composition of d-LNCs (% w/v)
Labrafac™ lipophile WL 1349	6.2	5.89
Octanoic-d15 acid (dC8)	-	0.17
Decanoic-d19 acid (dC10)	-	0.14
Kolliphor® HS 15	4.8	4.8
Phospholipon® 90 H	0.4	0.4
Sodium Chloride	0.5	0.5
Milli-Q water/deuterium oxide (D_2O)	q.s.	q.s.
DF003#	0.19	0.19

#DF003 is only present in drug-loaded LNCs.

4.3.2 Preparation of liposomes

Liposomes were prepared using an established thin-film hydration method (Zhang, 2017). The components POPC, cholesterol, DSPE-PEG_{2000}, and DiO in the molar ratio of 63.3:31.7:5:0.2 were dissolved in chloroform. Thin layer of lipids was formed by evaporating the chloroform using a rotary evaporator (model RC600, KNF Neuberger, Trenton, NJ, USA) at 100 rpm and at a pressure of 300 mbar for 1 to 2 h. The dried lipid film was hydrated in PBS by mixing and vortexing. Hydrated lipid structures were extruded using a mini-extruder (Avanti Polar Lipids, Alabaster, AL, USA) by passing the solution back and forth between a 100 nm porous polycarbonate membrane eleven times with Hamilton syringes. The liposomes were stored at 2-8 °C until further use.

4.3.3 Large-scale manufacturing of LNCs

Upscaling of LNCs to higher volumes of 1 L and 10 L was performed to evaluate the feasibility of the phase inversion process in producing LNCs with similar characteristics as those manufactured at lower volume scales of 0.01 L. These higher volumes of 1 L and 10 L corresponds to 100 and 1000 times the lab-scale volumes, respectively. For this purpose, LNCs were prepared without the drug loading and the detailed composition is given in Table 6.

Table 6. Composition of LNCs for large-scale manufacturing.

Excipient	Composition (% w/v)	Weight of excipients (g) for 1 L scale	Weight of excipients (g) for 10 L scale
Labrafac™ lipophile WL 1349	6.2	62	620
Kolliphor® HS 15	4.8	48	480
Phospholipon® 90 H	0.4	4	40
Sodium chloride	0.5	5	50
milli-Q water	17	170	1700
milli-Q water for quenching	71.1	711	7110

4.3.3.1 Large-scale manufacturing with batch and continuous processes

Batch manufacturing of LNCs at 1 L and 10 L involves an initial mixing and heating of Labrafac™, Kolliphor®, Phospholipon® 90 H, Sodium chloride, milli-Q water (17 %) until the components dissolves completely. This solution was then transferred directly into a double jacketed reaction vessel containing a mechanical stirrer. This reaction vessel was connected to a bath containing a mix of 50/50 ethylene glycol/water to control the temperature of the component mixture at a desired level during both heating and cooling steps. The temperature of the excipient mixture was raised to 90 °C followed by cooling back to 60 °C, above and below the phase inversion temperature of the composition. A total of three such heating-cooling cycles (90-60 °C) were applied to the mixture. During the last cooling cycle, at around 80 °C, when the solution turned translucent, the solution was directly transferred into a flask containing water at ~4 °C which resulted in the formation of nanoparticles. The nanoparticle dispersion was kept for stirring in an ice-bath for at least five minutes. Two batches of LNCs at 1 L scale were manufactured to check the repeatability and reproducibility of the process.

In addition, a continuous manufacturing process was attempted to prepare LNCs to improve the process control and to reduce the manufacturing time intervals. For this, few modifications were introduced to the above-described batch manufacturing process

and the LNCs were manufactured at 1 L volume scale. The first modification was using a medium scale vertical oscillatory reactor fitted with baffles instead of a normal jacketed reaction vessel (Figure 14a and Figure 14c). Secondly, two baths were connected to the baffled reactor to control the temperature of the components as opposed to one bath in the batch manufacturing process. These baths were maintained at temperatures of 20 °C and 95 °C and were used for cooling and heating steps, respectively and the connections to the baffled reactor were switched to reach the desired temperature of the component mixture. Heated excipient mixture was transferred into the oscillatory baffled reactor and a similar process as described above was used to manufacture LNCs.

In addition to adapting the batch process to continuous manufacturing process, the batch process was further adjusted by including additional unit operations in an attempt to lower the bioburden, thereby resulting in sterile nanoparticles. For this, pre-heated mixture containing Labrafac™, Kolliphor®, sodium chloride, and water as listed in Table 6 (except Phospholipon® 90 H and water for quenching) were filtered using a 0.2 µm syringe filter (Supor® EKV Membrane) into a pre-sterilized glass bottle. To this, Phospholipon® 90 H was added and heated until it dissolves completely. This complete mixture was heat sterilized at 121 °C for 15 min with ~2 bar pressure and the resulting sterile solution was subjected to heat-cool cycles and transferred into sterile water for quenching (maintained at ~4 °C) to obtain LNCs. Formed nanoparticles were filtered through a 0.2 µm syringe filter (Supor® EKV Membrane) into sterile containers under a pre-sanitized laminar air-flow chamber. Samples were tested for bioburden.

During all these manufacturing processes, temperature and conductivity of the component mixture were monitored continuously. Manufactured LNCs from each of these processes were characterized for particle size, polydispersity index (PDI), zeta potential, and derived count rate (DCR). Physical stability of these nanoparticles with respect to the particle size and zeta potential was also studied.

4.4 *In vitro* characterization of LNCs

4.4.1 Particle size and particle size distribution

Dynamic light scattering (DLS) is a common and widely used technique for measuring the size and size distribution of particles which are typically in the submicron size range. Particles in this size range experience Brownian motion when suspended in a liquid and the velocity of Brownian motion is related to particle size. In DLS, when the laser light is focused on a sample, Brownian motion of the particles in the sample causes the incident laser light to be scattered at different intensities. Analyzing these intensity fluctuations yields the velocity of the Brownian motion, which is defined by the Diffusion coefficient, D. This Diffusion coefficient allows for the calculation of hydrodynamic radius (R_h) using the Stokes-Einstein relationship, assuming spherical particles.

$$D = \frac{k_B T}{6\pi\eta R_h}$$

Where k_B is the Bolzmann constant, T is the absolute temperature and η the viscosity of the dispersion medium.

In the present work, DLS was used to measure the particle size, PDI and derived count rate (DCR) of LNCs. Samples in the concentration range of 1-62 mg/mL were measured at 25 °C after necessary dilution in a Zetasizer Nano ZS instrument (Malvern Instruments, U.K.) using disposable plastic cuvettes. Each sample was measured in triplicate and the data was presented as mean ± SD.

4.4.2 ζ-potential

ζ-potential is a measure of the magnitude of electrostatic charge on the surface of the particles dispersed in a liquid. This gives information about stability of these particles. Higher zeta potential indicates highly charged particles, which prevents them from being aggregated, and the stability is achieved by electric repulsion. Particles with a near zero zeta potential are unstable due to the lack of particle repulsion, unless other mechanisms of stabilization (e.g. steric stabilization) exist (Samimi et al., 2019).

Under the influence of an applied electric field, charged particles tend to migrate towards the electrode of opposite charge and the speed of migration is proportional to the magnitude of surface charge or zeta potential. In the present work, the ζ-potential of the particles was determined indirectly by measuring the electrophoretic mobility of the nanoparticles at 25 °C in a folded capillary cell. Measurements were made in a Zetasizer Nano ZS instrument (Malvern Instruments, U.K.). Each sample was measured in triplicate and the data was presented as mean ± SD.

4.4.3 Morphology by cryogenic transmission electron microscopy (cryo-TEM)

In cryogenic transmission electron microscopy (cryo-TEM), a very thin liquid film is vitrified and maintained at very low temperatures. This enables the imaging of colloidal particles in their native and hydrated state (Almgren et al., 2000; Bellare et al., 1988). In this technique, an electron beam which is accelerated over a high voltage is focussed on the thin film and as the electron beam passes through such thin sample film, digital images can be acquired on a detector/CCD camera.

In the present work, samples were analyzed using cryo-TEM as described by Almgren et al. (Almgren et al., 2000). Initially, samples were equilibrated at 25 °C and high relative humidity (> 90 %) within a climate chamber. A small drop (< 1 µl) of each sample was deposited on a carbon-sputtered copper grid pre-covered with a perforated polymer film. Excess liquid was thereafter removed by blotting with a filter paper, leaving a thin film of the solution on the grid. Subsequently, the sample

was vitrified in liquid ethane and transferred to the microscope. Samples were kept below −160 °C and protected against atmospheric conditions during both transfer and examination. Analyses were performed with a Zeiss Libra 120 Transmission Electron Microscope (Carl Zeiss AG, Oberkochen, Germany) operating at 80kV and in zero-loss bright-field mode. Digital images were recorded under low-dose conditions with a BioVision Pro-SM Slow Scan CCD camera (Proscan elektronische Systeme GmbH, Scheuring, Germany).

Freeze-dried samples were measured after reconstitution to their initial volume with milli-Q water. Cryo-TEM specimens were prepared on Quantifoil TEM grids covered with a thin continuous carbon film by plunge freezing using a Leica EM GP2 with the following parameters: Initial sample volume: 3 µl, blotting time: 2-3 seconds, temperature: 15 °C, relative humidity: 95 %. The specimens were transferred to a Gatan Elsa cryo-TEM holder and imaged in a JEOL JEM-2100Plus TEM at cryogenic conditions. Low-dose measurements at an acceleration voltage of 200 kV were performed using the software SerialEM.

4.4.4 Entrapment efficiency and drug loading

The amount of DF003 associated with LNCs was calculated indirectly, by measuring the free drug which is not associated with LNCs. For this purpose, Amicon Ultra-0.5 Centrifugal Filter Units (0.5 mL, MWCO 50 kDa) were used. 0.5 mL of DF003-LNCs were added to the centrifugal device and centrifuged at 10000*g* for 5 min. During centrifugation, LNCs which are bigger than the membrane pore size remained inside the filter device. Clear filtrate which passed through the filter membrane was free from LNCs and was collected from the centrifuge tube. Free drug concentration from the filtrate was quantified using UPLC method as described in 4.1, and the % EE and drug loading were calculated using the below mentioned equations.

$$\% \text{ EE} = \frac{\text{Total amount of DF003-Amount of free DF003}}{\text{Total amount of DF003}}$$

$$\text{Drug loading} = \frac{\text{Amount of entraped DF003 in LNCs}}{\text{Amount of LNCs (mL)}}$$

4.4.5 Drug release in phosphate buffer and simulated vitreous fluid

Spectra-Por® Float-A-Lyzer® G2 dialysis devices (1 mL, MWCO 100 kDa) were used for evaluating the release of DF003 from DF003-LNCs. Prior to release experiments, dialysis devices were treated with 10 % of ethanol for 10 min followed by soaking in purified water for 15-20 min. 1 mL of DF003-LNCs were added to the pre-treated dialysis devices and immersed in 18 mL of phosphate buffer, pH 7.2-7.4. A drug solution of 2 mg/mL prepared in phosphate buffer, pH 7.2-7.4 was used as a control. Throughout the study duration, samples were maintained at 37 °C and magnetic stirring

was applied in the phosphate buffer to ensure sufficient mixing. At regular time intervals of 0.5, 1, 2, 4, 8, 24, 48, and 144 h, 1 mL of sample was withdrawn and the whole buffer was replaced with fresh phosphate buffer in order to maintain sink conditions. Drug content in the collected samples was quantified using a UPLC method as described previously and the cumulative drug release from the LNCs was calculated.

In another study, hyaluronic acid solution (HA; concentration of ~ 375 µg/mL) was used as a release medium instead of phosphate buffer, and the release experiments on DF003-LNCs were performed in the same way as explained above.

For the purpose of *ex vivo* experiments, LNCs were prepared with DiO as a loading agent and the release of loaded DiO in phosphate buffer was tested using the same process described for drug-loaded LNCs. For the quantification of released DiO, fluorescence intensity from the collected samples was measured with a Varioskan™ LUX multimode microplate reader (ThermoFisher Scientific).

4.4.6 Stability of LNCs

4.4.6.1 Colloidal stability

Colloidal stability of LNCs and DF003-LNCs prepared at lab-scale was evaluated in their native state by storing them at room temperature (25 °C) and at refrigerated conditions (2-8 °C) for one month. Further, LNCs prepared at higher scales were also stored at 2-8 °C for a period of 6 months to check for their colloidal stability over an extended time frame. At different time points, colloidal stability was assessed by measuring particle size, size distribution, zeta potential, and % EE.

4.4.6.2 Stability in simulated vitreous fluid

The LNCs prepared in the present work are intended for retinal drug delivery applications. Hence there is a potential for these particles to interact with the components of vitreous fluid. Hyaluronic acid is a negatively charged polymer that makes up a predominant part of vitreous fluid (Del Amo et al., 2017). Thus, the structural integrity of LNCs after a possible interaction was measured by incubating them in hyaluronic acid. For this, LNCs were diluted 20 times in hyaluronic acid (2.4 million Da, ~ 375 µg/mL) and incubated at 37 °C for 7 days. Particle and PDI of the samples were measured on different days to check for any noticeable changes.

4.4.7 Testing for microbial purity

LNCs prepared using the batch process included with additional unit operations were examined for microbial purity as per the membrane filtration method described in the European Pharmacopoeia (Ph. Eur. 10.0, 2020). For this, Staphylococcus aureus (ATCC 6538), Pseudomonas aeruginosa (ATCC 9027), Bacillus subtilis (ATCC 6633), Candida albicans (ATCC 10231), Aspergillus brasiliensis (ATCC 16404) were used as

challenge microorganisms (reference strains) for the determination of Total Aerobic Microbial Count (TAMC) as an indication of microbial purity. These test organisms were prepared from freeze-dried and ready-to-use pellets. Method suitability was carried out by filtering (a) 10-100 CFU of challenge microorganisms in 100 mL of peptone water (positive controls) and (b) test samples spiked with 10-100 CFU of challenge microorganisms, using Milliflex filtration system pre-fitted with 0.2 µm membrane. After the filtration, membranes were separated and incubated in Milliflex cassettes containing prefilled tryptic soy agar (TSA) for three days at 30-35℃. Percentage recovery of microbial count was calculated using the formula mentioned below and the acceptance criteria was set from 50 % to 200 %. Test samples were prepared by mixing 1 mL of formulations in 100 mL peptone water and examined for microbial purity using the same method as described above. TAMC of the samples was compared against the limits mentioned in the European Pharmacopoeia.

$$\% \text{ Recovery} = \frac{\text{Count on TSA cassette of samples spiked with challenge organisms}}{\text{Count on TSA cassette of positive control}} \times 100$$

4.5 Freeze-drying of LNCs

For freeze-drying, LNCs (both unloaded and drug-loaded) were mixed with the selected cytoprotectants dissolved in water (sucrose, trehalose, raffinose) to obtain a mass mixing ratio (MMR: mass of carbohydrate/mass of LNCs) from 5 to 25. These cytoprotectants were studied at 5 % and 10 % of the final concentration. 2 mL of these resulting dispersions were taken in 6 mL capacity glass vials and freeze-dried using an Epsilon 2–4 LSCplus (Martin Christ Gmbh, Germany) freeze-dryer. For freeze-drying, initially the liquid dispersions were frozen at -45 °C for 4 h by placing the samples inside the freeze dryer at atmospheric pressure. This was followed by primary drying of the samples at -30 °C and 0.02 mbar pressure for 36 h. Then the temperature of the samples was raised to 20 °C for final drying (secondary drying step). This final drying was performed at a reduced pressure of 0.005 mbar for 17 h. Freeze-dried samples were sealed and stored in low humid environment until further use.

4.5.1 Reconstitution and characterization of LNCs

Freeze-dried LNCs were reconstituted with water equivalent to the initial volume before freeze-drying. Samples were left for 10 minutes with occasional stirring to ensure sufficient reconstitution. The reconstituted freeze-dried samples were characterized for particle size, PDI, zeta potential, morphology, % EE and drug release.

4.6 Structural characterization of LNCs using small-angle scattering techniques

4.6.1 Theory of small-angle scattering

Although nanoparticles offer various advantages in drug delivery, understanding their structure, properties, interaction with drugs upon loading, and how they behave under physiological conditions is often challenging. This is especially true in the case of complex systems, and they need an array of techniques to get relevant and useful structural information. Dynamic light scattering (DLS) technique, for instance, provide information about the apparent hydrodynamic particle size and particle size distribution based on the estimated diffusion coefficient. However, it is not possible to obtain the internal structure of the nanoparticles with this technique. Cryo-TEM on the other hand provide very useful information regarding the morphology by preserving the original and hydrated state of nanoparticles. However, for nanoparticles with poor contrast differences in different regions in their structure, for instance for LNCs used in this work, it is highly challenging to obtain information about their internal structure. Moreover, the information from the technique is based on a very limited sample quantity and this may not wholly represent the entire sample (Gommes et al., 2021). Here small-angle scattering techniques (SAXS and SANS) become very useful as they enable measurement of samples in the original liquid state and relatively large sample volumes are studied. These techniques have similar working principle that involves exposing the sample to a collimated beam of X-rays (SAXS) or neutrons (SANS), which then scatter the beam at different angles (Figure 7), and the intensity of the scattered beam is collected by a two-dimensional detector (Di Cola et al., 2016; Tuukkanen et al., 2017). The output is radially integrated to obtain one-dimensional scattering function *I(Q)*. *Q* represents the magnitude of the scattering wave vector and is defined by $Q = 4\pi/\lambda \sin(\theta/2)$, where λ is the wavelength of incident beam and θ is the scattering angle. The scattered intensity from the particles is obtained using the equation given below (Hellsing et al., 2012; Long et al., 1994).

$$I(Q) = n \Delta\rho^2 P(Q) S(Q)$$

Where *n* is the number density of the particles in the sample, ρ is the scattering length density (SLD) difference between the particles and the dispersion medium (can be calculated from known values of the measured systems) (Candau & Ottewill, 1989; Ghosh et al., 2000). SLD is a measure of the scattering power of a material. *P (Q)* represents the form factor which is related to size and shape of the nanoparticles in dispersion medium and *S (Q)* represents the structure factor and is related to the interparticle interactions in the dispersion medium.

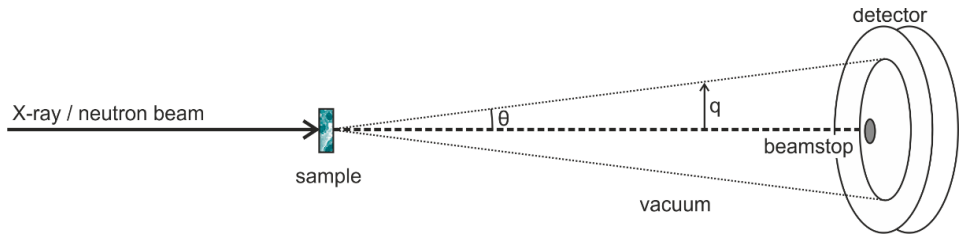

Figure 7. Layout of small-angle X-ray and/or neutron scattering setup, adapted from (Di Cola et al., 2016)

Despite a broadly similar working principle, SAXS and SANS techniques have fundamental differences in the way X-rays/neutrons interact with the samples. In case of SAXS, scattering from the sample arises following an interaction of photons with the electron cloud present in the sample. The samples with atoms of higher atomic number shows higher x-ray scattering cross sections due to the presence of more electrons. In contrast to SAXS, in neutron scattering, neutron beam interacts with the nuclei of the atoms present and the interaction is therefore sensitive to isotopes of the same element. This means that hydrogen and its isotope deuterium have completely different neutron scattering cross sections. This is a potential advantage with SANS for studying complex structures by specifically deuterating a specific portion of complex nanoparticle system (LNCs in the present work) and by altering the solvent contrast by mixing varied proportions of H_2O and D_2O. Additionally, by matching the contrast of part(s) of the particle with the dispersion medium, it is possible to study a specific region of interest for e.g. the shell of core–shell particles.

In a nutshell, SAXS and SANS are complementary techniques and combined analysis of the data from these techniques can provide critical information about particle size, particle shape, polydispersity, in-depth structure and interparticle interactions at nanometre-scale resolution (Di Cola et al., 2016; Hyland et al., 2013; Tuukkanen et al., 2017).

4.6.1.1 Small-angle X-ray scattering measurements on LNCs

SAXS experiments were performed using a SAXSpoint 2.0 instrument from Anton Paar. This instrument is equipped with a Supernova microfocus Copper radiation source (wavelength of 1.541 Å) and an Eiger R 1M Horizontal 2D detector. With the setup employed in the present study, data was collected from lowest q of 0.076 nm^{-1} which corresponds to around 82 nm. SAXS instrument was setup under vacuum and the LNCs samples with a particle concentration of 62 mg/mL were measured in reusable quartz capillaries. Under the same conditions, background measurement was performed with the buffer using the same capillary. Sample were maintained at 25 °C and measured for 30 min. Background subtracted data was used for further analysis and model fitting.

4.6.1.2 Small-angle neutron scattering measurements on LNCs

For SANS, LNCs were measured on Sans2d instrument using a pulsed 'white' beam at ISIS Neutron and Muon Source (Oxfordshire, UK). Data in the *q* range of 0.0076-0.7164 nm^{-1} was collected when operating in a time-of-flight mode with a neutron wavelength range of 1.75—16.5 Å and at sample-detector distances of 2.4 and 4 m.

Both d-LNCs and h-LNCs prepared in either H_2O or D_2O to highlight different parts of the LNC structure were measured at different particle concentrations ranging from 1.24 mg/mL to 6.2 mg/mL. Both the samples and the solvent contrasts for backgrounds were measured in standard quartz cells with the same parameters at different temperatures of 5 °C, 25 °C, and 37 °C. The measured data were reduced and scaled using software provided at ISIS facility, making allowance for the measured sample transmission, detector uniformity and instrument noise and background scattering. The data were set to an absolute scale using the scattering from a standard sample (comprising a solid blend of protiated and perdeuterated polystyrene) in accordance with established procedures, and converted to one-dimensional scattering intensity profiles *I(Q)* versus the momentum transfer, *Q*. Further details of the components such as detectors as well as the data reduction software can be found in Heenan et al. (2011).

4.6.2 SAXS and SANS data analysis and interpretation

Scattering data obtained from SAXS and SANS measurements was analyzed using SasView 5.0.3 software (Doucet, 2020). During SANS data analysis, instrumental smearing effects were considered and accounted for. Data collected from LNCs in different contrasts were simultaneously fitted to a core-shell sphere model. For the data analysis, the scattering length density (SLD) of the core and the solvent were kept constant at the calculated values (calculated using SLD Calculator Tool in SasView 5.0.3 software). The fitted parameters were SLD of the shell, core radius, shell thickness, polydispersity of the radius, and the volume fraction. Effective size/radius of LNCs was computed from the core radius and the shell thickness and compared with the data obtained from other techniques. Chemical formulas and SLD values of LNCs components are tabulated in Table 7.

Table 7. Material properties and scattering length densities (SLD) of LNCs components.

Component of LNCs	Chemical formula	Neutron SLD (10^{-6}Å^{-2})#	X-ray SLD (10^{-6}Å^{-2})#
Labrafac™	$C_8H_{16}O_2 + C_{10}H_{20}O_2$	0.15	8.93
Labrafac™:(dC8+dC10) (5.89:0.31 % w/v)	$C_8H_{16}O_2 + C_{10}H_{20}O_2 + C_8d_{15}O_2H + C_8d_{15}O_2H$	0.45	-
Kolliphor® HS 15*	$C_{20}H_{40}O_4$	0.13	9.92
Light water	H_2O	-0.56	9.44
Heavy water	D_2O	6.35	-

*Considering one ethylene glycol moiety.

#Calculated using SLD Calculator Tool in SasView 5.0.3 software.

4.7 *Ex vivo* characterization of LNCs

4.7.1 Permeation testing of free drug and drug-loaded LNCs using Franz diffusion cells

Fresh porcine eyes were obtained from a local slaughterhouse and were frozen at -80 °C within 2 h of collection until their use (Nicoli et al., 2009). Just before collecting the tissues, the frozen eyes were maintained in PBS until they thawed completely. For tissue collection, a small cut was made in the thawed eyes with the scalpel at the limbus and full-thickness corneas and the conjunctiva-sclera-choroid-retina complex were isolated. The permeability studies were performed with jacketed glass Franz-diffusion cells (area of 2.54 cm^2; PermeGear Inc., Pennsylvania, USA) (Figure 8) using a similar process described by Pescina et al. (Pescina et al., 2015; Pescina et al., 2012) with some modifications. The isolated tissues were placed between the donor and the receptor compartment of the Franz-cell with the endothelial side facing the receiving compartment. Donor compartment was filled with 1 mL of either free drug or drug-loaded LNCs at a concentration of 2 mg/mL, and the receiving compartment was filled with 5 mL of phosphate buffer. Experiments were performed for up to 6 h at 37 ± 0.2 °C with constant stirring in the receptor buffer to avoid any boundary layer effect. At predetermined time intervals, 0.2 mL of sample was collected from the receiving compartment and was replaced with an equal volume of fresh buffer. Drug concentrations were measured using a microplate reader equipped with a UV—Vis spectrophotometric detector (SpectraMax, Molecular Devices, San Jose, CA). All experiments were carried out in triplicate using different ocular bulbs from different animals. The permeability coefficients were calculated using the equation below (Niedorf et al., 2008). Data were presented as the cumulative amount of drug permeated per area (μg/cm^2) as a function of time (min).

$$P_{app}\ (cm/s) = J_{ss}\ (C_d/A)$$

where J_{ss} is the steady-state flux, C_d is the concentration in the donor compartment and A is the area of exposed tissue.

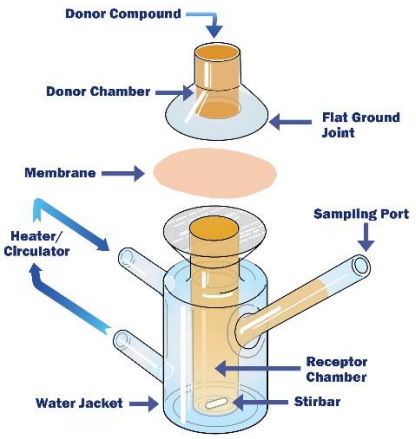

Figure 8. Jacketed Franz-diffusion cell (Image was obtained from PermeGear webpage: https://permegear.com/franz-cells/)

4.7.2 Intraocular bio-distribution of LNCs in *ex vivo* porcine eyes

Porcine eyes were obtained from a local slaughterhouse in the morning of the day of slaughter, followed by washing them in 70 % ethanol and sterile PBS. Later, the excess tissue was removed from the eyes. Before the sample injection, background green fluorescence was measured along the axial length within the eyes using an ocular fluorometer (FM-2 Fluorotron Master, OcuMetrics, CA, USA). For measuring the bio-distribution, nanoparticles were prepared by loading them with DiO, a lipophilic green fluorescent dye. A 50 µL volume of DiO-loaded LNCs or DiO-loaded liposomes was injected into the center of the vitreous using a 22-gauge needle (Hamilton 1705 RN syringe, Hamilton, Reno, NV, USA). From the eyes injected with DiO-loaded LNCs or DiO-loaded liposomes, the green fluorescence signal was measured on the fluorometer directly after injection (t = 0), followed by incubation on a rotation shaker at 45 rpm. At 0.5 h, 1 h, 2 h, 6 h, and 24 h of incubation, additional fluorescence measurements were recorded to follow the distribution of the particles in the eyes. After the 24 h time-point, the eyes were fixed in a 4 % PFA solution following a previously established protocol (Christensen et al., 2021) and incubated at 2-8 °C for 5 days. After 5 days, the eyes were washed twice in PBS and submerged in embedding medium (Tissue-Tek O.C.T. Compound, Sakura Finetek Europe, Alphen aan den Rijn, Netherlands) and frozen with liquid nitrogen. The frozen eyes were sectioned at −16 °C in 40 µm thick sections on a cryostat (NX50, Thermo Fisher, Waltham, MA, USA), which were then

transferred onto glass slides (Superfrost Plus™, R. Langenbrinck, Emmendingen, Germany). The slides were dried at 37 °C for 1-2 h in the dark, rehydrated with PBS for 10 min and mounted with Vectashield medium containing DAPI (Vector laboratories, Burlingame, CA, USA). The slides were kept at 2-8 °C for at least 0.5 h before imaging with fluorescent microscopy. The green signal was measured from different regions in the eye sections i.e., the cornea, the lens, the ciliary body, the vitreous, and the retina. Sections from eyes where no particles were injected were used to qualitatively determine the baseline for a positive signal. For both DiO-loaded LNCs or DiO-loaded liposomes, sections from 5 different eyes were measured (n = 5). Statistical differences were computed using One-way ANOVA with Tukey's multiple comparison test.

4.7.3 Retinal toxicity profile of LNCs

Possible toxicity profile of LNC carrier system prepared without drug loading was evaluated at different particle concentrations of 0, 1, 5, or 10 mg/mL. For this, mice were sacrificed at post-natal day (P) 9 by cervical dislocation. Then the eyes were collected and used for preparing the organotypic retinal explant cultures by following a previously established protocol (Belhadj et al., 2020). At P11, a 20 µL drop of LNCs were added on top of the retinal explain cultures. Here the particles come into contact with the retinal surface that would usually be in contact with the vitreous in intact eyes. At P13, another drop of LNC solution was applied to the explants. At P15, the retinal explant cultures were fixed in PFA for 45 min, followed by washing twice in PBS. The cultures were then cryoprotected in 10 %, 20 %, and 30 % sucrose for 10 min, 20 min, and 30 min, consecutively. The retinal cultures were placed in embedding medium (Tissue-Tek O.C.T. Compound, Sakura Finetek Europe, Alphen aan den Rijn, Netherlands), snap-frozen in liquid N_2, and sectioned on a cryostat (NX50, Thermo Fisher, Waltham, MA, USA) at −20 °C into 14 µm sections, which were collected onto glass slides (Superfrost Plus™, R. Langenbrinck, Emmendingen, Germany). The slides were dried at 37 °C for 45 min and stored at −20 °C. The amount of dying cells in the retinal tissue sections followed by treatment with LNCs was determined by TUNEL assay (Terminal deoxynucleotidyl transferase dUTP nick end labeling; TMR red, Product No. 12156792910, Sigma Aldrich, Darmstadt, Germany), as described under (Loo, 2011). Afterwards, the slides were mounted with Vectashield containing DAPI and imaged with fluorescent microscopy which is described in section 4.7.5. The relative amount of dying cells (TUNEL+ cells: TUNEL positive) from the imaged sections were calculated using the equation mentioned below.

$$\text{TUNEL+ cells (\%)} = \frac{N_{TUNEL}}{A_L/A_N} * 100$$

Where N_{TUNEL} is the absolute number of TUNEL+ cells in either the outer nuclear layer (ONL) or the inner nuclear layer (INL) in the retinal tissue sections, A_L is the area of each layer, and A_n is the average area of the cells in each layer. For each condition, the

relative TUNEL+ cells were determined for 4-5 different cultures (n = 4-5). Statistical differences were computed using One-way ANOVA with Tukey's multiple comparison test.

4.7.4 Treatment efficacy of free drug and drug-loaded LNCs

Treatment efficacy of free DF003 and DF003 loaded LNCs was performed on organotypic retinal explant cultures derived from the retinal degeneration *rd1* mouse model. Retinal explants were prepared at P5 from *rd1* mouse. At P7, a solution of free DF003 in 25 mM HEPES and 125 mM NaCl (pH 7.4) and drug-loaded LNCs, both at a drug concentration of 200 µM were applied to the ganglion cell side of the explant cultures. This was done since the LNCs will reach the retina from the ganglion side followed by their intravitreal administration under *in vivo* setup. Assuming equal distribution of the drug or the LNCs in the tissue and culture medium, the final drug concentration was 4 µM. Non-treated cultures were used as controls. At P9, administration of drug-loaded LNCs was repeated. At P11, the cultures were fixed, cryoprotected, frozen, and sectioned as described under 4.7.3. Additionally, organotypic retinal explant cultures from wild-type mice were prepared and left non-treated following the same paradigm. The effect of DF003 on retinal explant cultures was determined by following the cell death using the TUNEL assay as described above in the section 4.7.3. The relative TUNEL+ cells were determined for 5-6 different cultures (n = 5-6). Statistical differences were computed using One-way ANOVA with Tukey's multiple comparison test.

4.7.5 Fluorescent microscopy

Sections from either porcine eyes or organotypic retinal explant cultures were imaged with fluorescent microscopy (Axio Imager Z2 with ApoTome function, Zeiss, Oberkochen, Germany). A CCD camera with 10X or 20X objectives were used. For DiO signal: green channel of Ex./Em. of 483/501 nm. TUNEL assay: red channel of Ex./Em. 548/561 nm. DAPI signal: blue channel of Ex./Em. 353/465 nm. In all cases, the ApoTome function was used. Z-stacks were collected 1 µm across 25 images for porcine eye sections or 11 images for retinal explant cultures using the microscope software (ZEN 2.6, Zeiss). The images were projected using the Maximum Intensity Projection function, and these images were used for data analysis.

4.8 Statistical data analysis

The statistical analysis of the data generated in this thesis was performed with GraphPad Prism 8, GraphPad Software, San Diego, California, USA. Data is represented as mean ± standard deviation (SD), unless stated otherwise.

5 Results and discussion

5.1 Solubility of DF003

DF003, a cyclic GMP derivative, is a small molecule compound with calculated log *P* and pKa of 1.9 and 1.4, respectively (MarvinSketch 19.3). It is important to know the solubility of DF003 in aqueous buffer and in LNC formulation components to understand how the drug might interact and localize when loaded into the nanoparticles. Thus, the solubility evaluation was performed in purified water, 0.1 N HCl with pH 1.5, phosphate buffer with pH 7.2–7.4, LNC components such as Labrafac™, and Kolliphor® HS 15. DF003 showed a solubility of 1.4 mg/mL in water. Solubilities of 0.3 mg/mL and 3.6 mg/mL were found in HCl buffer and phosphate buffer, respectively. As expected, the solubility increases with increasing pH due to the acidic nature of the compound. Further, the solubility testing in the formulation components revealed that DF003 has higher solubility in the surfactant (Kolliphor®), that predominantly makes up the shell (>25 mg/g) of the LNCs, than in Labrafac™ oil (0.4 mg/g), which constitutes the core of the LNCs. Interestingly, the dissolution of DF003 in Kolliphor® was fast and the saturation point was not reached even at the highest tested concentration of 25 mg/g. The solubility data in the formulation components points to a preferential localization of DF003 in the shell part rather than in the oily core of LNCs. This preferential drug localization in the shell of nanoparticles was later confirmed by the findings reported in **Paper II**.

5.2 Formulation development, optimization, and characterization of LNCs

5.2.1 Lab-scale development and characterization of LNCs

LNCs either unloaded or loaded, were prepared following an established protocol as described by Valcourt et al., (Valcourt et al., 2016) and a similar process was adopted in all the papers included in the present thesis. In the present work, effect of differences in the composition of LNCs, especially the impact of varying concentrations of Labrafac™ and Kolliphor®, was evaluated on the physicochemical properties of the resulting LNCs. As described in the introduction, oily core of the nanoparticles is stabilized by a combination of Kolliphor® and Phospholipid based surfactants. Initially, the impact of phospholipids was tested by preparing the LNCs without including the phospholipids (F1 in Table 8). The resulted dispersion was phase separated almost instantly after the addition of quenching water, indicating the stabilizing role of

phospholipids. This stabilizing role of phospholipids is in line with the previously reported findings (Minkov et al., 2005a; Vonarbourg et al., 2005). This led to the study of different types of phospholipids (Phospholipon 90® H, Lipoid S 75, Phospholipon® 80 H, and Lipoid S PC-3) and their effect on the LNCs properties which is described in detail in **Paper I**. Briefly, all the LNC formulations prepared with different phospholipids were found to be stable without any signs of phase separation. Moreover, particle size of these LNCs remained similar with a narrow particle size distribution. The zeta potential, however, was found to be different when different phospholipids were used. LNCs containing Lipoid S 75 and Phospholipon® 80 H resulted in a more negative zeta potential compared to LNCs that contained Lipoid S PC-3 and Phospholipon® 90 H. Characterization data of LNCs prepared with different phospholipids is given in Figure 9. Phospholipon® 90 H was selected for further formulation development due to its suitability for parenteral administration over the other tested phospholipids.

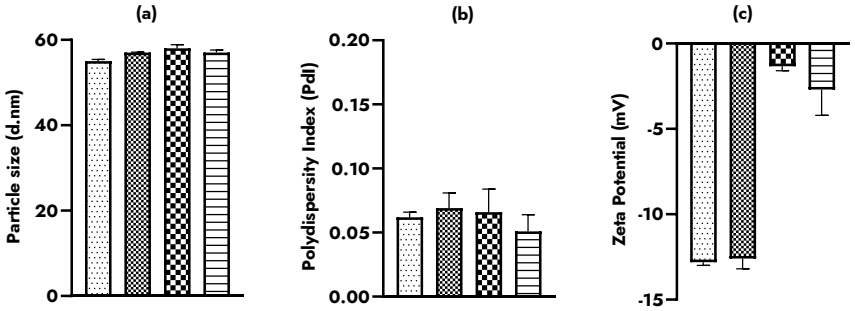

Figure 9. Particle size (a), polydispersity index (b), and zeta potential (c) of LNCs prepared with Lipoid S 75 (▭), Phospholipon 80® H (▩), Lipoid S PC-3 (▩) and Phospholipon 90® H (▭) (mean ± SD; n=3).

Later, the optimization and understanding of the effect of varied composition on the physico-chemical properties of the resulting LNCs was performed, and the data is presented in Table 8. The optimization studies of the LNCs composition showed the importance of the surfactant to oil ratio. At higher concentration of Labrafac™ (i.e., lower surfactant to oil ratio) (6.2 % w/v to 9.3 % w/v), larger sized particles were formed. While at higher concentrations of Kolliphor® (4.8 % w/v to 9.6 % w/v), giving a higher surfactant to oil ratio, a better stabilization of smaller particles was found, i.e. smaller sized particles were formed. These results are in accordance with previously reported findings on LNCs by other authors (Anton & Saulnier, 2013; Aparicio-Blanco et al., 2019). The size distribution of the LNCs as reported by PDI values was found to be less sensitive towards any change in the composition. Detailed optimization data can be found in **Paper I**. In addition to particle size and PDI, zeta potential was also measured for the LNCs prepared with varied concentrations of Kolliphor® and

Labrafac™. For the unloaded particles, the zeta potential remained closer to zero owing to the non-ionic nature of Kolliphor® that is surrounding and stabilizing the particles.

Upon addition of drug, DF003, the hydrodynamic size and PDI of LNCs obtained from DLS appeared to increase compared to unloaded particles (F5 vs F6 in Table 8). Nevertheless, the average particle size and PDI of LNCs prepared with different concentrations of excipients were found to be less than 100 nm and 0.25, respectively. Additionally, the drug-loaded particles acquired a negative surface charge and hence the zeta potential values were more negative compared to unloaded LNCs. Based on the optimization data, the zeta potential is dependent mainly on the drug loading and the amount of non-ionic surfactant, Kolliphor®. The amount of Kolliphor® in the LNCs, on the other hand, has a major impact on the EE (F6, F7 and F8 in Table 8). With increasing concentrations of Kolliphor®, higher EE was observed. This is most likely due to the fact that the drug is highly soluble in Kolliphor®, thereby higher affinity of the drug for the LNCs. In case of Labrafac™, where the drug is less soluble, the EE was not improved with higher concentrations. Although LNCs with varied compositions showed good physico-chemical characteristics, formulation with 6.2 % w/v Labrafac™, 4.8 % w/v Kolliphor®, and a drug to lipid ratio of 1:32 was chosen for further studies described hereafter.

Table 8. Optimization and characterization data of LNCs

Formulation	Labrafac (% w/v)	Kolliphor (% w/v)	Phospholipid (% w/v)	Drug: lipid ratio	Type of phospholipid	Particle size (d.nm)	PdI	% EE	Drug loading (mg/mL)	Zeta potential (mV)
F1	6.2	4.8	0	1:32	-	Immediate signs of phase separation				
F2	6.2	4.8	0.4	-	Lipoid S 75	55 ± 0.4	0.06 ± 0.00	-	-	-12.8 ± 0.2
F3	6.2	4.8	0.4	-	P 80® H	57 ± 0.1	0.07 ± 0.01	-	-	-12.6 ± 0.6
F4	6.2	4.8	0.4	-	Lipoid S PC-3	58 ± 0.9	0.07 ± 0.02	-	-	-1.3 ± 0.3
F5	6.2	4.8	0.4	-	P 90® H	57 ± 0.6	0.05 ± 0.01	-	-	-2.7 ± 1.5
F6	6.2	4.8	0.4	1:32	P 90® H	76 ± 1.2	0.16 ± 0.02	69 ± 0.5	1.4 ± 0.07	-11.6 ± 0.4
F7	6.2	7.2	0.4	1:32	P 90® H	51 ± 0.0	0.16 ± 0.00	82 ± 2.2	1.6 ± 0.05	-7.7 ± 0.5
F8	6.2	9.6	0.4	1:32	P 90® H	54 ± 2.9	0.25 ± 0.04	89 ± 0.5	1.8 ± 0.02	-7.4 ± 0.4
F9	9.3	7.2	0.4	1:32	P 90® H	91 ± 8.7	0.21 ± 0.03	84 ± 2.1	1.6 ± 0.00	-12.5 ± 0.1
F10	6.2	4.8	0.4	1:64	P 90® H	68 ± 1.4	0.12 ± 0.03	82 ± 6.3	0.8 ± 0.11	-8.2 ± 0.2

Formulation development of the LNCs with deuterated excipients was necessary for **Paper II**, which describes the structural investigation of LNCs (both with and without drug loading) using the small-angle scattering techniques, SAXS and SANS.

For SAXS experiments, LNCs with a particle concentration of 62 mg/mL were used, and a particle radius of 35 ± 1 and 45 ± 1 nm were observed for unloaded and drug-loaded LNCs, respectively. Additionally, a PDI of 0.14 ± 0.01 was observed with drug-loaded LNCs, which is higher compared to that for unloaded LNCs (0.09 ± 0.01). Nevertheless, both the particle size and PDI of LNCs were higher at a higher particle concentration compared to LNCs with lower particle concentrations that were used for SANS measurements.

As described earlier in the introduction, deuteration of the samples was necessary to achieve higher neutron contrast to enable the SANS measurements. This was done by replacing 5 % of the core components with an equal proportion of its deuterated counterpart. Hence, LNCs with deuterated core components (d-LNCs) were prepared in H_2O, D_2O and a mixture of H_2O and D_2O to obtain different neutron contrasts highlighting different regions in the nanoparticle (schematic of these contrasts is presented in Figure 25). Samples with a particle concentration of 1.2-6.2 mg/mL were used for the measurements. Initially, d-LNCs were characterized for particle size, PDI and zeta potential using Malvern Zetasizer and compared with original LNCs data (termed as h-LNCs in **Paper II**) to ensure that the deuteration to the core did not alter the physico-chemical properties of the particles and the data is presented in supporting information to **Paper II**. Unloaded LNCs prepared in D_2O as dispersion medium resulted in particle radius and PDI of 29 ± 1 nm and 0.04 ± 0.01, respectively. These values are very similar to the LNCs prepared in H_2O. This shows that changing the dispersion medium has no major impact on the particle properties. Further, upon deuteration in the core (d-LNCs), particle radius and PDI were noticed at 27 ± 1 nm and 0.04 ± 0.01, respectively. A very small reduction in particle size compared to the original LNCs was thus observed for the d-LNCs. A similar slight reduction in particle size was noticed for drug-loaded d-LNCs compared to the drug-loaded original formulation. Further, morphology of drug-loaded d-LNCs as determined with cryo-TEM was comparable to that of original formulation, demonstrating the minimal impact by the presence of a deuterated core in the particles (Figure 23d). Apart from the particle size and PDI, zeta potential was also unaffected upon inclusion of deuterium either in the particle core or in the dispersion medium, making these deuterated particles suitable for SANS measurements.

In **Paper III**, LNCs with selected composition were used for *in vitro/ex vivo* investigation to check for their suitability for ocular administration. For ocular bio-distribution studies, LNCs loaded with a lipophilic green fluorescent dye, DiO were prepared. Particle size and zeta potential of these DiO loaded LNCs were found to be

58 ± 0.2 nm and -0.3 ± 0.1 mV and these results are very similar to that of unloaded LNCs. DiO, being lipophilic is expected to be predominantly located in the core of the particles, thereby causing a little or no change to either the particle size or the surface charge.

Further, LNCs prepared both with and without the drug were subjected to freeze-drying using the selected composition from **Paper I**. For ease of understanding, the data is presented separately under section 5.3.

5.2.1.1 Drug release testing in phosphate buffer

Drug release testing provides valuable information about how efficiently the drug is associated with the nanoparticles and how the nanoparticles may affect drug release and absorption kinetics. The drug release kinetics are influenced by various factors such as drug and nanoparticle properties, formulation composition, interaction between drug and nanoparticle and testing conditions (Herdiana et al., 2021). Measuring in vitro release kinetics offers a possibility in predicting the formulation behavior upon administration (Kim et al., 2021; Weng et al., 2020). Based on this data, further formulation optimization can be performed to attain the desired release kinetics for a specific application of interest.

In the present work, the drug release from the LNCs was performed using a dialysis method where the LNCs loaded in a dialysis bag were placed in a vial containing phosphate buffer as a release medium. Sink conditions were maintained during the whole experiment and the concentration of DF003 in the release medium did not exceed 17 % of the drug concentration in the particles. From these experiments, it was observed that the release from LNCs is much slower compared to the free drug and that the particles sustained the drug release for up to 6 days with an early burst release phase (Figure 10). This release data of DF003 is comparable with previously reported release data for LNCs loaded with hydrophobic drugs like amiodarone and tripentone (A. Lamprecht et al., 2002; Malzert-Fréon et al., 2006), despite its high aqueous solubility, possibly due to its strong association with Kolliphor®.

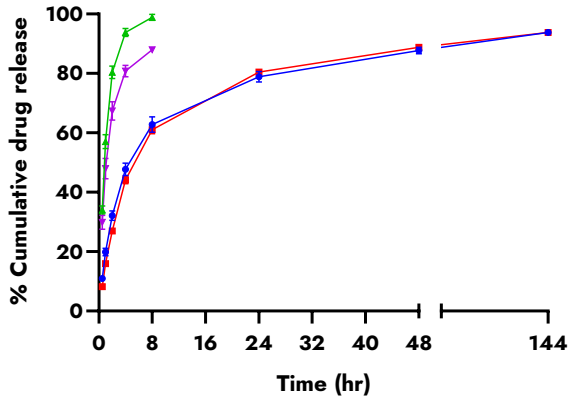

Figure 10. *In vitro* release testing of free drug in phosphate buffer (—▲—), free drug in hyaluronic acid (—▼—), drug-loaded LNCs (F6) in phosphate buffer (—●—) and drug-loaded LNCs (F6) in hyaluronic acid (—■—). (Mean ± SD, n=3)

5.2.1.2 Stability and drug release testing in HA

LNCs in the present work were developed with the ultimate goal to be used for intravitreal administration. The behavior of LNCs was, therefore studied in the presence of hyaluronic acid (HA) which is an important constituent of the vitreous along with water (98–99.7 %), collagen, and proteins (Rimpelä et al., 2018). Along with collagen, HA is responsible for maintaining the integrity of the eye structure (Christensen et al., 2021; Hyuncheol Kim et al., 2009). However, HA which is a negatively charged glycosaminoglycan, may hinder the movement of nanoparticles across the vitreous depending on factors such as particle size, surface charge, and protein binding. (X. Huang & Y. Chau, 2019; Mains & Wilson, 2013; Tavakoli et al., 2021). Nanoparticles, especially with a cationic charge, are prone to undergo aggregation as previously reported by several researchers (H. Kim et al., 2009; H. Koo et al., 2012; Martens et al., 2017; L. Peeters et al., 2005). Although the overall charge of LNCs is neutral to anionic depending on the presence or absence of loaded drug, it is important to study the physico-chemical stability and the drug release pattern in presence of HA. For this, drug-loaded LNCs were incubated in HA for one week at 37 °C, and the particle size and PDI were monitored. None of these parameters appeared to change over 7 days ($p > 0.05$, one-way ANOVA, Tukey's multiple comparison test) (Figure 11).

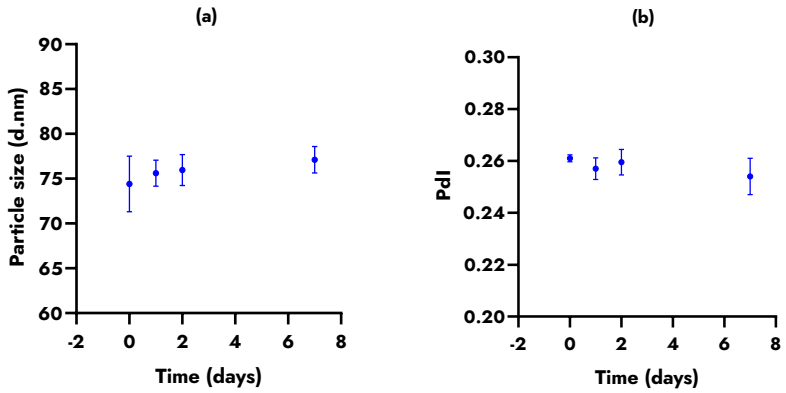

Figure 11. Stability of LNCs (F6) in presence of Hyaluronic acid sodium: (a) changes in particle size, (b) changes in polydispersity Index. (Mean ± SD, n=3)

Along with stability, drug release testing was also performed in presence of HA. A similar release profile was obtained as from the release profile obtained in phosphate buffer (Figure 10; $p > 0.05$, two-tailed paired t-test). This suggests that the LNCs are stable and maintain their sustained release properties for DF003 in presence of HA.

5.2.2 Large scale manufacturing of LNCs

Early-stage drug product development often relies on small quantities of API and drug formulation. However, as the development progresses from pre-clinical phase to commercial phase, there is a need to manufacture at a much larger volume scale. This translation from lab-scale production to a commercial scale often requires scale-up of the process several times and this may lead to various challenges in the manufacturing of the final product (Felton, 2012; Thomas & Lagarce, 2013). Over the decades, a large number of nanoparticulate systems have been developed for a variety of drug delivery applications, yet few made their way to market (Ventola, 2017). Many nanoparticulate systems are restricted to research purpose with limited industrial scope because of numerous underlying complexities. Scale-up difficulties such as batch to batch reproducibility, sterility/bioburden, long-term stability and stringent regulatory requirements, make it complicated for these systems to get market access (Muthu & Wilson, 2012). Most common challenges encountered while scaling up the nanoformulations includes changes in particle size, size distribution, stability of resulting formulation thereby changing the end product quality at higher scales compared to lab-scale. To address these challenges, the process may need to be accommodated with additional unit operations to facilitate a smoother transition to a large scale.

In the present work, the scalability of the phase inversion process was studied by manufacturing LNCs (without drug loading) at 1 L and 10 L volume scales that corresponds to 100 and 1000 times the lab-scale volumes. Different processes were

evaluated including conventional process, continuous process, and a process suitable for producing sterile LNCs. Initially, two batches of LNCs at 1 L scale were manufactured with a batch process to study the process reproducibility. It was found that none of the product characteristics like size, size distribution, particle concentration as expressed by DCR did not change between these two batches indicating that the setup used produced LNCs of similar quality. This was followed by a batch production of LNCs at 10 L scale and the product parameters obtained were similar to the LNCs prepared at lab-scale as well as at 1 L scale. Characterization data from upscaled LNCs with different processes is given in Table 9.

During the phase inversion process, the solution undergoes a phase change from O/W emulsion at low temperatures to W/O emulsion at higher temperatures, based on the temperature dependent changes in surfactant (Kolliphor®). The phase conversion leads to a change in the conductivity of the system i.e. from higher conductivity to a lower conductivity with rise in temperature. Hence, conductivity measurements were performed during the heating-cooling cycles to monitor the scale up process. The measured conductivity changes over the three temperature cycles followed the same pattern for both 1 L and 10 L scale-up as shown in Figure 12. Further, in Figure 13, conductivity measurements performed at a cycle when the temperature changed from 60 °C to 90 °C, during 1 L scale-up with the batch manufacturing process are visualized. High conductivity values were recorded at lower temperatures and when the temperature approaches 90 °C, a sudden decline in conductivity is evident indicating the formation of a W/O emulsion. These observations were found to follow the previous findings by Heurtault et al., (Heurtault et al., 2002). Hence, by monitoring the conductivity values, it is possible to monitor the manufacturing process, and deviations in the conductivity values may be an indicative for a possible impact on the product quality.

Table 9. Characterization of LNCs prepared at different manufacturing scales with different processes.

Batch/ (volume)	Type of process	Particle size (d.nm)	PdI	Zeta Potential (mV)	DCR (kcps)
Lab-scale/ (0.01 L)#	Batch	58 ± 0.7	0.06 ± 0.01	-2.0 ± 1.0	122273 ± 6990
Scale-up/ (1 L)*	Batch	57 ± 0.0	0.06 ± 0.01	-1.6 ± 0.2	115002 ± 1317
Scale-up/ (1 L)**	Continuous	59	0.08	-	117012
Scale-up/ (10 L)**	Batch	59	0.01	-1.8	113505
Scale-up/ (1 L) ** (with sterilization steps)	Batch	65	0.12	-1.7	133748

#n=3, *n=2 (data represented as mean ± SD), **n=1

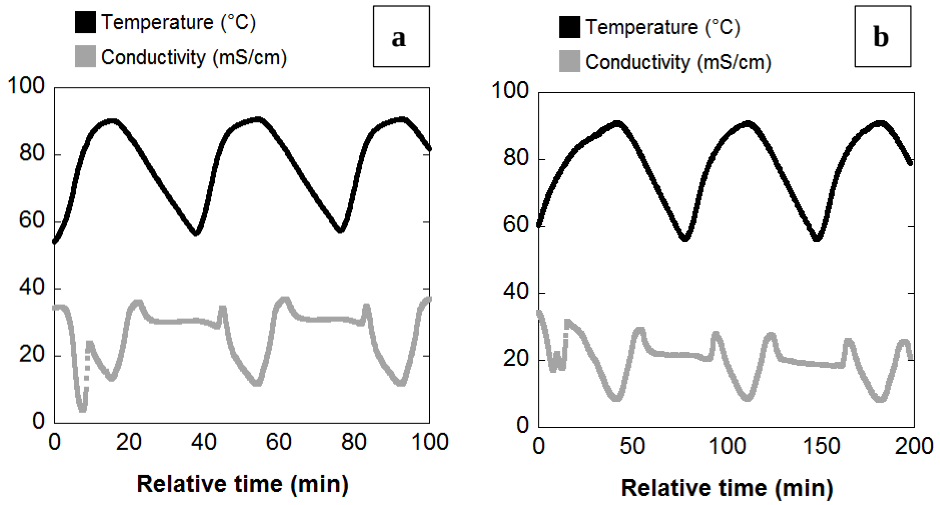

Figure 12. Dispersion temperature and conductivity as a function of time during the LNCs manufacturing process. (a) scale-up at 1 L volume (b) scale-up at 10 L volume, both with batch process.

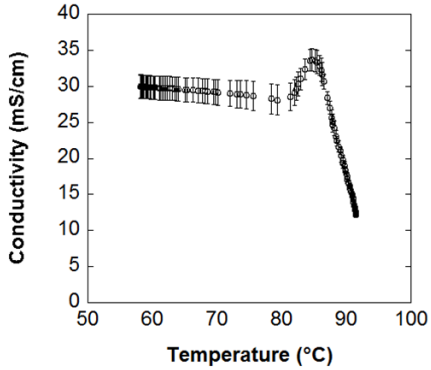

Figure 13. Conductivity as a function of the dispersion temperature for the last heating cycle when the temperature is raised from 60 °C to 90 °C, for 1 L with batch process. (n=2)

From Figure 12, it can be seen that the time frame for the heating-cooling cycles for the 10 L batch was higher than for the 1 L batch, indicating prolonged manufacturing times for the higher scales. To reduce this higher manufacturing time at higher scale, modifications were made to the batch process in an attempt to make it to a continuous process. For this purpose, LNCs were manufactured at a 1 L scale using a medium scale vertical oscillatory baffled reactor vessel that is connected to two different baths meant for heating and cooling (Figure 14c and Figure 14d). Agitation in this reactor is caused by oscillating baffles to achieve improved heat transfer and better mixing of the excipient mixture and thereby increasing the process efficiency and reducing the process times (Abbott et al., 2013; Bianchi et al., 2020). Additionally, the flow patterns observed in this type of flow reactor are similar to that of a large scale continuous oscillatory baffled reactor. Hence, scaling up to much higher volumes is possible by connecting several oscillatory baffled reactors into a continuous oscillatory baffled reactor without changing the flow properties of the liquid and thereby producing LNCs with the same quality. LNCs obtained using this process oscillatory reactor were found to be of the same quality as of the other processes (Table 9).

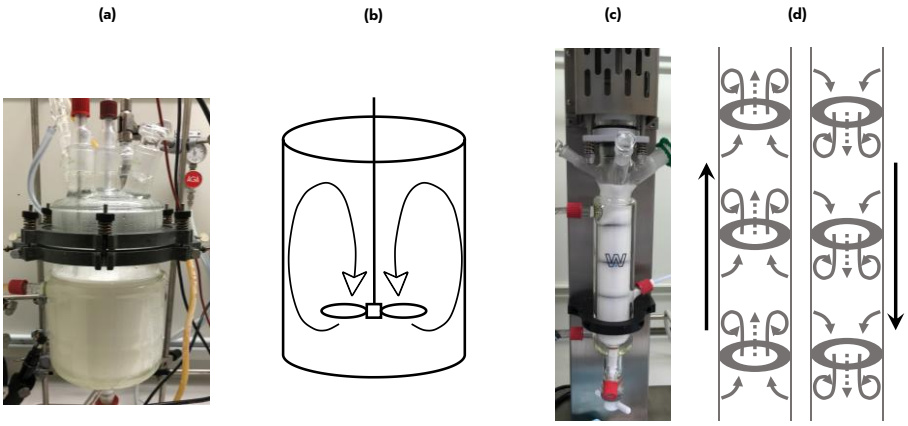

Figure 14. Manufacturing of LNCs at large scale. (a), (b) represents the reaction vessel and predicted liquid flow pattern in a batch operation and (c), (d) indicates the oscillatory baffled reactor and its flow pattern. In figure (d), liquid flow is indicated by dashed arrows and the solid arrows outside the drawing indicates the movement of baffles (Abbott et al., 2013).

In addition to modifying the batch process for a continuous process, the batch process was modified with additional unit operations to produce LNCs with a low bioburden. The resulting LNCs were tested for their ability to be sterile filtered. This method included a sterile filtration (0.22 µm) and a subsequent heat sterilization of the excipient mixture. When Phospholipon® 90 H was used in the mixture for sterile filtration, filter clogging was observed. Hence, Phospholipon® 90 H was included after the successful sterile filtration and heat sterilization of the rest of the components. Additionally, a final sterile filtration step was included after the preparation of LNCs, and this step was found to have no measurable effect on the particle properties (Table 10). Further, TAMC values for the resulting LNCs were found to be at 0 CFU/mL demonstrating that this process is effective at producing LNCs with low microbial burden and that the resulting LNCs are suitable for sterile filtration. Particle size distribution of LNCs prepared using various processes is shown in Figure 15.

Table 10. Characterization of upscaled LNCs prepared with a sterile manufacturing process

Sample type	Particle size (d.nm)	PdI	Zeta Potential (mV)	DCR (kcps)
Non-filtered	66	0.11	-1.6	131044
Sterile filtered	65	0.12	-1.7	133748

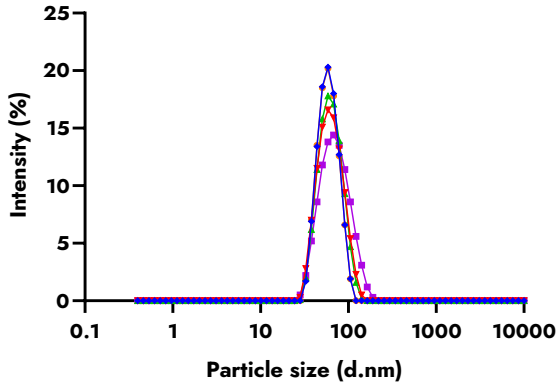

Figure 15. Comparison of the particle size data of LNCs manufactured at different scales and processes: lab-scale ( ), 100 times scale-up with batch process ( ), 1000 times scale-up with batch process ( ), continuous process ( ), sterile manufacturing process ( )

5.2.2.1 Colloidal stability testing

Different parameters like particle and surface charge plays an important role in maintaining the stability of nanoparticles. Formulations with poor inherent stability tend to show an increase in particle size with time, leading to aggregation thereby losing their functionality. Formulations intended for pre-clinical and clinical testing should have a sufficient stability. In this work LNCs prepared at both lab-scale and higher manufacturing scales were tested for their colloidal stability and the data is presented in Table 11 and Figure 16. For drug-loaded LNCs prepared at lab-scale, stability was monitored at room temperature and at refrigerated conditions. None of the samples showed physical instability. Except for the EE, remaining formulation properties were unchanged for both storage conditions compared to the initial data. For EE, a drop of up to 10 % was seen after 1 month and is due to the release of drug from nanoparticles into the dispersion medium. In addition, the data between the storage conditions is statistically similar suggesting that the stability for tested duration is independent of storage conditions ($p > 0.05$ for all parameters between both storage conditions, paired t-test). Further, LNCs (unloaded) prepared at higher scales were also found to be stable for at least 6 months after storage at 2-8 °C (Table 11).

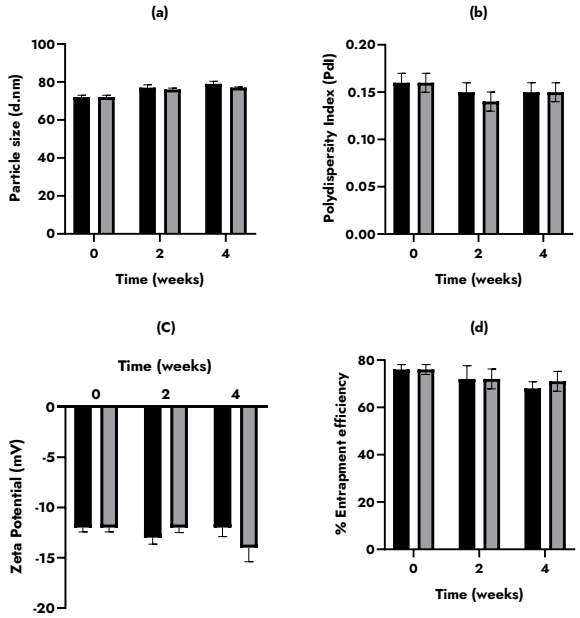

Figure 16. Colloidal stability evaluation of drug-loaded LNCs prepared at lab-scale: room temperature (■); 2-8 °C (▭). (Mean ± SD, n=3)

Table 11. Stability data of unloaded LNCs prepared at different manufacturing scales

Stability duration	**Lab-scale**	**100 times scale-up with batch process (1 L)**	**1000 times scale-up with batch process (10 L)**	**Continuous process (1 L)**	**Sterile manufacturing process (1 L)**
Particle size (d.nm)					
Initial	57	57	59	59	65
1 month	62	59	59	60	67
6 months	-	-	-	64	-
Polydispersity Index (PdI)					
Initial	0.05	0.07	0.10	0.08	0.12
1 month	0.03	0.04	0.05	0.05	0.11
6 months	-	-	-	0.06	-
Zeta Potential (mV)					
Initial	-2.7	-1.7	-1.8	-	-1.7
1 month	-1.9	-3.5	-3.7	-	-2.2

5.3 Freeze-drying of LNCs

The majority of nanoparticle-based formulations for pharmaceutical use are usually prepared in an aqueous dispersant. These formulations often encounter stability related issues like degradation and/or aggregation of nanoparticles, sedimentation, creaming, uncontrolled release kinetics and a limited microbiological shelf-life (Abdelwahed, Degobert, & Fessi, 2006; Degobert & Aydin, 2021; Smith et al., 2010; Trenkenschuh & Friess, 2021). The types of instabilities are mainly dependent on the formulation type and the storage conditions. These instabilities may lead to significant changes in the physico-chemical attributes of the nanoparticles and render them unsuitable for their intended applications especially upon long-term storage. This necessitates the need for extreme storage conditions like -20 °C or even at -80 °C depending on the complexity of the formulation. To alleviate these extreme storage conditions, there exists several ways of improving the storage or shelf-life stability. These include freeze-drying or lyophilization, spray drying, and spray-freeze-drying with an objective of converting the liquid formulation to dry powder with an enhanced long-term storage (Chen et al., 2010; Tang & Pikal, 2004; Trenkenschuh & Friess, 2021). All these processes involve removal of water from the formulation thereby preventing or delaying major physical and chemical stability challenges associated with the product (Abdelwahed, Degobert, Stainmesse, et al., 2006; Muramatsu et al., 2022; Umerska et al., 2020). Of these techniques, freeze-drying has been the preferred choice for various colloidal nanoparticulate systems, including lipid-based systems as this process avoid using very high temperatures resulting in better end-product characteristics (Abdelwahed, Degobert, Stainmesse, et al., 2006; Ali & Lamprecht, 2017; Smith et al., 2010).

Freeze-drying is a slow and energy demanding process that needs to be tailored to suit individual applications. This process involves three main steps namely (i) freezing the mixture where water in the mixture forms ice and is separated from the colloidal particles, thus leading to the formation of freeze concentrate (ii) primary drying or ice sublimation at low pressure and high temperature to facilitate ice sublimation, (iii) secondary drying at low pressure and elevated temperatures, to reduce the residual moisture content (Roy & Gupta, 2004; Tang & Pikal, 2004). Although freeze-drying is aimed at improving the stability behavior, the process itself may induce stresses on the formulation during different steps, leading to altered physico-chemical attributes for e.g., particle size increase, changes in particle structure, and poor drug retention (Guimarães et al., 2019). Thus, selection of a suitable cryoprotectant in combination with a better process is needed to preserve the product characteristics during freeze-drying.

A variety of cryoprotectants such as sucrose, glucose, trehalose, lactose, sorbitol, PEG 4000, aerosil, mannitol have been evaluated in the freeze-drying of LNCs loaded with different drug molecules, by various authors (Aparicio-Blanco et al., 2019; Ashour et al., 2020; Dulieu & Bazile, 2005; Heurtault et al., 2002; Molaahmadi et al., 2019; Varshosaz et al., 2018; Zhao et al., 2013). However, these studies were done either at fixed carbohydrate concentration or showed particle size data that was significantly

higher than the original formulation before freeze-drying. Further, these studies lack morphological information about the freeze-dried cake or the redispersed formulation. Changes in formulation caused by freeze-drying may vary depending on the type of drug molecule and how it is associated with the particles.

In the present work, an attempt was made to address the behavior of LNCs with freeze-drying with different cryoprotectants (sucrose, trehalose, and raffinose), and how the drug association with the LNCs is affected by the freeze-drying process. Both unloaded and drug-loaded formulations with chosen composition from the work described in **Paper I** were used for studying the freeze-drying process. For this, LNCs were mixed with different cryoprotectants to study the impact of these cryoprotectants at different concentrations on the physicochemical properties of the LNCs. These cryoprotectants at different final concentrations (5 % and 10 %) were mixed with LNCs to obtain an MMR of 5.0, 10.0, 25.0 and were subsequently freeze-dried. The freeze-dried cakes were redispersed with milli-Q water to the original volume and characterized for particle size, PDI, zeta potential, morphology with cryo-TEM, EE, and drug release in the same way as that of initial liquid formulation before freeze-drying step.

5.3.1 Characterization of freeze-dried and reconstituted LNCs

5.3.1.1 Particle size, size distribution

As mentioned in the previous sections the particle diameter of unloaded and drug-loaded LNCs was at 60.0 ± 1.0 and 72.0 ± 1.0 nm, respectively. Upon freeze-drying and redispersion of these formulations containing cryoprotectants, an increased particle size and PDI were clearly seen compared to their initial sizes (Figure 17). The increase in size was found to be dependent mainly on the type of cryoprotectant used. Among those studied, sucrose offered minimal increase in size, whereas raffinose showed highest increase in size. This observation is valid irrespective of the presence or absence of drug in the LNCs. However, the overall increase in size was relatively higher for drug-loaded LNCs compared to unloaded LNCs. For the same cryoprotectant, variations in size increase were observed at different MMRs. Different MMRs resulted in larger variations for drug-loaded particles. At 5 % and 10 % of cryoprotectant concentration, the cryoprotectants had a very little effect protecting from particle size increase.

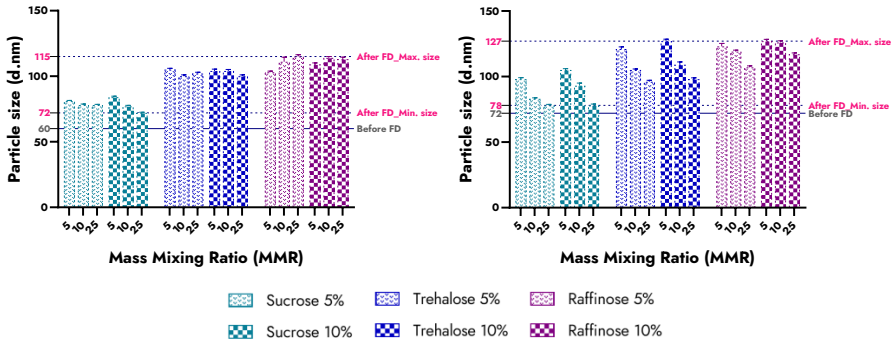

Figure 17. Impact of freeze-drying on particle size of unloaded (left) and drug-loaded LNCs (right) with different cryoprotectants.

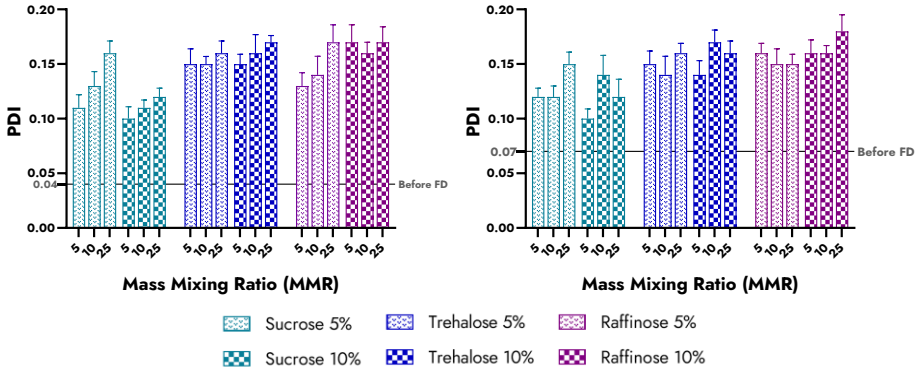

Figure 18. Impact of freeze-drying on PDI of unloaded (left) and drug-loaded LNCs (right) with different cryoprotectants.

Similar to particle size, the PDI of both unloaded and drug-loaded formulations also showed considerable increase after redispersion (Figure 18). Increase in PDI was relatively lower both for unloaded and drug-loaded LNCs, when sucrose was used as a cryoprotectant. However, the PDI values in all the tested combinations was lower than 0.2 indicating that they still maintain a monodisperse nature.

Morphology of these redispersed formulations was studied using cryo-TEM and the micrographs are presented in Figure 19. These micrographs shows that variability in particle sizes has increased with freeze-drying compared to original formulations (Figure 23). In addition, clear differences can be seen in overall morphology of LNCs when different cryoprotectants were used. LNCs containing sucrose shows a relatively better size distribution without visible signs of particle aggregation. When trehalose and raffinose were used, there was an apparent evidence of particle aggregation and an overall increase in particle size. In all the cases, a higher population of smaller particles was clearly seen compared to the micrographs obtained before freeze-drying (Figure 23).

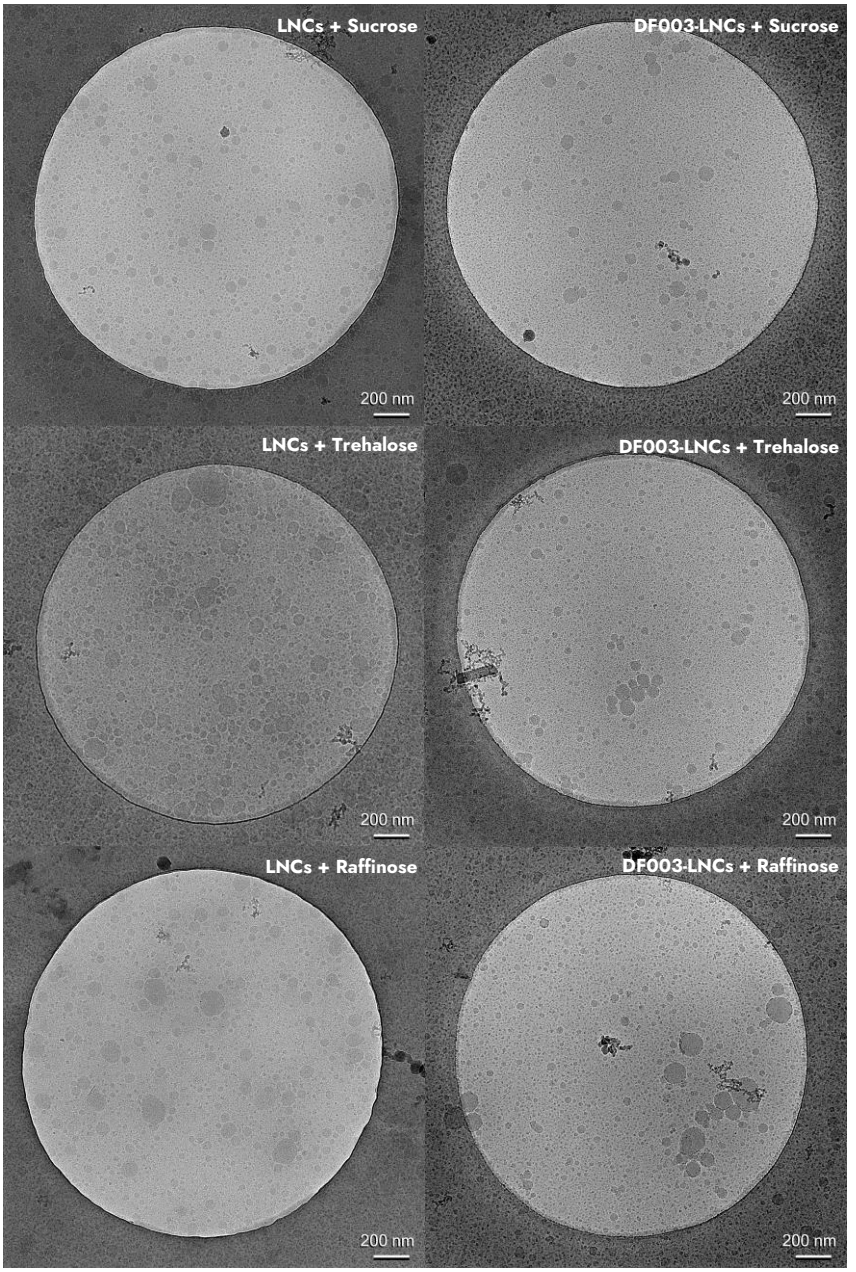

Figure 19. cryo-TEM micrographs of redispersed LNCs containing 10 % final carbohydrate concentration at MMR 10. (a, c, e) represents unloaded LNCs containing sucrose, trehalose, and raffinose respectively. (b, d, f) represents drug-loaded LNCs containing sucrose, trehalose, and raffinose respectively.

To obtain the structural information and to check if the core-shell spherical structure of the nanoparticles reported in **Paper II** is retained after freeze-drying and redispersion, synchrotron SAXS measurements were performed. Although this data is yet to be fully modelled, qualitative evaluation of the data demonstrated an increase in both particle size and PDI upon freeze-drying with all the cryoprotectants tested. Sucrose showed the least increase in size and PDI compared to raffinose that showed a larger increase in both size and PDI (data not shown in the thesis). These findings are in line with the DLS and cryo-TEM observations.

Further, zeta potential and EE of drug-loaded LNCs was tested for the reconstituted formulations. Irrespective of type of cryoprotectant used and its concentration, the zeta potential remained similar to that of the original formulation before freeze-drying.

In the case of EE, all the formulations showed a great reduction in EE. Only formulations containing 10 % of carbohydrate concentration at an MMR of 5 showed relatively better EE at around 60 %, although this is much lower than the original EE of ~ 86 % before freeze-drying. Formulations at MMR 25 had the highest reduction in EE. Since the drug is majorly located on the surface of the nanoparticles as shown in **Paper II**, the drug association to the particles was most likely adversely affected by the freeze-drying process eventually leading to reduced EE.

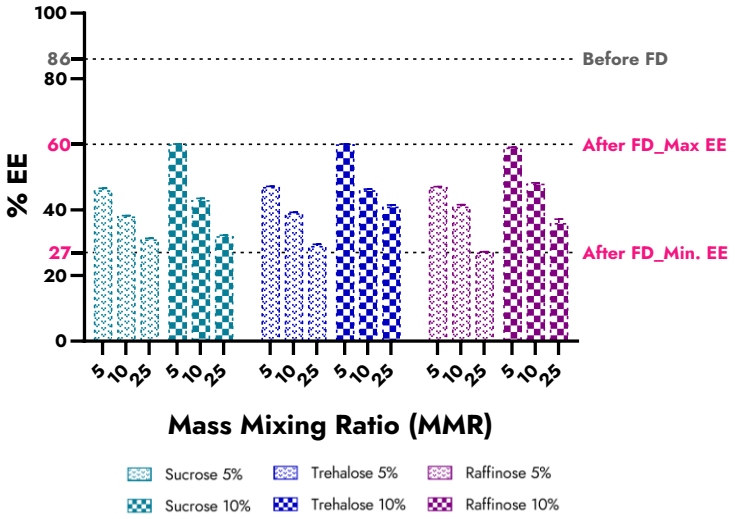

Figure 20. Effect of freeze-drying on entrapment efficiency of LNCs

Further, drug release from the LNCs that showed ~ 60 % of EE after freeze-drying was performed. This data was compared to the release from samples before freeze-drying (Figure 10). The release data from the freeze-dried and resuspended formulations is shown in Figure 21. Similar to the EE, the release of drug from the formulations was also greatly affected by the freeze-drying process. Redispersed formulations showed complete release within 24 h whereas the samples without the freeze-drying step had a

much-delayed drug release profile of up to 6 days. This study in combination with the EE testing demonstrates that the freeze-drying has induced significant changes in the drug association behavior to the nanoparticles.

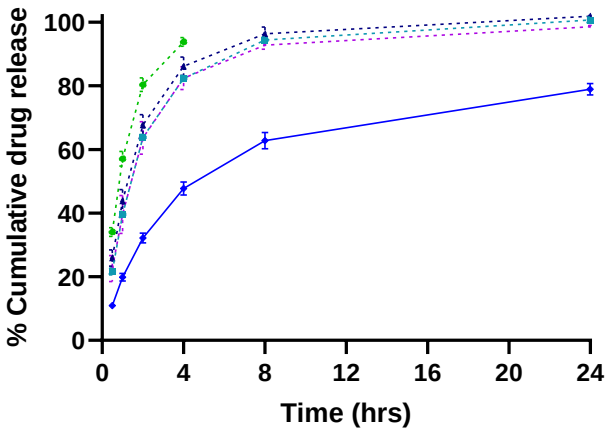

Figure 21. *In vitro* drug release testing of redispersed drug-loaded LNCs containing sucrose ( ), trehalose ( ), raffinose ( ). These redispersed formulations contain 10 % of final carbohydrate concentration at an MMR of 5. Release data from free drug in phosphate buffer ( ), drug-loaded LNCs (F6) in phosphate buffer ( ) is extracted from Figure 10. (Mean ± SD, n=3).

Overall, the characterization of redispersed LNCs (both with and without loaded drug) revealed the significant effect of the freeze-drying process on their physicochemical attributes. These effects were magnified especially in case of drug-loaded formulation, where most of the drug is associated on the particle surface. Nevertheless, the particles as such without any loaded drug showed good compatibility with the freeze-drying process, specifically the formulations containing sucrose, although the particle size increase was evident on a narrow range. It would be interesting to understand if the core-shell spherical structure would remain retained upon freeze-drying and if the drug loading would play a role in morphological changes in the particle structure. This would be a part of continuation of this work beyond this thesis.

5.4 Structural investigation of LNCs using small-angle scattering approaches

Most commonly used characterization techniques for nanosized drug delivery systems like DLS and cryo-TEM provide valuable information about particle size and morphology. However, these techniques fall short of providing insight into the detailed structural aspects of the nanoparticles. Advanced characterization techniques are therefore necessary to obtain structural information e.g. internal structure, and effect of drug loading on the internal structure, that is accurate to the extent of Å scale due to

the nanometer size of these particles. Thus, in this present work, to investigate the internal structure of LNCs, small-angle scattering approaches like SAXS and SANS techniques were utilized. This work was published in **Paper II**.

5.4.1 Small-angle x-ray scattering of LNCs

As mentioned earlier, SAXS does not require any sample modifications and hence the particles in their native undiluted state were measured at 62 mg/mL concentration. Both unloaded and drug-loaded particles were measured in a similar way. The measured scattering data was analyzed for pair distance distribution function *P(r)*. The obtained *P(r)* profiles for both unloaded and drug-loaded particles are presented in Figure 22, and they resemble Gaussian distribution or a bell-shaped curve. This confirms the spherical nature of LNCs both in presence and absence of drug. The spherical nature of the particle can also be seen in the cryo-TEM micrographs presented in Figure 23. Along with the morphology, the cryo-TEM micrographs show the presence of small and large particles indicating polydispersity of the samples. Polydispersity seems to be higher in case of LNCs containing the drug. (Figure 23a vs b). *P(r)* profiles further demonstrate that the average radius of drug-loaded LNCs is slightly smaller with a radius of gyration (Rg) of 15.8 ± 0.05 nm compared to an Rg of 17.3 ± 0.09 nm for unloaded LNCs. These values are significantly lower than those obtained with DLS, where drug-loaded and unloaded LNCs showed sizes of 36.0 ± 1.0 nm and 30.0 ± 1.0 nm, respectively (Table 12). This deviation may be explained by how these techniques measure the size of the particles. DLS measured diffusion coefficient thereby gives information about hydrodynamic size rather than actual size of the particles. The hydrodynamic size is affected by various parameters including the size and surface properties of the particles and properties of the dispersion medium (Maguire et al., 2018). This hydrodynamic size is usually higher than the actual particle size. Additionally, DLS is sensitive to the presence of small quantities of large particles or clusters of particles (Hackley et al., 2015). However, SAXS and SANS provide accurate size information by measuring individual particles directly and hence the size values obtained from these techniques were smaller than those from DLS.

Further, with SAXS technique, a smaller average radius was obtained for drug-loaded LNCs compared to unloaded LNCs. This contrasts with DLS data where drug-loaded LNCs showed higher size compared to unloaded LNCs. This may be explained by differences in polydispersity values obtained with different techniques. Model fitting of SAXS and SANS data for drug-loaded LNCs showed a higher polydispersity, indicating a wider size distribution than that was obtained with DLS.

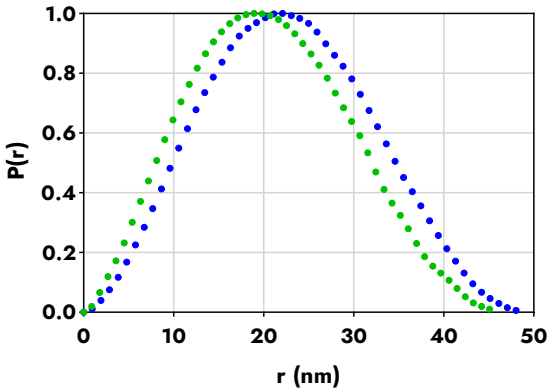

Figure 22. Normalized *P(r)* profile of unloaded (●) and drug-loaded (●) LNCs.

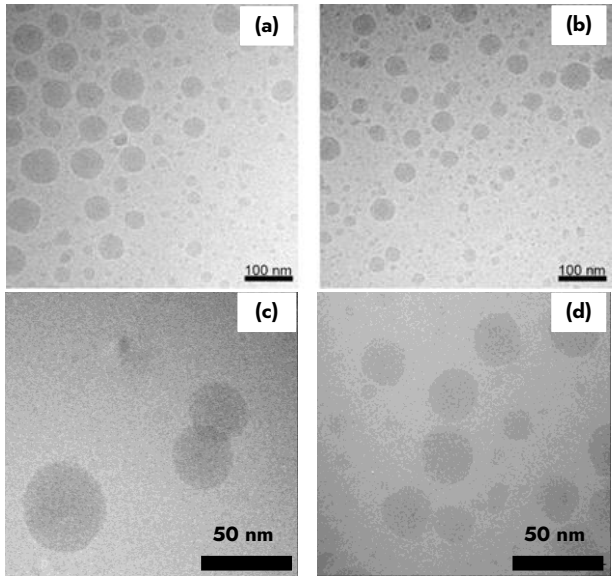

Figure 23. Cryo-TEM micrographs of (a) unloaded LNCs; (b, c) drug-loaded LNCs; (d) drug-loaded d-LNCs.

Based on the spherical morphology of the LNCs, scattering data from both unloaded and drug-loaded LNCs was initially fitted with a simple sphere model (Guinier et al., 1955) where the fit is clearly off from the experimental scattering data (Figure 24a). This suggests that the sphere model is unable to explain the data completely and that the particles have additional structural aspects. Thus, the data was fitted to a core-shell sphere model (Guinier et al., 1955), and this model fits the data well (Figure 24b). This demonstrates that the LNCs have a core-shell structure and this structure remained unchanged after the drug loading. However, similar to the findings from *P(r)* analysis, model fitting also showed a reduction in average particle radius upon drug loading (22.1 ± 0.3) compared to unloaded particles (24.3 ± 0.3). However, this reduction is mainly due to the reduction in the core radius, however, interestingly, the shell

thickness has increased from 2.6 ± 0.1 nm for the unloaded particles to 3.6 ± 0.1 nm for the drug-loaded particles. It is also evident from the data fitting that the polydispersity for drug-loaded LNCs was rather high as previously confirmed with DLS and cryo-TEM data. This higher PDI was one of the factors leading to an overall average size reduction of LNCs upon drug loading. Nonetheless, the increased shell thickness suggests that the drug is predominantly localized in the shell.

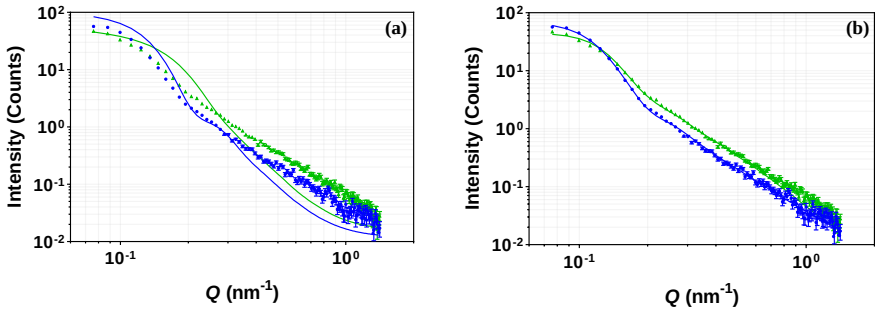

Figure 24. SAXS data from unloaded (●) and drug-loaded (●) LNCs fitted with (a) sphere model; (b) core-shell sphere model. Solid lines represent the best fits to the experimental scattering data. Error bars are almost within the size of the symbols for most of the scattering data at low *Q* values.

5.4.2 Small-angle neutron scattering of LNCs

Based on the observations from SAXS data analysis, a core-shell sphere model was fitted to the SANS scattering data and the fits are presented in Figure 26 for unloaded and drug-loaded h-LNCs and d-LNCs prepared in H_2O and D_2O. Also, a schematic model is presented in Figure 25 about how LNCs with differences in core components and in dispersion medium (H_2O or D_2O) would contrast in neutron scattering, based on a core-shell sphere model. Based on the contrast, either the core or the shell or both the core and the shell can be seen as highlighted.

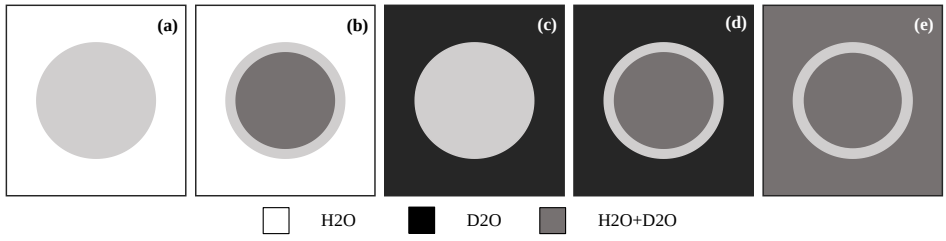

Figure 25. Schematic depiction of contrast variation in the core and in the dispersion medium of LNCs. (a) original LNCs in H_2O; (b) d-LNCs in H_2O; (c) original LNCs in D_2O; (d) d-LNCs in D_2O; (e) d-LNCs in contrast matched dispersion medium with a mixture of H_2O and D_2O. At each contrast, both unloaded and drug-loaded particles were prepared and measured for SANS.

For both unloaded and drug-loaded particles, best fits from a core-shell sphere model were obtained as seen in Figure 26. A perfect fit was not obtained from the experimental scattering data at Q = 0.2-0.8 nm^{-1}. The deviations can be due to many reasons one of which is the soft nature of the particles where a clear boundary is lacking between the core and the shell of the particles. Deviations were however judged not to have a significant impact on the outcomes of the data fitting. A higher scattering intensity was evident for drug-loaded LNCs compared to unloaded LNCs, suggesting an overall increase in particle size with drug loading. Besides this, no major changes were noticed in scattering intensity profiles upon drug loading leading to our conclusion that the particles show a core-shell structure both with and without drug loading. From the best fits, the core radius of unloaded and drug-loaded particles was found to be 20.0 ± 0.9 nm and 20.2 ± 0.6 nm and this indicates that the core of the particles remained unchanged regardless of presence or absence of loaded drug.

For resolving the shell region of the particles, SLD of the shell was allowed to vary in the software. While fitting the SANS data for unloaded LNCs, a marked increase in SLD from a calculated value of 0.13 to 3.3 was noticed. This happened mainly due to the hydration of the shell with molecules of D_2O which have higher neutron contrast, when D_2O was used as a dispersion medium. Based on the fitting, the shell thickness was found to be <1.5 nm for unloaded LNCs. In case of drug-loaded LNCs, SLD of the shell was observed to be at 4.5, indicating an even higher hydration compared to the shell of unloaded particles. This additional increase in shell hydration might be explained by a predominant localization of drug on the particle surface that possibly form hydrogen bonds with the dispersion medium which is D_2O. This surface localization of drug was further supported by the particles acquiring a negative surface charge upon drug loading, as described earlier. This surface charge may lead to some sort of a repulsion between surfactant monomers thereby these monomers may have a different and a disordered orientation around the particle core as depicted in Figure 27. These combined effects have led to an increase in the thickness of the shell to around ~2 ± 0.5 nm for drug-loaded particles.

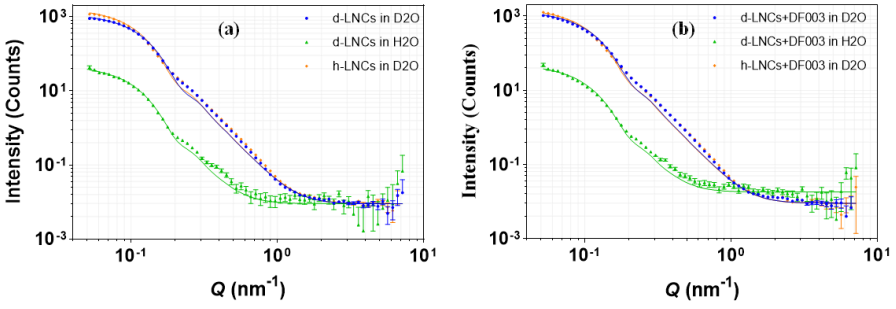

Figure 26. SANS scattering data from (a) unloaded LNCs, and (b) DF003-loaded LNCs prepared with varied contrast in the core and in the dispersion medium. Solid lines represent the best fits to the experimental scattering data. Error bars are almost within the size of the symbols for most of the scattering data.

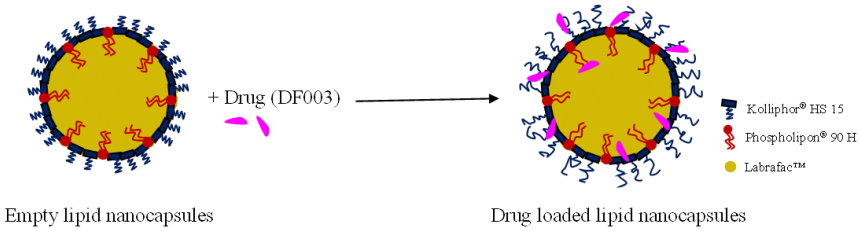

Figure 27. Proposed structure of empty and DF003-loaded lipid nanocapsules. Drug-loaded LNCs are proposed to have a higher disorder in the way the surfactants are packed around the oily core by the presence of the drug.

Table 12. Structural information about the LNCs as determined by SAXS, SANS, and DLS techniques.

Parameter	Unloaded LNCs	DF003-loaded LNCs
P(r) analysis of Small-angle X-ray scattering (SAXS) data		
R_g (nm)	17.3 ± 0.09	15.8 ± 0.05
D_{max} (nm)	49 ± 0.5	46 ± 0.5
Shape model analysis of Small-angle X-ray scattering (SAXS) data		
Core radius (nm)	21.7 ± 0.2	18.5 ± 0.2
Shell thickness (nm)	2.6 ± 0.1	3.6 ± 0.1
Total radius (nm)	24.3 ± 0.3	22.1 ± 0.3
Volume fraction[a]	0.092	0.092
Polydispersity	0.20	0.35
$\chi 2$	2.4	3.7
Small-angle neutron scattering (SANS)		
Core radius (nm)	20.0 ± 0.9	20.2 ± 0.6
Shell thickness (nm)	≤ 1.5	~ 2 ± 0.5
Total radius (nm)	21.5 ± 0.9	22.2 ± 1.1
Shell hydration (%)	50	70
Volume fraction[b]	0.009	0.009
Polydispersity	0.20	0.25
SLD of shell	3.3	4.5
Dynamic light scattering (DLS)		
Hydrodynamic radius (nm)	30.0 ± 1.0	36.0 ± 1.0
Polydispersity	0.04 ± 0.02	0.07 ± 0.01
Zeta potential (mV)	-3.7 ± 1.6	-13.6 ± 0.8

[a]Volume fractions estimated using a core–shell sphere model and the values are in close approximation to a theoretical volume fraction of 0.062. [b]Volume fractions estimated using a core–shell sphere model and the values are in close approximation to a theoretical volume fraction of 0.0062.

Combined analysis of the information obtained from SAXS, and SANS measurements increased the understanding and helped resolve the internal structure of LNCs. Structural parameters obtained from SAXS and SANS measurements of the LNCs are summarized in Table 12. Both the techniques supported the presence of a core-shell structure in the LNC particles with the shell predominantly composed of a combination of Kolliphor® and phospholipid as they are associated together at the interface of the particle and the surrounding medium. Although there is a significant evidence of presence of shell and its increased thickness in presence of drug, precise measurements of shell thickness were rather challenging owing to the dynamic and interfacial nature of the shell components and polydispersity associated with the actual particles. Previous findings by Heurtault, B et al., confirms that Kolliphor® orients towards the aqueous phase, and that the shell constitutes only a sufficient rigidity to the particle to prevent its opening and releasing the contents of the core (Heurtault et al., 2003). Further, the higher shell hydration led to a weaker signal from the shell and therefore an uncertainty in the accurate shell thickness parameter.

Scattering data were collected for samples measured at different particle concentrations (1.2-6.2 mg/mL), and at different temperatures of 5, 25, and 37 °C Neither the concentration nor the temperature did have any noticeable impact of the collected scattering data, indicating that the particle concentration and temperature do not influence the structure of the LNCs to a large extent. Similarly, LNCs were diluted with D_2O containing NaCl at a final concentration of 5 mg/mL and SANS measurements were performed. The collected data did not show any sign of changes in scattering pattern and thereby indicating a lack of instability of these particles. Scattering data generated at different conditions mentioned above can be found in **Paper II**.

5.5 *Ex vivo* investigation of LNCs

To determine the suitability of LNCs as drug carriers for retinal applications, the LNC formulation with selected composition from the work described in **Paper I** was chosen for further characterization. For this, various *ex vivo* and *in vitro* techniques were utilized to understand the behavior of this formulation.

In vivo experiments that use for e.g. rabbits for testing intravitreal drug delivery systems (Bakri et al., 2007; Del Amo & Urtti, 2015) are expensive and often associated with ethical considerations especially for preliminary screening during early formulation work. Apart from this rabbit eyes contain only around 1.5 mL of vitreous which is significantly lower than the human vitreous of approximately 4 mL (Del Amo et al., 2015). Here, porcine eyeballs serve as a better alternative to *in vivo* formulation testing. The use of porcine eyeballs carries several advantages such as possibility of obtaining fast results about formulation behavior, reducing the animal use, wider availability, and low cost (Christensen et al., 2021; Heikkinen et al., 2018). Thus, in a recent report by Christensen et al., the authors have demonstrated the usefulness of porcine eyeballs for

pharmacokinetic measurements using intravitreally administered liposomal drug delivery system (Christensen et al., 2021). However, despite various advantages, isolated porcine eyeballs have certain limitations including tissue degradation with visual signs of degradation after 5-7 days even under sterile conditions. Topical ocular permeability and intraocular bio-distribution of LNCs were, therefore, tested using excised porcine eye tissues and the whole intact porcine eyes, respectively and were used within approximately 4 h following their excision. Yet, the data generated in this work using porcine eyes still showed considerable variation of up to 100 % for 5-6 experiments. This may be due to experimental differences in individual intravitreal injections in addition to the differences in the porcine eyes themselves. Similar variations were also reported elsewhere in literature (Eriksen et al., 2017).

The bio-distribution of LNCs in the eye would lead to an accumulation of particles at different tissues and this distribution is dependent on particle properties that define their affinity to different ocular tissues. Although various reports suggest the biocompatible nature of LNCs, it is imperative to study their toxicity and the maximum tolerable concentration at the retinal level which is the target tissues in the present work. Hence, toxicity measurements were performed on the retinal explant cultures obtained from the eyes of heathy mice (wild type: *wt*).

Finally, drug-loaded LNCs were tested for their efficacy against photoreceptor cell death using organotypic retinal explant cultures derived from the retinal degeneration mouse model, *rd1*. This *rd1* model is characterized by accumulation of cGMP leading to photoreceptor cell degeneration with preservation of all other retinal cell types (Arango-Gonzalez et al., 2014; Chang et al., 2002). Testing of DF003 loaded LNCs using this model would enable better understanding of the formulation efficacy in preserving the function of retinal photoreceptor cells.

5.5.1 Permeability testing on excised ocular tissues

Topical administration, as previously described in the introduction, is a non-invasive and patient-friendly ocular drug delivery technique, yet not an ideal route for retinal applications owing to the barrier properties imposed by cornea to the drug permeation. However, many reports suggests that lipid-based nanoformulations enhance the ocular penetration of drugs which are targeted for both anterior and posterior chambers when administered topically to the eye (Davis et al., 2014; Gaballa et al., 2020; Khalil et al., 2017; Lakhani et al., 2019; Navarro-Partida et al., 2021; Tatke et al., 2018). Thus, to understand the role of LNCs in enhancing the ocular penetration of DF003, permeability screening of free DF003 and DF003-loaded LNCs was conducted on both full-thickness cornea and conjunctiva-sclera-choroid-retina excised from fresh porcine eyeballs using Franz-diffusion cells (Pescina et al., 2015; Pescina et al., 2012). Permeability coefficients and the cumulative drug permeation are presented in Table 13 and Figure 28, respectively. From the data, the conjunctiva-sclera-choroid-retina was

found to be 4.6 and 3 times more permeable to free DF003 and DF003-loaded LNCs compared to permeation across full-thickness cornea. Moreover, the permeability of DF003 was found to be improved across both these tissues when formulated with LNCs compared to DF003 alone in solution.

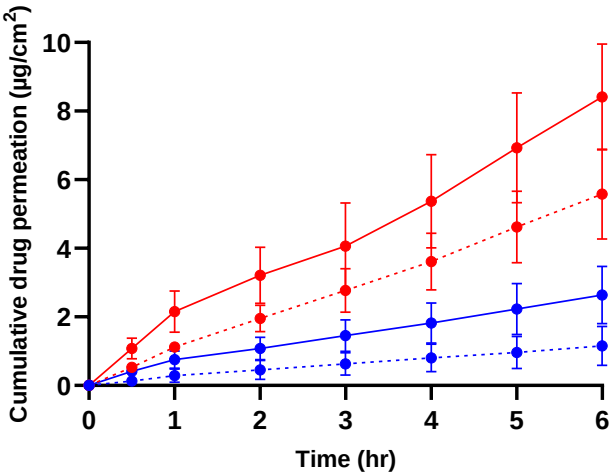

Figure 28. Cumulative amount permeated per area (µg/cm2, mean ± SD, n = 3) of CN03 (dashed lines) and drug-loaded LNCs (solid lines). Data in Blue indicates the permeation through full-thickness cornea and the data in Red indicates the permeation through conjunctiva-sclera-choroid-retina.

However, these permeability values were considerably lower in comparison to reported permeability of other ophthalmic drugs that were tested using a similar methodology (Table 13). In a recent study by Lorenzo-Soler et al. wherein 27 different compounds were tested for permeability in their free form and these drugs showed better permeability characteristics compared to that of DF003 (Table 13). This poorly permeable nature of DF003 suggests that the topical route of administration is not an efficient route for its delivery to the retinal photoreceptors. This led to the investigation of LNCs for their suitability for intravitreal administration.

Table 13. Permeability of DF003 and other ophthalmic drugs tissues derived from porcine eyeballs.

Compound	Application	Tissue permeability (cm/s)		Reference(s)
		Full-thickness cornea	Conjunctiva-sclera-choroid-retina	
Free DF003	cGMP analogue used in treatment of IRD.	$2.2 \pm 1.2 \times 10^{-8}$	$1.0 \pm 0.2 \times 10^{-7}$	Data from this thesis
DF003 loaded LNCs		$5.1 \pm 1.7 \times 10^{-8}$	$1.60 \pm 0.4 \times 10^{-7}$	
Dexamethasone	Glucocorticoid used in treatment of allergic reactions in the eye	$0.2 \pm 0.1 \times 10^{-6}$ - $7.6 \pm 1.2 \times 10^{-6}$	$1.0 \pm 0.2 \times 10^{-6}$	(Hahne et al., 2012; Juretić et al., 2018; Loch et al., 2012; Ramsay et al., 2018)
Propranolol	Beta-blockers used in the treatment of intraocular pressure	$1.5 \pm 1.4 \times 10^{-6}$ - $14.6 \pm 0.5 \times 10^{-6}$	$7.0 \pm 2.5 \times 10^{-6}$	(Pescina et al., 2015; Pescina et al., 2012; Ramsay et al., 2018)
Timolol maleate		$5.1 \pm 0.6 \times 10^{-6}$ - $10.7 \pm 2.1 \times 10^{-6}$	$1.3 \pm 0.4 \times 10^{-6}$	(Hahne et al., 2012; Juretić et al., 2018; Loch et al., 2012)
Library of compounds with varied molecular properties (n = 27)	Varied applications	$5.0 \pm 0.3 \times 10^{-6}$	$16.0 \pm 0.9 \times 10^{-6}$	Unpublished*

*Data reported as mean permeability values from 27 different compounds

5.5.2 Intraocular bio-distribution of LNCs

For studying the diffusion kinetics of LNCs in the vitreous, DiO-loaded LNCs were injected intravitreously into intact *ex vivo* porcine eyes. DiO is a hydrophobic, green fluorescence that enables the distribution studies using Fluorophotometry. Following the intravitreal injection, intensity plots were collected for up to 24 h post-injection and the area under the curve (AUC) for each time-point was plotted to follow the distribution of LNCs (Figure 29A). The measurements indicated an even distribution of the injected LNCs, and that the AUC at the site of injection was reduced to about 10 % of the AUC_{max}, which was observed at 2 h post-injection. This demonstrates that the movement of LNCs is unrestricted by the matrix properties of vitreous.

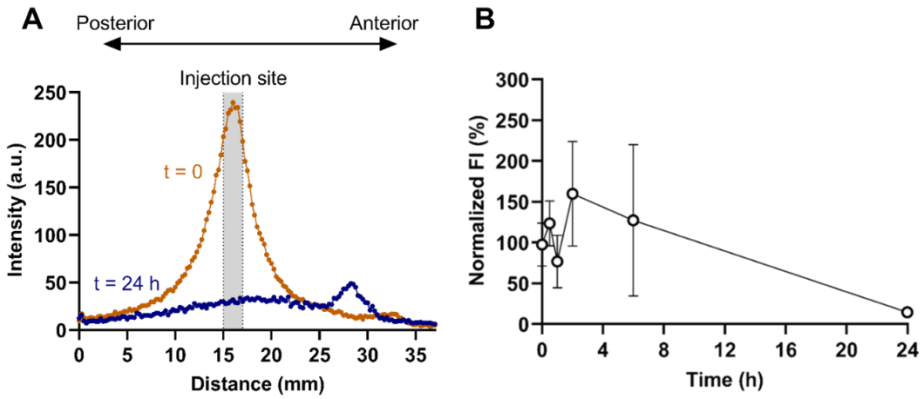

Figure 29. Intravitreal movement of LNCs as determined by Fluorophotometry. (A) Example profile of LNC-DiO signal from injected pig eyes at t = 0 (orange) and at t = 24 h (purple) along the axial length. The approximate positions of regions within the eye are labelled. (B) Area under the curve (AUC) at distinct time-points from 0 to 24 h. Data is presented as mean ± SD (n = 5 eyes).

At 24 h post-injection, injected eyes were sectioned and the fluorescent signal from different regions of the eyes was quantified. For comparison purpose, data was generated for DiO-loaded conventional POPC-liposomes prepared with 5 mol % 2 kDa PEG. From Figure 30, It can be seen that both the LNC and liposome systems were able to reach most of the ocular tissues and showed similar total fluorescence intensities 24 h after injection. Except for the ciliary body, the distribution data of different parts of the eye showed no statistically significant differences between LNCs and liposomes. However, distinctive differences were evidenced between the distribution of LNCs and liposomes in the ciliary body. LNCs showed a significantly higher accumulation at ciliary body than liposomes. This could be due to the presence of a well-defined PEG layer on the surface of liposomes that limits their uptake by the ciliary epithelium (Hatakeyama et al., 2013).

Within the retina, LNCs and liposomes appeared to show differences in their distribution pattern, although quantitatively these differences were statistically insignificant. DiO signal from LNCs was mostly observed around the vitreoretinal interface, whereas the DiO signal from liposomes was observed throughout the whole retina. Previously Tavakoli et al. showed an improved permeation of PEGylated liposomes across inner limiting membrane of the retina owing to the PEG layer (Tavakoli et al., 2020). Importantly, however, it should be noted that, since hydrophobic molecules were used as tracers, transfer of the tracer from the lipid carriers (both LNCs and liposomes) to hydrophobic biological membranes in the retina is possible. This transfer is likely to be higher for the lipids with a low phase transition temperature like POPC used in the liposomes in the present study. (Urquhart & Eriksen,

2019). In case of LNCs, as the DiO is encapsulated in the inner core of the LNC, the transfer will be less likely than for the liposomes.

Further, for both LNCs and liposomes, a fluorescence signal was evident in the lens. This may be due to the lipophilic nature of DiO, and is in accordance with the previous reports that suggested a higher affinity and permeation of lipophilic molecules into the lens (Heikkinen et al., 2019).

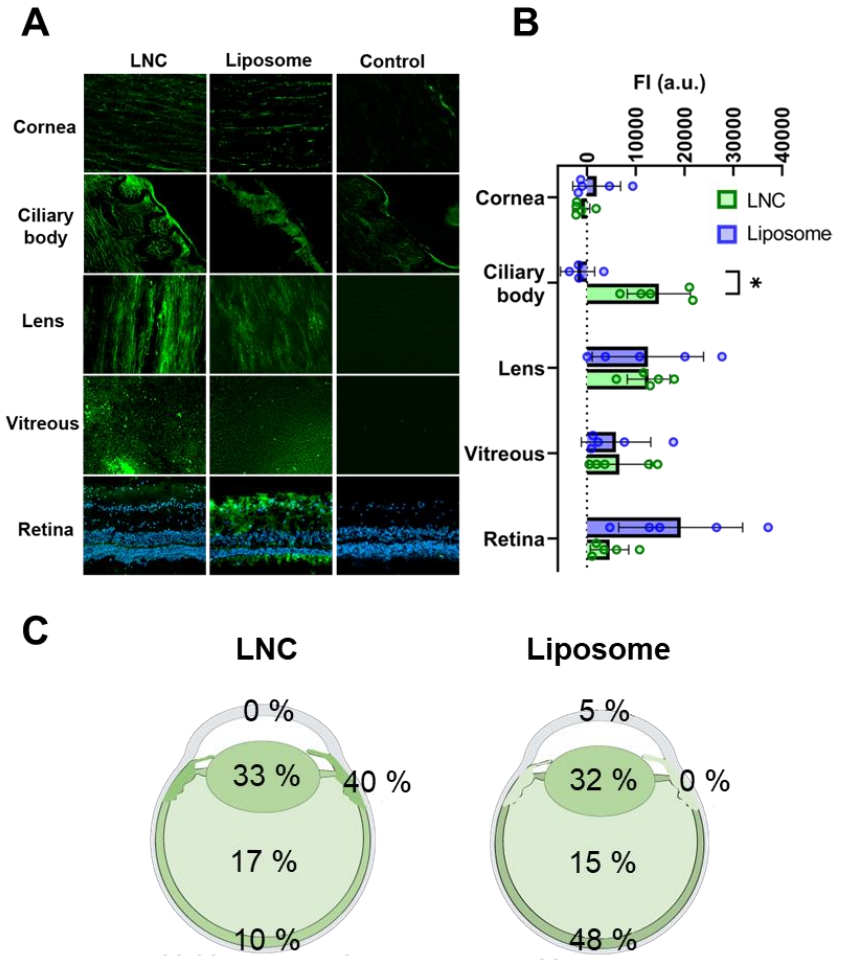

Figure 30. Bio-distribution of LNCs and liposomes after intravitreal administration in whole porcine eyes. A Microscopy images of different tissues from sections of porcine eyes 24 h after injection of either LNC/DiO formulation or liposome/DiO formulation or non-injected eyes (control). Scale bar = 50 µm. B Fluorescent intensities (FI) from relevant ocular tissues after injection of LNCs or liposomes. Negative value is due to subtracted with background signal. Results represent mean ± SD for n = 5, * $p \leq 0.05$. Data analysis: Two-way ANOVA with Šidák's multiple comparison test. C Schematics over the relative distribution in the pig eyes.

5.5.3 Retinal toxicity profile of LNCs

Retinal toxicity of LNCs was evaluated using the retinal explants derived from P9 *WT* mice. The retinal cultures themselves without added LNCs contained 2 % TUNEL-positive cells in the outer nuclear layer (ONL). Whereas the cell death in the inner nuclear layer (INL) was very low indicating that INL cells were less sensitive than the photoreceptors.

LNCs were found to be largely non-toxic to the retina and the toxicity is presented in Figure 31. It can be clearly noticed that the cultures tolerated LNCs at a concentration of 1 mg/mL. At a 5 mg/mL concentration an increased cell death was evident, although it was statistically insignificant. At a 10 mg/mL concentration, cell death became statistically significant. In all these instances, cell death deeper into the retinal tissue in the INL showed no change compared to untreated explants.

Liposomes on the other hand were found to trigger significant cell death at a concentration of 5 mg/mL under similar study conditions, as reported by Christensen et al. (Christensen et al., 2021). These differences in toxicity may be partly attributed to their extent of retinal distribution. LNCs which showed a poor retinal uptake were more tolerated compared to liposomes that distributed across the whole retina (Figure 30). In addition to the liposomes, many other formulations like albumin-based nanoparticles, and PLGA-based nanoparticles showed better retinal permeability compared to LNCs reported in this study (Bourges et al., 2003; Camelo et al., 2007; Christensen et al., 2021; Hyuncheol Kim et al., 2009; Heebeom Koo et al., 2012; Lee et al., 2017).

It is important to consider that in the current studies the retina was directly exposed to the LNCs. *In vivo*, the particles will be injected intravitreously and diluted in the vitreous and only a fraction of particles would reach the retina. Considering the volume of human vitreous which is around 4-5 mL (Azhdam et al., 2020), a dose of 50 µL of the formulation at a concentration of 80 mg/mL would give around 1 mg/mL of LNCs at the retinal level, assuming an even distribution in the eye. However, the present study showed that only ~ 10 % of the injected formulation at the retina (Figure 30). Thus, based on the current data on cell death, the LNCs formulation may be well tolerated for IVT injection at a much higher concentration than 1 mg/mL.

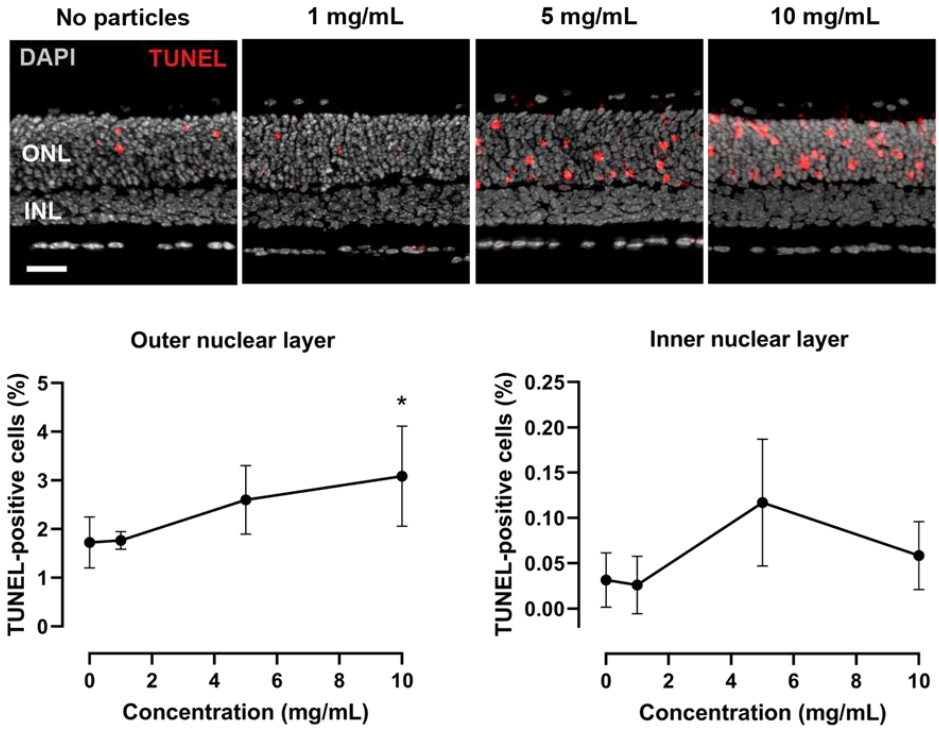

Figure 31. Retinal toxicity profile of LNCs. Retinal explant cultures derived from *WT* mice were incubated with LNCs at different concentrations for 4 days. The TUNEL-assay (red) was employed to label dying cells in tissue sections. DAPI (gray) was used as nuclear counterstain to visualize the ONL and the INL. The number of TUNEL-positive cells in either layer was analyzed. Notice that the scales between the two graphs are very different, meaning that the majority of cell death came from the photoreceptors in the ONL. Scale bar = 50 µm. Results represent mean ± SD for n = 4-5 animals. * $p \leq 0.05$. Statistical analysis: One-way ANOVA with Tukey's post-hoc test.

5.5.4 Treatment efficacy of free drug and drug-loaded LNCs

Efficacy testing of DF003 and DF003-loaded LNCs was performed using the retinal explants obtained from *rd1* mouse model. *rd1* mouse model is characterized by an increased photoreceptor cell death compared to *WT* type. Upon treatment of *rd1* explants with free DF003 and DF003-loaded LNCs, a significant reduction (~ 25 %) in cell death was observed (Figure 32). This protective effect of free DF003 was previously showed by Vighi et al. (Vighi et al., 2018). In case of treatment with the formulation where the drug is associated with the particles, the release of DF003 from LNCs was fast enough to have a similar effect on the *rd1* model, although not statistically different to that of free DF003. Even though the LNCs showed poor retinal uptake as shown in Figure 30, they elicited a strong protective effect on photoreceptor cells due to the release of DF003. Thus, the LNCs may not need to be taken up by the retina to allow the loaded drug to exert its effect. Since, retinal uptake is a route of

elimination from the vitreous (Del Amo et al., 2017), a poor retinal uptake of LNCs could be advantageous in prolonging their vitreous exposure. Thus, the main benefit of the LNCs as an intraocular drug delivery system may be their ability to provide a drug depot and sustain the release of DF003 in the vitreous over a prolonged period thereby extending its pharmacological effect.

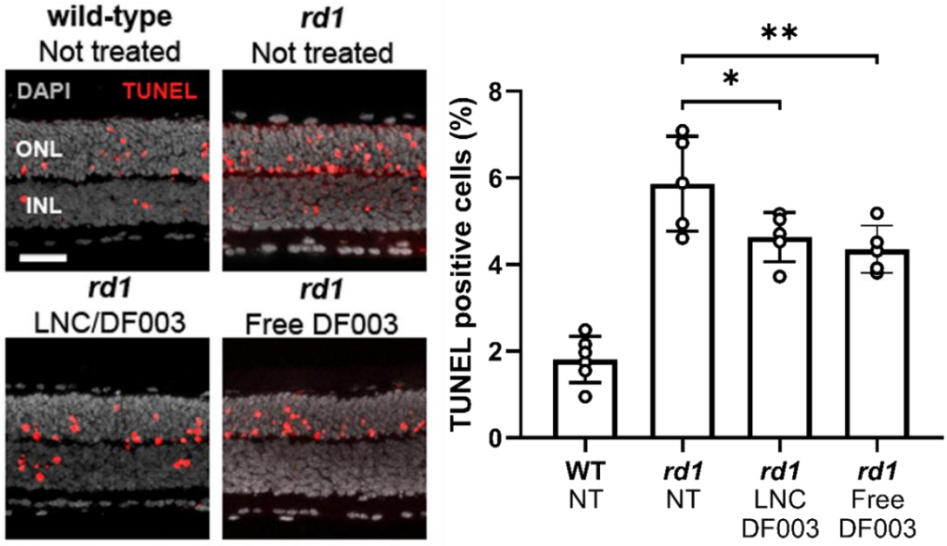

Figure 32. Treatment efficacy of the LNC/drug formulation. Retinal explant cultures derived from the *rd1* mouse model were treated with the retinoprotective drug CN03, either in a particle-free solution (Free CN03) or encapsulated in the LNCs (LNC/CN03). In both cases, drug concentration in the treatment solutions was 200 µM, and all were applied on top of the retinal culture. Assuming equal distribution in the culture medium, the final concentration was 4 µM. Treatment period was from P7 to P11. A TUNEL-assay (red) was used to detect dying cells in cross-sections of the cultures, and DAPI (gray) was used to localize the outer nuclear layer (ONL) and inner nuclear layer (INL). The amount of dying cells (TUNEL-positive cells) in the ONL was counted to assess treatment effects. Scale bar = 50 µm. Results represent mean ± SD for n = 5-6 animals. * $p \leq 0.05$, ** $p \leq 0.01$ compared to the *rd1* not treated (NT) condition. Statistical analysis: One-way ANOVA with Tukey's post-hoc test.

6 Summary and conclusions

This dissertation focused on the suitability evaluation of LNCs as a drug carrier system for retinal applications and covers various studies i.e., formulation development with a novel cGMP analogue, DF003; characterization of resulting nanoparticles for their *in vitro* behaviour including their structural investigation using X-ray and neutron based techniques; *ex vivo* and *in vitro* evaluation using porcine eye balls, and retinal explants derived from healthy and diseased mouse models to check for the performance of LNCs and their toxicity.

This work started with the preparation of LNCs using the novel drug molecule, DF003 that has demonstrated protective effects against photoreceptor cell death. LNCs with varied composition were prepared using a phase inversion methodology to understand the effect of compositional changes on the physico-chemical properties of the resulting formulations. These studies demonstrated the dominant role of Kolliphor®, a predominantly hydrophilic surfactant, in determining the size and entrapment efficiency of the resulting formulations. Drug-loaded LNCs which were also made using a similar process showed a relatively larger particle size (when measured using DLS) and a more negative zeta potential compared to the unloaded LNCs. Both the formulations showed a similar morphology when measured with cryo-TEM except that the PDI of drug containing LNCs was relatively higher than the unloaded LNCs. Further the formulations demonstrated a prolonged drug release over 6 days despite the hydrophilic nature of the drug.

In a continuation, LNCs were upscaled up to 10 L volume scale using a phase inversion process and the resulted LNCs showed comparable size and PDI to that of LNCs prepared at lab-scale volumes, demonstrating that the phase inversion process is capable of being upscaled to higher volume scales. Furthermore, the formulation was found to be stable for at least 6 months. Freeze-drying of LNCs was performed using sucrose, trehalose and raffinose as cryo-protectants. Freeze-dried formulations upon reconstitution showed considerably different characteristics compared to the original formulations. The level of protection of LNCs towards the freeze-drying induced stresses was higher when using sucrose over other tested cryoprotectants.

Further, structural investigation of the LNCs using x-ray and neutron scattering techniques (SAXS and SANS) revealed the presence of a core-shell structure in the nanoparticles, which was well retained even after drug loading. Observations from the small-angle scattering techniques, combined with zeta potential measurements confirmed the surface localization of drug in LNCs.

The suitability of LNCs for ocular administration was also evaluated using a combination of *in vitro* and *ex vivo* techniques. Permeability of drug upon topical administration of drug-loaded LNCs was considerably lower, although the permeability enhancing effect of LNCs was evident. Upon IVT administration in porcine eyeballs, LNCs distributed across the vitreous and most of the ocular tissues. The ocular distribution of LNCs was comparable to that of liposomes studied under similar conditions. In addition to the retina, LNCs were found to be permeated more towards the ciliary body. Further, the LNCs demonstrated a protective effect on retinal photoreceptor cells of *rd1* mouse model while being safe and non-toxic.

This work significantly adds to furthering the understanding on LNCs as a drug carrier for the treatment of various diseases. In conclusion, LNCs in combination with loaded drug, DF003 can be a potentially viable system in the treatment of RD.

References

Abbott, M., Harvey, A., Perez, G. V., & Theodorou, M. (2013). Biological processing in oscillatory baffled reactors: operation, advantages and potential. *Interface focus*, *3*(1), 20120036.

Abdel-Mottaleb, M. M., Neumann, D., & Lamprecht, A. (2011). Lipid nanocapsules for dermal application: a comparative study of lipid-based versus polymer-based nanocarriers. *European Journal of Pharmaceutics and Biopharmaceutics*, *79*(1), 36-42.

Abdelwahed, W., Degobert, G., & Fessi, H. (2006). Investigation of nanocapsules stabilization by amorphous excipients during freeze-drying and storage. *European Journal of Pharmaceutics and Biopharmaceutics*, *63*(2), 87-94.

Abdelwahed, W., Degobert, G., Stainmesse, S., & Fessi, H. (2006). Freeze-drying of nanoparticles: formulation, process and storage considerations. *Advanced drug delivery reviews*, *58*(15), 1688-1713.

Abrishami, M., Ganavati, S. Z., Soroush, D., Rouhbakhsh, M., Jaafari, M. R., & Malaekeh-Nikouei, B. (2009). Preparation, characterization, and in vivo evaluation of nanoliposomes-encapsulated bevacizumab (avastin) for intravitreal administration. *Retina*, *29*(5), 699-703.

Agrahari, V., Agrahari, V., Mandal, A., Pal, D., & Mitra, A. K. (2017). How are we improving the delivery to back of the eye? Advances and challenges of novel therapeutic approaches. *Expert Opinion on Drug Delivery*, *14*(10), 1145-1162.

Albanawany, N. M., Samy, D. M., Zahran, N., El-Moslemany, R. M., Elsawy, S. M., & Abou Nazel, M. W. (2022). Histopathological, physiological and biochemical assessment of resveratrol nanocapsules efficacy in bleomycin-induced acute and chronic lung injury in rats. *Drug Delivery*, *29*(1), 2592-2608.

Ali, M. E., & Lamprecht, A. (2017). Spray freeze drying as an alternative technique for lyophilization of polymeric and lipid-based nanoparticles. *International journal of pharmaceutics*, *516*(1-2), 170-177.

Allard, E., Passirani, C., Garcion, E., Pigeon, P., Vessières, A., Jaouen, G., & Benoit, J.-P. (2008). Lipid nanocapsules loaded with an organometallic tamoxifen derivative as a novel drug-carrier system for experimental malignant gliomas. *Journal of controlled release*, *130*(2), 146-153.

Almgren, M., Edwards, K., & Karlsson, G. (2000). Cryo transmission electron microscopy of liposomes and related structures. *Colloids and Surfaces A: Physicochemical and Engineering Aspects*, *174*(1-2), 3-21.

Amara, R. O., Ramadan, A. A., El-Moslemany, R. M., Eissa, M. M., El-Azzouni, M. Z., & El-Khordagui, L. K. (2018). Praziquantel–lipid nanocapsules: an oral

nanotherapeutic with potential Schistosoma mansoni tegumental targeting. *International journal of nanomedicine*, *13*, 4493.

Anton, N., & Saulnier, P. (2013). Adhesive water-in-oil nano-emulsions generated by the phase inversion temperature method. *Soft Matter*, *9*(28), 6465-6474.

Anton, N., Saulnier, P., Beduneau, A., & Benoit, J.-P. (2007). Salting-out effect induced by temperature cycling on a water/nonionic surfactant/oil system. *The Journal of Physical Chemistry B*, *111*(14), 3651-3657.

Aparicio-Blanco, J., Sebastián, V., Rodríguez-Amaro, M., García-Díaz, H. C., & Torres-Suárez, A. I. (2019). Size-tailored design of highly monodisperse lipid nanocapsules for drug delivery. *Journal of Biomedical Nanotechnology*, *15*(6), 1149-1161.

Arango-Gonzalez, B., Trifunović, D., Sahaboglu, A., Kranz, K., Michalakis, S., Farinelli, P., Koch, S., Koch, F., Cottet, S., & Janssen-Bienhold, U. (2014). Identification of a common non-apoptotic cell death mechanism in hereditary retinal degeneration. *PLoS One*, *9*(11), e112142.

Ashour, A. A., El-Kamel, A. H., Abdelmonsif, D. A., Khalifa, H. M., & Ramadan, A. A. (2021). Modified Lipid Nanocapsules for Targeted Tanshinone IIA Delivery in Liver Fibrosis. *International journal of nanomedicine*, *16*, 8013.

Ashour, A. A., Ramadan, A. A., Abdelmonsif, D. A., & El-Kamel, A. H. (2020). Enhanced oral bioavailability of Tanshinone IIA using lipid nanocapsules: formulation, in-vitro appraisal and pharmacokinetics. *International journal of pharmaceutics*, *586*, 119598.

Azhdam, A. M., Goldberg, R. A., & Ugradar, S. (2020). In vivo measurement of the human vitreous chamber volume using computed tomography imaging of 100 eyes. *Translational Vision Science & Technology*, *9*(1), 2-2.

Bakri, S. J., Snyder, M. R., Reid, J. M., Pulido, J. S., Ezzat, M. K., & Singh, R. J. (2007). Pharmacokinetics of intravitreal ranibizumab (Lucentis). *Ophthalmology*, *114*(12), 2179-2182.

Balguri, S. P., Adelli, G. R., & Majumdar, S. (2016). Topical ophthalmic lipid nanoparticle formulations (SLN, NLC) of indomethacin for delivery to the posterior segment ocular tissues. *European Journal of Pharmaceutics and Biopharmaceutics*, *109*, 224-235.

Barras, A., Mezzetti, A., Richard, A., Lazzaroni, S., Roux, S., Melnyk, P., Betbeder, D., & Monfilliette-Dupont, N. (2009). Formulation and characterization of polyphenol-loaded lipid nanocapsules. *International journal of pharmaceutics*, *379*(2), 270-277.

Battaglia, L., Serpe, L., Foglietta, F., Muntoni, E., Gallarate, M., Del Pozo Rodriguez, A., & Solinis, M. A. (2016). Application of lipid nanoparticles to ocular drug delivery. *Expert Opinion on Drug Delivery*, *13*(12), 1743-1757.

Belhadj, S., Tolone, A., Christensen, G., Das, S., Chen, Y., & Paquet-Durand, F. (2020). Long-Term, Serum-Free Cultivation of Organotypic Mouse Retina Explants with Intact Retinal Pigment Epithelium. *Journal of Visualized Experiments*. https://doi.org/https://doi.org/10.3791/61868

Bellare, J. R., Davis, H., Scriven, L., & Talmon, Y. (1988). Controlled environment vitrification system: an improved sample preparation technique. *Journal of electron microscopy technique*, *10*(1), 87-111.

Bianchi, P., Williams, J. D., & Kappe, C. O. (2020). Oscillatory flow reactors for synthetic chemistry applications. *Journal of Flow Chemistry*, *10*(3), 475-490.

Bourges, J.-L., Gautier, S. E., Delie, F., Bejjani, R. A., Jeanny, J.-C., Gurny, R., BenEzra, D., & Behar-Cohen, F. F. (2003). Ocular drug delivery targeting the retina and retinal pigment epithelium using polylactide nanoparticles. *Investigative ophthalmology & visual science*, *44*(8), 3562-3569.

Camelo, S., Lajavardi, L., Bochot, A., Goldenberg, B., Naud, M., Fattal, E., Behar-Cohen, F., & de Kozak, Y. (2007). Ocular and systemic bio-distribution of rhodamine-conjugated liposomes loaded with VIP injected into the vitreous of Lewis rats. *Molecular vision*, *13*, 2263.

Candau, F., & Ottewill, R. H. (1989). *Scientific methods for the study of polymer colloids and their applications* (Vol. 303). Springer.

Chang, B., Hawes, N., Hurd, R., Davisson, M., Nusinowitz, S., & Heckenlively, J. (2002). Retinal degeneration mutants in the mouse. *Vision research*, *42*(4), 517-525.

Chen, C., Han, D., Cai, C., & Tang, X. (2010). An overview of liposome lyophilization and its future potential. *Journal of controlled release*, *142*(3), 299-311.

Chen, T.-C., Huang, D.-S., Lin, C.-W., Yang, C.-H., Yang, C.-M., Wang, V. Y., Lin, J.-W., Luo, A. C., Hu, F.-R., & Chen, P.-L. (2021). Genetic characteristics and epidemiology of inherited retinal degeneration in Taiwan. *NPJ genomic medicine*, *6*(1), 1-8.

Chetoni, P., Burgalassi, S., Monti, D., Tampucci, S., Tullio, V., Cuffini, A. M., Muntoni, E., Spagnolo, R., Zara, G. P., & Cavalli, R. (2016). Solid lipid nanoparticles as promising tool for intraocular tobramycin delivery: Pharmacokinetic studies on rabbits. *European Journal of Pharmaceutics and Biopharmaceutics*, *109*, 214-223.

Chizzolini, M., Galan, A., Milan, E., Sebastiani, A., Costagliola, C., & Parmeggiani, F. (2011). Good epidemiologic practice in retinitis pigmentosa: from phenotyping to biobanking. *Current genomics*, *12*(4), 260-266.

Chouchou, A., Aubert-Pouëssel, A., Dorandeu, C., Zghaib, Z., Cuq, P., Devoisselle, J.-M., Bonnet, P.-A., Bégu, S., & Deleuze-Masquefa, C. (2017). Lipid nanocapsules formulation and cellular activities evaluation of a promising anticancer agent: EAPB0503. *International journal of pharmaceutical investigation*, *7*(4), 155.

Christensen, G., Barut, L., Urimi, D., Schipper, N., & Paquet-Durand, F. (2021). Investigating Ex Vivo Animal Models to Test the Performance of Intravitreal Liposomal Drug Delivery Systems. *Pharmaceutics*, *13*(7), 1013.

Clavreul, A., Roger, E., Pourbaghi-Masouleh, M., Lemaire, L., Tétaud, C., & Menei, P. (2018). Development and characterization of sorafenib-loaded lipid nanocapsules for the treatment of glioblastoma. *Drug Delivery*, *25*(1), 1756-1765.

Cross, N., van Steen, C., Zegaoui, Y., Satherley, A., & Angelillo, L. (2022). Current and Future Treatment of Retinitis Pigmentosa. *Clinical Ophthalmology*, *16*, 2909-2921.

Davis, B. M., Normando, E. M., Guo, L., Turner, L. A., Nizari, S., O'Shea, P., Moss, S. E., Somavarapu, S., & Cordeiro, M. F. (2014). Topical delivery of Avastin to the posterior segment of the eye in vivo using annexin A5-associated liposomes. *Small*, *10*(8), 1575-1584.

Degobert, G., & Aydin, D. (2021). Lyophilization of nanocapsules: instability sources, formulation and process parameters. *Pharmaceutics*, *13*(8), 1112.

Del Amo, E. M., Rimpelä, A.-K., Heikkinen, E., Kari, O. K., Ramsay, E., Lajunen, T., Schmitt, M., Pelkonen, L., Bhattacharya, M., & Richardson, D. (2017). Pharmacokinetic aspects of retinal drug delivery. *Progress in retinal and eye research*, *57*, 134-185.

Del Amo, E. M., & Urtti, A. (2015). Rabbit as an animal model for intravitreal pharmacokinetics: Clinical predictability and quality of the published data. *Experimental eye research*, *137*, 111-124.

Del Amo, E. M., Vellonen, K.-S., Kidron, H., & Urtti, A. (2015). Intravitreal clearance and volume of distribution of compounds in rabbits: In silico prediction and pharmacokinetic simulations for drug development. *European Journal of Pharmaceutics and Biopharmaceutics*, *95*, 215-226.

Di Cola, E., Grillo, I., & Ristori, S. (2016). Small angle X-ray and neutron scattering: powerful tools for studying the structure of drug-loaded liposomes. *Pharmaceutics*, *8*(2), 10.

Ding, B., Chen, H., Wang, C., Zhai, Y., & Zhai, G. (2013). Preparation and in vitro evaluation of apigenin loaded lipid nanocapsules. *Journal of nanoscience and nanotechnology*, *13*(10), 6546-6552.

Ding, B., Chen, P., Kong, Y., Zhai, Y., Pang, X., Dou, J., & Zhai, G. (2014). Preparation and evaluation of folate-modified lipid nanocapsules for quercetin delivery. *Journal of Drug Targeting*, *22*(1), 67-75.

Dos Santos, G. A., Ferreira-Nunes, R., Dalmolin, L. F., dos Santos Ré, A. C., Anjos, J. L. V., Mendanha, S. A., Aires, C. P., Lopez, R. F., Cunha-Filho, M., & Gelfuso, G. M. (2020). Besifloxacin liposomes with positively charged additives for an improved topical ocular delivery. *Scientific reports*, *10*(1), 1-18.

Doucet, M. C., Jae Hie; Alina, Gervaise; Attala, Ziggy; Bakker, Jurrian; Bouwman, Wim; Butler, Paul; Campbell, Kieran; Cooper-Benun, Torin; Durniak, Celine; Forster, Laura; Gonzales, Miguel; Heenan, Richard; Jackson, Andrew; King, Stephen; Kienzle, Paul; Krzywon, Jeff; Nielsen, Torben; O'Driscoll, Lewis; Potrzebowski, Wojciech; Prescott, Stewart; Ferraz Leal, Ricardo; Rozycko, Piotr; Snow, Tim; Washington, Adam. (2020). *SasView version 5.0.3. Zenodo.* In

Dulieu, C., & Bazile, D. (2005). Influence of lipid nanocapsules composition on their aptness to freeze-drying. *Pharmaceutical research*, *22*, 285-292.

Duvvuri, S., Majumdar, S., & Mitra, A. K. (2003). Drug delivery to the retina: challenges and opportunities. *Expert opinion on biological therapy*, *3*(1), 45-56.

Ekström, P., Paquet-durand, F., Gaillard, P. J., Marigo, V., Genieser, H.-G., Rentsch, A., Trifunovic, D., & Tekgoz, A. S. (2019). *Targeted liposomal delivery of cGMP analogues*.

Eldesouky, L. M., El-Moslemany, R. M., Ramadan, A. A., Morsi, M. H., & Khalafallah, N. M. (2021). Cyclosporine lipid nanocapsules as thermoresponsive gel for dry eye management: promising corneal mucoadhesion, biodistribution and preclinical efficacy in rabbits. *Pharmaceutics*, *13*(3), 360.

Eriksen, A. Z., Brewer, J., Andresen, T. L., & Urquhart, A. J. (2017). The diffusion dynamics of PEGylated liposomes in the intact vitreous of the ex vivo porcine eye: a fluorescence correlation spectroscopy and biodistribution study. *International journal of pharmaceutics*, *522*(1-2), 90-97.

Farber, D. B., & Lolley, R. N. (1974). Cyclic guanosine monophosphate: elevation in degenerating photoreceptor cells of the C3H mouse retina. *Science*, *186*(4162), 449-451.

Farrar, G. J., Carrigan, M., Dockery, A., Millington-Ward, S., Palfi, A., Chadderton, N., Humphries, M., Kiang, A. S., Kenna, P. F., & Humphries, P. (2017). Toward an elucidation of the molecular genetics of inherited retinal degenerations. *Human Molecular Genetics*, *26*(R1), R2-R11.

Felton, L. A. (2012). Pharmaceutical Process Scale-Up, 3rd edition. *Drug Development and Industrial Pharmacy*, *38*(4), 512-512. https://doi.org/10.3109/03639045.2011.633523

Formica, M. L., Gamboa, G. U., Tártara, L., Luna, J., Benoit, J., & Palma, S. D. (2020). Triamcinolone acetonide-loaded lipid nanocapsules for ophthalmic applications. *International journal of pharmaceutics*, *573*, 118795.

Formica, M. L., Legeay, S., Bejaud, J., Montich, G. G., Gamboa, G. V. U., Benoit, J.-P., & Palma, S. D. (2021). Novel hybrid lipid nanocapsules loaded with a therapeutic monoclonal antibody—Bevacizumab—and Triamcinolone acetonide for combined therapy in neovascular ocular pathologies. *Materials Science and Engineering: C*, *119*, 111398.

Förster, T., Schambil, F., & Tesmann, H. (1990). Emulsification by the phase inversion temperature method: the role of self-bodying agents and the influence of oil polarity. *International journal of cosmetic science*, *12*(5), 217-227.

Gaballa, S. A., El Garhy, O. H., Moharram, H., & Abdelkader, H. (2020). Preparation and evaluation of cubosomes/cubosomal gels for ocular delivery of beclomethasone dipropionate for management of uveitis. *Pharmaceutical research*, *37*(10), 1-23.

Genieser, H.-G., Schwede, F., Rentsch, A. Rentsch, New equatorially modified polymer linked multimers of guanosine-3′, 5′-cyclic monophosphates. 2018, Google Patents.

Germain, M., Caputo, F., Metcalfe, S., Tosi, G., Spring, K., Åslund, A. K., Pottier, A., Schiffelers, R., Ceccaldi, A., & Schmid, R. (2020). Delivering the power of nanomedicine to patients today. *Journal of controlled release*, *326*, 164-171.

Ghasemiyeh, P., & Mohammadi-Samani, S. (2018). Solid lipid nanoparticles and nanostructured lipid carriers as novel drug delivery systems: Applications, advantages and disadvantages. *Research in pharmaceutical sciences*, *13*(4), 288.

Ghosh, R., Egelhaaf, S., & Rennie, A. (2000). *A computing guide for small-angle scattering experiments*. Inst. Max von Laue.

Gommes, C. J., Jaksch, S., & Frielinghaus, H. (2021). Small-angle scattering for beginners. *Journal of Applied Crystallography*, *54*(6).

Groo, A.-C., Matougui, N., Umerska, A., & Saulnier, P. (2018). Reverse micelle-lipid nanocapsules: a novel strategy for drug delivery of the plectasin derivate AP138 antimicrobial peptide. *International journal of nanomedicine*, *13*, 7565.

Gross, N., Ranjbar, M., Evers, C., Hua, J., Martin, G., Schulze, B., Michaelis, U., Hansen, L. L., & Agostini, H. T. (2013). Choroidal neovascularization reduced by targeted drug delivery with cationic liposome-encapsulated paclitaxel or targeted photodynamic therapy with verteporfin encapsulated in cationic liposomes. *Molecular vision*, *19*, 54.

Guimarães, D., Noro, J., Silva, C., Cavaco-Paulo, A., & Nogueira, E. (2019). Protective effect of saccharides on freeze-dried liposomes encapsulating drugs. *Frontiers in bioengineering and biotechnology*, *7*, 424.

Guinier, A., Fournet, G., & Yudowitch, K. L. (1955). Small-angle scattering of X-rays.

Hackley, V. A., Hackley, V., & Clogston, J. (2015). *Measuring the Size of Nanoparticles in Aqueous Media Using Batch-mode Dynamic Light Scattering: NIST-NCL Joint Assay Protocol, PCC-1 Version 1.2*.

Hahne, M., Zorn-Kruppa, M., Guzman, G., Brandner, J. M., Haltner-Ukomado, E., Wätzig, H., & Reichl, S. (2012). Prevalidation of a human cornea construct as an alternative to animal corneas for in vitro drug absorption studies. *Journal of pharmaceutical sciences*, *101*(8), 2976-2988.

Hatakeyama, H., Akita, H., & Harashima, H. (2013). The polyethyleneglycol dilemma: advantage and disadvantage of PEGylation of liposomes for systemic genes and nucleic acids delivery to tumors. *Biological and Pharmaceutical Bulletin*, *36*(6), 892-899.

Heikkinen, E. M., Auriola, S., Ranta, V.-P., Demarais, N. J., Grey, A. C., Del Amo, E. M., Toropainen, E., Vellonen, K.-S., Urtti, A., & Ruponen, M. (2019). Distribution of small molecular weight drugs into the porcine lens: studies on imaging mass spectrometry, partition coefficients, and implications in ocular pharmacokinetics. *Molecular pharmaceutics*, *16*(9), 3968-3976.

Heikkinen, E. M., Del Amo, E. M., Ranta, V.-P., Urtti, A., Vellonen, K.-S., & Ruponen, M. (2018). Esterase activity in porcine and albino rabbit ocular tissues. *European Journal of Pharmaceutical Sciences*, *123*, 106-110.

Hellsing, M. S., Rennie, A. R., Heenan, R. K., & Rogers, S. E. (2012). Structure of a large colloidal crystal–controlling orientation and three-dimensional order. *Rsc Advances*, *2*(18), 7091-7098.

Herdiana, Y., Wathoni, N., Shamsuddin, S., & Muchtaridi, M. (2021). Drug release study of the chitosan-based nanoparticles. *Heliyon*, e08674.

Heurtault, B., Saulnier, P., Pech, B., Benoıt, J., & Proust, J. (2003). Interfacial stability of lipid nanocapsules. *Colloids and Surfaces B: Biointerfaces*, *30*(3), 225-235.

Heurtault, B., Saulnier, P., Pech, B., Proust, J.-E., & Benoit, J.-P. (2002). A novel phase inversion-based process for the preparation of lipid nanocarriers. *Pharmaceutical research*, *19*(6), 875-880.

Hirsjärvi, S., Dufort, S., Gravier, J., Texier, I., Yan, Q., Bibette, J., Sancey, L., Josserand, V., Passirani, C., & Benoit, J.-P. (2013). Influence of size, surface coating and fine chemical composition on the in vitro reactivity and in vivo biodistribution of lipid nanocapsules versus lipid nanoemulsions in cancer models. *Nanomedicine: Nanotechnology, biology and medicine*, *9*(3), 375-387.

Huang, X., & Chau, Y. (2019). Intravitreal nanoparticles for retinal delivery. *Drug Discovery Today*, *24*(8), 1510-1523.

Huang, X., & Chau, Y. (2019). Intravitreal nanoparticles for retinal delivery. *Drug Discov Today*, *24*(8), 1510-1523. https://doi.org/10.1016/j.drudis.2019.05.005

Hureaux, J., Lacoeuille, F., Lagarce, F., Rousselet, M.-C., Contini, A., Saulnier, P., Benoit, J.-P., & Urban, T. (2017). Absence of lung fibrosis after a single pulmonary delivery of lipid nanocapsules in rats. *International journal of nanomedicine*, *12*, 8159.

Hureaux, J., Lagarce, F., Gagnadoux, F., Vecellio, L., Clavreul, A., Roger, E., Kempf, M., Racineux, J.-L., Diot, P., & Benoit, J.-P. (2009). Lipid nanocapsules: ready-to-use nanovectors for the aerosol delivery of paclitaxel. *European Journal of Pharmaceutics and Biopharmaceutics*, *73*(2), 239-246.

Huynh, N. T., Passirani, C., Saulnier, P., & Benoît, J.-P. (2009). Lipid nanocapsules: a new platform for nanomedicine. *International journal of pharmaceutics*, *379*(2), 201-209.

Hyland, L. L., Taraban, M. B., & Yu, Y. B. (2013). Using small-angle scattering techniques to understand mechanical properties of biopolymer-based biomaterials. *Soft Matter*, *9*(43), 10218-10228.

Juretić, M., Cetina-Čižmek, B., Filipović-Grčić, J., Hafner, A., Lovrić, J., & Pepić, I. (2018). Biopharmaceutical evaluation of surface active ophthalmic excipients using in vitro and ex vivo corneal models. *European Journal of Pharmaceutical Sciences*, *120*, 133-141.

Kang-Mieler, J. J., Dosmar, E., Liu, W., & Mieler, W. F. (2017). Extended ocular drug delivery systems for the anterior and posterior segments: biomaterial options and applications. *Expert Opinion on Drug Delivery*, *14*(5), 611-620.

Kang-Mieler, J. J., Osswald, C. R., & Mieler, W. F. (2014). Advances in ocular drug delivery: emphasis on the posterior segment. *Expert Opinion on Drug Delivery*, *11*(10), 1647-1660.

Kang-Mieler, J. J., Rudeen, K. M., Liu, W., & Mieler, W. F. (2020). Advances in ocular drug delivery systems. *Eye*, *34*(8), 1371-1379.

Kaur, I. P., & Kakkar, S. (2014). Nanotherapy for posterior eye diseases. *Journal of controlled release*, *193*, 100-112.

Khalil, R. M., Abdelbary, G. A., Basha, M., Awad, G. E., & El-Hashemy, H. A. (2017). Enhancement of lomefloxacin Hcl ocular efficacy via niosomal encapsulation: in vitro characterization and in vivo evaluation. *Journal of liposome research*, *27*(4), 312-323.

Kim, H., Robinson, S. B., & Csaky, K. G. (2009). Investigating the movement of intravitreal human serum albumin nanoparticles in the vitreous and retina. *Pharmaceutical research*, *26*(2), 329-337.

Kim, H., Robinson, S. B., & Csaky, K. G. (2009). Investigating the movement of intravitreal human serum albumin nanoparticles in the vitreous and retina. *Pharm Res*, *26*(2), 329-337. https://doi.org/10.1007/s11095-008-9745-6

Kim, H. M., & Woo, S. J. (2021). Ocular drug delivery to the retina: current innovations and future perspectives. *Pharmaceutics*, *13*(1), 108.

Kim, Y., Park, E. J., Kim, T. W., & Na, D. H. (2021). Recent progress in drug release testing methods of biopolymeric particulate system. *Pharmaceutics*, *13*(8), 1313.

Koo, H., Moon, H., Han, H., Na, J. H., Huh, M. S., Park, J. H., Woo, S. J., Park, K. H., Kwon, I. C., & Kim, K. (2012). The movement of self-assembled amphiphilic polymeric nanoparticles in the vitreous and retina after intravitreal injection. *Biomaterials*, *33*(12), 3485-3493.

Koo, H., Moon, H., Han, H., Na, J. H., Huh, M. S., Park, J. H., Woo, S. J., Park, K. H., Kwon, I. C., Kim, K., & Kim, H. (2012). The movement of self-assembled amphiphilic polymeric nanoparticles in the vitreous and retina after intravitreal injection. *Biomaterials*, *33*(12), 3485-3493. https://doi.org/10.1016/j.biomaterials.2012.01.030

Lacoeuille, F., Hindré, F., Moal, F., Roux, J., Passirani, C., Couturier, O., Calès, P., Le Jeune, J.-J., Lamprecht, A., & Benoit, J.-P. (2007). In vivo evaluation of lipid nanocapsules as a promising colloidal carrier for paclitaxel. *International journal of pharmaceutics*, *344*(1-2), 143-149.

Lai, S., Wei, Y., Wu, Q., Zhou, K., Liu, T., Zhang, Y., Jiang, N., Xiao, W., Chen, J., & Liu, Q. (2019). Liposomes for effective drug delivery to the ocular posterior chamber. *Journal of nanobiotechnology*, *17*(1), 1-12.

Lakhani, P., Patil, A., Wu, K.-W., Sweeney, C., Tripathi, S., Avula, B., Taskar, P., Khan, S., & Majumdar, S. (2019). Optimization, stabilization, and characterization of amphotericin B loaded nanostructured lipid carriers for ocular drug delivery. *International journal of pharmaceutics*, *572*, 118771.

Lamprecht, A., & Benoit, J.-P. (2006). Etoposide nanocarriers suppress glioma cell growth by intracellular drug delivery and simultaneous P-glycoprotein inhibition. *Journal of controlled release*, *112*(2), 208-213.

Lamprecht, A., Bouligand, Y., & Benoit, J.-P. (2002). New lipid nanocapsules exhibit sustained release properties for amiodarone. *Journal of controlled release*, *84*(1-2), 59-68.

Lamprecht, A., Bouligand, Y., & Benoit, J. P. (2002). New lipid nanocapsules exhibit sustained release properties for amiodarone. *J Control Release*, *84*(1-2), 59-68. https://doi.org/10.1016/s0168-3659(02)00258-4

Le Moal, B., Lepeltier, É., Rouleau, D., Le Visage, C., Benoit, J.-P., Passirani, C., Guicheux, J., Fusellier, M., & Clouet, J. (2022). Lipid nanocapsules for intracellular delivery of microRNA: A first step towards intervertebral disc degeneration therapy. *International journal of pharmaceutics*, *624*, 121941.

Lee, J., Goh, U., Lee, H.-J., Kim, J., Jeong, M., & Park, J.-H. (2017). Effective retinal penetration of lipophilic and lipid-conjugated hydrophilic agents delivered by engineered liposomes. *Molecular pharmaceutics*, *14*(2), 423-430.

Li, Q., Weng, J., Wong, S. N., Thomas Lee, W. Y., & Chow, S. F. (2020). Nanoparticulate drug delivery to the retina. *Molecular pharmaceutics*, *18*(2), 506-521.

Lim, S. B., Banerjee, A., & Önyüksel, H. (2012). Improvement of drug safety by the use of lipid-based nanocarriers. *Journal of controlled release*, *163*(1), 34-45.

Liu, L., & Liu, X. (2019). Roles of drug transporters in blood-retinal barrier. *Drug Transporters in Drug Disposition, Effects and Toxicity*, 467-504.

Loch, C., Zakelj, S., Kristl, A., Nagel, S., Guthoff, R., Weitschies, W., & Seidlitz, A. (2012). Determination of permeability coefficients of ophthalmic drugs through different layers of porcine, rabbit and bovine eyes. *European Journal of Pharmaceutical Sciences*, *47*(1), 131-138.

Lollo, G., Ullio-Gamboa, G., Fuentes, E., Matha, K., Lautram, N., & Benoit, J.-P. (2018). In vitro anti-cancer activity and pharmacokinetic evaluation of curcumin-loaded lipid nanocapsules. *Materials Science and Engineering: C*, *91*, 859-867.

Lombardo, D., Kiselev, M. A., & Caccamo, M. T. (2019). Smart nanoparticles for drug delivery application: development of versatile nanocarrier platforms in biotechnology and nanomedicine. *Journal of Nanomaterials*, *2019*.

Long, M. A., Kaler, E. W., Lee, S. P., & Wignall, G. D. (1994). Characterization of lecithin-taurodeoxycholate mixed micelles using small-angle neutron scattering and static and dynamic light scattering. *The Journal of Physical Chemistry*, *98*(16), 4402-4410.

Loo, D. T. (2011). In situ detection of apoptosis by the TUNEL assay: an overview of techniques. *Methods in molecular biology*, *682*, 3-13. https://doi.org/https://doi.org/10.1007/978-1-60327-409-8_1

Maguire, C. M., Rösslein, M., Wick, P., & Prina-Mello, A. (2018). Characterisation of particles in solution—a perspective on light scattering and comparative technologies. *Science and Technology of Advanced Materials*, *19*(1), 732-745.

Mains, J., & Wilson, C. G. (2013). The vitreous humor as a barrier to nanoparticle distribution. *J Ocul Pharmacol Ther*, *29*(2), 143-150. https://doi.org/10.1089/jop.2012.0138

Malzert-Fréon, A., Vrignaud, S., Saulnier, P., Lisowski, V., Benoît, J. P., & Rault, S. (2006). Formulation of sustained release nanoparticles loaded with a tripentone, a new anticancer agent. *Int J Pharm*, *320*(1-2), 157-164. https://doi.org/10.1016/j.ijpharm.2006.04.007

Mandal, A., Cholkar, K., Khurana, V., Shah, A., Agrahari, V., Bisht, R., Pal, D., & Mitra, A. K. (2017). Topical formulation of self-assembled antiviral prodrug nanomicelles for targeted retinal delivery. *Molecular pharmaceutics*, *14*(6), 2056-2069.

Marigo, V., Ekström, P., Schwede, F., Rentsch, A., & Paquet-Durand, F. (2018). Modulation of cGMP-signalling to Prevent Retinal Degeneration. In *Therapies for Retinal Degeneration* (pp. 88-98).

Martens, T. F., Peynshaert, K., Nascimento, T. L., Fattal, E., Karlstetter, M., Langmann, T., Picaud, S., Demeester, J., De Smedt, S. C., Remaut, K., & Braeckmans, K. (2017). Effect of hyaluronic acid-binding to lipoplexes on intravitreal drug delivery for retinal gene therapy. *Eur J Pharm Sci*, *103*, 27-35. https://doi.org/10.1016/j.ejps.2017.02.027

Meyer, C. H., Krohne, T. U., Issa, P. C., Liu, Z., & Holz, F. G. (2016). Routes for drug delivery to the eye and retina: intravitreal injections. *Retinal Pharmacotherapeutics*, *55*, 63-70.

Minkov, I., Ivanova, T., Panaiotov, I., Proust, J., & Saulnier, P. (2005a). Reorganization of lipid nanocapsules at air–water interface: I. Kinetics of surface film formation. *Colloids and Surfaces B: Biointerfaces*, *45*(1), 14-23.

Minkov, I., Ivanova, T., Panaiotov, I., Proust, J., & Saulnier, P. (2005b). Reorganization of lipid nanocapsules at air–water interface: part 2. Properties of the formed surface film. *Colloids and Surfaces B: Biointerfaces*, *44*(4), 197-203.

Mohsen, K., Azzazy, H. M., Allam, N. K., & Basalious, E. B. (2020). Intranasal lipid nanocapsules for systemic delivery of nimodipine into the brain: In vitro optimization and in vivo pharmacokinetic study. *Materials Science and Engineering: C*, *116*, 111236.

Molaahmadi, M. R., Varshosaz, J., Taymouri, S., & Akbari, V. (2019). Lipid nanocapsules for imatinib delivery: Design, optimization and evaluation of anticancer activity against melanoma cell line. *Iranian journal of pharmaceutical research: IJPR*, *18*(4), 1676.

Mouzouvi, C. R., Umerska, A., Bigot, A. K., & Saulnier, P. (2017). Surface active properties of lipid nanocapsules. *PLoS One*, *12*(8), e0179211.

Mukubwa, G. K., Safari, J. B., Walker, R. B., & Krause, R. W. (2022). Design, Manufacturing, Characterization and Evaluation of Lipid Nanocapsules to Enhance the Biopharmaceutical Properties of Efavirenz. *Pharmaceutics*, *14*(7), 1318.

Muramatsu, H., Lam, K., Bajusz, C., Laczkó, D., Karikó, K., Schreiner, P., Martin, A., Lutwyche, P., Heyes, J., & Pardi, N. (2022). Lyophilization provides long-term stability for a lipid nanoparticle-formulated, nucleoside-modified mRNA vaccine. *Molecular Therapy*, *30*(5), 1941-1951.

Muthu, M. S., & Wilson, B. (2012). Challenges posed by the scale-up of nanomedicines. *Nanomedicine*, *7*(3), 307-309.

Natarajan, J. V., Ang, M., Darwitan, A., Chattopadhyay, S., Wong, T. T., & Venkatraman, S. S. (2012). Nanomedicine for glaucoma: liposomes provide sustained release of latanoprost in the eye. *International journal of nanomedicine*, *7*, 123.

Natarajan, J. V., Darwitan, A., Barathi, V. A., Ang, M., Htoon, H. M., Boey, F., Tam, K. C., Wong, T. T., & Venkatraman, S. S. (2014). Sustained drug release in nanomedicine: a long-acting nanocarrier-based formulation for glaucoma. *ACS nano*, *8*(1), 419-429.

Navarro-Partida, J., Altamirano-Vallejo, J. C., Gonzalez-De la Rosa, A., Armendariz-Borunda, J., Castro-Castaneda, C. R., & Santos, A. (2021). Safety and tolerability of topical ophthalmic triamcinolone acetonide-loaded liposomes formulation and evaluation of its biologic activity in patients with diabetic macular edema. *Pharmaceutics*, *13*(3), 322.

Nicoli, S., Ferrari, G., Quarta, M., Macaluso, C., Govoni, P., Dallatana, D., & Santi, P. (2009). Porcine sclera as a model of human sclera for in vitro transport experiments: histology, SEM, and comparative permeability. *Molecular vision*, *15*, 259.

Niedorf, F., Schmidt, E., & Kietzmann, M. (2008). The automated, accurate and reproducible determination of steady-state permeation parameters from percutaneous permeation data. *Alternatives to Laboratory Animals*, *36*(2), 201-213.

O'Neal, T. B., & Luther, E. E. (2021). Retinitis pigmentosa. In *StatPearls [Internet]*. StatPearls Publishing.

Paquet-Durand, F., Hauck, S. M., Van Veen, T., Ueffing, M., & Ekström, P. (2009). PKG activity causes photoreceptor cell death in two retinitis pigmentosa models. *Journal of neurochemistry*, *108*(3), 796-810.

Peeters, L., Sanders, N. N., Braeckmans, K., Boussery, K., Van de Voorde, J., De Smedt, S. C., & Demeester, J. (2005). Vitreous: a barrier to nonviral ocular gene therapy. *Invest Ophthalmol Vis Sci*, *46*(10), 3553-3561. https://doi.org/10.1167/iovs.05-0165

Peeters, L., Sanders, N. N., Braeckmans, K., Boussery, K., Van de Voorde, J., De Smedt, S. C., & Demeester, J. (2005). Vitreous: a barrier to nonviral ocular gene therapy. *Investigative ophthalmology & visual science*, *46*(10), 3553-3561.

Perazzo, A., Preziosi, V., & Guido, S. (2015). Phase inversion emulsification: Current understanding and applications. *Advances in Colloid and Interface Science*, *222*, 581-599.

Pérez, O., Schipper, N., & Bollmark, M. (2021). Preparative Synthesis of an R P-Guanosine-3′, 5′-Cyclic Phosphorothioate Analogue, a Drug Candidate for the Treatment of Retinal Degenerations. *Organic process research & development*, *25*(11), 2453-2460.

Pescina, S., Govoni, P., Potenza, A., Padula, C., Santi, P., & Nicoli, S. (2015). Development of a convenient ex vivo model for the study of the transcorneal permeation of drugs: histological and permeability evaluation. *Journal of pharmaceutical sciences*, *104*(1), 63-71.

Pescina, S., Santi, P., Ferrari, G., Padula, C., Cavallini, P., Govoni, P., & Nicoli, S. (2012). Ex vivo models to evaluate the role of ocular melanin in trans-scleral drug delivery. *European Journal of Pharmaceutical Sciences*, *46*(5), 475-483.

Ph. Eur. 10.0. (2020). *Microbiological examination of non-sterile products: Microbial enumeration tests* (2.6.12) [Monograph]. https://extranet.edqm.eu/4DLink1/4DCGI/Web_View/mono/20612

Radwan, S. A. A., El-Maadawy, W. H., ElMeshad, A. N., Shoukri, R. A., & Yousry, C. (2020). Impact of reverse micelle loaded lipid nanocapsules on the delivery of gallic acid into activated hepatic stellate cells: a promising therapeutic approach for hepatic fibrosis. *Pharmaceutical research*, *37*(9), 1-17.

Ramadan, A., Lagarce, F., Tessier-Marteau, A., Thomas, O., Legras, P., Macchi, L., Saulnier, P., & Benoit, J. P. (2011). Oral fondaparinux: use of lipid nanocapsules as nanocarriers and in vivo pharmacokinetic study. *International journal of nanomedicine*, *6*, 2941.

Ramsay, E., Del Amo, E. M., Toropainen, E., Tengvall-Unadike, U., Ranta, V.-P., Urtti, A., & Ruponen, M. (2018). Corneal and conjunctival drug permeability: Systematic comparison and pharmacokinetic impact in the eye. *European Journal of Pharmaceutical Sciences*, *119*, 83-89.

Rimpelä, A. K., Reunanen, S., Hagström, M., Kidron, H., & Urtti, A. (2018). Binding of Small Molecule Drugs to Porcine Vitreous Humor. *Mol Pharm*, *15*(6), 2174-2179. https://doi.org/10.1021/acs.molpharmaceut.8b00038

Roy, I., & Gupta, M. N. (2004). Freeze-drying of proteins: some emerging concerns. *Biotechnology and applied biochemistry*, *39*(2), 165-177.

Sahaboglu, A., Paquet-Durand, O., Dietter, J., Dengler, K., Bernhard-Kurz, S., Ekström, P. A., Hitzmann, B., Ueffing, M., & Paquet-Durand, F. (2013). Retinitis pigmentosa: rapid neurodegeneration is governed by slow cell death mechanisms. *Cell death & disease*, *4*(2), e488-e488.

Salehi-Had, H., Roh, M. I., Giani, A., Hisatomi, T., Nakao, S., Kim, I. K., Gragoudas, E. S., Vavvas, D., Guccione, S., & Miller, J. W. (2011). Utilizing targeted gene therapy with nanoparticles binding alpha v beta 3 for imaging and treating choroidal neovascularization. *PLoS One*, *6*(4), e18864.

Samimi, S., Maghsoudnia, N., Eftekhari, R. B., & Dorkoosh, F. (2019). Lipid-based nanoparticles for drug delivery systems. *Characterization and biology of nanomaterials for drug delivery*, 47-76.

Sánchez-López, E., Espina, M., Doktorovova, S., Souto, E., & García, M. (2017). Lipid nanoparticles (SLN, NLC): Overcoming the anatomical and physiological barriers of the eye—Part II-Ocular drug-loaded lipid nanoparticles. *European Journal of Pharmaceutics and Biopharmaceutics*, *110*, 58-69.

Sancho-Pelluz, J., Arango-Gonzalez, B., Kustermann, S., Romero, F. J., Van Veen, T., Zrenner, E., Ekström, P., & Paquet-Durand, F. (2008). Photoreceptor cell death mechanisms in inherited retinal degeneration. *Molecular neurobiology*, *38*(3), 253-269.

Shaukat, A., & Kolter, K. K. (2019). Kolliphor® HS 15—an enabler for parenteral and oral formulations. *Am. Pharm. Rev*, *22*, 22-34.

Shen, Y., & Tu, J. (2007). Preparation and ocular pharmacokinetics of ganciclovir liposomes. *The AAPS journal*, *9*(3), E371-E377.

Shinoda, K., & Kunieda, H. (1983). Phase properties of emulsions: PIT and HLB. *Encyclopedia of emulsion technology*, *1*, 337-367.

Shinoda, K., & Saito, H. (1969). The stability of O/W type emulsions as functions of temperature and the HLB of emulsifiers: the emulsification by PIT-method. *Journal of colloid and interface science*, *30*(2), 258-263.

Singh, S., Grossniklaus, H., Kang, S., Edelhauser, H., Ambati, B., & Kompella, U. (2009). Intravenous transferrin, RGD peptide and dual-targeted nanoparticles enhance anti-VEGF intraceptor gene delivery to laser-induced CNV. *Gene therapy*, *16*(5), 645-659.

Smith, P. B., Dendramis, K. A., & Chiu, D. T. (2010). Investigating lyophilization of lipid nanocapsules with fluorescence correlation spectroscopy. *Langmuir*, *26*(12), 10218-10222.

Solans, C., Izquierdo, P., Nolla, J., Azemar, N., & Garcia-Celma, M. J. (2005). Nano-emulsions. *Current opinion in colloid & interface science*, *10*(3-4), 102-110.

Sun, R., Zhang, A., Ge, Y., Gou, J., Yin, T., He, H., Wang, Y., Zhang, G., Kong, J., & Shang, L. (2020). Ultra-small-size Astragaloside-IV loaded lipid nanocapsules eye drops for the effective management of dry age-related macular degeneration. *Expert Opinion on Drug Delivery*, *17*(9), 1305-1320.

Tang, X., & Pikal, M. J. (2004). Design of freeze-drying processes for pharmaceuticals: practical advice. *Pharmaceutical research*, *21*, 191-200.

Tatke, A., Dudhipala, N., Janga, K. Y., Balguri, S. P., Avula, B., Jablonski, M. M., & Majumdar, S. (2018). In situ gel of triamcinolone acetonide-loaded solid lipid nanoparticles for improved topical ocular delivery: Tear kinetics and ocular disposition studies. *Nanomaterials*, *9*(1), 33.

Tavakoli, S., Kari, O. K., Turunen, T., Lajunen, T., Schmitt, M., Lehtinen, J., Tasaka, F., Parkkila, P., Ndika, J., Viitala, T., Alenius, H., Urtti, A., & Subrizi, A. (2021). Diffusion and Protein Corona Formation of Lipid-Based Nanoparticles in the

Vitreous Humor: Profiling and Pharmacokinetic Considerations. *Mol Pharm*, *18*(2), 699-713. https://doi.org/10.1021/acs.molpharmaceut.0c00411

Tavakoli, S., Peynshaert, K., Lajunen, T., Devoldere, J., Del Amo, E. M., Ruponen, M., De Smedt, S. C., Remaut, K., & Urtti, A. (2020). Ocular barriers to retinal delivery of intravitreal liposomes: Impact of vitreoretinal interface. *Journal of controlled release*, *328*, 952-961.

Thomas, O., & Lagarce, F. (2013). Lipid nanocapsules: a nanocarrier suitable for scale-up process. *Journal of Drug Delivery Science and Technology*, *23*(6), 555-559.

Tolone, A., Belhadj, S., Rentsch, A., Schwede, F., & Paquet-Durand, F. (2019). The cGMP pathway and inherited photoreceptor degeneration: targets, compounds, and biomarkers. *Genes*, *10*(6), 453.

Tolone, A., Haq, W., Fachinger, A., Rentsch, A., Herberg, F. W., Schwede, F., & Paquet-Durand, F. (2021). Retinal degeneration: Multilevel protection of photoreceptor and ganglion cell viability and function with the novel PKG inhibitor CN238. *BioRxiv*.

Trenkenschuh, E., & Friess, W. (2021). Freeze-drying of nanoparticles: How to overcome colloidal instability by formulation and process optimization. *European Journal of Pharmaceutics and Biopharmaceutics*, *165*, 345-360.

Tuukkanen, A. T., Spilotros, A., & Svergun, D. I. (2017). Progress in small-angle scattering from biological solutions at high-brilliance synchrotrons. *IUCrJ*, *4*(5), 518-528.

Umerska, A., Matougui, N., Groo, A.-C., & Saulnier, P. (2016). Understanding the adsorption of salmon calcitonin, antimicrobial peptide AP114 and polymyxin B onto lipid nanocapsules. *International journal of pharmaceutics*, *506*(1-2), 191-200.

Umerska, A., Mugheirbi, N. A., Kasprzak, A., Saulnier, P., & Tajber, L. (2020). Carbohydrate-based Trojan microparticles as carriers for pulmonary delivery of lipid nanocapsules using dry powder inhalation. *Powder Technology*, *364*, 507-521.

Urquhart, A. J., & Eriksen, A. Z. (2019). Recent developments in liposomal drug delivery systems for the treatment of retinal diseases. *Drug Discovery Today*, *24*(8), 1660-1668.

Valcourt, C., Saulnier, P., Umerska, A., Zanelli, M., Montagu, A., Rossines, E., & Joly-Guillou, M.-L. (2016). Synergistic interactions between doxycycline and terpenic components of essential oils encapsulated within lipid nanocapsules against gram negative bacteria. *International journal of pharmaceutics*, *498*(1-2), 23-31.

Varshosaz, J., Taymouri, S., Jahanian-Najafabadi, A., & Alizadeh, A. (2018). Efavirenz oral delivery via lipid nanocapsules: formulation, optimisation, and ex-vivo gut permeation study. *IET nanobiotechnology*, *12*(6), 795-806.

Ventola, C. L. (2017). Progress in nanomedicine: approved and investigational nanodrugs. *Pharmacy and Therapeutics*, *42*(12), 742.

Vighi, E., Trifunović, D., Veiga-Crespo, P., Rentsch, A., Hoffmann, D., Sahaboglu, A., Strasser, T., Kulkarni, M., Bertolotti, E., & Van Den Heuvel, A. (2018). Combination of cGMP analogue and drug delivery system provides functional protection in

hereditary retinal degeneration. *Proceedings of the National Academy of Sciences*, *115*(13), E2997-E3006.

Vonarbourg, A., Saulnier, P., Passirani, C., & Benoit, J. P. (2005). Electrokinetic properties of noncharged lipid nanocapsules: influence of the dipolar distribution at the interface. *Electrophoresis*, *26*(11), 2066-2075.

Vrignaud, S., Hureaux, J., Wack, S., Benoit, J.-P., & Saulnier, P. (2012). Design, optimization and in vitro evaluation of reverse micelle-loaded lipid nanocarriers containing erlotinib hydrochloride. *International journal of pharmaceutics*, *436*(1-2), 194-200.

Weng, J., Tong, H. H., & Chow, S. F. (2020). In vitro release study of the polymeric drug nanoparticles: development and validation of a novel method. *Pharmaceutics*, *12*(8), 732.

Yamada, N., & Olsen, T. W. (2016). Routes for drug delivery to the retina: topical, transscleral, suprachoroidal and intravitreal gas phase delivery. *Retinal Pharmacotherapeutics*, *55*, 71-83.

Zeng, S., Hu, C., Wei, H., Lu, Y., Zhang, Y., Yang, J., Yun, G., Zou, W., & Song, B. (1993). Intravitreal pharmacokinetics of liposome-encapsulated amikacin in a rabbit model. *Ophthalmology*, *100*(11), 1640-1644.

Zhai, Q., Li, H., Song, Y., Wu, R., Tang, C., Ma, X., Liu, Z., Peng, J., Zhang, J., & Tang, Z. (2018). Preparation and optimization lipid nanocapsules to enhance the antitumor efficacy of cisplatin in hepatocellular carcinoma HepG2 cells. *AAPS PharmSciTech*, *19*(5), 2048-2057.

Zhang, H. (2017). Thin-film hydration followed by extrusion method for liposome preparation. In *Liposomes* (pp. 17-22). Springer.

Zhang, R., He, R., Qian, J., Guo, J., Xue, K., & Yuan, Y.-f. (2010). Treatment of experimental autoimmune uveoretinitis with intravitreal injection of tacrolimus (FK506) encapsulated in liposomes. *Investigative ophthalmology & visual science*, *51*(7), 3575-3582.

Zhang, W., Li, X., Ye, T., Chen, F., Sun, X., Kong, J., Yang, X., Pan, W., & Li, S. (2013). Design, characterization, and in vitro cellular inhibition and uptake of optimized genistein-loaded NLC for the prevention of posterior capsular opacification using response surface methodology. *International journal of pharmaceutics*, *454*(1), 354-366.

Zhao, Y.-q., Wang, L.-p., Ma, C., Zhao, K., Liu, Y., & Feng, N.-p. (2013). Preparation and characterization of tetrandrine-phospholipid complex loaded lipid nanocapsules as potential oral carriers. *International journal of nanomedicine*, *8*, 4169.

Paper I

International Journal of Pharmaceutics 602 (2021) 120640

Contents lists available at ScienceDirect

International Journal of Pharmaceutics

journal homepage: www.elsevier.com/locate/ijpharm

Formulation development and upscaling of lipid nanocapsules as a drug delivery system for a novel cyclic GMP analogue intended for retinal drug delivery

Dileep Urimi [a,b], Ronja Widenbring [a], Raúl Oswaldo Pérez García [a,b], Lars Gedda [c], Katarina Edwards [c], Thorsteinn Loftsson [b], Nicolaas Schipper [a,*]

[a] RISE Research Institutes of Sweden, SE-151 36 Södertälje, Sweden
[b] Faculty of Pharmaceutical Sciences, School of Health Sciences, University of Iceland, Hofsvallagata 53, IS-107 Reykjavík, Iceland
[c] Department of Chemistry – Ångström Laboratory, Uppsala University, Box 573, Uppsala SE-751 23, Sweden

ARTICLE INFO

Keywords:
Lipid nanocapsules
Retinal degenerations
Drug Release
Upscaling
Continuous manufacture
Clinical translation

ABSTRACT

Lipid nanocapsules (LNCs) were prepared with a novel cyclic GMP analogue, DF003, intended for the treatment of neurodegenerative retinal degenerations. LNCs loaded with DF003 were prepared by a phase inversion method and characterized for particle size, polydispersity index, drug loading, entrapment efficiency, stability, and *in vitro* drug release. Particle size, PdI and zeta potential of selected optimized formulation were 76 ± 1.2 nm, 0.16 ± 0.02, and −11.6 ± 0.4 mV, respectively, with an entrapment efficiency of 69 ± 0.5%. The selected formulation showed a sustained drug release for up to 6 days in phosphate buffer as well as in vitreous components. Stability evaluation of LNCs in presence of vitreous components demonstrated structural stability and compatibility. Further, the nanoparticle preparation process was upscaled to 1000 times (10 L) of the typical lab scale (0.01 L). Product parameters were observed to be unaffected by the upscaling, demonstrating that the LNCs were of the same quality as those prepared at lab scale. Additionally, the manufacturing process was adapted and assessed for a continuous production of LNCs to leverage it for industrial viability. Overall, these findings reveal the remarkable potential of LNCs as drug delivery vehicles and their possibility for clinical translation.

1. Introduction

Lipid nanocapsules (LNCs) are nanoparticles prepared by a solvent-free, low-energy phase inversion method (Hirsjärvi et al., 2013; Huynh et al., 2009; Thomas and Lagarce, 2013; Valcourt et al., 2016), and consist of an oily core composed of medium chain triglycerides which is enveloped by a layer of hydrophilic and hydrophobic surfactants (Heurtault et al., 2002; Mouzouvi et al., 2017; Valcourt et al., 2016). The components of LNCs are pharmaceutically acceptable and are regarded as generally recognized as safe (i.e. are included in FDA's GRAS list), and pharmacopoeial grades are commercially available. The characteristics of these nanoparticles can be adjusted to suit various applications with a possibility of loading both hydrophobic and hydrophilic drugs (Thomas and Lagarce, 2013). Previous studies on LNCs demonstrated their potential for loading various actives for drug delivery (e.g., ibuprofen, amiodarone, tripentone, paclitaxel, docetaxel, tamoxifen, cisplatin, and antimicrobial peptides) (Groo et al., 2018; Huynh et al., 2009; Lamprecht et al., 2002; Malzert-Freon et al., 2006; Umerska et al., 2016; Zhai et al., 2018) and their suitability for various administration routes like oral, dermal, pulmonal and parenteral including ocular routes (Abdel-Mottaleb et al., 2011; Formica et al., 2020, 2021; Hureaux et al., 2009; Sun et al., 2020). The present study mainly focused on lab scale development of LNCs loaded with a novel cyclic guanosine- 3′,5′-monophosphate (cGMP) analogue (DF003), their characterization, and scale-up studies of the manufacturing process.

A novel class of cGMP analogues (Ekström et al., 2019; Vighi et al., 2018) were recently developed and have shown to be potentially effective in the treatment of retinal degenerations (RD). DF003, in particular, was found to inhibit both cyclic nucleotide–gated ion channel (CNGC) and cGMP-dependent protein kinase (PKG), and thus proved to be effective against photoreceptor cell death. Extensive preclinical animal studies in three different RD models demonstrated the effectiveness of DF003 in functional preservation of both rods and cones (Vighi et al., 2018). Remarkably, no strong toxicological adversities were noted when

* Corresponding author.
E-mail address: nicolaas.schipper@ri.se (N. Schipper).

https://doi.org/10.1016/j.ijpharm.2021.120640
Received 11 February 2021; Received in revised form 12 April 2021; Accepted 21 April 2021
Available online 24 April 2021

administrating DF003 to mice and rats. According to these studies, DF003 (Fig. 1) could become a potential molecule for the treatment of inherited retinal degeneration.

Although DF003 has proved to be effective, its delivery to the retinal photoreceptors is extremely challenging given the anatomical complexity of the eye and the fast clearance from the anterior chamber owing to its physicochemical properties. This can be addressed by formulating the drug into nanoparticles as they have established effectiveness (Germain et al., 2020; Lombardo et al., 2019; Patra et al., 2018; Ventola, 2017) in carrying drug molecules to most complex body tissues and organs, thereby reducing the clearance rate and improving the half-life and bioavailability of the drugs. Lipid based nanoparticles are particularly superior for ocular drug delivery over other kinds of nanoparticles due to their ability to increase the bioavailability by interacting with biological membranes of the eye. Furthermore, if the right lipids are chosen, the particles can have a high biocompatibility and biodegradability. Lipid nanoparticles offer high prospects for clinical translation as supported by the vast number of approved drug products in the market for different routes of administration including the eye (e.g., liposomal doxorubicin, liposomal amphotericin) (Beloqui et al., 2016; Gan et al., 2013; Lim et al., 2012). Many different lipid systems have been evaluated and developed for the treatment of disorders related with the anterior part of the eye, while modest progress has been seen on treating posterior chamber related disorders. However, over the recent years there has been a paradigm shift towards developing treatment options for the posterior part as well. This is augmented by an increased need for novel treatment approaches, due to the current lack of clinical therapies for many of the posterior segment associated anomalies. Successful treatment to the posterior segment of the eye requires a formulation with a sustained release behavior and that is suitable for intravitreal administration (Agrahari et al., 2017; Fung, 2010).

Previous studies on liposomes (Vighi et al., 2018), were shown to be effective in delivering DF003 to the retinal photoreceptors after intravenous (IV) administration. However, systemic administration may not be the ideal route for delivering drugs to retinal tissues due to the barrier properties of the blood-retinal barrier and non-specific off-target adverse effects (Sahoo et al., 2008). The present investigation addresses these issues by looking into the development of LNCs as delivery vehicles for DF003, their physicochemical characterization including stability in vitreous components to test their suitability for intravitreal administration.

Alongside the lab scale evaluation of LNCs, a pilot manufacturing process was developed to facilitate their clinical translation. Treatment of many diseases is just not possible not because of absence of drug molecules but due to the complexity of delivering them to the target tissues, here nanoparticles can show significant advantages. Over the decades, a large number of nanoparticulate systems have been developed for a variety of drug delivery applications, yet few made their way to market (Ventola, 2017). Many nanoparticulate systems are restricted to research purpose with limited industrial scope because of numerous underlying complexities. Scale-up difficulties such as batch to batch reproducibility, sterility/bioburden, long-term stability and stringent regulatory requirements, make it complicated for these systems to get market access (Thomas and Lagarce, 2013). Unfortunately, the lab scale process is not always suitable for large scale production and poses a multitude of predicaments for higher manufacturing scales. This necessitates the development of suitable manufacturing methods. The present investigation attempts to bridge this gap from lab to production scale by manufacturing the LNCs at 1000 times the lab scale volumes. Furthermore, the feasibility of a continuous manufacturing process and a process suitable for sterile manufacturing was evaluated. The upscaled batches of LNCs were tested for stability, microbial purity and all the quality parameters similar to lab scale.

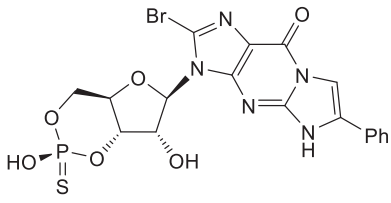

Fig. 1. Molecular structure of DF003.

2. Materials

The drug candidate (DF003: β-Phenyl-1,N^2-etheno-8-bromoguanosine-3′,5′-cyclic monophosphorothioate, sometimes referred to as CN03 in previous publications) was internally synthesized within RISE Research Institutes of Sweden (Södertälje, Sweden) as part of the *trans*Med project (H2020-MSCA-765441). Labrafac™ lipophile WL 1349, medium chain triglycerides (Ph. Eur. Grade, Gattefossé, France), Kolliphor® HS 15 i.e. Polyethylene glycol (15)-hydroxystearate (Ph. Eur. Grade, BASF), Phospholipids namely Phospholipon® 90 H (hydrogenated phosphatidylcholine ≥ 90%), Phospholipon® 80 H (hydrogenated phosphatidylcholine ≥ 70%), Lipoid S 75 (phosphatidylcholine approx. 70% with predominantly unsaturated fatty acids) and Lipoid S PC-3 (hydrogenated phosphatidylcholine ≥ 98%) from Lipoid GmbH, Germany, were used to prepare LNCs. Sodium phosphate dibasic dihydrate ($Na_2HPO_4{\cdot}2H_2O$), sodium dihydrogen phosphate (NaH_2PO_4), ammonium acetate, sodium chloride, 100 kD Float-A-Lyzer® G2 Dialysis Device (Spectrum Labs), 50 kD Amicon Ultra-0.5 Centrifugal Filter Units (Millipore®) were from Sigma-Aldrich Sweden AB (Stockholm, Sweden). Ultrapure milli-Q water (ELGA, Purelab Prima) made in-house was utilized for all experiments. All excipients and reagents were of analytical grade, unless specifically mentioned otherwise.

3. Methods

3.1. Lab scale development and characterization of LNCs

3.1.1. Solubility measurement of DF003

The solubility of DF003 in water, 0.1 N HCl (pH 1.5), Phosphate buffer (pH 7.2–7.4), Labrafac™ lipophile WL 1349, Kolliphor® HS 15 was studied. Approximately 5–6 mg of DF003 was weighed into separate glass vials and 0.5 mL of aqueous buffer media was added. In case of Labrafac™ and liquified Kolliphor® HS 15, 0.5 g was weighed and added to the individual vials. The vials were kept on a mixing board and observed at 15 min intervals for two hours for the presence of particles. Excess DF003 was added to the vials that showed no visible particles. The vials with aqueous buffers were then left on a mixing board for 48 h at 25℃ to reach the saturation point. In case of Labrafac™ and Kolliphor® HS 15, vials were maintained at 37°C for 3 h and 6 h respectively. At the end of stated time points, the experiment was stopped, and the vials were centrifuged at 14000*g* for 30 min to remove undissolved particles. Clear supernatant was collected and diluted with acetonitrile: water (30:70) or ethanol (in case of Labrafac™ and Kolliphor® HS 15) and the solubility of DF003 was quantified by UPLC-UV using the parameters stated in section 3.1.3.

3.1.2. Formulation development and optimization of LNCs

LNCs were prepared by a phase inversion method as described by Valcourt et al. (Valcourt et al., 2016) (Fig. 2). Briefly, Labrafac™, DF003, Kolliphor® HS 15, phospholipid, sodium chloride, and milli-Q water (17%) were weighed into a glass vial. The mixture was heated under stirring until the components were dissolved, and a clear solution was formed. Thereafter, the solution was subjected to three successive heat cool cycles, above and below the phase inversion temperature, from 90°C to 60°C, whilst stirring. During the last cooling cycle, when the solution was close to phase inversion, excess cold water (2–8°C) was

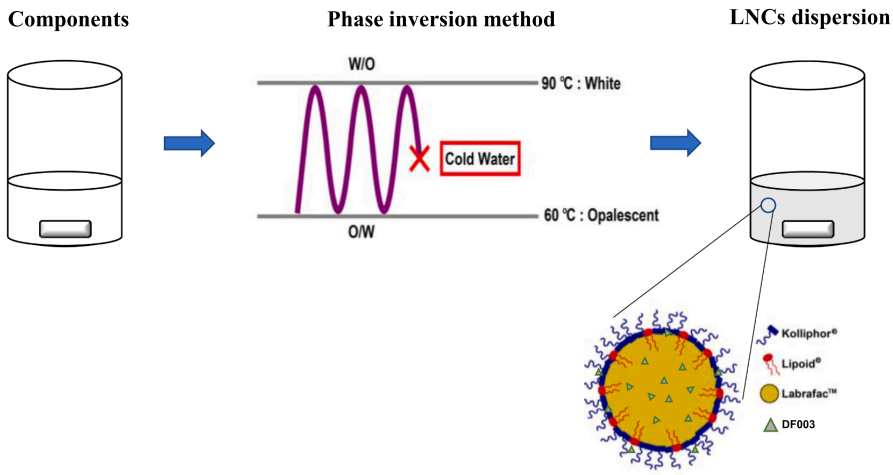

Fig. 2. Schematic representation of lipid nanocapsules (LNCs) preparation by a phase inversion method.

added. This mixture was kept under stirring for 5 min to stabilize the LNCs. Formulation was optimized by varying the proportions of Labrafac™ lipophile WL 1349, Kolliphor® HS 15, and phospholipids (Table 1). Moreover, blank LNCs without drug were prepared using different phospholipids (Phospholipon® 90 H, Lipoid S 75, Phospholipon® 80 H, and Lipoid S PC-3) to check their impact on the formulation behavior. Initially, formulations were visually inspected for phase separation as an indication of physical instability. Formulations with no observable signs of phase separation were characterized for particle size, particle size distribution, zeta potential, entrapment efficiency, and drug loading.

3.1.3. UPLC-UV method to quantify the drug concentration

DF003 was quantified using UPLC system (ACQUITY UPLC, Waters Corporation) which was comprised of an autosampler, a pump for mobile phases/solvents, column oven, a UV detector, and a column (Acquity BEH shield RP18, 2.1 mm internal diameter, particle size 1.7 μm). Mobile phases consisted of 5 mM ammonium acetate (A) and acetonitrile (B), and elution was carried out in a gradient manner from 100% A to 100% B over 10 min. 2 μL of sample was injected and eluted at 0.5 mL/min at 40°C. Detection was performed at 256 nm at a peak retention time of ~ 3.5 min. A standard curve was generated between 20 and 100 μg/mL by dissolving DF003 in acetonitrile:water (30:70). Test solutions were prepared and quantified in the same way as standard samples, either undiluted or diluted with acetonitrile:water (30:70). Data analysis was carried out using Chromeleon software (Dionex Corporation).

3.1.4. Characterization of LNCs

3.1.4.1. Physicochemical properties. The mean hydrodynamic diameter and Polydispersity Index (PdI) of the prepared LNCs (with or without drug) were measured by dynamic light scattering (DLS) at 25°C with a detection angle of 173°. Samples for particle size, zeta potential (ZP), and derived count rate (DCR) were measured undiluted or diluted to 60 times with milli-Q water before the measurement. Both size and zeta potential were measured using Malvern Zetasizer Nano ZS (Malvern Instruments, UK).

3.1.4.2. Entrapment efficiency and drug loading. Entrapment efficiency (% EE) calculates the fraction of drug that is associated, or entrapped, in the nanoparticles. In the present study, entrapment efficiency was quantified by an indirect method wherein the formulations were centrifuged in Amicon Ultra-0.5 centrifugal filter units with 50 kD molecular weight cut-off membrane for 5 min at 10000*g*. Clear filtrate which is devoid of LNCs was collected and analyzed for unentrapped drug using UPLC-UV. Absence of nanoparticles in the clear filtrate was confirmed by particle size measurements. Entrapment efficiency (% EE) was calculated by

$$\% \text{ EE} = (\text{Wt-Wo})/\text{Wt} \times 100 \quad (1)$$

where Wt and Wo corresponds to the total and unentrapped drug, respectively. Drug loading of LNCs was calculated by

Table 1
Optimization of LNCs with varied compositions.

Formulation	Labrafac™ WL 1349 (% w/v)	Kolliphor® HS 15 (% w/v)	Phospholipid (% w/v)	NaCl (% w/v)	Drug: lipid ratio	Type of phospholipid
F1	6.2	4.8	0	0.5	1:32	–
F2	6.2	4.8	0.4	0.5	–	Lipoid S 75
F3	6.2	4.8	0.4	0.5	–	Phospholipon® 80 H
F4	6.2	4.8	0.4	0.5	–	Lipoid S PC-3
F5	6.2	4.8	0.4	0.5	–	Phospholipon® 90 H
F6	6.2	4.8	0.4	0.5	1:32	Phospholipon® 90 H
F7	6.2	7.2	0.4	0.5	1:32	Phospholipon® 90 H
F8	6.2	9.6	0.4	0.5	1:32	Phospholipon® 90 H
F9	9.3	7.2	0.4	0.5	1:32	Phospholipon® 90 H
F10	6.2	4.8	0.4	0.5	1:64	Phospholipon® 90 H

$$\text{Drug loading (mg/mL)} = \frac{\text{Amount of entrapped drug in LNCs (mg)}}{\text{volume of LNCs (mL)}} \quad (2)$$

3.1.4.3. Cryogenic transmission electron microscopy. Samples were analyzed by cryogenic transmission electron microscopy (cryo-TEM) as described by Almgren et al. (Almgren et al., 2000). Initially, samples were equilibrated at 25°C and high relative humidity (> 90%) within a climate chamber. A small drop (< 1 μL) of each sample was deposited on a carbon-sputtered copper grid precovered with perforated polymer - film. Excess liquid was thereafter removed by blotting with a filter paper, leaving a thin film of the solution on the grid. Subsequently, the sample was vitrified in liquid ethane and transferred to the microscope. Samples were kept below –160°C and protected against atmospheric conditions during both transfer and examination. Analyses were performed with a Zeiss Libra 120 Transmission Electron Microscope (Carl Zeiss AG, Oberkochen, Germany) operating at 80 kV and in zero-loss bright-field mode. Digital images were recorded under low-dose conditions with a BioVision Pro-SM Slow Scan CCD camera (Proscan elektronische Systeme GmbH, Scheuring, Germany).

3.1.4.4. In vitro drug release. In the present study, release testing was carried out in a dialysis setup. A Float-A-Lyzer® G2 dialysis device fitted with 100 kD molecular weight cut-off membrane was selected and pretreated with 10% ethanol and purified water as per the standard instruction provided by the supplier. Thereafter, 1 mL of formulation was added to the individual devices and kept in the release buffer (phosphate buffer pH 7.2–7.4 or hyaluronic acid ~375 μg/mL), at 37°C. The ratio of formulation to release buffer volume was kept constant at 1 mL to 18 mL. Samples were collected and the buffer was replaced completely with fresh buffer at predetermined time intervals to maintain sink conditions. Samples were quantified for released drug using UPLC.

3.1.4.5. Stability testing

3.1.4.5.1. Colloidal stability. Drug loaded formulations in their native state were evaluated for colloidal stability by storing them at 2–8°C and 25°C for one month. Additionally, LNCs manufactured at higher volumes were also studied for stability by storing them at 2–8°C for up to 6 months. Samples were collected and investigated for any possible changes in physical appearance, particle size, particle size distribution, zeta potential, % entrapment efficiency.

3.1.4.5.2. Stability in simulated vitreous fluid. A solution of hyaluronic acid (2.4 million Da; ~375 μg/mL) was used as a simulated vitreous fluid (del Amo et al., 2017). Nanoparticles were diluted 20 times with the simulated vitreous fluid and incubated at 37°C for seven days. Samples were tested for changes in particle size and particle size distribution, as an indication of aggregation or degradation.

3.2. Large-scale manufacturing of LNCs

LNCs without drug loading were prepared by a phase inversion method at two different manufacturing volumes, 1 L and 10 L scales which are 100 and 1000 times the lab scale volumes, respectively. Additionally, different manufacturing processes were also evaluated. Samples were collected and characterized for particle size, zeta potential, and derived count rate. Temperature and conductivity values were continuously monitored during the whole process. Detailed composition of LNCs used for large-scale production is given in Table 2.

3.2.1. Manufacturing of LNCs with batch and continuous processes

The same phase inversion method as for lab scale was used when scaling up the procedure from lab scale to a volume of 1 L and 10 L. In brief, Labrafac™ lipophile WL 1349, Kolliphor® HS 15, Phospholipon® 90 H, Sodium chloride, milli-Q water (17%) were mixed and heated to obtain a clear solution which was then transferred directly into a double jacketed reaction vessel. A mechanical stirrer was mounted into the reaction vessel and a water bath with a mix of 50/50 ethylene glycol/water was attached to the setup to maintain the required temperature in the reaction vessel. Three heating–cooling cycles (90–60°C) were performed to the component mixture and during the last cooling cycle, at around 80°C, the solution was transferred into a flask with cold (~4°C) quenching water (and with a magnetic stirring bar) directly, followed by stirring in an ice-bath for at least five minutes. Two batches at 1 L scale were manufactured to check the repeatability and reproducibility of the process.

Table 2
Composition of LNCs for large-scale manufacturing.

Excipient	Composition (% w/v)	Weight of excipients (g) for 1 L scale	Weight of excipients (g) for 10 L scale
Labrafac™ lipophile WL 1349	6.2	62	620
Kolliphor® HS 15	4.8	48	480
Phospholipon® 90 H	0.4	4	40
Sodium chloride	0.5	5	50
milli-Q water	17	170	1700
milli-Q water for quenching	71.1	711	7110

In addition, the batch manufacturing process was assessed and modified for its suitability to convert into a continuous process. For this purpose, LNCs were manufactured to a 1 L volume scale. Firstly, a vertical oscillatory reactor fitted with baffles was employed instead of a normal jacketed reaction vessel (Fig. 10a and Fig. 10c). This medium scale oscillatory reactor typically simulates the flow patterns observed with continuous oscillatory baffled reactors for which better process control, as compared to standard batch processes, is possible. Two water baths were connected to the reactor to control the temperature as opposed to one bath in the batch manufacturing process. These water baths were maintained at temperatures of 20°C and 95°C and the connections to the oscillatory reactor were switched for cooling and heating of the reaction mixture during the preparation of LNCs. Clear excipient mixture was transferred into the oscillatory reactor and subjected to heating and cooling cycles, followed by transferring into the quenching water, in the same manner as described for the batch process.

3.2.2. Sterile manufacturing of LNCs at 1L scale

The individual components listed in Table 2, except Phospholipon® 90 H and water for quenching, were melted and sterile filtered using a 0.2 μm syringe filter (Supor® EKV Membrane) into a heat sterilized glass bottle. Phospholipon® 90 H was added to the glass bottle and the solution was heated until a clear solution was formed. The complete mixture was heat sterilized at 121°C for 15 min with ~2 bar pressure. This sterile solution was subsequently subjected to heat-cool cycles and transferred into sterilized cold quenching water to obtain LNCs as described in Section 3.2.1. Finally, these nanocapsules were filtered through a 0.2 μm syringe filter (Supor® EKV Membrane) into sterile containers under a pre-sanitized laminar air-flow chamber. Samples were tested for bioburden as described in Section 3.2.3.

3.2.3. Testing of LNCs for microbial purity

Testing of microbial purity of the formulations prepared in Section 3.2.2 was performed using the membrane filtration method described in the European Pharmacopoeia (Ph. Eur. 10.0, 2020). In short, Staphylococcus aureus (ATCC 6538), Pseudomonas aeruginosa (ATCC 9027), Bacillus subtilis (ATCC 6633), Candida albicans (ATCC 10231), Aspergillus brasiliensis (ATCC 16404) were used as challenge microorganisms (reference strains) for the determination of Total Aerobic Microbial Count (TAMC) as an indication of microbial purity. These test organisms were prepared from freeze-dried and ready-to-use pellets. Method suitability was carried out by filtering (a) 10–100 CFU of challenge

microorganisms in 100 mL of peptone water (positive controls) and (b) test samples spiked with 10–100 CFU of challenge microorganisms, using Milliflex filtration system pre-fitted with 0.2 μm membrane. After the filtration, membranes were separated and incubated in Milliflex cassettes containing prefilled tryptic soy agar (TSA) for three days at 30-35℃. Percentage recovery of microbial count was calculated using Equation (3)and the acceptance criteria was set from 50% to 200%. Test samples were prepared by mixing 1 mL of formulations in 100 mL peptone water and examined for the microbial purity using the same method as described above. TAMC of the samples was compared against the limits mentioned in the European Pharmacopoeia.

$$\% \text{ Recovery} = \frac{\text{Count on TSA cassette of samples spiked with challenge organisms}}{\text{Count on TSA cassette of positive control}} \text{ x } 100 \quad (3)$$

3.3. Statistical analysis

The statistical analysis of generated data was performed using GraphPad Prism version 8.2.1, GraphPad Software, San Diego, California USA. Data is represented as mean ± standard deviation (SD).

4. Results and discussion

4.1. Lab scale formulation development of DF003 loaded LNCs

4.1.1. Solubility of DF003

DF003 is a small molecule with calculated log *P* and pKa of 1.9 and 1.4, respectively (MarvinSketch 19.3). The first step in the formulation development for DF003 was to determine the solubility of DF003 in various aqueous buffers and formulation components. Solubility of DF003 in water was found to be 1.4 mg/mL. DF003 showed lower solubility in 0.1 N HCl buffer pH 1.5 (0.3 mg/mL) than in phosphate buffer pH 7.2–7.4 (3.6 mg/mL). Labrafac™ oil, which forms the core of the LNCs, showed lower solubility of DF003 (0.4 mg/g) as compared to the solubility in pure water. On the other hand, Kolliphor® HS 15, which makes up the shell of the LNCs, showed the highest solubility of more than 25 mg/g. Interestingly, for Kolliphor® HS 15, DF003 dissolved quickly, and saturation was not reached at the highest concentration tested of 25 mg/g.

4.1.2. Formulation development, optimization, and characterization of LNCs

The DF003 nanoformulations were prepared and optimized using a phase inversion method with various combinations of excipients (Valcourt et al., 2016). LNCs consists of an oil, Labrafac™ lipophile WL 1349 which forms the core of the nanocapsules, surrounded and stabilized by a mixture of hydrophilic (Kolliphor® HS 15) and hydrophobic (phospholipids) surfactants. LNCs prepared without phospholipids showed signs of immediate phase separation as shown for formulation F1 in Table 3. This suggests an important role of phospholipids in preserving the formulation stability which was previously also been shown by by Minkov et al. and Vonarbourg et al. (Minkov et al., 2005a; 2005b;; Vonarbourg et al., 2005). This led to studying the impact of different phospholipids on the stability and properties of the LNC formulations (F2, F3, F4, F5) prepared without drug loading. The use of different phospholipids (Phospholipon® 90 H, Lipoid S 75, Phospholipon® 80 H, and Lipoid S PC-3) did not affect the stability of the formulations as all the formulations were found to be stable. The different phospholipids vary in the fraction of phosphatidylcholine and the ratio of the different phospholipids in the excipient (phosphatidylcholine and phosphatidylethanolamine) and different ratios of fatty acids (palmitic acid, stearic acid, and other unsaturated fatty acids). The particle size was not dependent on the choice of phospholipid preparation and the PdI remained low in all cases, demonstrating a narrow size distribution (Fig. 3, Table 3). In addition, all tested phospholipid preparations resulted in physically stable negatively charged particles as shown by the zeta potential (Fig. 3, Table 3). The zeta potential is more negative for LNCs prepared with Lipoid S 75 (F2) and Phospholipon® 80 H (F3) as compared to LNCs with Lipoid S PC-3 (F4) and Phospholipon® 90 H (F5). Although the zeta potential was larger for formulations containing Lipoid S 75, Phospholipon® 80 H, this did not result in differences in particle size and polydispersity. Phospholipon® 90 H was selected for further formulation development due to its suitability for parenteral administration, whereas Phospholipon® 80 H is not approved for parenteral use and Lipoid S 75, the surfactant used in the original method as described by Valcourt et al. (Valcourt et al., 2016), was discontinued by the supplier. Overall, the use of different phospholipids exhibited similar formulation characteristics.

In Table 3, the particle size and PdI of all the studied combinations with and without drug loading are summarized. Particle size and PdI of all the combinations were less than 100 nm and 0.25, respectively. It is apparent from the results in Table 3 that an increased amount of Labrafac™ (6.2% w/v in F7 and 9.3% w/v in F9), which forms the core of LNCs, results in an increased size of the nanoparticles. On the other hand, an increased amount of Kolliphor® HS 15 results in a decreased particle size of LNCs (F6, F7 and F8). Apparently, the ratio between Labrafac™ and surfactant (Kolliphor® HS 15) is important for the size of nanoparticles. The more surfactant the better stabilization of smaller nanoparticles, and this can be achieved due to reduced interfacial tension during their formation. An increased oil proportion reduces the surfactant to oil ratio and thus results in particles with larger diameter. This behavior is in line with previous findings by Anton and Saulnier (Anton and Saulnier, 2013) and Aparicio-Blanco et al. (Aparicio-Blanco

Table 3
Optimization and characterization data of LNCs.

Formulation	Particle size (d.nm)	PdI	% EE	Drug loading (mg/mL)	Zeta potential (mV)
F1	Immediate signs of phase separation				
F2	55 ± 0.4	0.06 ± 0.00	–	–	−12.8 ± 0.2
F3	57 ± 0.1	0.07 ± 0.01	–	–	−12.6 ± 0.6
F4	58 ± 0.9	0.07 ± 0.02	–	–	−1.3 ± 0.3
F5	57 ± 0.6	0.05 ± 0.01	–	–	−2.7 ± 1.5
F6	76 ± 1.2	0.16 ± 0.02	69 ± 0.5	1.4 ± 0.07	−11.6 ± 0.4
F7	51 ± 0.0	0.16 ± 0.00	82 ± 2.2	1.6 ± 0.05	−7.7 ± 0.5
F8	54 ± 2.9	0.25 ± 0.04	89 ± 0.5	1.8 ± 0.02	−7.4 ± 0.4
F9	91 ± 8.7	0.21 ± 0.03	84 ± 2.1	1.6 ± 0.00	−12.5 ± 0.1
F10	68 ± 1.4	0.12 ± 0.03	82 ± 6.3	0.8 ± 0.11	−8.2 ± 0.2

Values are expressed as mean ± SD (n = 3)

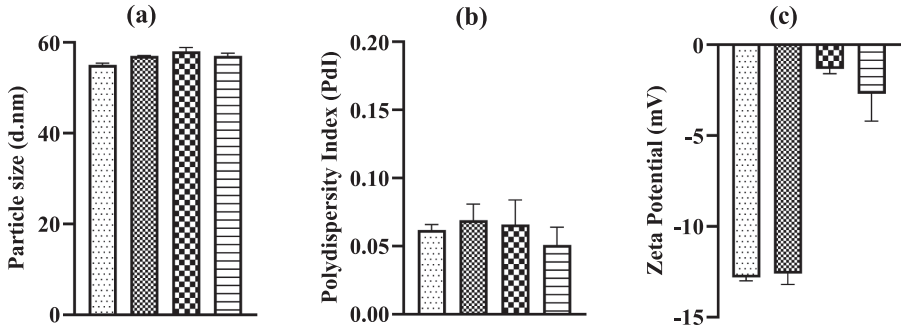

Fig. 3. Particle size (a), polydispersity index (b) and zeta potential (c) of LNCs prepared with Lipoid S 75 (Table 1: F2) (▭), Phospholipon® 80 H (Table 1: F3) (▨), Lipoid S PC-3 (Table 1: F4) (▩) and Phospholipon® 90 H (Table 1: F5) (▭) (mean ± SD; n = 3).

et al., 2019). Drug loaded LNCs in formulations F6 to F10 showed polydispersity values of 0.25 or smaller. A polydispersity of less than 0.25 is indicative of a narrow distribution of particles sizes of the lipid vehicles. Unloaded particles appear to show lower polydispersity index compared to the LNCs prepared without drug (F2 to F5 compared to F6 to F10, Table 3). This may indicate an even narrower size distribution for unloaded particles. The difference may however also be due to experimental differences as the unloaded particles were diluted 60 times with water prior to measurement. Dilution of the LNCs did not affect particle size and zeta potential but decreased PdI (data not shown).

Drug loaded LNCs showed higher surface charge (more negative zeta potential compared to the formulations prepared without drug (F6 to F9 vs F2 to F5; Table 3) indicating that incorporation of the drug in the particles increases the surface charge and that the resulting LNCs are more stable than the unloaded LNCs. For the drug loaded formulations, the zeta potential showed less variability between varying compositions than between loaded and unloaded LNCs. In formulations F6, F7, and F8 at a fixed concentration of Labrafac™ 6.2% w/v, and drug to lipid ratio of 1:32, a zeta potential of −11.6 was evident with F6 having 4.8% w/v of Kolliphor® HS 15, whereas in F7 and F8, slightly less negative zeta potentials of −7.7 mV and −7.4 mV, respectively, were observed. The higher amount of non-ionic surfactant (Kolliphor® HS 15) in F7 and F8 compared to F6, may hide the overall charge on the particle surface. Further, the zeta potential of F6 and F9 was similar as the surfactant to oil ratio and lipid to drug ratio remains the same. Formulations F6 and F10 have similar composition except that F10 has a lower drug ratio, resulting in lower surface charge for F10. Overall, the zeta potential of LNCs is mainly related to the drug loading and the amount of Kolliphor® HS 15.

The drug entrapment efficiency and drug loading are also shown in Table 3. Drug entrapment efficiency and drug loading are high for all compositions tested. Entrapment efficiency of DF003 is comparable to earlier data by Lamprecht at al. and Malzert-Fréon et al. for more lipophilic drugs like amiodarone and tripentone (Lamprecht et al., 2002; Malzert-Freon et al., 2006). It shows that LNCs may be good drug carriers also for more hydrophilic drugs such as DF003. As can be seen from Table 3, drug entrapment efficiency and drug loading are not dependent on the amount of oil (F7 and F9). The solubility of DF003 in Labrafac™ (0.4 mg/g) is poor and a larger amount of oil does not increase the entrapment efficiency and drug loading in the LNCs. In contrast, the solubility of DF003 is very high in Kolliphor® HS 15 (> 25 mg/g) and an increased entrapment efficiency is evident for higher proportions of Kolliphor® HS 15. An entrapment efficiency of 70% was found with 4.8% w/v of Kolliphor® HS 15 (F6) while, F7 and F8 with 7.2% and 9.6% of Kolliphor® HS 15 resulted in LNCs with an entrapment efficiency of 82% and 89%, respectively. At higher drug to lipid ratio of 1:32 (F6), compared to 1:64 in F10, a lower entrapment efficiency was observed but with an overall increase in drug loading (Table 3). Although LNCs at each composition showed good characteristics, F6 was chosen for further characterization.

4.1.2.1. Morphology by cryogenic transmission electron microscopy. Formulations without and with DF003 (F5 and F6 respectively) were analyzed by cryo-TEM and the micrographs are presented in Fig. 4. It can be seen from the micrographs that the employed phase inversion process resulted in the formation of LNCs. The LNCs are of spherical shape and look similar for both unloaded and drug loaded LNCs, suggesting that drug loading does not alter the structure of the formed

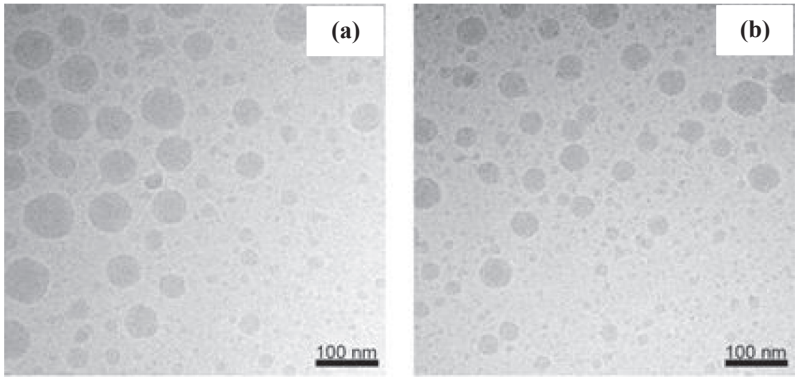

Fig. 4. Cryogenic transmission electron micrographs of (a) unloaded, and (b) drug loaded LNCs.

nanoparticles. Moreover, the size distribution of LNCs from cryo-TEM analysis is in accordance with the size distribution profile obtained with DLS for lab scale process (Fig. 11).

4.1.3. In vitro drug release testing of LNCs formulations

Drug release testing serves as a performance indicator for the sustained release behavior of the formulation. Additionally, it can demonstrate how strongly the drug is entrapped in the nanoparticles. In the present investigation, drug release testing from LNCs was done by measuring the drug diffusion across a 100 kD dialysis membrane. Sink conditions were maintained by keeping small donor and large acceptor volumes in the experimental setup. Concentrations of DF003 at the receptor site of the membrane did not exceed 17% of donor concentration. Additionally, gentle stirring was applied in the acceptor side to ensure uniform mixing of released drug. As can be seen in Fig. 5, the drug diffusion across the dialysis membrane was much slower for drug loaded LNCs compared to free drug. The diffusion of free DF003 was fast and > 80% of the drug was diffused within 4 h. Interestingly, DF003 loaded LNCs showed a much longer release profile with a duration of 6 days with an initial burst release phase. Previous studies on LNCs loaded with more hydrophobic drugs like amiodarone and tripentone showed sustained release behavior of 10 days (approximately 60% drug release) and 14 days, respectively (Lamprecht et al., 2002; Malzert-Freon et al., 2006). For more hydrophilic molecules like DF003, the main challenge of nanolipid formulations like LNCs is encapsulating the drug with a significant encapsulation yield and at the same time controlling the release induced by diffusion of the hydrophilic drug to the aqueous bulk phase. In a study by Vrigneaud et al. using hydrophilic doxorubicin hydrochloride, sustained release was achieved when the doxorubicin was loaded in a reverse micellar form in the oily core of the LNCs (Vrignaud et al., 2011). Although DF003 also is a hydrophilic drug, substantial loading was achieved and the obtained drug release profile was similar to that of some lipophilic drugs like amiodarone and tripentone, with extended release up to 6 days. Several attempts were made to load DF003 also in a reversed micellar form into the LNCs, but these were unsuccessful (data not shown). The data suggests that DF003 interacts strongly with Kolliphor® HS 15 resulting in sustained drug release to the aqueous environment.

Additionally, drug release was studied in an aqueous buffer containing hyaluronic acid. Hyaluronic acid (HA) is a major component of the vitreous that forms the largest anatomical region in the eye. The vitreous body is mainly composed of water, proteins and HA. Along with collagen, HA is responsible for maintaining the integrity of the eye structure. Drugs administered by the intravitreal route will be exposed to vitreous components and an interaction is possible. For example, nanoparticles could interact with the negatively charged HA which could lead to nanoparticle destabilization. The drug release profile in hyaluronic acid was found to be similar to the release profile in phosphate buffer and no significant differences were evident ($p > 0.05$, two-tailed paired *t*-test) (Fig. 5).

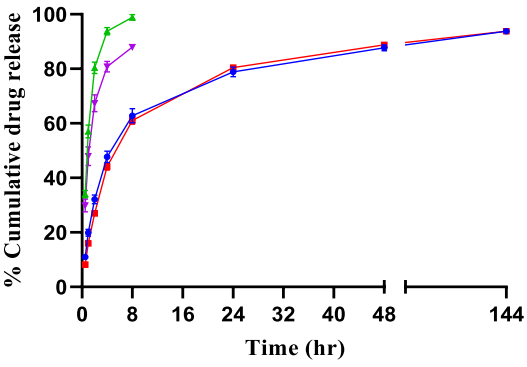

Fig. 5. *In vitro* release testing of free drug in phosphate buffer (-•-), free drug in hyaluronic acid (-•-), drug loaded LNCs (F6) in phosphate buffer (-•-) and drug loaded LNCs (F6) in hyaluronic acid (-•-). (Mean ± SD, n = 3).

4.1.4. Stability testing of formulations

4.1.4.1. Colloidal stability evaluation of LNCs. Nanoparticle preparations, especially dispersion systems, often encounter various stability challenges. LNCs, like any other emulsion systems, could potentially show particle aggregation or creaming phenomena that leads to phase separation and instability. Thus, it is crucial that the formulations are stable until their use, and for this reason, formulated lipid nanocapsules were tested for their physical stability by storing them at room temperature (25°C) and at refrigerated conditions (2–8°C). Firstly, samples were studied for their physical appearance and none of the formulations showed any signs of a phase separation during storage for one month at 25°C or 2–8°C. This is further supported by minimal changes in both particle size and particle size distribution as indicated by the low PdI values (Fig. 6). Additionally, the zeta potential values remain unchanged, further demonstrating a good physical stability of the LNCs. A slight decrease (< 10% of drug load) in the amount of drug associated to the particles was observed during storage as expressed by the entrapment efficiency. Overall, it can be concluded that the drug loaded formulations are physicochemically stable during storage for at least one month. ($p > 0.05$ for all parameters between both storage conditions, paired *t*-test).

4.1.4.2. Stability of LNCs in vitreous components by direct incubation in hyaluronic acid sodium. Stability of LNCs was studied in presence of hyaluronic acid to simulate vitreous fluid for seven days. The data demonstrate that neither the particle size nor the polydispersity index changed significantly during a seven-day study period at 37°C ($p > 0.05$, one-way ANOVA, Tukey's multiple comparison test) (Fig. 7). The negative surface charge of both HA and LNCs may prohibit interactions between the polymer and the particles, thereby preventing effects on the physical stability. This study along with the drug release testing in hyaluronic acid concludes that the LNC particles are compatible with HA at the concentrations found in the eye.

4.2. Manufacture of LNCs at large scale

The phase inversion process is highly energy efficient as this process uses internal chemical energy, arising from the changes in surfactant behavior, to form the nanoparticles and does not require a high-energy equipment like high pressure homogenizer or microfluidizer (Solans and Solé, 2012). Moreover, organic solvents are not needed to produce LNCs, making this process environmental friendly and viable for commercial applications. In the present paper, the scalability of the LNCs manufacturing process has been studied. Here, the volume scale of the process was increased from a lab scale of a few mL to the volumes of 10 L to understand the impact of scale on the LNCs production and their quality parameters. Initially two batches of LNCs at 1 L volume were manufactured using a similar process as for lab scale to check the reproducibility and robustness of the process. The resultant LNCs were characterized for particle size and size distribution which did not differ between these two batches (Table 4). Furthermore, particle concentration as expressed by the derived count rate values obtained from DLS did not vary between the batches indicating the consistency in product characteristics between these two batches, demonstrating that the process is reproducible. Manufacturing of LNCs even at a higher scale of 10 L using the same batch wise process resulted in nanocapsules with comparable characteristics as for lab scale and 1 L scale-up, as demonstrated in Table 4. Thus, the process can be scaled up to higher volumes with little impact on product quality parameters such as particle size,

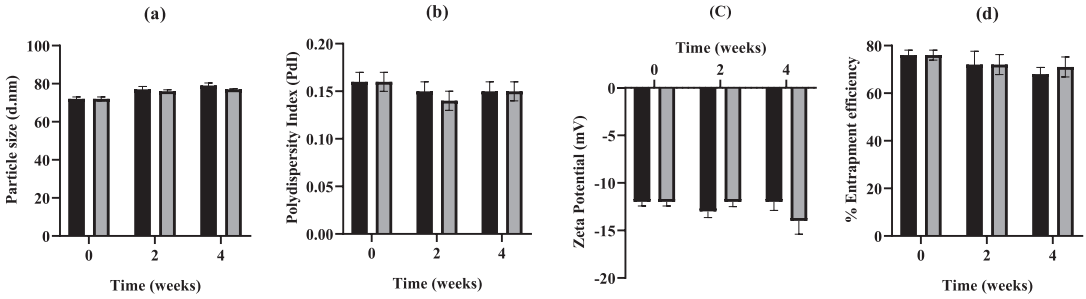

Fig. 6. Colloidal stability evaluation of drug loaded LNCs (F6) stored at room temperature (■) and at 2–8°C (▭). (Mean ± SD, n = 3).

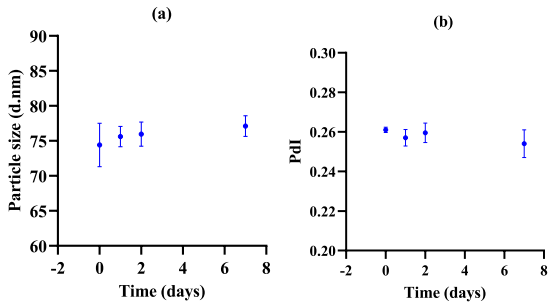

Fig. 7. Stability of LNCs (F6) in presence of Hyaluronic acid sodium: (a) changes in particle size, (b) changes in polydispersity Index. (Mean ± SD, n = 3).

Table 4
Characterization of upscaled LNCs manufactured with batch and continuous manufacturing processes.

Batch/ (volume)	Type of process	Particle size (d.nm)	PdI	Zeta Potential (mV)	DCR (kcps)
Lab scale/ (0.01 L)#	Batch	58 ± 0.7	0.06 ± 0.01	−2.0 ± 1.0	122273 ± 6990
Scale-up/(1 L)*	Batch	57 ± 0.0	0.06 ± 0.01	−1.6 ± 0.2	115002 ± 1317
Scale-up/(1 L)**	Continuous	59	0.08	–	117012
Scale-up/ (10 L)**	Batch	59	0.01	−1.8	113505

#n = 3, *n = 2 (data represented as mean ± SD), **n = 1.

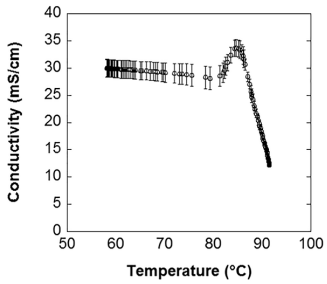

Fig. 8. Conductivity as a function of the dispersion temperature for the last heating cycle when the temperature is raised from 60°C to 90 C, for 1 L with batch process. (Mean ± SD, n = 2).

polydispersity, and particle concentration.

Phase inversion methodology employed in this investigation to produce LNCs is governed by a temperature dependent changes in the surfactant behavior. At low temperatures, surfactant is in a hydrated state with a positive curvature that favors the formation of an O/W emulsion. With increase in temperature, the surfactant loses its ability to form hydrogen bonds with water and undergoes dehydration with a negative curvature that prefers the formation of a W/O emulsion. This whole process can be characterized by a higher conductivity at lower temperature and vice versa. In Fig. 8, the conductivity as a function of the dispersion temperature for the last cycle (60°C to 90°C) during 1 L scale-up with the batch manufacturing process is visualized. High conductivity values can be seen at lower temperatures and a lower conductivity is visible at higher temperatures which is similar to the previous findings by Heurtault et al. (Heurtault et al., 2002). This phenomenon is an indication of a phase inversion from O/W to W/O emulsion with increase in temperature, and the conductivity measurements offer a possibility of monitoring the LNCs preparation process and can thus be used as an in-process control. The conductivity changes over the three temperature cycles follow the same pattern for both 1 L and 10 L scale-up (Fig. 9). However, from Fig. 9, it can also be seen that the heating and cooling cycles are scale dependent. It obviously takes longer time to heat and cool at larger scale and this will increase the manufacturing time.

In the above-mentioned batch manufacturing process, only a single water bath was used for both heating and cooling the excipient mixture and there was a significant time consumption to obtain the desired temperature. This will result in long manufacturing time scales, especially at high manufacturing volumes. To reduce the impact of scale on the process time for heating and cooling cycles, the batch process was modified to be suitable for a continuous operation. For this purpose, a medium scale of a vertical oscillatory baffled reactor vessel (Fig. 10c) was tested. The vertical reactor was connected to two water baths for

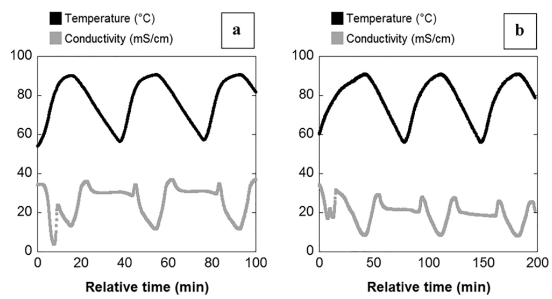

Fig. 9. Dispersion temperature and conductivity as a function of time during the LNCs manufacturing process. (a) scale-up at 1 L volume (b) scale-up at 10 L volume, both with batch process.

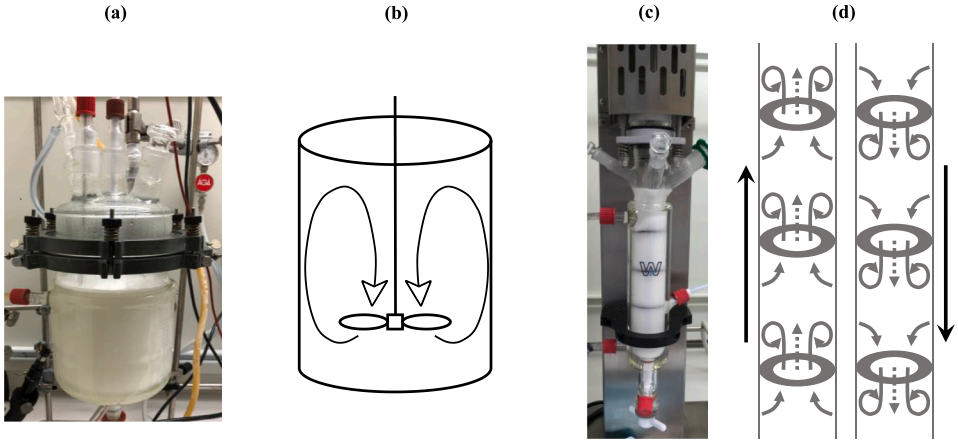

Fig. 10. Manufacturing of LNCs at large scale. (a), (b) represents the reaction vessel and predicted liquid flow pattern in a batch operation and (c), (d) indicates the oscillatory baffled reactor and its flow pattern. In figure (d), liquid flow is indicated by dashed arrows and the solid arrows outside the drawing indicates the movement of baffles (Abbott et al., 2013).

heating and cooling the excipient mixture to reduce the process time. This oscillatory reactor setup generates liquid flow patterns that are similar to the patterns achieved with a large scale continuous oscillatory baffled reactor. Agitation in the utilized baffled reactor is caused by oscillating baffles to achieve improved heat transfer and better mixing of the excipient mixture (Abbott et al., 2013; Bianchi et al., 2020) thereby increasing the process efficiency and reducing the process times. This manufacturing process resulted in particles with a size around 59 nm, a size that correlates well with the batch method. Moreover, both the PdI and the derived count rate are in the same range as for the batch method (Table 4). Upscaling of this medium scale process to manufacture large volumes of particles can simply be achieved by connecting several oscillatory baffled reactors into a continuous oscillatory baffled reactor without changing the flow properties of the liquid and thereby producing LNCs with the same quality.

4.2.1. Manufacturing of sterile LNCs at 1 L scale

For parenteral applications it is essential that the manufacturing process can be adapted for introduction of sterilization steps. Indeed, although the manufacturing was not performed under aseptic sterile conditions, we tested the critical steps for sterile manufacture. The batch process was modified to accommodate the necessary sterilization steps to reduce the bioburden during the manufacturing. This method included a sterile filtration (0.22 μ) and a subsequent heat sterilization of the excipient mixture. Phospholipon® 90 H was added after the filtration as it caused clogging of the filter used for sterile filtration. Additionally, a final sterile filtration step was included after the preparation of LNCs. These process steps to reduce the bioburden did not affect the properties of the LNCs to a large extent. Stable nanosized particles were obtained following heat sterilization of the excipient mixture and sterile filtration of the final product (Table 5).

The method suitability test for TAMC by filtration according to European Pharmacopoeia was established successfully to test the bioburden of the formulation. For test formulations, microbial colonies were not detected on the surface of TSA cassettes, giving a TAMC value

Table 5
Characterization of upscaled LNCs prepared with sterile manufacturing process.

Sample type	Particle size (d.nm)	PdI	Zeta Potential (mV)	DCR (kcps)
Non-filtered	66	0.11	−1.6	131044
Sterile filtered	65	0.12	−1.7	133748

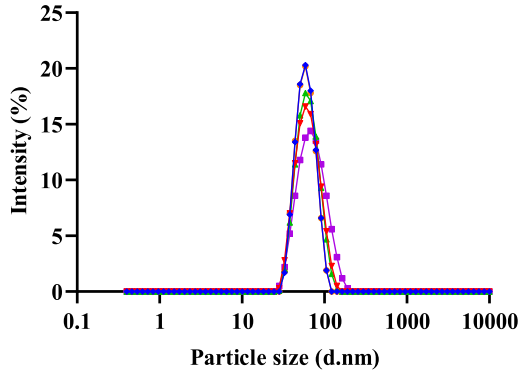

Fig. 11. Comparison of the particle size data of LNCs manufactured at different scales and processes: lab scale (), 100 times scale-up with batch process (), 1000 times scale-up with batch process (), continuous process (), sterile manufacturing process ().

Table 6
Stability data of LNCs prepared at different manufacturing scales.

Stability duration	Lab scale	100 times scale-up with batch process (1 L)	1000 times scale-up with batch process (10 L)	Continuous process (1 L)	Sterile manufacturing process (1 L)
			Particle size (d.nm)		
Initial	57	57	59	59	65
1 month	62	59	59	60	67
6 months	–	–	–	64	–
			Polydispersity Index (PdI)		
Initial	0.05	0.07	0.10	0.08	0.12
1 month	0.03	0.04	0.05	0.05	0.11
6 months	–	–	–	0.06	–
			Zeta Potential (mV)		
Initial	−2.7	−1.7	−1.8	–	−1.7
1 month	−1.9	−3.5	−3.7	–	−2.2

of 0 CFU/mL. Overall, the physicochemical properties of nanoparticles and subsequent testing of the LNCs formulation for microbial purity demonstrated that the inclusion of several sterilization steps led to the manufacture of LNCs with very low microbial burden, without affecting the nanoparticles to any greater extent.

Overall, LNCs manufactured at different volume scales using different setups resulted in highly monodisperse nanoparticles with similar product characteristics (Fig. 11). Further, the LNCs were assessed for their stability by storing them at 2–8°C. Samples were measured for changes in particle size, polydispersity index and zeta potential for at least one month and the data is presented in Table 6. No significant deviations from initial values were seen with respect to all the studied parameters for one month. Further, the formulation made with the continuous manufacturing process was studied for an extended duration of 6 months and it was observed that the studied parameters were unchanged. These results indicate that the large-scale production processes resulted in stable LNCs.

5. Conclusion

In the present work, lipid nanocapsules were developed as a lipid nano delivery system for the novel drug molecule, DF003 that has showed neuroprotective properties in previous studies. Varied compositions of nanocapsules were prepared with a phase inversion method and thoroughly characterized. All the studied compositions resulted in stable nanoparticles with high entrapment efficiency and drug loading. The selected formulation showed a significantly extended release over a 6-day time period as compared to the free drug. The interaction of the hydrophilic DF003 with the lipid nanoparticles will need to be studied further and will be the subject of future investigations. Due to the invasive nature of intravitreal administration, the dosing frequency of an intravitreal drug should be as low as possible. For DF003, the current *in vitro* release rate of the drug in the LNCs may still be too fast and require additional development of the drug delivery system. *In vivo* release studies combined with appropriate knowledge of drug concentration requirements at the target site will set the stage for such development. The formulation manufacturing process was developed to produce LNCs at high volumes without any noticeable deviation from the lab scale data. Additionally, sterilization steps were included to reduce the bioburden and to produce sterile nanoparticles. Combining a continuous manufacturing method with the sterilization steps could become a successful strategy for manufacturing LNCs at higher volume scales. Such a manufacturing process will be suitable for technology transfer to production lines that is needed for the introduction of new drugs to treat patients.

CRediT authorship contribution statement

Dileep Urimi: Investigation, Methodology, Writing - review & editing. **Ronja Widenbring:** Investigation, Methodology, Supervision. **Raúl Oswaldo Pérez García:** Methodology. **Lars Gedda:** Investigation, Methodology. **Katarina Edwards:** Investigation, Methodology. **Thorsteinn Loftsson:** Supervision. **Nicolaas Schipper:** Funding acquisition, Supervision.

Declaration of Competing Interest

The authors declare that they have no known competing financial interests or personal relationships that could have appeared to influence the work reported in this paper.

Acknowledgment and Funding

This work was financially supported by grants from the European Union (*trans*Med, H2020-MSCA-ITN-2017-765441 and FORMAMP, FP7/2007-2013-604182)

References

Abbott, M., Harvey, A., Perez, G.V., Theodorou, M., 2013. Biological processing in oscillatory baffled reactors: operation, advantages and potential. Interface Focus 3, 20120036.
Abdel-Mottaleb, M.M., Neumann, D., Lamprecht, A., 2011. Lipid nanocapsules for dermal application: a comparative study of lipid-based versus polymer-based nanocarriers. Eur. J. Pharm. Biopharm. 79, 36–42.
Agrahari, V., Agrahari, V., Mandal, A., Pal, D., Mitra, A.K., 2017. How are we improving the delivery to back of the eye? Advances and challenges of novel therapeutic approaches. Expert Opinion on Drug Delivery 14, 1145–1162.
Almgren, M., Edwards, K., Karlsson, G., 2000. Cryo transmission electron microscopy of liposomes and related structures. Colloids Surf., A 174, 3–21.
Anton, N., Saulnier, P., 2013. Adhesive water-in-oil nano-emulsions generated by the phase inversion temperature method. Soft Matter 9, 6465–6474.
Aparicio-Blanco, J., Sebastián, V., Rodríguez-Amaro, M., García-Díaz, H.C., Torres-Suárez, A.I., 2019. Size-tailored design of highly monodisperse lipid nanocapsules for drug delivery. J. Biomed. Nanotechnol. 15, 1149–1161.
Beloqui, A., Solinís, M.Á., Rodríguez-Gascón, A., Almeida, A.J., Préat, V., 2016. Nanostructured lipid carriers: promising drug delivery systems for future clinics. Nanomed.: Nanotechnol. Biol. Med. 12, 143–161.
Bianchi, P., Williams, J.D., Kappe, C.O., 2020. Oscillatory flow reactors for synthetic chemistry applications. J. Flow Chem. 1–16.
del Amo, E.M., Rimpelä, A.-K., Heikkinen, E., Kari, O.K., Ramsay, E., Lajunen, T., Schmitt, M., Pelkonen, L., Bhattacharya, M., Richardson, D., 2017. Pharmacokinetic aspects of retinal drug delivery. Progr. Retinal Eye Res. 57, 134–185.
Ekström, P., Paquet-durand, F., Gaillard, P.J., Marigo, V., Genieser, H.-G., Rentsch, A., Trifunovic, D., Tekgoz, A.S., 2019. Targeted liposomal delivery of cGMP analogues. Google Patents.
Formica, M.L., Gamboa, G.U., Tártara, L., Luna, J., Benoit, J., Palma, S.D., 2020. Triamcinolone acetonide-loaded lipid nanocapsules for ophthalmic applications. Int. J. Pharm. 573, 118795.
Formica, M.L., Legeay, S., Bejaud, J., Montich, G.G., Gamboa, G.V.U., Benoit, J.-P., Palma, S.D., 2021. Novel hybrid lipid nanocapsules loaded with a therapeutic monoclonal antibody–Bevacizumab–and Triamcinolone acetonide for combined therapy in neovascular ocular pathologies. Mater. Sci. Eng., C 119, 111398.
Fung, A.E., 2010. A novel sustained-release intravitreal drug delivery system for retinal vascular disease. Retina Today 5, 51–53.
Gan, L., Wang, J., Jiang, M., Bartlett, H., Ouyang, D., Eperjesi, F., Liu, J., Gan, Y., 2013. Recent advances in topical ophthalmic drug delivery with lipid-based nanocarriers. Drug Discovery Today 18, 290–297.
Germain, M., Caputo, F., Metcalfe, S., Tosi, G., Spring, K., Åslund, A.K., Pottier, A., Schiffelers, R., Ceccaldi, A., Schmid, R., 2020. Delivering the power of nanomedicine to patients today. J. Control. Release 326, 164–171.
Groo, A.-C., Matougui, N., Umerska, A., Saulnier, P., 2018. Reverse micelle-lipid nanocapsules: a novel strategy for drug delivery of the plectasin derivate AP138 antimicrobial peptide. Int. J. Nanomed. 13, 7565.
Heurtault, B., Saulnier, P., Pech, B., Proust, J.-E., Benoit, J.-P., 2002. A novel phase inversion-based process for the preparation of lipid nanocarriers. Pharm. Res. 19, 875–880.
Hirsjärvi, S., Dufort, S., Gravier, J., Texier, I., Yan, Q., Bibette, J., Sancey, L., Josserand, V., Passirani, C., Benoit, J.-P., 2013. Influence of size, surface coating and fine chemical composition on the in vitro reactivity and in vivo biodistribution of lipid nanocapsules versus lipid nanoemulsions in cancer models. Nanomed. Nanotechnol. Biol. Med. 9, 375–387.
Hureaux, J., Lagarce, F., Gagnadoux, F., Vecellio, L., Clavreul, A., Roger, E., Kempf, M., Racineux, J.-L., Diot, P., Benoit, J.-P., 2009. Lipid nanocapsules: ready-to-use nanovectors for the aerosol delivery of paclitaxel. Eur. J. Pharm. Biopharm. 73, 239–246.
Huynh, N.T., Passirani, C., Saulnier, P., Benoît, J.-P., 2009. Lipid nanocapsules: a new platform for nanomedicine. Int. J. Pharm. 379, 201–209.
Lamprecht, A., Bouligand, Y., Benoit, J.-P., 2002. New lipid nanocapsules exhibit sustained release properties for amiodarone. J. Control. Release 84, 59–68.
Lim, S.B., Banerjee, A., Önyüksel, H., 2012. Improvement of drug safety by the use of lipid-based nanocarriers. J. Control. Release 163, 34–45.
Lombardo, D., Kiselev, M.A., Caccamo, M.T., 2019. Smart nanoparticles for drug delivery application: development of versatile nanocarrier platforms in biotechnology and nanomedicine. Journal of Nanomaterials 2019.
Malzert-Freon, A., Vrignaud, S., Saulnier, P., Lisowski, V., Benoit, J., Rault, S., 2006. Formulation of sustained release nanoparticles loaded with a tripentone, a new anticancer agent. Int. J. Pharm. 320, 157–164.
Minkov, I., Ivanova, T., Panaiotov, I., Proust, J., Saulnier, P., 2005a. Reorganization of lipid nanocapsules at air–water interface: I. Kinetics of surface film formation. Colloids Surf., B 45, 14–23.
Minkov, I., Ivanova, T., Panaiotov, I., Proust, J., Saulnier, P., 2005b. Reorganization of lipid nanocapsules at air–water interface: part 2. Properties of the formed surface film. Colloids Surf., B 44, 197–203.
Mouzouvi, C.R., Umerska, A., Bigot, A.K., Saulnier, P., 2017. Surface active properties of lipid nanocapsules. PLoS ONE 12, e0179211.
Patra, J.K., Das, G., Fraceto, L.F., Campos, E.V.R., del Pilar Rodriguez-Torres, M., Acosta-Torres, L.S., Diaz-Torres, L.A., Grillo, R., Swamy, M.K., Sharma, S., 2018. Nano based drug delivery systems: recent developments and future prospects. J. Nanobiotechnol. 16, 71.
Ph. Eur. 10.0, 2020. Microbiological examination of non-sterile products: Microbial enumeration tests, 01/01/2020 ed.

Sahoo, S.K., Dilnawaz, F., Krishnakumar, S., 2008. Nanotechnology in ocular drug delivery. Drug Discovery Today 13, 144–151.
Solans, C., Solé, I., 2012. Nano-emulsions: formation by low-energy methods. Curr. Opin. Colloid Interface Sci. 17, 246–254.
Sun, R., Zhang, A., Ge, Y., Gou, J., Yin, T., He, H., Wang, Y., Zhang, G., Kong, J., Shang, L., 2020. Ultra-small-size Astragaloside-IV loaded lipid nanocapsules eye drops for the effective management of dry age-related macular degeneration. Expert Opinion on Drug Delivery 17, 1305–1320.
Thomas, O., Lagarce, F., 2013. Lipid nanocapsules: a nanocarrier suitable for scale-up process. J. Drug Delivery Sci. Technol. 23, 555–559.
Umerska, A., Matougui, N., Groo, A.-C., Saulnier, P., 2016. Understanding the adsorption of salmon calcitonin, antimicrobial peptide AP114 and polymyxin B onto lipid nanocapsules. Int. J. Pharm. 506, 191–200.
Valcourt, C., Saulnier, P., Umerska, A., Zanelli, M., Montagu, A., Rossines, E., Joly-Guillou, M.-L., 2016. Synergistic interactions between doxycycline and terpenic components of essential oils encapsulated within lipid nanocapsules against gram negative bacteria. Int. J. Pharm. 498, 23–31.
Ventola, C.L., 2017. Progress in nanomedicine: approved and investigational nanodrugs. Pharmacy and Therapeutics 42, 742.
Vighi, E., Trifunović, D., Veiga-Crespo, P., Rentsch, A., Hoffmann, D., Sahaboglu, A., Strasser, T., Kulkarni, M., Bertolotti, E., Van Den Heuvel, A., 2018. Combination of cGMP analogue and drug delivery system provides functional protection in hereditary retinal degeneration. Proc. Natl. Acad. Sci. 115, E2997–E3006.
Vonarbourg, A., Saulnier, P., Passirani, C., Benoit, J.P., 2005. Electrokinetic properties of noncharged lipid nanocapsules: influence of the dipolar distribution at the interface. Electrophoresis 26, 2066–2075.
Vrignaud, S., Anton, N., Gayet, P., Benoit, J.-P., Saulnier, P., 2011. Reverse micelle-loaded lipid nanocarriers: a novel drug delivery system for the sustained release of doxorubicin hydrochloride. Eur. J. Pharm. Biopharm. 79, 197–204.
Zhai, Q., Li, H., Song, Y., Wu, R., Tang, C., Ma, X., Liu, Z., Peng, J., Zhang, J., Tang, Z., 2018. Preparation and optimization lipid nanocapsules to enhance the antitumor efficacy of cisplatin in hepatocellular carcinoma HepG2 cells. AAPS PharmSciTech 19, 2048–2057.

Paper II

molecular pharmaceutics

pubs.acs.org/molecularpharmaceutics

Article

Structural Characterization Study of a Lipid Nanocapsule Formulation Intended for Drug Delivery Applications Using Small-Angle Scattering Techniques

Dileep Urimi,* Maja Hellsing, Najet Mahmoudi, Christopher Söderberg, Ronja Widenbring, Lars Gedda, Katarina Edwards, Thorsteinn Loftsson, and Nicolaas Schipper

Cite This: https://doi.org/10.1021/acs.molpharmaceut.1c00648

Read Online

ACCESS | Metrics & More | Article Recommendations | Supporting Information

ABSTRACT: Lipid nanocapsules (LNCs) are increasingly being used for various drug delivery applications due to their versatile nature and ability to carry a wide variety of therapeutic drug molecules. In the present investigation, small-angle X-ray (SAXS) and neutron scattering (SANS) techniques were used to elucidate the structure of LNCs. Overall, size measurements obtained from SAXS and SANS techniques were complemented with dynamic light scattering, zeta potential, and cryogenic transmission electron microscopy measurements. The structural aspects of LNCs can be affected by drug loading and the properties of the drug. Here, the impact of drug loading on the overall structure was evaluated using DF003 as a model drug molecule. LNCs with varying compositions were prepared using a phase inversion method. Combined analysis of SAXS and SANS measurements indicated the presence of a core−shell structure in the LNCs. Further, the drug loading did not alter the overall core−shell structure of the LNCs. SANS data revealed that the core size remained unchanged with a radius of 20.0 ± 0.9 nm for unloaded LNCs and 20.2 ± 0.6 nm for drug-loaded LNCs. Furthermore, interestingly, the shell becomes thicker in an order of ∼1 nm in presence of the drug compared to the shell thickness of unloaded LNCs as demonstrated by SAXS data. This can be correlated with the strong association of hydrophilic DF003 with Kolliphor HS 15, a polyethylene glycol-based surfactant that predominantly makes up the shell, resulting in a drug-rich hydrated shell.

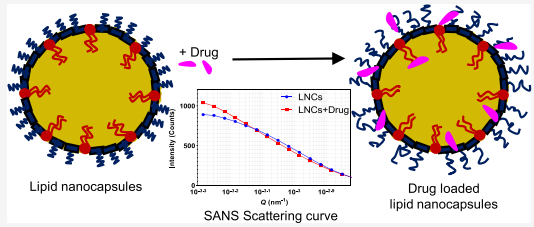

KEYWORDS: *lipid nanocapsules, LNC, nanoparticles, core−shell structure, DF003, small-angle X-ray scattering, SAXS, small-angle neutron scattering, SANS*

1. INTRODUCTION

Lipid nanocapsules (LNCs) are a versatile carrier system often used in drug delivery applications. LNCs are prepared by a phase inversion method[1] where the formation of LNCs is governed by a temperature-dependent behavior of a hydrophilic surfactant such as Kolliphor HS 15 (polyethylene glycol (15)-hydroxystearate). The properties of LNCs can be varied greatly by changing their composition, and they can be prepared in a variety of sizes to suit different applications. LNCs also offer a possibility to load both hydrophilic and hydrophobic drug molecules.[2] Due to their biomimetic nature,[3] LNCs have previously been studied for their suitability as drug delivery systems for treating conditions like cancer, antibiotic resistance, and ocular conditions, including age-related macular degeneration.[4−9]

LNCs comprise a hydrophobic oily core that is surrounded and stabilized by a combination of PEGylated surfactants and phospholipids.[3,10,11] Characterization tools such as dynamic light scattering, cryogenic transmission electron microscopy (cryo-TEM), drop tensiometry, Langmuir balance, and atomic force microscopy have been used to understand the structural properties of LNCs.[3,11,12] Previous studies demonstrate a preferential orientation of phospholipids toward the oily core, whereas a PEGylated surfactant orients toward the aqueous phase, collectively forming a tensioactive cohesive membrane surrounding the oily core.[10,11] Direct confirmatory studies using scattering techniques will provide further information on the internal structure of LNCs. Understanding the structural aspects of LNCs will give more insight into what factors govern their formation and the mechanism of drug interaction, and enable optimization of drug delivery systems for various therapeutic applications.[11,13,14] Furthermore, the structural information provides additional insight about the mechanisms

Received: August 19, 2021
Revised: February 10, 2022
Accepted: February 11, 2022

of LNC interactions with cell membranes. Drugs may selectively deposit in certain parts of LNCs, or they may distribute uniformly depending on their physicochemical properties. By studying the structural aspects of LNCs in combination with understanding the drug localization, a better correlation of in vitro and in vivo performance can be made. This will in turn allow for a further improvement in the nanoparticle properties and performance to suit diverse applications.

Loading of drugs into nanoparticles may induce structural changes of the nanoparticles that have the potential to affect the drug loading efficiency. This is advantageous in certain cases; for instance, encapsulation of doxorubicin into liposomes may result in nanoprecipitation inside the core of liposomes. As a result, morphologically they look like ellipsoidal vesicles compared to spherical structures when they have no drug.[15,16] This nanoprecipitation ultimately results in increased drug loading and a prolonged drug release.[17] However, many novel drug delivery systems that have showed potential for treating various diseases remain poorly characterized at the nanoscale, and how the drug interacts with the drug delivery systems is still unknown in many cases.[18,19] Structural elucidation will thus offer possibilities for a better formulation optimization to suit the desired applications.

A diverse range of experimental methods and tools are available for a detailed structural characterization of nanoparticles. The selection of suitable techniques depends on the part of the system to be studied and on the type and composition of nanoparticles and drugs. More general characterization techniques like dynamic light scattering (DLS) and cryo-TEM are very useful tools, but they may not give a complete and necessary information about the structure of the formulation. DLS, for example, gives information about the apparent hydrodynamic particle size and polydispersity, based on the estimated diffusion coefficient, but it does not measure the internal structure of the particles. However, DLS is often easily accessible and does, in most cases, not require specific sample modifications. On the other hand, advanced characterization techniques like tomography and small-angle X-ray and neutron scattering (SAXS and SANS) allow more accurate size estimation as well as provide insight into the internal structure of nanoparticles.[14] By combining complementary techniques, it is possible to fully characterize particle size, size distribution, shape, internal structure, and intermolecular interactions, resulting in better understanding and prediction of the formulation properties.[20]

In this investigation, in addition to studying unloaded LNCs, drug-loaded LNCs were prepared with DF003, a novel cyclic guanosine-3′,5′-monophosphate (cGMP) analogue. In previous studies, DF003 was found to provide a protective effect on the survival of photoreceptors in cell cultures and animal models of retinal degeneration.[21] The present investigation combines different characterization techniques to unravel the structural properties of unloaded and drug-loaded LNCs. SAXS and SANS are mainly used to determine the structure of LNCs and any influence of drug loading or temperature on the structure. Additionally, an attempt to understand the preferential distribution of drug in LNCs is made. Observations from these experiments are compared and complemented with DLS, zeta potential, and cryo-TEM studies.

2. THEORY OF SMALL-ANGLE SCATTERING

SAXS and SANS are two small-angle scattering techniques, which offer detailed investigation possibilities of samples at colloidal length scales. The structure of particles is obtained from the absolute scattering intensity of X-rays and neutrons, which can be expressed as eq 1.[22,23]

$$I(Q) = n\Delta\rho^2 P(Q)S(Q) \quad (1)$$

where n is the number density of the particles in the sample, and ρ is the scattering length density (SLD) difference between the particles and the dispersion medium (can be calculated from known values of the measured systems).[24,25] Q represents the magnitude of the scattering wave vector $Q = 4\pi/\lambda\sin(\theta/2)$, where θ is the scattering angle and λ is the wavelength of the incident beam. $P(Q)$ represents the form factor, which is related to the size and shape of the nanoparticles in the dispersion medium, and $S(Q)$ represents the structure factor and is related to the interparticle interactions in the dispersion medium.

SAXS can detect nanoscale density differences of electrons in a sample. This means that it can resolve nanoparticle size distributions, study the size and shape of (monodisperse) macromolecules, determine pore sizes, study characteristic distances of partially ordered materials, and much more. LNCs are soft nanoparticles with similar electron density profiles across their whole internal structure, and SAXS alone may not be enough to study their internal structural layers. SANS is in many respects very similar to SAXS, but SANS has a higher sensitivity to lighter elements and has the possibility of isotope labeling. In X-ray scattering, photons interact with the electronic cloud, so the larger the element, the larger the effect. In neutron scattering, neutrons interact with nuclei of atoms, and the interaction is therefore sensitive to isotopes; some light elements like deuterium show similar scattering cross sections as heavy elements. In aqueous dispersions, combinations of normal (H_2O) and heavy (D_2O) water can be used to achieve good signal from a sample. Additionally, by matching the contrast of part(s) of the particle with the dispersion medium, signal can be obtained from a specific region in the particles of interest, e.g., shell of core−shell nanoparticles. Hence, with the proper contrast differences, one can study individual components in complex structures as for example nanoparticles like LNCs. By preparing LNCs with deuterated components, it is possible to extract detailed information about the internal structure of LNCs.[26] SANS with contrast variation provides information about the average particle size, shape, internal structure, and interactions between particles.

3. EXPERIMENTAL SECTION

3.1. Materials. Labrafac lipophile WL 1349, (caprylic−capric acid triglycerides at 54.0%:45.2% as per the certificate of analysis, Ph. Eur. Grade, Gattefossé, France), Kolliphor HS 15 (polyethylene glycol (15)-hydroxystearate, Ph. Eur. Grade, BASF), Phospholipon 90 H (hydrogenated phosphatidylcholine ≥90%, Lipoid, Germany), octanoic-d15 acid, decanoic-d19 acid, sodium chloride, and 50 kD Amicon Ultra-0.5 Centrifugal Filter Units (Sigma-Aldrich Sweden AB, Stockholm) were used in preparation and characterization of LNCs. Drug, DF003 (β-phenyl-1,N^2-etheno-8-bromoguanosine-3′,5′-cyclic monophosphorothiotic acid, sometimes referred to as CN03 in previous publications), was synthesized within RISE Research Institutes

https://doi.org/10.1021/acs.molpharmaceut.1c00648
Mol. Pharmaceutics XXXX, XXX, XXX−XXX

of Sweden (Södertälje, Sweden) as part of the *trans*Med project (H2020-MSCA-765441) to prepare drug-loaded LNCs. Milli-Q water from ELGA, Purelab Prima and D_2O (Cambridge Isotope Laboratories, Inc.) were utilized for all experiments. All other excipients and reagents were of analytical grade. The chemical structures of Kolliphor HS 15 and DF003 are provided in the Supporting Information (Figures SI1 and SI2).

4. METHODS

4.1.1. Preparation of LNCs. A phase inversion method was employed for preparing LNCs as described by Valcourt et al.[1] and Urimi et al.[9] In short, for preparing fully hydrogenated LNCs (h-LNCs), 620 mg of Labrafac, 480 mg of Kolliphor HS 15, 50 mg of sodium chloride, 40 mg of Phospholipon 90 H, and 1.7 mL of purified water/deuterium oxide (D_2O) were heated to 50 °C until a clear solution was observed. This clear solution was then further heated to 90 °C followed by cooling it to 60 °C. Three such heat−cool cycles were applied followed by rapid addition of 7.1 mL of cold water or D_2O near the phase inversion temperature during the last heat−cool cycle. This resulted in spontaneous formation of LNCs. Additionally, LNCs with a deuterated core (d-LNCs) were prepared with a combination of Labrafac and a mixture of deuterated fatty acids as an oil phase to achieve higher contrast in the core, to be suitable for SANS experiments. For this, 95% of Labrafac was mixed with a 5% mixture of octanoic-d15 (dC8) and decanoic-d19 acid (dC10) (dC8/dC10 corresponds to 54.0%:45.2% as per the certificate of analysis of Labrafac). Using this as an oil phase, d-LNCs were prepared in a similar manner as described above. All samples were filtered using a 0.22 μM membrane filter before further characterization. The composition of h-LNCs and d-LNCs is given in Table 1.

Table 1. Composition of Hydrogenated (h-LNCs) and Deuterated (d-LNCs) LNCs

excipient	composition of h-LNCs (% w/v)	composition of d-LNCs (% w/v)
Labrafac lipophile WL 1349	6.2	5.89
octanoic-d15 acid (dC8)		0.17
decanoic-d19 acid (dC10)		0.14
Kolliphor HS 15	4.8	4.8
Phospholipon 90 H	0.4	0.4
sodium chloride	0.5	0.5
Milli-Q water/deuterium oxide (D_2O)	q.s.	q.s.
DF003[a]	0.19	0.19

[a]DF003 is only present in drug-loaded LNCs.

4.1.2. Particle Size and Zeta Potential Measurements. The mean particle size and polydispersity index (PDI) of unloaded and DF003-loaded LNCs were measured using a Malvern Zetasizer Nano ZS setup (Malvern Instruments, U.K.) at a backscattering detection angle of 173°. Using the same setup, the zeta potential of the LNCs was determined by measuring the electrophoretic mobility of the samples in a folded capillary cell and then applying the Smoluchowski equation. The samples were measured in the concentration range of 1.2−62 mg/mL after making necessary dilutions of the original formulation.

4.1.3. Morphology by Cryogenic Transmission Electron Microscopy. Drug-loaded LNCs with and without a deuterated core were analyzed by cryo-TEM as described by Almgren et al.[27] Samples were equilibrated at 25 °C and at a high relative humidity within a climate chamber. A small drop of sample was deposited on a carbon-sputtered copper grid precovered with a perforated polymer film. Excess liquid was thereafter removed by blotting with a filter paper, leaving a thin film of the solution on the grid. The sample was vitrified in liquid ethane and transferred to the microscope, continuously kept below −160 °C, and protected against atmospheric conditions. Analyses were performed with a Zeiss Libra 120 transmission electron microscope (Carl Zeiss AG, Oberkochen, Germany) operating at 80 kV and in zero-loss bright-field mode. Digital images were recorded under low-dose conditions with a BioVision Pro-SM Slow Scan CCD camera (Proscan elektronische Systeme GmbH, Scheuring, Germany).

4.1.4. Small-Angle Scattering Experiments. 4.1.4.1. Small-Angle X-Ray Scattering Experiments. SAXS measurements were made using a SAXSpoint 2.0 instrument by Anton Paar with point collimation (microfocus tube), equipped with a Supernova Copper radiation source (wavelength of 1.541 Å) and a 2D detector (Eiger R 1M Horizontal). This SAXS instrument can deliver structural information of dimensions between 1 and 100 nm. Small- and wide-angle data can be measured using the same sample setup at scattering angles up to 60°. In the present investigation, for LNCs of up to 74 nm (from DLS), data collection started at 0.076 nm^{-1}. For a lower signal to background, the SAXS was setup under vacuum using quartz capillary sample holders. Each sample with a particle concentration of 62 mg/mL was measured for 30 min at 25 °C. A background measurement of air/buffer in the same capillary was acquired using the same settings and subtracted from the sample measurements for the data analysis.

4.1.4.2. Small-Angle Neutron Scattering Experiments. SANS measurements on the LNC samples were performed at ISIS Neutron and Muon Source (Oxfordshire, UK) with a Sans2d instrument using a pulsed "white" beam, operating in a time-of-flight mode with a neutron wavelength range of 1.75−16.5 Å. The collimation of the incident beam is provided by apertures that could be selected together with the effective source distance, which is altered by inserting neutron guides to provide an appropriate beam divergence for each measurement configuration. Data were recorded on two two-dimensional detectors situated 2.4 and 4 m from the sample.

Samples with varied particle concentrations (1.24 to 6.2 mg/mL) and solvent contrasts were measured in standard quartz cells with the same parameters at temperatures of 5, 25, and 37 °C. The measured data were reduced using software provided at ISIS facility for background scattering, making allowance for the measured sample transmission, detector uniformity, and instrument noise. The data were placed on an absolute scale using the scattering from a standard sample (comprising a solid blend of protiated and perdeuterated polystyrene) in accordance with established procedures[28] and converted to one-dimensional scattering intensity profiles $I(Q)$ versus the momentum transfer, Q. Further details of the components such as detectors as well as the data reduction software can be found in the report by Heenan et al.[29]

4.1.5. SAXS and SANS Data Analysis and Interpretation. SasView 5.0.3 software[30] was used for analysis of the data obtained from SAXS and SANS experiments. Here, we also accounted for instrumental smearing effects of the SANS data.

https://doi.org/10.1021/acs.molpharmaceut.1c00648
Mol. Pharmaceutics XXXX, XXX, XXX−XXX

Data collected with the same LNC formulation with different solvent contrasts were simultaneously fitted to a core−shell sphere model. When analyzing the data, the SLD of the core and the solvent were kept constant at the calculated values (calculated using SLD Calculator Tool in SasView 5.0.3 software). The modeled parameters were the SLD of the shell, core radius, shell thickness, polydispersity of the radius, and the volume fraction. From the core radius and the shell thickness, the effective size of the LNCs was computed and compared with the DLS measurements. Chemical formulas and the scattering density values of the LNC components are tabulated in Table 2.

Table 2. Material Properties and Scattering Length Densities of LNC Components

component of LNCs	chemical formula	neutron SLD (10^{-6} Å^{-2})[b]	X-ray SLD (10^{-6} Å^{-2})[b]
Labrafac	$C_8H_{16}O_2$ + $C_{10}H_{20}O_2$	0.15	8.93
Labrafac: (dC8 + dC10) (5.89:0.31% w/v)	$C_8H_{16}O_2$ + $C_{10}H_{20}O_2$ + $C_8d_{15}O_2H$ + $C_8d_{15}O_2H$	0.45	
Kolliphor HS 15[a]	$C_{20}H_{40}O_4$	0.13	9.92
light water	H_2O	−0.56	9.44
heavy water	D_2O	6.35	

[a]Considering one ethylene glycol moiety. [b]Calculated using SLD Calculator Tool in SasView 5.0.3 software.

5. RESULTS AND DISCUSSION

5.1. Particle Size, Zeta Potential, and Entrapment Efficiency. LNCs were initially characterized for particle size, PDI, entrapment efficiency, and zeta potential. For SAXS experiments, LNCs with a particle concentration of 62 mg/mL were used, and for SANS experiments, LNCs were diluted to get a particle concentration in the range of 1.2−6.2 mg/mL. At a higher particle concentration of 62 mg/mL, particle radii of 35 ± 1 and 45 ± 1 nm were observed for unloaded and drug-loaded LNCs, respectively. Additionally, a PDI of 0.14 ± 0.01 was observed with drug-loaded LNCs, which is higher compared to that for unloaded LNCs (0.09 ± 0.01). Nevertheless, both the particle size and PDI of LNCs were higher at a higher particle concentration compared to LNCs with lower particle concentrations that were used for SANS measurements. LNCs at particle concentrations of 1.2−6.2 mg/mL prepared with Labrafac lipophile WL 1349 in water showed a hydrodynamic radius of 30 ± 1 nm with a PDI of 0.04 ± 0.02. For the SANS experiments, LNCs with Labrafac were prepared in deuterium oxide (D_2O), and in a separate experiment, 5% of Labrafac was replaced with a mixture of deuterated caprylic (dC8) and deuterated capric acids (dC10). Changing the dispersion medium from water to D_2O resulted in LNCs with a radius and PDI of 29 ± 1 nm and 0.04 ± 0.01, respectively, very similar to LNCs prepared in water. Furthermore, replacing 5% Labrafac with a mixture of dC8 and dC10 did not affect the properties of the LNCs to any greater extent, although a slight reduction in size could be seen compared to h-LNCs (Figure SI3 in the Supporting Information). The particle size and PDI values of d-LNCs were observed to be 27 ± 1 nm and 0.04 ± 0.01, respectively. These results indicate that the behavior of LNCs is little affected by inclusion of deuterium, either in the core or in the dispersion medium, making them suitable for further characterization using contrast variation and isotopic labeling for SANS experiments. In addition to unloaded LNCs, DF003-loaded LNCs were prepared in a similar manner and the formulation behavior was unaffected by the presence of deuterium. However, in all the cases where LNCs were prepared with DF003, the hydrodynamic radius was increased by about 6−8 nm compared to the unloaded LNCs. Both drug-loaded and unloaded h-LNCs and d-LNCs were measured in the concentration range of 1.2−6.2 mg/mL, and the particle size and polydispersity were unaffected in this concentration range. A detailed composition of h-LNCs and d-LNCs used for SAXS and SANS experimentation along with their characterization data can be found in Tables SI1 and SI2 in the Supporting Information.

Unloaded LNCs showed a near zero zeta potential, irrespective of the presence or absence of deuterium. However, similar to earlier results by Urimi et al.,[9] upon loading of DF003, LNCs showed a more negative zeta potential of about −10 mV, values that were also independent of deuterium. This increase in negative zeta potential could be attributed to the strong interaction of hydrophilic DF003 with the hydrophilic headgroup region of the amphiphilic surfactant (Kolliphor HS 15). This strong interaction can be supported by the higher solubility of DF003 in Kolliphor HS 15 compared to the other components of the LNCs, as demonstrated by Urimi et al.[9] This indicates that the drug is preferentially localized on the outer surface of the LNCs possibly in a shell-like structure formed by Kolliphor HS 15 and Phospholipon 90 H surrounding the core of LNCs, leading to a more negative surface charge. Thus, drug loading increases the size and zeta potential of LNCs. Furthermore, the entrapment efficiency of drug-loaded LNCs (both h-LNCs and d-LNCs) showed to be at >80% (detailed methodology for entrapment efficiency can be found in the Supporting Information).

5.2. Morphology of LNCs by Cryo-TEM. To investigate the possible presence of a shell-like structure, the morphology of DF003-loaded LNCs prepared without and with a deuterated fatty acid mixture was investigated using cryo-TEM (Figure 1). The micrographs indicate the presence of

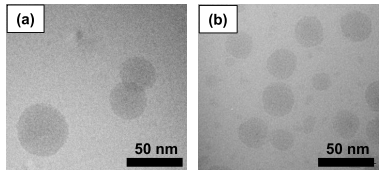

Figure 1. Cryogenic transmission electron micrographs of drug-loaded (a) h-LNCs and (b) d-LNCs.

spherical-shaped LNC particles. LNCs in both samples appear similar in morphology, indicating that the inclusion of d-oil for preparing d-LNCs has not affected the morphology of the resulting LNCs, as also suggested by the particle size, PDI, and zeta potential measurements. The size distribution profile of both samples is comparable to the size data measured with DLS (Figure SI3 in the Supporting Information). However, despite the presence of smaller particle population as can be seen in Figure 1, DLS showed very low PDI values (Table SI2 in the Supporting Information). This could be due to their negligible contribution to the overall scattering intensity measured with DLS. These micrographs did not reveal the

https://doi.org/10.1021/acs.molpharmaceut.1c00648
Mol. Pharmaceutics XXXX, XXX, XXX−XXX

internal structure of LNC particles. Due to the limited resolution of the currently used cryo-TEM technique and the poor contrast provided by polyethylene glycol, it is not possible to visualize a likely thin shell built from Kolliphor HS 15 and Phospholipon 90 H surrounding the oily core using cryo-TEM.[31] In previous studies, it has also been demonstrated that the LNCs appear very similar with and without drug loading.[9]

5.3. Resolving the Structure of LNCs. *5.3.1. Small-Angle X-Ray Scattering.* Unloaded and drug-loaded LNCs were prepared with pure Labrafac in water and were measured using SAXS at a concentration of 62 mg/mL. Initially, the scattering data from both unloaded and drug-loaded LNCs were analyzed to obtain the pair distance distribution function $P(r)$ (Figure 2). From $p(r)$ profiles, it is clear that the particles

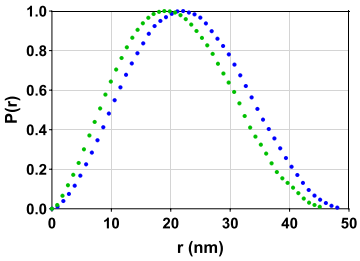

Figure 2. Normalized $P(r)$ profile of unloaded (blue solid circle) and drug-loaded (green solid circle) LNCs.

have a spherical structure, which was also confirmed from cryo-TEM measurements (Figure 1). $P(r)$ analysis of unloaded LNCs indicated an average radius of gyration (R_g) of 17.3 ± 0.09 nm with a 49 ± 0.5 nm maximum distance between any two points in the system (D_{max}). For the drug-loaded LNCs, the obtained R_g and D_{max} values were 15.8 ± 0.05 and 46 ± 0.5 nm, respectively. These R_g and D_{max} values indicate that the LNCs with the drug are slightly smaller in size compared to unloaded LNCs.

Based on these observations, a sphere model and a core−shell sphere model[32] were fitted to the scattering data to get the structural details of the LNC particles. Scattering data along with the best model fits are presented in Figure 3. It can be seen from Figure SI4 in the Supporting Information that the scattering data did not fit well with the sphere model, suggesting the presence of additional structural features.

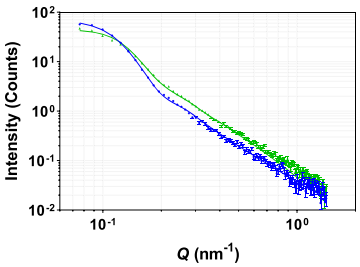

Figure 3. SAXS data from unloaded (blue solid circle) and drug-loaded (green solid circle) LNCs fitted with a core−shell sphere model. Solid lines represent the best fits to the experimental scattering data. Error bars are almost within the size of the symbols for most of the scattering data at low Q values.

Significant improvement was observed when a shell was added to the sphere model (Figure 3). Structural parameters from the data fitting of the LNCs are tabulated in Table 3.

Table 3. Structural Information about the LNCs as Determined by SAXS, SANS, and DLS Techniques

parameter	unloaded LNCs	DF003-loaded LNCs
$P(r)$ analysis of small-angle X-ray scattering (SAXS) data		
R_g (nm)	17.3 ± 0.09	15.8 ± 0.05
D_{max} (nm)	49 ± 0.5	46 ± 0.5
shape model analysis of small-angle X-ray scattering (SAXS) data		
core radius (nm)	21.7 ± 0.2	18.5 ± 0.2
shell thickness (nm)	2.6 ± 0.1	3.6 ± 0.1
total radius (nm)	24.3 ± 0.3	22.1 ± 0.3
volume fraction[a]	0.092	0.092
polydispersity	0.20	0.35
χ^2	2.4	3.7
small-angle neutron scattering (SANS)		
core radius (nm)	20.0 ± 0.9	20.2 ± 0.6
shell thickness (nm)	≤1.5	∼2 ± 0.5
total radius (nm)	21.5 ± 0.9	22.2 ± 1.1
shell hydration (%)	50	70
volume fraction[b]	0.009	0.009
polydispersity	0.20	0.25
SLD of shell	3.3	4.5
dynamic light scattering (DLS)		
hydrodynamic radius (nm)	30.0 ± 1.0	36.0 ± 1.0
polydispersity	0.04 ± 0.02	0.07 ± 0.01
zeta potential (mV)	−3.7 ± 1.6	−13.6 ± 0.8

[a]Volume fractions estimated using a core−shell sphere model and the values are in close approximation to a theoretical volume fraction of 0.062. [b]Volume fractions estimated using a core−shell sphere model and the values are in close approximation to a theoretical volume fraction of 0.0062.

Furthermore, it is evident from the scattering profiles shown in Figure 3 that the structures of unloaded and drug-loaded LNCs are similar and were well fitted with a core−shell sphere model, but they differ in size. From the best data fits, the average core radius and shell thickness of unloaded LNCs were found to be 21.7 ± 0.2 and 2.6 ± 0.1 nm, respectively. Upon drug loading, the average core radius was reduced to 18.5 ± 0.2 nm, but the shell thickness was increased to 3.6 ± 0.1 nm. Taken together, this means that drug loading into LNCs led to a decrease in the average overall size of core−shell LNC particles. These size parameters obtained from modeling SAXS data correlate well with the $P(r)$ analysis (Figure 2) but appear to go against the results from DLS presented above where the particles appeared larger in response to the drug being present (Table SI2). DLS measures the diffusion coefficient, and binding the drug molecule on the surface of LNCs can potentially change the diffusion coefficient. SAXS is more accurate in determining the size of these LNC particles, as it measures the particle size directly.

With SAXS, we measure the average particle size; thus, in conclusion, the decrease in the average size of the LNC particle upon drug loading could be explained by a shift in particle size distribution to smaller dimensions, resulting in a smaller average size. Despite the average decrease in size, the shell is larger in drug-loaded LNCs compared to the unloaded ones, indicating the presence of the drug on the surface of the LNC particles as measured by SAXS.

https://doi.org/10.1021/acs.molpharmaceut.1c00648
Mol. Pharmaceutics XXXX, XXX, XXX−XXX

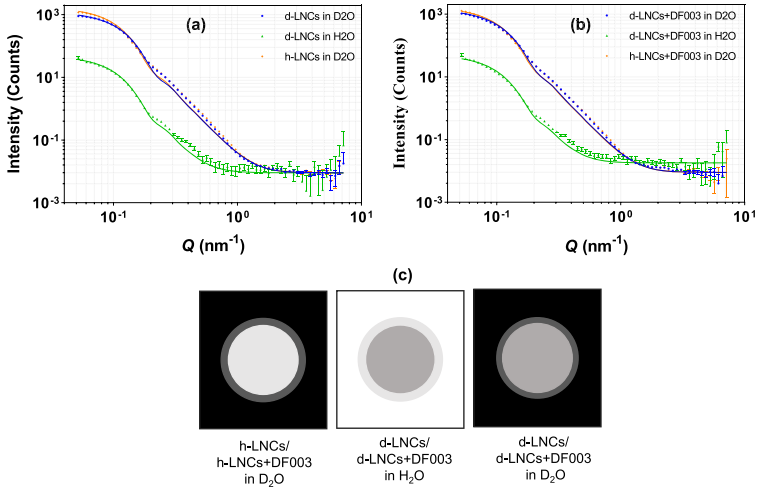

Figure 4. SANS scattering data from (a) unloaded LNCs and (b) DF003-loaded LNCs prepared with varied contrast in the core and in the dispersion medium. Solid lines represent the best fits to the experimental scattering data. (c) Schematic depiction of varied contrasts in the core and in the dispersion medium. Error bars are almost within the size of the symbols for most of the scattering data.

5.3.2. Small-Angle Neutron Scattering. Building on the SAXS data of LNCs, the SANS data were fitted to a core−shell sphere model. Figure 4 displays the scattering intensity curves along with a schematic sketch of contrast differences for LNCs with varying contrasts.

5.3.2.1. Resolving the Core. To investigate the structural details of the nanoparticles, LNCs were prepared with pure hydrogenous oil (i.e., Labrafac) and Labrafac mixed with a 5% mixture of dC8 and dC10 oils to increase the contrast in the core for neutrons. Along with this, the dispersion medium was changed from H_2O to D_2O to highlight different structural aspects of LNCs. In Figure 4a, the scattering data from unloaded h-LNCs and d-LNCs prepared in H_2O and D_2O are displayed, where most of the signal comes from the core. The best fits from a core−shell sphere model were obtained with a core radius of 20.0 ± 0.9 nm. The fits slightly deviate from the scattering data between Q = 0.2−0.8 nm^{-1}. The model was kept simple to get the best possible and relevant structural information of the LNCs. A schematic picture with contrast variation in the core of LNCs and the dispersion medium is shown in Figure 4c.

5.3.2.2. Resolving the Shell. SANS data fitting with a core−shell sphere model demonstrated the presence of a highly hydrated shell surrounding the core of LNCs. In the case of unloaded LNCs, the shell hydration was found to be of the order 50% and this was seen by an increase in SLD from a calculated value of 0.13 to 3.3 from the data fitting. Based on the data fitting, the shell thickness was found to be <1.5 nm; however, this diffuse shell is difficult to model precisely with respect to thickness, as the signal is weak. The high hydration of the shell was further confirmed by experiments where the signal of the core was matched out by the dispersion medium and the remaining very weak signal only came from the shell (Figure SI5 in the Supporting Information). It is clear that the hydration of the shell of these soft particles makes it difficult to model their exact thickness. Previously, it has been found that Kolliphor HS 15 orients toward the aqueous phase and does constitute a sufficiently rigid shell,[11] and data represented herein support this speculation.

Taking together, the information obtained with SAXS and SANS suggests that the LNC particles have a core−shell structure. The shell is assumed to be made up of a combination of the surface active agents Kolliphor HS 15 and Phospholipon 90 H, as they are associated together at the interface of the particle and the surrounding medium. The predominant thickness of the shell results from the PEG chains of Kolliphor HS 15. Data from SAXS and SANS experiments provide an indication on the extent of the contribution of shell thickness to the overall size of the LNCs. However, owing to the dynamic and interfacial nature of the shell components and polydispersity associated with the actual particles, it is highly challenging to precisely measure the thickness of the shell even with the advanced characterization tools. Polydispersity values of 0.2 and 0.25 for the unloaded and drug-loaded LNCs, respectively, were obtained through modeling the SANS data. A similar increase in the polydispersity of LNCs with drug loading was observed with DLS measurements (Table SI2) and cryo-TEM observations.

5.3.2.3. Addition of the Drug. Drug-loaded h-LNCs and d-LNCs were measured with SANS in the same way as unloaded LNCs (Figure 4b). The scattering intensity profiles followed a similar pattern and a core−shell sphere model fits well, similar to the unloaded LNCs (Figure 4a vs Figure 4b), indicating a retained overall core−shell structure upon drug loading. The drug loading resulted in a higher scattering intensity relative to unloaded LNCs, indicating an increased overall size with drug loading. The best possible fit showed a core radius of 20.2 ± 0.6 nm for drug-loaded LNCs, which is very similar to 20.0 ± 0.9 nm obtained for unloaded LNCs (Table 3). Additionally, similar to unloaded LNCs, the shell in drug-loaded LNCs is highly hydrated; however, this hydration is even higher at ∼70%, compared to the shell hydration of unloaded LNCs (50%). Further data analysis showed a shell thickness of ∼2 ± 0.5 nm, which is thicker compared to the shell thickness observed for unloaded LNCs. This increased shell hydration

https://doi.org/10.1021/acs.molpharmaceut.1c00648
Mol. Pharmaceutics XXXX, XXX, XXX−XXX

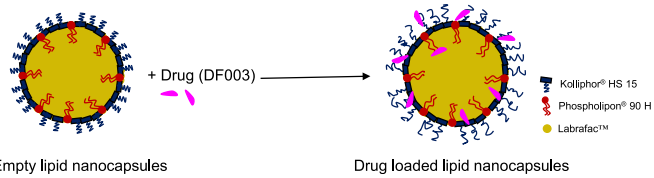

Figure 5. Proposed structure of empty and DF003-loaded lipid nanocapsules. Drug-loaded LNCs are proposed to have a higher disorder in the way the surfactants are packed around the oily core by the presence of the drug.

and thickness can be explained by the hydrophilic nature of DF003 localizing it on the surface of the particles (as confirmed by particles becoming more negatively charged with drug loading, Table SI2). DF003 may form hydrogen bonds with water, making the shell more hydrated compared to unloaded LNCs. Additionally, drug localization and surface charge may imply a different positioning of the surfactant monomers surrounding the core of LNCs. These combined effects may lead to an increase in the shell thickness. A schematic illustration of empty and drug-loaded LNCs is shown in Figure 5.

5.3.2.4. Effect of Concentration. Drug-loaded and unloaded LNCs with or without a deuterated core were prepared using H_2O or D_2O as the dispersant and were measured with SANS at different particle concentrations, 1.24, 3.1, and 6.2 mg/mL. Figures 6 and 7 represent the scattering intensity profile and

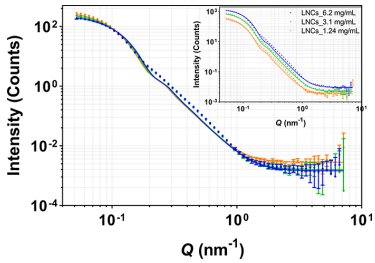

Figure 6. Effect of particle concentration on SANS scattering data from unloaded h-LNCs prepared in D_2O. Data were normalized with respect to concentration, and the inset shows non-normalized SANS data. Error bars are almost within the size of the symbols for most of the scattering data.

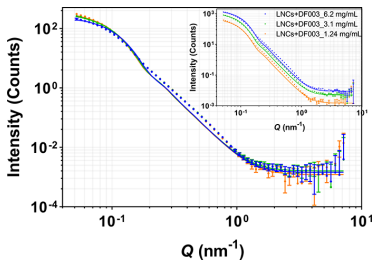

Figure 7. Effect of particle concentration on SANS scattering data from DF003-loaded h-LNCs prepared in D_2O. Data were normalized with respect to concentration, and the inset shows non-normalized SANS data. Error bars are almost within the size of the symbols for most of the scattering data.

the model fit from unloaded and drug-loaded h-LNCs prepared in D_2O. The data indicate that the overall structure is retained upon dilution (for both unloaded and drug-loaded LNCs). The signal intensities vary according to volume fractions of LNCs. The average core radii for unloaded and drug-loaded LNCs at different concentrations were observed to be 20.9 ± 1.0 and 20.7 ± 1.0 nm, respectively, indicating that the core remains unchanged in size with particle concentration irrespective of the presence or absence of the drug.

5.3.2.5. Effect of Temperature. SANS measurements on h-LNCs and d-LNCs (with and without the drug) were carried out at 5, 25, and 37 °C to investigate the impact of temperature on the internal structure of LNCs. The scattering intensity profile with the best fit from nondeuterated LNCs prepared in D_2O is given in Figure 8. The samples were diluted 20 times with D_2O before the measurement. It can be noted that the scattering intensity profiles generated at different temperatures are very similar to each other, indicating that the structure of these LNCs is stable and that the measurements are unaffected over this temperature range. All different temperatures showed the best fit with a core diameter of 21.5 nm.

5.3.2.6. Effect of Salt. In our previous work, we have demonstrated the stability of DF003-loaded LNCs with hyaluronic acid sodium to check for the suitability of LNCs for ocular administration.[9] To further investigate their stability, both unloaded and drug-loaded h-LNCs were diluted with sodium chloride dissolved in D_2O to a final salt concentration of ∼5 mg/mL and SANS profiles were generated (Figure 9). Scattering profiles remained the same with and without the presence of excess NaCl. This indicates that excess salt did not change the overall core−shell structure for neither unloaded nor drug-loaded LNCs. SANS data along with size data measured with DLS (Table SI2) show that the LNCs are stable and nonaggregating without any changes in the internal structure at the studied salt concentration.

6. CONCLUSIONS

Structural aspects of LNCs were studied using a combination of different characterization techniques, including DLS, cryo-TEM, SAXS, and SANS. Information about the overall particle size and morphology was obtained from DLS and cryo-TEM, whereas SAXS and SANS provided more detailed information about the internal structure of LNCs. The results indicate the presence of a core−shell structure, which is retained after drug loading into LNCs. Modeling of both SAXS and SANS data showed an increase in the thickness of the shell for drug-loaded LNCs, compared to unloaded LNCs. It could be further observed from SANS data that drug loading of LNCs resulted in higher hydration of the shell, leading to the increase in shell thickness. The hydrophilic nature of DF003 correlates well

https://doi.org/10.1021/acs.molpharmaceut.1c00648
Mol. Pharmaceutics XXXX, XXX, XXX−XXX

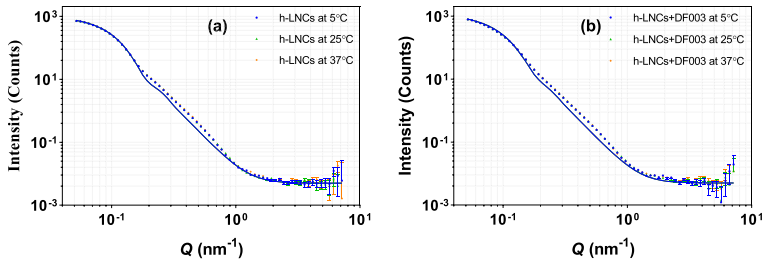

Figure 8. Effect of temperature (5, 25, and 37 °C) on SANS scattering data from (a) unloaded h-LNCs and (b) DF003-loaded h-LNCs prepared in D_2O. Error bars are almost within the size of the symbols for most of the scattering data.

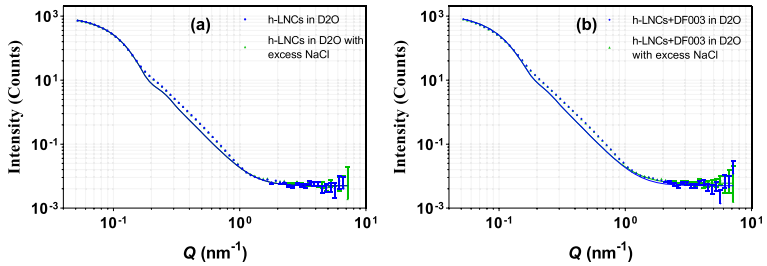

Figure 9. Effect of excess salt on SANS scattering data from (a) unloaded h-LNCs and (b) DF003-loaded h-LNCs prepared in D_2O. Error bars are almost within the size of the symbols for most of the scattering data.

with the increased hydration of the shell and strengthens the conclusion of a preferential localization of DF003 to the shell. Moreover, the concluded localization of DF003 to the shell was further confirmed by a negative surface potential of drug-loaded LNCs, compared to a near neutral surface potential of unloaded LNCs. The LNC core−shell configuration was found to be unaffected by particle concentration, temperature, or the presence of excess salt, demonstrating the stability of these particles. However, for drug-loaded LNCs at higher LNC particle concentrations (62 mg/mL) as used for SAXS measurements, we found that the average LNC particle size decreased, indicating a shift in the size distribution of the core−shell particles to smaller sizes. Further investigation into the effect of LNC assembly with the drug present at different particle concentrations could shed more light onto what causes this shift in dynamics as seen with the SAXS measurements. The findings from this work can help in better understanding of the physicochemical properties of LNCs and the effect of drug loading. Overall, this complementary approach can be implemented in finding out the structural details of various other novel drug delivery systems.

■ ASSOCIATED CONTENT

Supporting Information

The Supporting Information is available free of charge at https://pubs.acs.org/doi/10.1021/acs.molpharmaceut.1c00648.

Chemical structures of the drug (DF003), Kolliphor HS 15, additional experimental methods, DLS and encapsulation efficiency results of LNC samples, SAXS model fitting with a sphere model, and SANS data in contrast match conditions (PDF)

■ AUTHOR INFORMATION

Corresponding Author

Dileep Urimi − *RISE Research Institutes of Sweden, Division Bioeconomy and Health, Chemical Process and Pharmaceutical Development, Södertälje 151 36, Sweden; Faculty of Pharmaceutical Sciences, School of Health Sciences, University of Iceland, Reykjavík IS-107, Iceland;* orcid.org/0000-0002-1463-4990; Phone: +46-703486575; Email: dileep.urimi@ri.se

Authors

Maja Hellsing − *RISE Research Institutes of Sweden, Division Bioeconomy and Health, Chemical Process and Pharmaceutical Development, Södertälje 151 36, Sweden;* Present Address: Department for Research Infrastructure, Swedish Research Council, Västra Järnvägsgatan 3, Box 1035, 101 38 Stockholm

Najet Mahmoudi − *ISIS Pulsed Neutron and Muon Source, Rutherford Appleton Laboratory, Didcot OX11 0QX, U.K.*

Christopher Söderberg − *RISE Research Institutes of Sweden, Division Bioeconomy and Health, Chemical Process and Pharmaceutical Development, Södertälje 151 36, Sweden*

Ronja Widenbring − *RISE Research Institutes of Sweden, Division Bioeconomy and Health, Chemical Process and Pharmaceutical Development, Södertälje 151 36, Sweden*

Lars Gedda − *Department of Chemistry − Ångström laboratory, Uppsala University, Uppsala SE-751 23, Sweden*

Katarina Edwards − *Department of Chemistry − Ångström laboratory, Uppsala University, Uppsala SE-751 23, Sweden*

Thorsteinn Loftsson − *Faculty of Pharmaceutical Sciences, School of Health Sciences, University of Iceland, Reykjavík IS-107, Iceland;* orcid.org/0000-0002-9439-1553

Nicolaas Schipper − *RISE Research Institutes of Sweden, Division Bioeconomy and Health, Chemical Process and Pharmaceutical Development, Södertälje 151 36, Sweden*

Complete contact information is available at: https://pubs.acs.org/10.1021/acs.molpharmaceut.1c00648

Funding

This work was financially supported by the grant from the European Union (*trans*Med, H2020-MSCA-ITN-2017-765441) and VINNOVA (2019-03616).

Notes

The authors declare no competing financial interest.

■ ACKNOWLEDGMENTS

The authors acknowledge the ISIS facility for the award of beam time on Sans2d (doi:10.5286/ISIS.E.RB2010513). This work benefited from the use of the SasView application, originally developed under NSF Award DMR-0520547. SasView also contains code developed with funding from the EU Horizon 2020 programme under the SINE2020 project Grant No 654000.

■ REFERENCES

(1) Valcourt, C.; Saulnier, P.; Umerska, A.; Zanelli, M.; Montagu, A.; Rossines, E.; Joly-Guillou, M.-L. Synergistic interactions between doxycycline and terpenic components of essential oils encapsulated within lipid nanocapsules against gram negative bacteria. *Int. J. Pharm.* **2016**, *498*, 23−31.

(2) Thomas, O.; Lagarce, F. Lipid nanocapsules: a nanocarrier suitable for scale-up process. *J. Drug Delivery Sci. Technol.* **2013**, *23*, 555−559.

(3) Mouzouvi, C. R.; Umerska, A.; Bigot, A. K.; Saulnier, P. Surface active properties of lipid nanocapsules. *PLoS One* **2017**, *12*, No. e0179211.

(4) Groo, A.-C.; Matougui, N.; Umerska, A.; Saulnier, P. Reverse micelle-lipid nanocapsules: a novel strategy for drug delivery of the plectasin derivate AP138 antimicrobial peptide. *Int. J. Nanomed.* **2018**, *13*, 7565.

(5) Hureaux, J.; Lagarce, F.; Gagnadoux, F.; Vecellio, L.; Clavreul, A.; Roger, E.; Kempf, M.; Racineux, J.-L.; Diot, P.; Benoit, J.-P. Lipid nanocapsules: ready-to-use nanovectors for the aerosol delivery of paclitaxel. *Eur. J. Pharm. Biopharm.* **2009**, *73*, 239−246.

(6) Sun, R.; Zhang, A.; Ge, Y.; Gou, J.; Yin, T.; He, H.; Wang, Y.; Zhang, G.; Kong, J.; Shang, L. Ultra-small-size Astragaloside-IV loaded lipid nanocapsules eye drops for the effective management of dry age-related macular degeneration. *Expert Opin. Drug Delivery* **2020**, *17*, 1305−1320.

(7) Umerska, A.; Matougui, N.; Groo, A.-C.; Saulnier, P. Understanding the adsorption of salmon calcitonin, antimicrobial peptide AP114 and polymyxin B onto lipid nanocapsules. *Int. J. Pharm.* **2016**, *506*, 191−200.

(8) Formica, M. L.; Legeay, S.; Bejaud, J.; Montich, G. G.; Gamboa, G. V. U.; Benoit, J.-P.; Palma, S. D. Novel hybrid lipid nanocapsules loaded with a therapeutic monoclonal antibody−Bevacizumab−and Triamcinolone acetonide for combined therapy in neovascular ocular pathologies. *Mater. Sci. Eng., C* **2021**, *119*, No. 111398.

(9) Urimi, D.; Widenbring, R.; García, R. O. P.; Gedda, L.; Edwards, K.; Loftsson, T.; Schipper, N. Formulation development and upscaling of lipid nanocapsules as a drug delivery system for a novel cyclic GMP analogue intended for retinal drug delivery. *Int. J. Pharm.* **2021**, *602*, No. 120640.

(10) Heurtault, B.; Saulnier, P.; Pech, B.; Proust, J.-E.; Benoit, J.-P. A novel phase inversion-based process for the preparation of lipid nanocarriers. *Pharm. Res.* **2002**, *19*, 875−880.

(11) Heurtault, B.; Saulnier, P.; Pech, B.; Benoıt, J.; Proust, J. Interfacial stability of lipid nanocapsules. *Colloids Surf., B* **2003**, *30*, 225−235.

(12) Hureaux, J.; Lagarce, F.; Gagnadoux, F.; Rousselet, M.-C.; Moal, V.; Urban, T.; Benoit, J.-P. Toxicological study and efficacy of blank and paclitaxel-loaded lipid nanocapsules after iv administration in mice. *Pharm. Res.* **2010**, *27*, 421−430.

(13) Sebastiani, F.; Yanez Arteta, M.; Lerche, M.; Porcar, L.; Lang, C.; Bragg, R. A.; Elmore, C. S.; Krishnamurthy, V. R.; Russell, R. A.; Darwish, T. Apolipoprotein E binding drives structural and compositional rearrangement of mRNA-containing lipid nanoparticles. *ACS Nano* **2021**, *15*, 6709−6722.

(14) Di Cola, E.; Grillo, I.; Ristori, S. Small angle X-ray and neutron scattering: powerful tools for studying the structure of drug-loaded liposomes. *Pharmaceutics* **2016**, *8*, 10.

(15) Nordström, R.; Zhu, L.; Härmark, J.; Levi-Kalisman, Y.; Koren, E.; Barenholz, Y.; Levinton, G.; Shamrakov, D. Quantitative Cryo-TEM Reveals New Structural Details of Doxil-Like PEGylated Liposomal Doxorubicin Formulation. *Pharmaceutics* **2021**, *13*, 123.

(16) Lasic, D. D.; Frederik, P.; Stuart, M.; Barenholz, Y.; McIntosh, T. Gelation of liposome interior A novel method for drug encapsulation. *FEBS Lett.* **1992**, *312*, 255−258.

(17) Johnston, M. J.; Edwards, K.; Karlsson, G.; Cullis, P. R. Influence of drug-to-lipid ratio on drug release properties and liposome integrity in liposomal doxorubicin formulations. *J. Liposome Res.* **2008**, *18*, 145−157.

(18) Cardellini, J.; Balestri, A.; Montis, C.; Berti, D. Advanced Static and Dynamic Fluorescence Microscopy Techniques to Investigate Drug Delivery Systems. *Pharmaceutics* **2021**, *13*, 861.

(19) Hallan, S. S.; Sguizzato, M.; Esposito, E.; Cortesi, R. Challenges in the Physical Characterization of Lipid Nanoparticles. *Pharmaceutics* **2021**, *13*, 549.

(20) Chu, B.; Liu, T. Characterization of nanoparticles by scattering techniques. *J. Nanopart. Res.* **2000**, *2*, 29−41.

(21) Vighi, E.; Trifunović, D.; Veiga-Crespo, P.; Rentsch, A.; Hoffmann, D.; Sahaboglu, A.; Strasser, T.; Kulkarni, M.; Bertolotti, E.; Van Den Heuvel, A. Combination of cGMP analogue and drug delivery system provides functional protection in hereditary retinal degeneration. *Proc. Natl. Acad. Sci. U. S. A.* **2018**, *115*, E2997−E3006.

(22) Hellsing, M. S.; Rennie, A. R.; Heenan, R. K.; Rogers, S. E. Structure of a large colloidal crystal−controlling orientation and three-dimensional order. *RSC Adv.* **2012**, *2*, 7091−7098.

(23) Long, M. A.; Kaler, E. W.; Lee, S. P.; Wignall, G. D. Characterization of lecithin-taurodeoxycholate mixed micelles using small-angle neutron scattering and static and dynamic light scattering. *J. Phys. Chem.* **1994**, *98*, 4402−4410.

(24) Candau, F.; Ottewill, R. H. *Scientific methods for the study of polymer colloids and their applications*; Springer, 1989; Vol. *303*.

(25) Ghosh, R.; Egelhaaf, S.; Rennie, A., *A computing guide for small-angle scattering experiments*. Inst Max von Laue, 2000.

(26) Hyland, L. L.; Taraban, M. B.; Yu, Y. B. Using small-angle scattering techniques to understand mechanical properties of biopolymer-based biomaterials. *Soft Matter* **2013**, *9*, 10218−10228.

(27) Almgren, M.; Edwards, K.; Karlsson, G. Cryo transmission electron microscopy of liposomes and related structures. *Colloids Surf., A* **2000**, *174*, 3−21.

(28) Wignall, G. T.; Bates, F. Absolute calibration of small-angle neutron scattering data. *J. Appl. Crystallogr.* **1987**, *20*, 28−40.

(29) Heenan, R.; Rogers, S.; Turner, D.; Terry, A.; Treadgold, J.; King, S. Small angle neutron scattering using Sans2d. *Neutron News* **2011**, *22*, 19−21.

(30) Doucet, M., Cho, J. H.; Alina, G.; Attala, Z.; Bakker, J.; Bouwman, W.; Butler, P.; Campbell, K.; Cooper-Benun, T.; Durniak, C.; Forster, L.; Gonzales, M.; Heenan, R.; Jackson, A.; King, S.; Kienzle, P.; Krzywon, J.; Nielsen, T.; O'Driscoll, L.; Potrzebowski, W.; Prescott, S.; Ferraz Leal, R.; Rozycko, P.; Snow, T.; Washington, A. *SasView version 5.0.3*; Zenodo, 2020.

(31) Askes, S. H.; Bossert, N.; Bussmann, J.; Talens, V. S.; Meijer, M. S.; Kieltyka, R. E.; Kros, A.; Bonnet, S.; Heinrich, D. Dynamics of

dual-fluorescent polymersomes with durable integrity in living cancer cells and zebrafish embryos. *Biomaterials* **2018**, *168*, 54−63.
(32) Guinier, A.; Fournet, G.; Yudowitch, K. L. *Small-angle scattering of X-rays*, 1955.

https://doi.org/10.1021/acs.molpharmaceut.1c00648
Mol. Pharmaceutics XXXX, XXX, XXX−XXX

Supporting information to

Structural characterization study of a lipid nanocapsule formulation intended for drug delivery applications using small angle scattering techniques

Dileep Urimi [†‡*], *Maja Hellsing*[†], *Najet Mahmoudi*[§], *Christopher Söderberg*[†], *Ronja Widenbring*[†], *Lars Gedda*[††], *Katarina Edwards*[††], *Thorsteinn Loftsson*[‡], *Nicolaas Schipper*[†]

[†]RISE Research Institutes of Sweden, Division Bioeconomy and Health, Chemical Process and Pharmaceutical Development, Forskargatan 18, 151 36 Södertälje, Sweden

[‡]Faculty of Pharmaceutical Sciences, School of Health Sciences, University of Iceland, Hofsvallagata 53, IS-107 Reykjavík, Iceland

[§]ISIS Pulsed Neutron and Muon Source, Rutherford Appleton Laboratory, Didcot OX11 0QX, UK.

[††]Department of Chemistry − Ångström laboratory, Uppsala University, Box 573, Uppsala, SE-751 23, Sweden

*Corresponding author: Dileep Urimi

E-mail: dileep.urimi@ri.se

Tel.: +46-703486575

Chemical structures

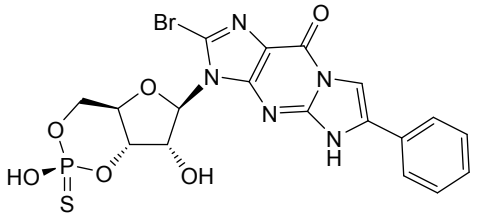

Figure SI1. Molecular structure of drug candidate, DF003

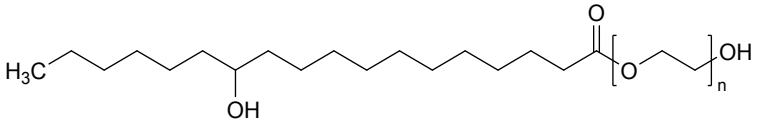

Figure SI2. Molecular structure of Kolliphor® HS 15

Preparation of lipid nanocapsules

Details of h-LNCs and d-LNCs prepared for SANS experiments are mentioned in Table SI1.

Table SI1. Details of the formulations used for structural characterization.

Formulation	Proportion of Labrafac™ (% w/v)	Proportion of dC8+dC10 (% w/v)	Dispersion medium	Drug loading (drug: total oil)
For SAXS experiments (particle concentration (62 mg/mL)				
F1	6.20	-	H_2O	-
F2	6.20	-	H_2O	1:32
For SANS experiments (Particle concentration (1.2-6.2 mg/mL)				
F3	6.20	-	H_2O	-
F4	6.20	-	D_2O	-
F5	5.89	0.31	D_2O	-
F6	6.20	-	H_2O	1:32
F7	6.20	-	D_2O	1:32
F8	5.89	0.31	D_2O	1:32
F9*	6.20	-	D_2O	-
F10*	6.20	-	D_2O	1:32

*Final NaCl concentration of 5 mg/mL for SANS measurements

Determination of encapsulation efficiency

Entrapment efficiency (% EE) and drug loading of DF003 into LNCs were measured with indirect method. Initially, soluble unentrapped drug was separated from the formulations by centrifuging 0.5 mL of drug loaded formulations at 10000x g for 5 minutes. Centrifugation was performed in individual Amicon® Ultra 0.5 centrifugal units with 50 kD membrane. After 5 min, clear filtrate without LNCs was collected and DF003 was quantified using UPLC-UV. The % EE was calculated using equations (2).

$$\% \text{ EE } = \frac{\text{Amount total DF003 - Amount of unentrapped DF003}}{\text{Amount total DF003}} \times 100 \qquad (1)$$

Characterization data of LNCs

Table SI2. Physicochemical characterization of LNCs used for the structural characterization.

Formulation	Particle radius (nm)	Polydispersity Index (PdI)	Zeta potential (mV)	Entrapment efficiency (%)
	For SAXS experiments (particle concentration (62 mg/mL)			
F1	35 ± 1	0.09 ± 0.01	-	-
F2	45 ± 1	0.14 ± 0.01	-	86
	For SANS experiments (Particle concentration (1.2-6.2 mg/mL)			
F3	30 ± 1	0.04 ± 0.02	-3.7 ± 1.6	-
F4	29 ± 1	0.04 ± 0.01	-1.3 ± 0.3	-
F5	27 ± 1	0.04 ± 0.01	-3.7 ± 2.1	-
F6	36 ± 1	0.07 ± 0.01	-13.6 ± 0.8	86
F7	37 ± 1	0.05 ± 0.01	-13.1 ± 0.2	93
F8	33 ± 1	0.04 ± 0.01	-9.6 ± 0.3	87
F9*	30 ± 1	0.03 ± 0.00	-2.0 ± 0.4	-
F10*	36 ± 1	0.07 ± 0.01	-4.5 ± 1.0	-

*Final NaCl concentration of 5 mg/mL for SANS measurements

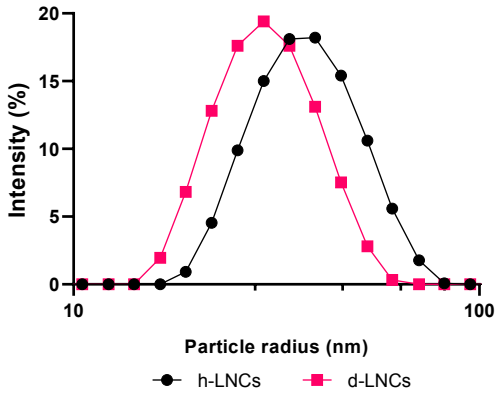

Figure SI3. Comparison of size distribution profiles of h-LNCs and d-LNCs obtained with dynamic light scattering technique. Samples were at a concentration of 6.2 mg/mL. Particle size in this graph refers to the intensity weighted mean hydrodynamic radius.

Small angle X-ray scattering (SAXS)

SAXS data of h-LNCs when fitted with a sphere model indicating a poor fit (Figure SI4) and thus emphasizing the presence of an internal structure in the LNC particles.

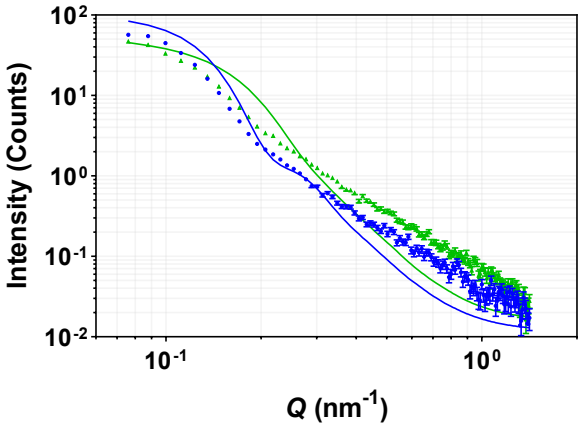

Figure SI4. SAXS data from unloaded (●) and drug-loaded (●) LNCs fitted with a sphere model. Solid lines represent the best fits to the experimental scattering data. Error bars are almost within the size of the symbols for most of the scattering data.

Small angle neutron scattering (SANS)

SANS data was generated on d-LNCs in a mixture of H_2O and D_2O to match out the contrast from the core with the contrast from the dispersion medium to be able to get a reasonable signal from the shell (Figure SI5). However, as can be seen in Figure SI5, the signal is very weak and moreover the shell is much more hydrated which made it difficult to estimate the accurate thickness of the shell.

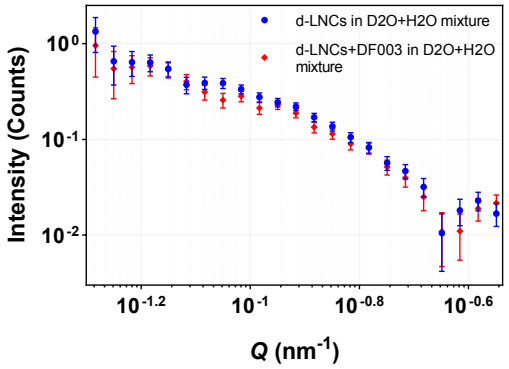

Figure SI5. SANS data from d-LNCs with and without drug loading prepared in a mixture of H_2O and D_2O for matching out the core with the solvent.

Paper III

European Journal of Pharmaceutics and Biopharmaceutics 187 (2023) 175–183

Contents lists available at ScienceDirect

European Journal of Pharmaceutics and Biopharmaceutics

journal homepage: www.elsevier.com/locate/ejpb

Research paper

Ocular permeability, intraocular biodistribution of lipid nanocapsule formulation intended for retinal drug delivery

Gustav Christensen [a,1], Dileep Urimi [b,c,1], Laura Lorenzo-Soler [c], Nicolaas Schipper [b,*], François Paquet-Durand [a,*]

[a] Institute for Ophthalmic Research, University of Tübingen, Elfriede-Aulhorn Straße 5-7, 72076 Tübingen, Germany
[b] Division Bioeconomy and Health, Chemical Process and Pharmaceutical Development, RISE Research Institutes of Sweden, Forskargatan 18, Södertälje 151 36, Sweden
[c] Faculty of Pharmaceutical Sciences, School of Health Sciences, University of Iceland, Hofsvallagata 53, Reykjavík IS-107, Iceland

ARTICLE INFO

Keywords:
Inherited retinal degenerations
Lipid nanocapsules
Liposomes
Intravitreal injections
Explant cultures
Drug delivery

ABSTRACT

Recently, cGMP analogues have been investigated for the treatment of inherited retinal degenerations (IRD) using intravitreal injections. However, higher vitreous elimination rates limit the possibility to treat the retina with small molecule drugs. Here, we investigated the potential of lipid nanocapsules (LNCs) as vehicles to reduce clearance and prolong the delivery of cGMP analogue, CN03 to the retinal photoreceptors. Initially LNCs were investigated for both topical/periocular and intravitreal administration routes. While LNC-mediated drug permeation through the cornea proved to be too low for clinical applications, intravitreal application showed significant promise. Intravitreally administered LNCs containing fluorescent tracer in *ex vivo* porcine eyes showed complete intravitreal dispersal within 24 h. Ocular bio-distribution on histological sections showed that around 10 % of the LNCs had reached the retina, and 40 % accumulated in the ciliary body. For comparison, we used fluorescently labeled liposomes and these showed a different intraocular distribution with 48 % accumulated in the retina, and almost none were in the ciliary body. LNCs were then tested in retinal explants prepared from wild-type (WT) and *rd1* mouse. In WT retina LNCs showed no significant toxic effects up to a concentration of 5 mg/mL. In *rd1* retina, the LNC/CN03 formulation protected *rd1* photoreceptors with similar efficacy to that of free CN03, demonstrating the usefulness of LNC/CN03 formulation in the treatment of IRD. Overall, our results indicate the suitability of LNCs for intraocular administration and drug delivery to both the retina and the ciliary body.

1. Introduction

Inherited retinal degeneration (IRD) relates to a group of rare diseases that result in the progressive loss of retinal photoreceptors, eventually leading to blindness [1–3]. Most of these diseases are untreatable to date and therapy development is hindered by, among other things, the vast genetic diversity of IRD combined with the various ocular barriers which limit drug access to photoreceptors [4].

In many IRD diseases, including in retinitis pigmentosa and Lebeŕs congenital amaurosis, pathological levels of intracellular cGMP have been identified [5]. Based on this mechanistic insight, cGMP analogues have been prepared to inhibit cGMP-activated targets within photoreceptors. One such analogue, CN03, was previously shown to produce morphological preservation of rod photoreceptors, as well as functional protection of cone photoreceptors in IRD mouse models, when administered in a liposomal drug delivery system [6]. The structure of CN03 is given in Fig. 1.

Recently, lipid-nanocapsules (LNC) have been investigated for CN03 encapsulation and release [7,8]. It was found that LNCs achieved high drug encapsulation efficiency and sustained the release *in vitro* for up to 6 days, noticeably superior to what might be expected for the liposomal release of small hydrophilic compounds [9,10]. LNCs are widely investigated for the treatment of various disease conditions mainly due to their biocompatibility, adaptability to modifications, and ease of

Abbreviations: IRD, inherited retinal degenerations; LNCs, lipid nanocapsules; cGMP, cyclic guanosine- 3′,5′-monophosphate; IVT, intravitreal administration; TUNEL, terminal deoxynucleotidyl transferase dUTP nick end labeling; ONL, outer nuclear layer; INL, inner nuclear layer.

* Corresponding authors.
E-mail addresses: nicolaas.schipper@ri.se (N. Schipper), francois.paquet-durand@uni-tuebingen.de (F. Paquet-Durand).

[1] Gustav Christensen and Dileep Urimi contributed equally to this work.

https://doi.org/10.1016/j.ejpb.2023.04.012
Received 31 January 2023; Received in revised form 5 April 2023; Accepted 17 April 2023
Available online 22 April 2023

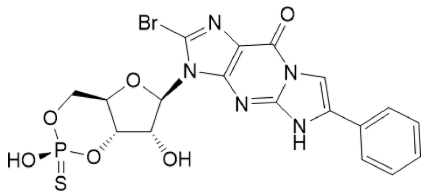

Fig. 1. Molecular structure of CN03.

preparation. LNCs are a type of core–shell nanoparticles that offer the possibility of loading various types of drug molecules including both hydrophilic and hydrophobic compounds of different molecular sizes. Unfortunately, LNC suitability for ocular administration is not very well understood and only a few reports are available, most of which focus on topical applications [11–13]. Due to ocular barrier restrictions, topical administration usually involves very little or no drug delivery to the retinal cells [14]. Intravitreal (IVT) administration is much more efficient for the treatment of retinal diseases as the injected solution is brought into close proximity to the target tissue [15,16].

Here, we studied the permeation of LNCs using excised ocular tissues, and the bio-distribution of LNCs after an IVT injection in whole *ex vivo* porcine eyeballs, which have previously been used as a model for studying IVT particle distribution [17,18]. IVT bio-distribution data was compared against that of liposomes. Moreover, the cytotoxicity of empty particles and the efficacy of CN03 loaded LNCs against photoreceptor cell death were assessed using organotypic retinal explant cultures derived from mice.

2. Materials

1-palmitoyl-2-oleoyl-*sn*-glycero-3-phosphocholine (POPC), cholesterol, 1,2-distearoyl-*sn*-glycero-3-phosphoethanolamine-N-[methoxy (polyethylene glycol)-2000] (ammonium salt) (DSPE-PEG$_{2000}$), 3,3′-Dioctadecyl-oxacarbocyanin-perchlorate, dioctadecyl-3,3,3,3 Tetramethylindodicarbocyanine (DiO), Float-A-Lyzer® G2 dialysis devices (MWCO 100 kDa), chloroform, PBS, 4 % paraformaldehyde in PBS (PFA), sucrose and sodium chloride were obtained from Sigma Aldrich. Labrafac™ lipophile WL 1349 (Medium chain triglycerides, Ph. Eur. Grade), Kolliphor® HS 15 (polyethylene glycol (15)-hydroxystearate, Ph. Eur. Grade), and Phospholipon® 90H (hydrogenated phosphatidylcholine ≥ 90 %) were obtained from Gattefossé (France), BASF and, Lipoid (Germany) respectively. The CN03 (also referred to as DF003 in previous publications) drug compound (R_P-8-Br-PET-cGMPS) was synthesized internally by RISE Research Institutes of Sweden [19].

3. Methods

3.1. Preparation of lipid nanocapsules

LNCs were prepared using a phase inversion process [7,8]. In brief, the components of LNCs (Labrafac lipophile WL 1349, Kolliphor HS 15, Phospholipon 90H, sodium chloride) along with DiO or CN03 were weighed and subjected to 3 heat-cool cycles of 90–60 °C. During the last cooling cycle, near the phase inversion temperature, an excess of cold water was added to the mixture to form the LNCs loaded with either DiO or CN03. For DiO the encapsulation efficiency was estimated to be around 100 % (from visual inspection of the aqueous phase). For comparison, blank LNC formulation was prepared in a similar way. Finally, LNCs were filtered using a 0.22 μM syringe filter and stored at 2–8 °C until further use.

3.2. Preparation of liposomes

Liposomes were prepared using an established protocol [20]. The compounds POPC, cholesterol, DSPE-PEG$_{2000}$, and DiO were dissolved in chloroform and mixed in the molar ratio 63.3:31.7:5:0.2. The chloroform was removed on a rotary evaporator (model RC600, KNF Neuberger, Trenton, NJ, USA) at 100 rpm and a pressure of 300 mbar for 1 to 2 h. The dried lipid film was hydrated in PBS and extruded using a mini-extruder (Avanti Polar Lipids, Alabaster, AL, USA) by passing the solution back and forth between a 100 nm porous polycarbonate membrane eleven times with Hamilton syringes. The liposomes were kept in the dark and stored at 2–8 °C until further use.

3.3. Characterization of lipid nanocapsules

3.3.1. Physico-chemical characterization

3.3.1.1. Particle size and zeta potential measurements. Particle size, size distribution and zeta potential of the prepared LNCs were measured with a Malvern Zetasizer ZS (Malvern Instruments, UK). Size measurements were performed by dynamic light scattering (DLS) with an angle of detection of 173°. The zetapotential of LNCs was calculated by determining the electrophoretic mobility. Both size and zeta potential measurements were performed at 25 °C.

3.3.1.2. Release of DiO from LNCs. Release experiments on DiO loaded LNCs were performed in phosphate buffer using a dialysis setup. 1 mL of DiO-LNCs were placed in a Float-A-lyzer device with a 50kD MWCO membrane and this was kept in 18 mL of phosphate buffer. Prior to the experiments, the dialysis device was pretreated as per the suppliers' standard instructions. Experiments were performed at 37 °C and stirring was maintained in the release buffer. At predetermined time intervals samples were collected for analysis and the whole buffer was replaced with fresh phosphate buffer. DiO released into the phosphate buffer was quantified by measuring the fluorescence intensity using a Varioskan™ LUX multimode microplate reader (ThermoFisher Scientific).

3.3.2. Ex vivo and in vitro characterization

3.3.2.1. Permeation of free drug and drug loaded LNCs in Franz-type diffusion cells. Fresh porcine eyes were obtained from a local slaughterhouse and were frozen at −80 °C within 2 h of collection until they were being used [21]. Before the tissue collection, the frozen eyes were brought to complete thaw by keeping them in PBS. After thawing, a small cut was made with the scalpel at the limbus and the corneas were dissected from the eyeballs. Full-thickness corneas and the conjunctiva-sclera-choroid-retina complex were isolated, and the permeability studies were performed using Franz-diffusion cells (PermeGear Inc., Pennsylvania, USA) using a similar process described by Pescina *et al.* [22,23] with some modifications. The dissected tissues were kept between the donor and the receptor compartment with the endothelial side facing the receiving compartment. The donor compartment was filled with 1 mL of either free drug or drug loaded LNCs (LNC/CN03) at a concentration of 2 mg/mL, and phosphate buffer (5 mL) was used in the receptor compartment. Experiments were performed for up to 6 h at 37 ± 0.2 °C with constant stirring in the receptor buffer to avoid any boundary layer effect. At predetermined time intervals, 0.2 mL of sample was collected from the receptor compartment and was replaced with an equal volume of fresh buffer. Drug concentrations were measured using a microplate reader equipped with a UV–Vis spectrophotometric detector (SpectraMax, Molecular Devices, San Jose, CA) and the permeability coefficients were calculated using the algorithm described by Niedorf *et al.* [24]. All experiments were carried out in triplicate using different ocular bulbs from different animals.

3.3.2.2. Intraocular bio-distribution in ex vivo porcine eyes. Porcine eyes were obtained from a local slaughterhouse in the morning of the day of slaughter. The eyes were washed briefly in 70 % ethanol and sterile PBS.

Excess tissue was removed. Before injection, the green background fluorescence along the axial length within the eyes were measured on an ocular fluorometer (FM-2 Fluorotron Master, OcuMetrics, CA, USA). A 50 μL volume of LNC/DiO or liposomes/DiO was injected into the center of the vitreous using a 22-gauge needle (Hamilton 1705 RN syringe, Hamilton, Reno, NV, USA). For LNC/DiO injected eyes, the green fluorescence signal from DiO was measured on the fluorometer directly after injection (t = 0), followed by incubation on a rotation shaker at 45 rpm. Additional measurements were recorded after 0.5 h, 1 h, 2 h, 6 h, and 24 h to follow the distribution of the particles. After the 24 h time-point, the eyes were fixed in a 4 % PFA solution following an established protocol [17]. After 5 days incubation at 2–8 °C, the eyes were washed twice in PBS and submerged in embedding medium (Tissue-Tek O.C.T. Compound, Sakura Finetek Europe, Alphen aan den Rijn, Netherlands) and frozen with liquid N_2. The eyes were sectioned on a cryostat (NX50, Thermo Fisher, Waltham, MA, USA) at –16 °C in 40 μm thick sections, which were transferred onto glass slides (Superfrost Plus™, R. Langenbrinck, Emmendingen, Germany). The slides were dried at 37 °C for 1–2 h in the dark, rehydrated with PBS for 10 min and mounted with Vectashield medium containing DAPI (Vector laboratories, Burlingame, CA, USA). They were kept at 2–8 °C for at least 0.5 h before imaging with fluorescent microscopy. The green signal was measured from different regions in the eye sections: the cornea, the lens, the ciliary body, the vitreous, and the retina. Sections from eyes where no particles were injected were used to qualitatively determine the baseline for a positive signal. For either LNC/DiO or liposome/DiO injected eyes, sections from 5 different eyes were measured (n = 5). One-way ANOVA with Tukey's multiple comparison test was calculated with GraphPad Prism 8 (GraphPad Software, San Diego, CA, USA) to determine statistical significances.

3.3.2.3. Retinal toxicity profile. Mice were sacrificed at post-natal day (P) 9 by cervical dislocation. The eyes were collected, and organotypic retinal explant cultures were prepared using an established protocol [25]. At P11, a 20 μL drop of either 0, 1, 5, or 10 mg/mL LNCs was added onto the side of the retina that would normally be in contact with the vitreous, *i.e.,* on top of retinal explant cultures. At P13, another drop of LNC solution was applied. At P15, the retinal explant cultures were fixed in PFA for 45 min, washed twice in PBS, and cryoprotected in 10 %, 20 %, and 30 % sucrose for 10 min, 20 min, and 30 min, consecutively. The retinal cultures were placed in embedding medium (Tissue-Tek O.C.T. Compound, Sakura Finetek Europe, Alphen aan den Rijn, Netherlands), snap-frozen in liquid N_2, and sectioned on a cryostat (NX50, Thermo Fisher, Waltham, MA, USA) at –20 °C into 14 μm sections, which were collected onto glass slides (Superfrost Plus™, R. Langenbrinck, Emmendingen, Germany). The slides were dried at 37 °C for 45 min and stored at –20 °C. To determine the amount of dying cells in the retinal tissue sections, a terminal deoxynucleotidyl transferase dUTP nick end labeling (TUNEL) assay was employed (TMR red, Product No. 12156792910, Sigma Aldrich, Darmstadt, Germany). The procedure is described under [26]. Afterwards, the slides were mounted with Vectashield containing DAPI and imaged using fluorescence microscopy. From the imaged sections, the relative amount of dying cells (TUNEL + cells) were calculated from the following equation:

$$TUNEL + cells(\%) = \frac{N_{TUNEL}}{A_L/A_n} \bullet 100$$

where N_{TUNEL} is the absolute number of TUNEL + cells in either the outer nuclear layer (ONL) or the inner nuclear layer (INL) of the retinal tissue sections, A_L is the area of each layer, and A_n is the average area of the cells in each layer. For each condition, the relative TUNEL + cells were determined for 4–5 different cultures (n = 4–5). Statistical analysis: One-way ANOVA with Tukey's multiple comparison test using GraphPad Prism 8.

Table 1
Characterization of LNCs. Data is represented as mean ± SD (n = 3).

Formulation	Particle size (diameter, nm)	PDI	Zeta potential (mV)
Blank LNCs	61 ± 1	0.03 ± 0.02	−2.5 ± 1.1
CN03-LNCs	72 ± 1	0.07 ± 0.02	−11.3 ± 0.8
DiO-LNCs	58 ± 0.2	0.04 ± 0.03	−0.3 ± 0.1

3.3.2.4. Treatment efficacy of encapsulated CN03. The retinal degeneration *rd1* mouse model was used to produce organotypic retinal explant cultures at P5. At P7, LNC/CN03 formulation was applied to the culture in a drop onto the ganglion cell side of the cultures. Alternatively, a solution of free CN03 in 25 mM HEPES and 125 mM NaCl (pH 7.4) was applied. In both instances, the initial drug concentration in the solution applied to the retinal cultures was 200 μM, which, if assuming an even distribution across the culture medium, produced a final concentration of 4 μM. Non-treated cultures were used as controls. LNC/CN03 administration was repeated at P9. At P11, the cultures were fixed, cryoprotected, frozen, and sectioned as described above. Additionally, organotypic retinal explant cultures from wild-type mice were prepared and left non-treated following the same paradigm. To determine the effect of CN03, cell death was determined using the TUNEL assay as described above. From the imaged sections, the relative amount of dying cells (TUNEL + cells) were calculated from the equation above. The relative TUNEL + cells were determined for 5–6 different cultures (n = 5–6). Statistical analysis: One-way ANOVA with Tukey's multiple comparison test.

3.3.2.5. Fluorescent microscopy. Sections from either porcine eyes or organotypic retinal explant cultures were images using fluorescence microscopy (Axio Imager Z2 with ApoTome function, Zeiss, Oberkochen, Germany). A CCD camera and 10X or 20X objectives were used. For DiO signal: green channel of Ex./Em. of 483/501 nm. TUNEL assay: red channel of Ex./Em. 548/561 nm. DAPI signal: blue channel of Ex./Em. 353/465 nm. In all cases, the ApoTome function was used. Z-stacks were collected 1 μm across 25 images for porcine eye sections or 11 images for retinal explant cultures using the microscope software (ZEN 2.6, Zeiss). The images were projected using the Maximum Intensity Projection function, and these images were used for data analysis.

4. Results

4.1. Physico-chemical characterization of LNCs

Blank LNCs and loaded LNCs (drug or DiO loaded) were analyzed for particle size and size distribution (poly dispersity index; PDI) along with the zeta potential (Table 1). Particle size and zeta potential of unloaded and DiO loaded LNCs were similar, however an increased size and zeta potential was observed in the presence of encapsulated CN03 in agreement with earlier published data [7,8]. Detailed physico-chemical characterization data on LNCs and liposomes ha been described in previous publications [7,17].

Further experiments were performed to quantify the release of DiO in phosphate buffer. Here, DiO release was insignificant and did not produce detectable levels of fluorescence even after 48 h of testing. This confirms that the dye is confined in the LNCs and can be used as a marker to study the distribution of LNC in the eye.

4.2. Tissue permeability studies

Permeability studies were performed with a Franz-diffusion cell system using excised tissues from intact porcine eyeballs. The permeability coefficients of free drug and the drug loaded particles across full-thickness cornea were $2.2 \pm 1.2 \times 10^{-8}$ cm/s, and $5.1 \pm 1.7 \times 10^{-8}$ cm/s respectively. For conjunctiva-sclera-choroid-retina the free drug and LNC/CN03 formulation showed a permeability coefficient of 1.0 ± 0.2

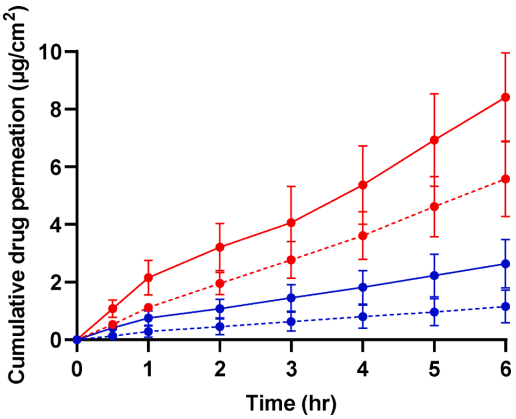

Fig. 2. Cumulative amount permeated per area (µg/cm^2, mean ± SD, n = 3) of CN03 (dashed lines) and LNC/CN03 formulation (solid lines). Data in Blue indicates the permeation through full-thickness cornea and the data in Red indicates the permeation through conjunctiva-sclera-choroid-retina. (For interpretation of the references to colour in this figure legend, the reader is referred to the web version of this article.)

× 10^{-7} cm/s and 1.60 ± 0.4 × 10^{-7} cm/s respectively. Based on the permeability coefficients, the conjunctiva-sclera-choroid-retina was 4.6 times more permeable to the free compound than the full-thickness cornea and 3 times more permeable for the LNCs formulation. The cumulative drug penetration of drug and LNC/CN03 formulation in the excised ocular tissues are shown in Fig. 2.

4.3. Intraocular bio-distribution in ex vivo porcine eye

Fluorophotometry was used on intact *ex vivo* porcine eyes obtained from the local slaughterhouse to analyze the kinetics of the intravitreal diffusion of LNC. The fluorescent marker DiO was formulated with the LNCs to localize the particles within the axial length of the eyeball. Intensity plots as shown in Fig. 3**A** were collected across different time points up to 24 h post-injection. The area under the curve (AUC) for each time-point was plotted (Fig. 3**B**) to analyze how fast the LNCs were diffusing within the eye. After 24 h the AUC was reduced to about 10 % the value of the peak, which occurred at 2 h post-injection. The initial increase in AUC from 0 to 2 h, may be due to a back-flow of the injected solution through the injection channel. The following decrease in signal is then caused by intravitreal diffusion.

4.4. Histological analysis of ex vivo porcine eyes

The fluorophotometry measurements revealed an almost even distribution of the injected LNC/DiO after 24 h (Fig. 3). Fluorescence microscopy was then used to record the DiO signal from different regions of the eye (Fig. 4**A**). For comparison, conventional POPC-liposomes with 5 mol% 2 kDa mPEG were also tested. The DiO signal was measured from the images using the same microscopy conditions across all specimens (Fig. 4**B**). No statistically significant differences were observed between LNCs and liposomes except at the ciliary body where more LNCs than liposomes accumulated. Liposomes tended to absorb more strongly to the retina, although this was not statistically significant. Qualitatively, it was observed that LNCs were primarily restricted to the surface of the retina around the vitreoretinal interface, while the liposomal DiO was transported through the whole retina (see Fig. 4**A**, panels labelled "retina"). Also, the liposomal distribution in the vitreous seemed to be more homogenous compared to the LNCs. An overview of the intraocular bio-distribution is shown in Fig. 4**C**.

4.5. Retinal toxicity profile

Retinal explants derived from P9 mice and cultured for four days were used to assess the toxicity of LNCs to the retina. Without LNC addition to the cultures, there were around 2 % TUNEL-positive cells in the ONL, reflecting the cell death rate caused by the explant situation itself. Cell death in the INL was very low, indicating that INL cells were less sensitive than photoreceptors. At a concentration of 1 mg/mL LNCs appeared to be well tolerated by the retina. However, at 5 mg/mL there was a tendency towards increased cell death. At an LNC concentration of 10 mg/mL, a statistically significant increase in the number of dying cells in the ONL was observed, suggesting that this concentration was toxic to photoreceptors (Fig. 5). In all cases, there was no change in the cell death in the INL.

It is important to consider that the LNC concentration was tested on the retina itself. Since an injected formulation would be diluted in the vitreous, the concentration of the highest tolerated dose could be a lot higher than 1 mg/mL. The human vitreous is about 4–5 mL [27], and if

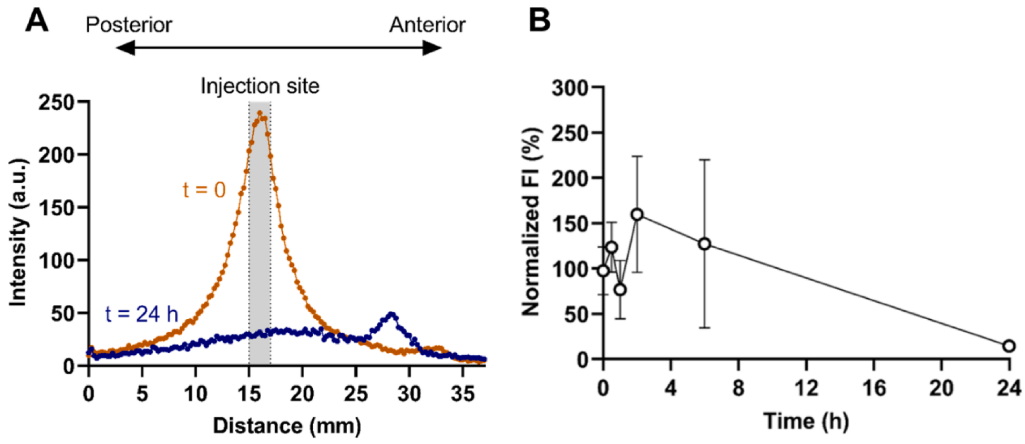

Fig. 3. Intravitreal movement of LNCs as determined by fluorophotometry. A Example profile of LNC-DiO signal from injected pig eyes at t = 0 (orange) and at t = 24 h (purple) along the axial length. B Normalized fluorescent intensity (FI) in the injection site from 0 to 24 h. Results present mean ± SD for n = 5 eyes. (For interpretation of the references to colour in this figure legend, the reader is referred to the web version of this article.)

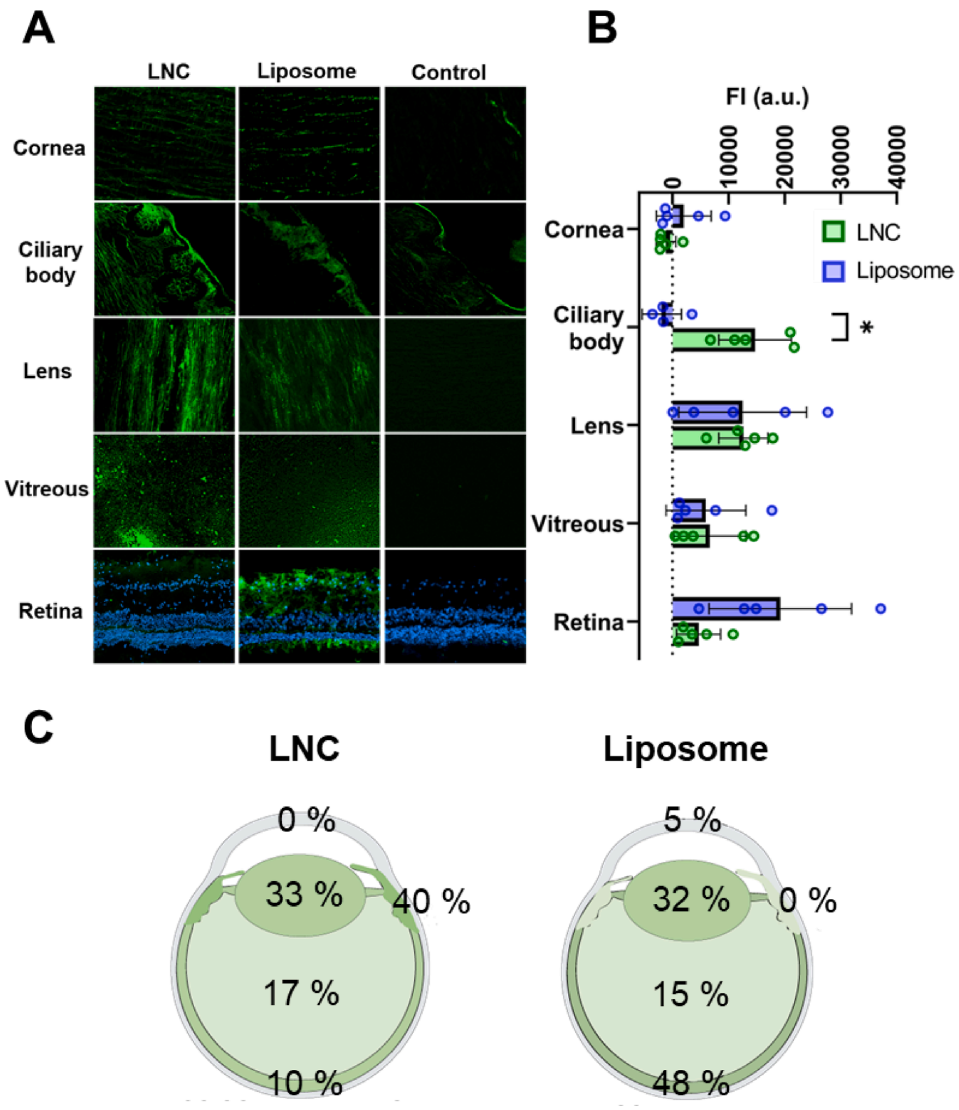

Fig. 4. Bio-distribution of LNCs and liposomes after intravitreal administration in whole porcine eyes. (A) Microscopy images of different tissues from sections of porcine eyes 24 h after injection of either LNC/DiO formulation or liposome/DiO formulation or non-injected eyes (control). Scale bar = 50 μm. (B) Fluorescent intensities (FI) from relevant ocular tissues after injection of LNCs or liposomes. Negative value is due to subtraction of background signal. Results represent mean ± SD for n = 5, * $p \leq 0.05$. Data analysis: Two-way ANOVA with Šidák's multiple comparison test. (C) Schematic drawings illustrating the relative distribution of LNCs and liposomes in pig eyes.

50 μL of the LNC formulation was injected, a dose of 80 mg/mL could be given to achieve a local concentration at the retina of 1 mg/mL. However, this is assuming an even distribution in the eye, which our bio-distribution results do not support (Fig. 4), so that the local concentration at the retina would likely be lower than expected.

4.6. Treatment efficacy of encapsulated drugs

Retinas from the retinal degeneration mouse model, *rd1*, were used to assess the treatment efficacy of CN03 encapsulated in LNC. Since the LNCs were tested for an intravitreal administration route, all drug solution was applied on top of the cultures (*i.e.*, from the ganglion cell side). In an *in vivo* setting, using intravitreal injection, the LNCs would reach the retina from this side. Either a free drug solution (free CN03), LNC/CN03 formulation, or non-treated control retinas were analyzed. For drug-containing solutions, the concentration in the solution administered was 200 μM. Assuming equal distribution in the tissue and culture medium, the final drug concentration was 4 μM. Explant cultures derived from wild-type mice were compared. As in the toxicity analysis, a TUNEL-assay was used to detect dying photoreceptors in cross-sections of the tissue (Fig. 6).

In *rd1* retinas, there was a significant increase in dying photoreceptors compared to wild-type. Both the free drug and the LNC encapsulated drug provided a protection of the photoreceptors as evidenced by a

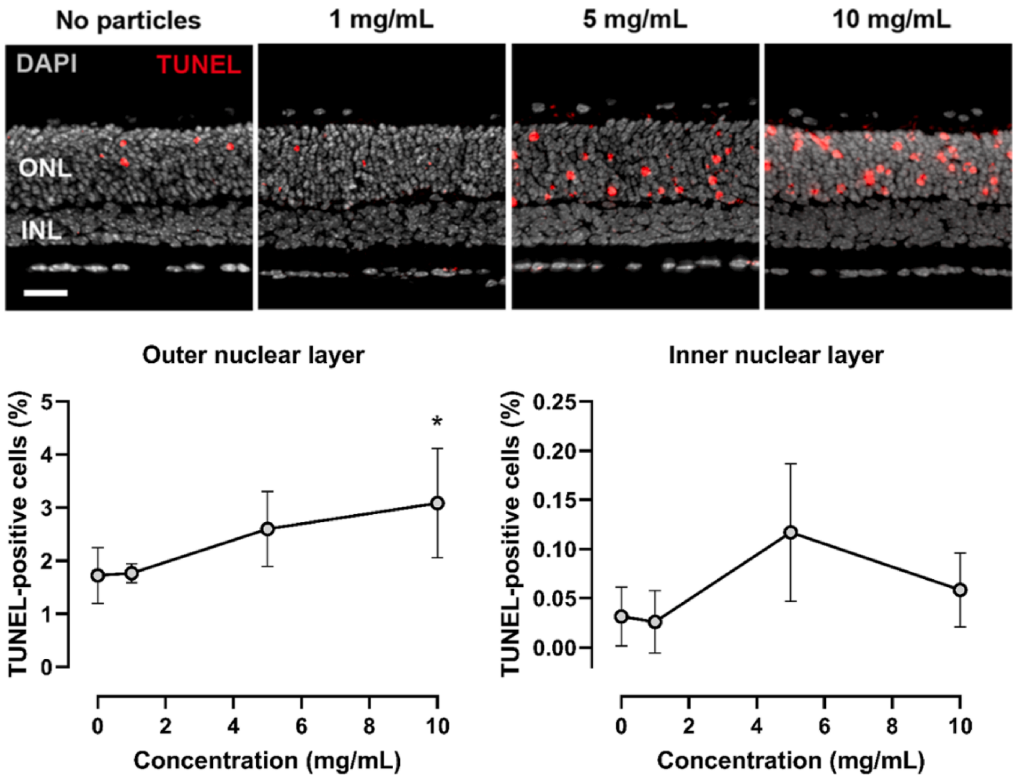

Fig. 5. Retinal toxicity profile of LNCs. Retinal explant cultures derived from WT mice were incubated with LNCs at different concentrations for 4 days. The TUNEL-assay (red) was employed to label dying cells in tissue sections. DAPI (gray) was used as nuclear counterstain to visualize the outer nuclear layer (ONL) and inner nuclear layer in the retina (INL). The number of TUNEL-positive cells in either layer was analyzed. Notice the differences in scales between the two graphs, indicating that cell death related mostly to photoreceptors in the ONL. Scale bar = 50 μm. Results represent mean ± SD for n = 4–5 animals. * $p \leq 0.05$. Statistical analysis: One-way ANOVA with Tukey's post-hoc test. (For interpretation of the references to colour in this figure legend, the reader is referred to the web version of this article.)

lower TUNEL-positive cell count. In both cases, cell death was reduced by 25 %. The release of CN03 from LNC/CN03 formulation was fast enough to have an effect on the *rd1* model, and this effect was found to be similar to that of free CN03. Although there was no difference between the CN03 and LNC/CN03 formulation treatments in this *in vitro* setting, in the *in vivo* situation LNCs could be advantageous to retain the drug within the vitreous and thereby improve the pharmacokinetics of CN03 and extend its pharmacological effect.

5. Discussion

In this study, we employed different *ex vivo* and *in vitro* techniques to determine the effectiveness of LNCs as an intraocular delivery system for the neuroprotective drug CN03. The data address several aspects that are useful for the development of ocular drug delivery systems, such as particle size, vitreal mobility, ocular tissue accumulation, retinal toxicity, and treatment efficacy in retinal cultures.

Characterization of LNCs indicated that the formulation, irrespective of presence or absence of a loaded cargo, resulted in particles with <100 nm in size and with a narrow particle size distribution. An increase in size as measured with DLS was observed when the drug CN03 was loaded in the particles. In such particles, the surface charge, as measured by the zeta potential, became more negative compared to unloaded LNCs, indicating that CN03 was present on the surface of the particles. These observations are in accordance with previous findings [7,8]. On the other hand, DiO loading did not seem to impact either particle size or zeta potential. Lipophilic DiO is expected to predominantly locate to the core of the particles, causing little change to the surface charge. To study the integrity of DiO loaded particles and confirm the suitability of DiO as a fluorescent label for LNCs, release experiments were performed in phosphate buffer. No DiO release to the medium could be detected for up to 48 h. Apparently, a strong interaction of DiO with the oily core, as well as poor solubility of DiO in phosphate buffer prevented the label release from the LNC.

The cornea of the eye forms a tremendous barrier for the penetration of drug substances. To reach therapeutic drug concentrations in the retina, topical administration is usually not sufficient and intravitreal injection may be required to achieve the desired effect [28,29]. It has however been reported that lipid-based nanoparticles enhance the ocular penetration of drugs which are targeted for both anterior and posterior chambers when administered topically to the eye [30–35]. Thus, to study the ability of the LNCs in improving the ocular penetration, permeability screening of free CN03 and CN03 loaded LNCs was conducted on both full-thickness cornea and conjunctiva-sclera-choroid-retina excised from fresh porcine eyeballs using Franz-diffusion cells methodology [22,23].

The permeability of CN03 was found to be improved across both full-thickness cornea and conjunctiva-sclera-choroid-retina when formulated with LNCs compared to CN03 alone in solution. Moreover, the permeability coefficients of both drug solution and the CN03-LNCs across conjunctiva-sclera-choroid-retina were higher than across full-thickness cornea. However, the LNC permeability values were

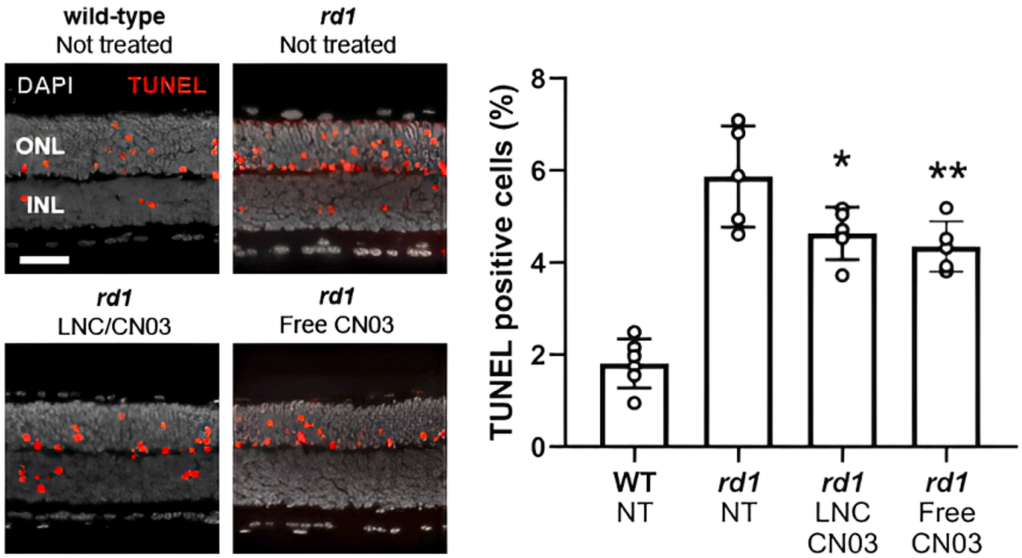

Fig. 6. Treatment efficacy of the LNC/drug formulation. Retinal explant cultures derived from the *rd1* mouse model were treated with the retinoprotective drug CN03, either in a particle-free solution (Free CN03) or LNC/CN03 formulation. In both cases, drug concentration in the treatment solutions was 200 μM, and all were applied on top of the retinal culture. Assuming equal distribution in the culture medium, the final concentration was 4 μM. Treatment period was from P7 to P11. A TUNEL-assay (red) was used to detect dying cells in cross-sections of the cultures, and DAPI (gray) was used to localize the outer nuclear layer (ONL) and inner nuclear layer (INL). The amount of dying cells (TUNEL-positive cells) in the ONL was counted to assess treatment effects. Scale bar = 50 μm. Results represent mean ± SD for n = 5–6 animals. * $p \leq 0.05$, ** $p \leq 0.01$ compared to the *rd1* not treated (NT) condition. Statistical analysis: One-way ANOVA with Tukey's post-hoc test. (For interpretation of the references to colour in this figure legend, the reader is referred to the web version of this article.)

Table 2
Permeability of drug compounds across ocular tissues derived from porcine eyeballs.

Compound	Application	Tissue permeability (cm/s)		Reference(s)
		Full-thickness cornea	Conjunctiva-sclera-choroid-retina	
Dexamethasone	Glucocorticoid used in treatment of allergic reactions in the eye	$0.2 \pm 0.1 \times 10^{-6}$ – $7.6 \pm 1.2 \times 10^{-6}$	$1.0 \pm 0.2 \times 10^{-6}$	[36–39]
Propranolol	Beta-blockers used in the treatment of intraocular pressure	$1.5 \pm 1.4 \times 10^{-6}$ – $14.6 \pm 0.5 \times 10^{-6}$	$7.0 \pm 2.5 \times 10^{-6}$	[22,23,37]
Timolol maleate		$5.1 \pm 0.6 \times 10^{-6}$ – $10.7 \pm 2.1 \times 10^{-6}$	$1.3 \pm 0.4 \times 10^{-6}$	[36,38,39]
Library of compounds with varied molecular properties (n = 27)	Varied applications	$5.0 \pm 0.3 \times 10^{-6}$	$16.0 \pm 0.9 \times 10^{-6}$	Unpublished *

* Data reported as mean permeability values from 27 different compounds.

relatively low in comparison to other ophthalmologic drugs, the *ex vivo* permeability of which has been tested by other authors using a similar methodology (Table 2). In a study performed by Lorenzo-Soler *et al.* (manuscript under revision), where 27 different drugs were tested in their free form using the methodology here described, the mean permeability coefficients across both tissues were calculated. The mean permeability values of the compounds tested were $5.0 \pm 0.3 \times 10^{-6}$ cm/s across full thickness cornea and $16.0 \pm 0.9 \times 10^{-6}$ cm/s for conjunctiva-sclera-choroid-retina. These values are considerably higher than those shown for CN03, indicating a poor permeability of the compound across both cornea and the scleral complex. This suggests that the topical route of administration is not an efficient route for delivering CN03 to the retinal photoreceptors.

For histology and ocular distribution experiments, we used fresh porcine eyes from the slaughterhouse. The excised porcine eyes have several advantages over *in vivo* studies such as cost, ethical concerns of animal use, and rapid production of data [40]. Moreover, porcine eyes from slaughterhouses are readily available in many parts of the world. However, it is also important to consider the limitations of using this model. Due to the degradation of the eyes following the tissue isolation, longer term studies are usually not possible. We have previously demonstrated that porcine eyes are useful in short term pharmacokinetic analyses in combination with fluorophotometry [17], but even under sterile conditions, obvious signs of tissue degradation can be seen after 5–7 days. In this study, we have used the porcine eyes within approximately 4 h following their excision, *i.e.* long before tissue degradation sets in. Our porcine eye data showed considerable variability with standard deviations in eye distribution of up to 100 % for 5 experiments. This may be due to experimental differences in individual intravitreal injections, as well as differences in the porcine eyes themselves. Other studies that used intact *ex vivo* porcine eyes also reported high variation [18].

Fluorophotometry measurements on intact porcine eyes showed a near complete distribution of DiO-LNCs 24 h post injection, showing that the distribution of particles is unhindered by the vitreous network. From the histological analysis of injected porcine eyes, both liposomes and LNCs showed similar total fluorescence intensities 24 h after injection, yet their distribution to different ocular tissues was markedly different. LNCs tended to accumulate on the surface of the ciliary body more than liposomes. Uptake of liposomes in the ciliary epithelium may

be limited by the PEG layer on the surface of the liposomes [41]. For the retina, on the other hand, the PEG layer may stimulate uptake as shown in the work of Tavakoli *et al.* [42]. They showed that PEGylation of liposomes improves the permeation across the inner limiting membrane of the retina, thereby increasing the possibilities for retinal cell uptake. Still, it should be noted that, since hydrophobic molecules were used as tracers, transfer of the tracer from the lipid bilayer to hydrophobic biological membranes in the retina is possible. This may happen more often for lipids with low transition temperatures like POPC used in this study [43]. Since DiO is encapsulated in the inner core in the LNC, it is likely that the transfer happens less than for the liposomes. Further, for both LNCs and liposomes, fluorescence signal was evident across the lens, which may be due to the lipophilic nature of DiO [44].

We found that LNCs were largely non-toxic to the retina with only a slight increase in the number of dying photoreceptors after *in vitro* exposure to concentrations of 10 mg/mL. Low cytotoxicity at the studied LNC concentration may in part be due to the poor retinal uptake of the LNCs. In comparison, liposomes, which showed higher retinal penetration, were found to be slightly toxic at 5 mg/mL [17]. Other studies have also found higher retinal penetration of liposomes [17,45,46], as well as other nano-systems like albumin-based nanoparticles [47,48] and PLGA-based nanoparticles [49] compared to LNCs. The poor retinal uptake of LNCs likely affects drug transport, which, in retinal cultures, was not improved by the LNCs. Yet, in the treatment of retinal explant cultures, the encapsulated drug provided the same level of protection as the free drug solution. Thus, the LNCs may not need to be taken up by the retina to allow the loaded drug to exert its effect. The main benefit of the LNCs as an intraocular drug delivery system may therefore be their ability to provide a drug depot and sustain the release of CN03 in the vitreous over a prolonged period of time [7]. Moreover, a poor retinal uptake of LNCs could prolong their half-life in the eye as retinal uptake is a route of elimination from the vitreous [50]. Both factors would reduce the required number of IVT injections, something highly advantageous in a clinical context.

6. Conclusion

In summary, LNCs were well suited for encapsulation of the small molecule drug CN03 and exhibited low retinal toxicity. The biodistribution of LNCs in the vitreous of *ex vivo* porcine eyes revealed a high degree of permeation in the ciliary body compared to the retina, indicating that LNCs might be useful for targeted delivery to the ciliary body. Nevertheless, in explanted *in vitro* retinal cultures LNC formulated CN03 could efficiently protect *rd1* mouse photoreceptors from mutation-induced degeneration.

Declaration of Competing Interest

The authors declare that they have no known competing financial interests or personal relationships that could have appeared to influence the work reported in this paper.

Data availability

Data will be made available on request.

Acknowledgements

The authors would like to thank Professor Thorsteinn Loftsson at the University of Iceland for his continued support and guidance, particularly to Dileep Urimi as an academic supervisor. The authors would like to thank Ronja Widenbring for her review and proof reading of this manuscript.

Funding sources

This work was financially supported by the German Research Council (DFG; PA1751/10-1), and the European Union (*trans*Med, H2020-MSCA-ITN-2017-765441), European Joint Programme on Rare Diseases - Joint Transnational Call 2020 (TreatRP).

References

[1] A. Sahaboglu, et al., Retinitis pigmentosa: rapid neurodegeneration is governed by slow cell death mechanisms, Cell Death Dis. 4 (2) (2013) e488.
[2] F. Paquet-Durand, et al., PKG activity causes photoreceptor cell death in two retinitis pigmentosa models, J. Neurochem. 108 (3) (2009) 796–810.
[3] J. Sancho-Pelluz, et al., Photoreceptor cell death mechanisms in inherited retinal degeneration, Mol. Neurobiol. 38 (3) (2008) 253–269.
[4] L. Liu, X. Liu, Roles of Drug Transporters in Blood-Retinal Barrier, in Drug Transporters in Drug Disposition, Effects and Toxicity, X. Liu and G. Pan, Editors. 2019, Springer Singapore, Singapore. p. 467-504.
[5] D.B. Farber, R.N. Lolley, Cyclic guanosine monophosphate: elevation in degenerating photoreceptor cells of the C3H mouse retina, Science 186 (4162) (1974) 449–451.
[6] E. Vighi et al., Combination of cGMP analogue and drug delivery system provides functional protection in hereditary retinal degeneration. Proc. National Acad. Sci. 115(13) (2018) E2997-E3006.
[7] D. Urimi, et al., Formulation development and upscaling of lipid nanocapsules as a drug delivery system for a novel cyclic GMP analogue intended for retinal drug delivery, Int. J. Pharm. 602 (2021), 120640.
[8] D. Urimi, et al., Structural characterization study of a lipid nanocapsule formulation intended for drug delivery applications using small-angle scattering techniques, Mol. Pharm. 19 (4) (2022) 1068–1077.
[9] P. Panwar, et al., Preparation, characterization, and in vitro release study of albendazole-encapsulated nanosize liposomes, Int. J. Nanomed. 5 (2010) 101–108.
[10] Z.L. Miao, et al., Preparation of a liposomal delivery system and its in vitro release of rapamycin, Exp. Ther. Med. 9 (3) (2015) 941–946.
[11] R. Sun, et al., Ultra-small-size Astragaloside-IV loaded lipid nanocapsules eye drops for the effective management of dry age-related macular degeneration, Exp. Opin. Drug Deliv. 17 (9) (2020) 1305–1320.
[12] M.L. Formica, et al., Novel hybrid lipid nanocapsules loaded with a therapeutic monoclonal antibody–Bevacizumab–and Triamcinolone acetonide for combined therapy in neovascular ocular pathologies, Mater. Sci. Eng. C 119 (2021), 111398.
[13] M.L. Formica, et al., Triamcinolone acetonide-loaded lipid nanocapsules for ophthalmic applications, Int. J. Pharm. 573 (2020), 118795.
[14] D.M. Maurice, Drug delivery to the posterior segment from drops, Surv. Ophthalmol. 47 (Suppl 1) (2002) S41–S52.
[15] A. Bochot, E. Fattal, Liposomes for intravitreal drug delivery: a state of the art, J. Control. Release 161 (2) (2012) 628–634.
[16] L. García-Quintanilla, et al., Pharmacokinetics of intravitreal anti-vegf drugs in age-related macular degeneration, Pharmaceutics 11 (8) (2019).
[17] G. Christensen, et al., Investigating ex vivo animal models to test the performance of intravitreal liposomal drug delivery systems, Pharmaceutics 13 (7) (2021).
[18] A.Z. Eriksen, et al., The diffusion dynamics of PEGylated liposomes in the intact vitreous of the ex vivo porcine eye: a fluorescence correlation spectroscopy and biodistribution study, Int. J. Pharm. 522 (1–2) (2017) 90–97.
[19] O. Pérez, N. Schipper, M. Bollmark, Preparative synthesis of an R P-guanosine-3′, 5′-cyclic phosphorothioate analogue, a drug candidate for the treatment of retinal degenerations, Org. Process Res. Dev. 25 (11) (2021) 2453–2460.
[20] H. Zhang, Thin-Film Hydration Followed by Extrusion Method for Liposome Preparation, in Liposomes: Methods and Protocols, G.G.M. D'Souza, Editor. 2017, Springer New York: New York, NY. p. 17-22.
[21] S. Nicoli, et al., Porcine sclera as a model of human sclera for in vitro transport experiments: histology, SEM, and comparative permeability, Mol. Vis. 15 (2009) 259.
[22] S. Pescina, et al., Development of a convenient ex vivo model for the study of the transcorneal permeation of drugs: histological and permeability evaluation, J. Pharm. Sci. 104 (1) (2015) 63–71.
[23] S. Pescina, et al., Ex vivo models to evaluate the role of ocular melanin in transscleral drug delivery, Eur. J. Pharm. Sci. 46 (5) (2012) 475–483.
[24] F. Niedorf, E. Schmidt, M. Kietzmann, The automated, accurate and reproducible determination of steady-state permeation parameters from percutaneous permeation data, Altern. Lab. Anim. 36 (2) (2008) 201–213.
[25] S. Belhadj, et al., Long-term, serum-free cultivation of organotypic mouse retina explants with intact retinal pigment epithelium, J. Vis. Exp. (2020).
[26] D.T. Loo, In situ detection of apoptosis by the TUNEL assay: an overview of techniques, Methods Mol. Biol. 682 (2011) 3–13.
[27] A.M. Azhdam, R.A. Goldberg, S. Ugradar, In vivo measurement of the human vitreous chamber volume using computed tomography imaging of 100 eyes, Transl. Vis. Sci. Technol. 9 (1) (2020) 2.
[28] V. Agrahari, et al., How are we improving the delivery to back of the eye? Advances and challenges of novel therapeutic approaches, Expert Opin. Drug Deliv. 14 (10) (2017) 1145–1162.
[29] I.P. Kaur, S. Kakkar, Nanotherapy for posterior eye diseases, J. Control. Release 193 (2014) 100–112.

[30] B.M. Davis, et al., Topical delivery of Avastin to the posterior segment of the eye in vivo using annexin A5-associated liposomes, Small 10 (8) (2014) 1575–1584.
[31] S.A. Gaballa, et al., Preparation and evaluation of cubosomes/cubosomal gels for ocular delivery of beclomethasone dipropionate for management of uveitis, Pharm. Res. 37 (10) (2020) 1–23.
[32] R.M. Khalil, et al., Enhancement of lomefloxacin Hcl ocular efficacy via niosomal encapsulation: in vitro characterization and in vivo evaluation, J. Liposome Res. 27 (4) (2017) 312–323.
[33] P. Lakhani, et al., Optimization, stabilization, and characterization of amphotericin B loaded nanostructured lipid carriers for ocular drug delivery, Int. J. Pharm. 572 (2019), 118771.
[34] J. Navarro-Partida, et al., Safety and tolerability of topical ophthalmic triamcinolone acetonide-loaded liposomes formulation and evaluation of its biologic activity in patients with diabetic macular edema, Pharmaceutics 13 (3) (2021) 322.
[35] A. Tatke, et al., In situ gel of triamcinolone acetonide-loaded solid lipid nanoparticles for improved topical ocular delivery: Tear kinetics and ocular disposition studies, Nanomaterials 9 (1) (2018) 33.
[36] M. Juretić, et al., Biopharmaceutical evaluation of surface active ophthalmic excipients using in vitro and ex vivo corneal models, Eur. J. Pharm. Sci. 120 (2018) 133–141.
[37] E. Ramsay, et al., Corneal and conjunctival drug permeability: Systematic comparison and pharmacokinetic impact in the eye, Eur. J. Pharm. Sci. 119 (2018) 83–89.
[38] C. Loch, et al., Determination of permeability coefficients of ophthalmic drugs through different layers of porcine, rabbit and bovine eyes, Eur. J. Pharm. Sci. 47 (1) (2012) 131–138.
[39] M. Hahne, et al., Prevalidation of a human cornea construct as an alternative to animal corneas for in vitro drug absorption studies, J. Pharm. Sci. 101 (8) (2012) 2976–2988.
[40] E.M. Heikkinen, et al., Esterase activity in porcine and albino rabbit ocular tissues, Eur. J. Pharm. Sci. 123 (2018) 106–110.
[41] H. Hatakeyama, H. Akita, H. Harashima, The polyethyleneglycol dilemma: advantage and disadvantage of PEGylation of liposomes for systemic genes and nucleic acids delivery to tumors, Biol. Pharm. Bull. 36 (6) (2013) 892–899.
[42] S. Tavakoli, et al., Ocular barriers to retinal delivery of intravitreal liposomes: Impact of vitreoretinal interface, J. Control. Release 328 (2020) 952–961.
[43] A.J. Urquhart, A.Z. Eriksen, Recent developments in liposomal drug delivery systems for the treatment of retinal diseases, Drug Discov. Today 24 (8) (2019) 1660–1668.
[44] E.M. Heikkinen, et al., Distribution of small molecular weight drugs into the porcine lens: studies on imaging mass spectrometry, partition coefficients, and implications in ocular pharmacokinetics, Mol. Pharm. 16 (9) (2019) 3968–3976.
[45] J. Lee, et al., Effective retinal penetration of lipophilic and lipid-conjugated hydrophilic agents delivered by engineered liposomes, Mol. Pharm. 14 (2) (2017) 423–430.
[46] S. Camelo, et al., Ocular and systemic bio-distribution of rhodamine-conjugated liposomes loaded with VIP injected into the vitreous of Lewis rats, Mol. Vis. 13 (2007).
[47] H. Kim, S.B. Robinson, K.G. Csaky, Investigating the movement of intravitreal human serum albumin nanoparticles in the vitreous and retina, Pharm. Res. 26 (2) (2009).
[48] H. Koo, et al., The movement of self-assembled amphiphilic polymeric nanoparticles in the vitreous and retina after intravitreal injection, Biomaterials 33 (12) (2012) 3485–3493.
[49] J.L. Bourges, et al., Ocular drug delivery targeting the retina and retinal pigment epithelium using polylactide nanoparticles, Invest. Ophthalmol. Vis. Sci. 44 (8) (2003) 3562–3569.
[50] E.M.D. Amo, et al., Pharmacokinetic aspects of retinal drug delivery, Prog. Retinal Eye Res. 57 (2017) 134–185.